Title
Isochorismate Synthase Enzymes in Arabidopsis

Author
Strawn, Marcus Antoninus

Publication Date
2010

Peer reviewed|Thesis/dissertation

Isochorismate Synthase Enzymes in *Arabidopsis*

by

Marcus Antoninus Strawn

A dissertation submitted in partial satisfaction of the

requirements for the degree of

Doctor of Philosophy

in

Chemistry

in the

Graduate Division

of the

University of California, Berkeley

Committee in charge:

Professor Mary C. Wildermuth, Co-chair
Professor Judith P. Klinman, Co-chair
Professor Paul A. Bartlett
Professor Bob B. Buchanan

Spring 2010

Isochorismate Synthase Enzymes in *Arabidopsis*

by

Marcus Antoninus Strawn

Abstract

Isochorismate Synthase Enzymes in *Arabidopsis*

by

Marcus Antoninus Strawn

Doctor of Philosophy in Chemistry

University of California, Berkeley

Professor Mary C. Wildermuth, Co-chair

Professor Judith Klinman, Co-chair

Plants biosynthesize many essential metabolites via the shikimate pathway end product chorismate, including the aromatic amino acids phenylalanine, tyrosine and tryptophan. Isochorismate is generated from chorismate by the action of isochorismate synthase enzymes, and this isochorismate is a precursor to both the important plant hormone salicylic acid, and to the photosystem I electron transport agent phylloquinone (vitamin K_1). *AtICS1* and *AtICS2* are two genes in the model plant organism *Arabidopsis thaliana* encoding proteins that are homologous to known bacterial isochorismate synthases. Though expression of these genes had previously been studied, prior to this work nothing was known about the function of their protein products. Herein, I describe the overexpression and purification of both wild type and mutant forms of recombinant AtICS1 and AtICS2 proteins. I also describe a thorough biochemical characterization of these various proteins.

The pathogen-induced accumulation of the salicylic acid involved in plant defense requires AtICS1. AtICS1 acts as a monofunctional isochorismate synthase enzyme instead of a bifunctional salicylic acid synthase, and the reaction that it catalyzes operates near equilibrium (apparent $K_{eq} = 0.89$). Using an irreversible coupled spectrophotometric assay, AtICS1 was found to have an apparent K_M of 41.5 μM and k_{cat} of 38.7 min^{-1} for chorismate. This affinity for chorismate would allow AtICS1 to successfully compete with other pathogen-induced chorismate-utilizing enzymes. Furthermore, the biochemical properties of AtICS1 indicate that its activity is not regulated by light-dependent changes in stromal pH, Mg^{2+} ion concentration, or redox balance, and that it is remarkably active at 4 °C, consistent with a role for AtICS1 in salicylic acid production for the mediation of cold-tolerant growth. Finally, these analyses support plastidic synthesis of stress-induced salicylic acid by AtICS1 – with the requirement for one or more additional enzymes responsible for the conversion of isochorismate to salicylic acid – as non-enzymatic conversion of isochorismate to salicylic acid under physiological conditions was negligible.

The similarity between the pattern of expression of *AtICS2* and that of other genes in the phylloquinone biosynthetic pathway strongly suggests that AtICS2 is involved in phylloquinone biosynthesis associated with plastid development during the dark-light transition. AtICS2 is also a monofunctional isochorismate synthase that catalyzes a reaction that operates near equilibrium

(apparent K_{eq} = 0.76). This is consistent with its proposed role in phylloquinone biosynthesis, and it rules out a role for AtICS2 as an isochorismate pyruvate lyase in salicylic acid biosynthesis. Using an irreversible coupled spectrophotometric assay, AtICS2 was found to have an apparent K_M of 17.2 μM and k_{cat} of 18.0 min^{-1} for chorismate – these reaction parameters would allow AtICS2 to efficiently channel chorismate into the phylloquinone biosynthetic pathway. The biochemical properties of AtICS2 indicate that the enzyme is active within a broad range of stromal pH values, Mg^{2+} ion concentrations, and temperatures, consistent with the need for AtICS2 to operate under a variety of conditions during induced phylloquinone biosynthesis.

An examination of the amino acid sequence of various chorismate-utilizing enzymes revealed that one of the residues located within 6 Å of the putative substrate binding site is an alanine in virtually all known monofunctional isochorismate synthase enzymes, but a threonine in most bifunctional anthranilate synthase and salicylic acid synthase enzymes. Furthermore, structural studies of several of these enzymes indicate that this residue is likely forming a hydrogen bond to the substrate. These factors suggest that the identity of this residue may determine whether the given enzyme catalyzes a secondary aromatization reaction after the initial substitution reaction common to all of these enzymes. Several mutants of AtICS1 and AtICS2 were overexpressed and purified, all possessing residues altered at this and adjacent positions. In every case, the mutant protein no longer possessed any isochorismate synthase activity, acting instead as a bifunctional chorismate mutase-prephenate dehydratase enzyme. This suggests that the active sites of isochorismate synthase enzymes require a highly organized amino acid configuration, and that even minor perturbations in it will abolish all activity. It further suggests that the default activity of this class of enzymes may be chorismate mutase activity.

Experiments were undertaken to determine whether any of the three known *Arabidopsis* chorismate mutase enzymes could be acting as an isochorismate pyruvate lyase enzymes *in vivo*, as they possess homology to *Pseudomonas aeruginosa* PchB, an enzyme known to possess this activity. These enzymes were overexpressed and purified in recombinant form, and exposed to isochorismate. AtCM2 and AtCM3 produced no salicylic acid, but AtCM1 possessed a very weak isochorismate pyruvate lyase specific activity of 0.864 nmoles min^{-1} mg $protein^{-1}$. This suggests the possibility that AtCM1 is operating as an isochorismate pyruvate lyase *in planta*, where other factors could enable AtCM1 to catalyze this reaction more efficiently.

To my late grandparents Wesley and Gladys Strawn, who will live in my heart forever

ACKNOWLEDGEMENTS

Above all others, I wish to thank my graduate advisor Mary Wildermuth. There is no doubt in my mind that without her steadfast support and constant encouragement, I would not be about to receive a Ph.D. Mary rescued me from scientific oblivion, and guided me through graduate school with extraordinary patience. There were many times when I wanted to just give up, but Mary would never let me. Probably no other professor could have done what she did. Joining the Wildermuth lab allowed me to finally learn all of the biochemistry that I had long wanted to, and it is not an exaggeration to say that Mary has taught me everything that I know about the field. Working with Mary was the first time in my life that I have experienced great loyalty and dedication from an authority figure, and for this I consider myself deeply fortunate. I owe everything to Mary. It is a debt that will be hard to repay.

I also want to thank all my compatriots in the Wildermuth lab. Rachel Okrent was always there to discuss enzyme assays with, and Xander Jones to answer all of my questions about plant physiology; both of them made graduate school much less lonely these last five years. Sharon Marr was the best lab manager ever, and a cloning superstar to boot; I missed her and Mike more than I first realized when they moved away. Noriko Inada was also missed, as much for her upbeat demeanor as for the impromptu Japanese lessons that she would administer. Divya Chandran has been a pleasure to work with the last few years, and I wish her much continued success in all of her scientific endeavors. Diane Burgess was a terrific labmate, and it was inspirational to see the intensity with which she worked. Isabel Chon was an undergraduate who began working in the lab on the same day that I did; she has moved on to law school now, but I will always think of her as a scientist.

I also want to thank a number of people in the Plant and Microbial Biology Department for their help and friendship in the time that I have been here. Thuy Truong is a wonderful friend, and has always been there with a kind word when I needed to hear one. Ben Gutman taught me a lot about politics, and was hugely entertaining during occasional trips to Triple Rock. David Lynch and Matt Brooks rotated in the lab, and ultimately became good friends. Last but not least, Luis Rubio, Leo Curatti, Jose Hernandez, Steve Singer, Rob Igarashi, Dehua Zhao, Basem Soboh, Marie Demuez, Sabrina Santiago, and Marissa Hirst – all members of the Ludden lab – were each helpful to me numerous times during my stay here.

The professors who have served on my thesis committee – Judith Klinman, Paul Bartlett, and Bob Buchanan – have given much useful feedback and positive support, and I am very thankful for their service. I would also like to thank the following other professors for their insight and attention during my time in graduate school: Carolyn Bertozzi, Jean Frechet, Eusebio Juaristi, Dan Portnoy, Jon Ellman, Bob Bergman, and Caroline Kane. They have all taught me a lot. There were, in addition, a number of students and postdocs from my days in the Chemistry department that made my stay there much more enjoyable and informative: Youngsook Shin, George Lemieux, Ali Lemieux, Dustin Maly, Brian Cook, Seth Rubin, David Huang, Tom McCormick, Nir Goldman, Andy Souers, Tony Tang, Josh Armstrong, and Steve Klei. I appreciate all the help and support that they gave me.

Lastly, I want to thank Minju Kim and Hoonyoung Kim, who have been like a family to me this past ten years. I think about them every day, and it always brings a smile to my face.

TABLE OF CONTENTS

LIST OF FIGURES

CHAPTER I – INTRODUCTION

CHAPTER II – CHARACTERIZATION OF *ARABIDOPSIS* ICS1

CHAPTER III – CHARACTERIZATION OF *ARABIDOPSIS* ICS2

CHAPTER IV – CANDIDATES FOR ISOCHORISMATE PYRUVATE LYASE ENZYMES IN *ARABIDOPSIS*

LIST OF ABBREVIATIONS USED

ACP – Acyl carrier protein
ADC – 4-Amino-4-deoxychorismate
ADCL – 4-Amino-4-deoxychorismate lyase
ADCS – 4-Amino-4-deoxychorismate synthase
ADIC – 2-Amino-2-deoxyisochorismate
ADICS – 2-Amino-2-deoxyisochorismate synthase
AIP – 2-Aminoindan-2-phosphonic acid
APX – Ascorbate peroxidase
AS – Anthranilate synthase
At – *Arabidopsis thaliana*
Avr – Avirulence protein
BA2H – Benzoic acid 2-hydroxylase
CAPS – 2-(Cyclohexylamino)propanesulfonic acid
CBP – Calmodulin-binding peptide
CHES – 2-(Cyclohexylamino)ethanesulfonic acid
CM – Chorismate mutase
CoA – Coenzyme A
COX – Cyclooxygenase
CPL – Chorismate pyruvate lyase
CTP – Chloroplast transit peptide
DAHPS – 3-Deoxy-D-arabinoheptulosonate 7-phosphate synthase
DHBA – Dihydroxybenzoic acid
DHNA – 1,4-Dihydroxy-2-naphthoic acid
DHNA-CoA – 1,4-Dihydroxy-2-naphthoic acid coenzyme A ester
DMNT – (*E*)-4,8-Dimethyl-1,3,7-nonatriene
$DMQH_2$ – Demethylmenaquinol
DOXP – 1-Deoxy-D-xylulose-5-phosphate
DTT – Dithiothreitol
E4P – D-Erythrose 4-phosphate
EDTA – Ethylenediaminetetraacetic acid
EGTA – Ethylene glycol tetraacetic acid
EPR – Electron paramagnetic resonance
EPSP – 5-Enolpyruvylshikimate-3-phosphate
EST – Expressed sequence tag
ETI – Effector-triggered immunity
FPLC – Fast protein liquid chromatography
GFP – Green fluorescent protein
GPX – Glutathione peroxidase
GSH – Glutathione (reduced)
GSNO – S-Nitrosoglutathione
GS-SG – Glutathione disulfide
GST – Glutathione S-transferase
HPLC – High-performance liquid chromatography

HR – Hypersensitive response
ICS – Isochorismate synthase
IPL – Isochorismate pyruvate lyase
IPP – Isopentenyl diphosphate
IPTG – Isopropyl-β-D-thiogalactopyranoside
JA – Jasmonic acid
k_{cat} – Turnover number
K_M – Michaelis constant
LDH – L-Lactic dehydrogenase
MAPK – Mitogen-activated protein kinase
MBP – Maltose-binding protein
MES – 2-(N-Morpholino)ethanesulfonic acid
MeSA – Methyl salicylate
MOPS – 3-(N-Morpholino)propanesulfonic acid
MST – Menaquinone, Siderophore, and Tryptophan
NAD^+ – Nicotinamide adenine dinucleotide
NADH – Nicotinamide adenine dinucleotide (reduced)
NADPH – Nicotinamide adenine dinucleotide phosphate (reduced)
NCBI – National Center for Biotechnology Information
Ni^{2+}-NTA – Ni^{2+}-Nitrilotriacetic acid
NMR – Nuclear magnetic resonance
NOS – NO Synthase
NSAID – Non-steroidal anti-inflammatory drug
OSB – *ortho*-Succinylbenzoate
OSB-CoA – *ortho*-Succinylbenzoic acid coenzyme A ester
PABA – *para*-Aminobenzoic acid
PAL – Phenylalanine ammonia lyase
PEP – Phosphoenolpyruvate
PG – Prostaglandin
PHBA – *para*-Hydroxybenzoic acid
PhQ – Phylloquinone
PKS – Polyketide synthase
PMSF – Phenylmethanesulfonyl fluoride
PR – Pathogenesis-related protein
PS I – Photosystem I
PS II – Photosystem II
R – Resistance protein
ROS – Reactive oxygen species
SA – Salicylic acid
SABP2 – Salicylic acid binding protein 2 (also known as MeSA esterase)
SAG – Salicylic acid 2-O-β-glucoside
SAM – S-Adenosylmethionine
SAMT – Salicylic acid carboxyl methyl transferase
SAR – Systemic acquired resistance
SAS – Salicylic acid synthase
SDS-PAGE – Sodium dodecyl sulfate polyacrylamide gel electrophoresis

SEPHCHC – 2-Succinyl-5-enolpyruvyl-6-hydroxy-3-cyclohexene-1-carboxylate
SHCHC – 2-Succinyl-6-hydroxy-2,4-cyclohexadiene-1-carboxylate
S_N2'' – Bimolecular nucleophilic substitution, doubly vinylogous
SOD – Superoxide dismutase
TAL – Tyrosine ammonia lyase
TB – Terrific broth media
THP – Tris(hydroxypropyl)phosphine
Tris – 2-Amino-2-(hydroxymethyl)-1,3-propanediol
TS – Tryptophan synthase
TTBS – Tris-buffered saline with Tween-20
TX – Thromboxane
WRKY – Transcription factor containing the amino acids encoded by WRKY in sequence

CHAPTER I

INTRODUCTION

PLANT NATURAL PRODUCTS

Introduction to Plant Natural Products. Humans have taken advantage of the industrial and therapeutic applications of plants throughout recorded history, using their extracts as dyes, fibers, oils, perfumes, and drugs. Interest in plant natural products has been particularly high in the medical and scientific communities since 1805, when morphine (see Figure 1.2) became the first active ingredient associated with a medicinal plant – the opium poppy – to be isolated; in 1826, Emanuel Merck made it the first commercial pure natural product to be marketed as a therapeutic agent. Plant natural products comprise the active ingredients of 25% of all prescriptions dispensed in the United States – as opposed to 13% for microbial natural products [1, 2]. An analysis of the drugs approved by the U.S. Food and Drug Administration in the 26 years between 1981 and 2007 showed that 537 of the 1010 total (53%) were natural products or their derivatives, the majority of which were derived from plants [3]. Furthermore, for indications in which novel activity was desired, this percentage rose dramatically: 78% of the anti-cancer agents and 69% of anti-infective agents approved during this period were natural products [3]. The World Health Organization has estimated that approximately 80% of the world's population relies upon traditional medicines for their primary health care, most of which are plant-based [4]. This is significant, and given that as little as 5% of the approximately 250,000 species of higher plants have been systematically investigated for the presence of bioactive compounds [5], it suggests that many molecules of potential therapeutic use remain undiscovered.

Most plant natural products are biosynthesized in response to external stimuli. In the past these were referred to as secondary metabolites as they were not found to be required for growth under standard conditions; however, the term specialized metabolite is now favored. The extraordinary diversity of plant metabolism results from the fact that plants are stationary organisms, and as such are faced with a number of challenges that animals are not. Plants biosynthesize small molecule toxins to protect themselves directly from herbivores and microbial pathogens, and generate signaling molecules to activate local and systemic defenses against them. Various small molecules are also biosynthesized in response to potentially harmful abiotic factors, among them excessively hot and cold temperatures, very high or low light levels, high concentrations of toxic inorganic solutes, extremes of water balance, and various kinds of oxidative stress. Furthermore, the survival of many plants relies upon attracting insects to pollinate flowers or herbivores to consume and excrete seed fruit, motivating the biosynthesis of brightly colored compounds, scented volatiles, and chemical flavoring agents. Plants effectively compete with one another for resources by releasing small molecules into the soil that are inhibitory to the growth of the other plants, a phenomenon known as allelopathy [6]. Plants also have to maintain defensive structures like the cuticle – a secreted coating in the outer cell walls of the plant epidermis – in order to provide a physical barrier to pathogens that have attached themselves to the plant surface, and to prevent dehydration of the organism due to its impermeability to water; this involves the inducible biosynthesis of cutin and suberin, which are polyesters of hydroxylated fatty acids, and of various waxes, which are extremely hydrophobic mixtures of long-chain fatty esters. All told, an enormous number of small molecule compounds are biosynthesized by plants, but because they are present only transiently, are usually available in small quantities, and are often limited taxonomically, the function of most of these molecules in plants is unknown. Using the techniques of biochemistry and molecular biology, it is possible

to define the roles of these metabolites in plant biology and to assay their potential for industrial and therapeutic use.

Three major types of specialized metabolites are particular to plants, and comprise the bulk of these plant natural products: plant terpenoids, nitrogenous amino acid derivatives, and phenolics [7]. Below, I describe the biosynthetic pathways of these three classes of metabolite, as well as specify the biological function of notable members of each. This survey of plant natural product diversity emphasizes the importance of aromatic amino acid biosynthesis, as a relatively high percentage of specialized metabolites are generated via pathways that use one of these amino acids (phenylalanine, tyrosine, and tryptophan) as precursors. This discussion serves as an entrée to a more detailed description of chorismate metabolism, as chorismate is a precursor to the biosynthesis of the three aromatic amino acids, as well as numerous other specialized metabolites. The metabolism of chorismate-derived isochorismate is given particular consideration, as it is a biosynthetic precursor to the important plant metabolites phylloquinone and salicylic acid. Finally, the biological function of salicylic acid and its derivatives in both plants and humans is discussed in some detail.

Plant Terpenoids. All terpenoids are derived from intermediates formed from multiple additions of the five-carbon precursor isopentenyl diphosphate (IPP), and they are usually quite hydrophobic (Figure 1.1). Plant terpenoids in general are biosynthesized from IPP derived from the 1-deoxy-D-xylulose-5-phosphate (DOXP) pathway present in the chloroplast [8]; these terpenoid products include the monoterpenes (10 carbon atoms), diterpenes (20 carbon atoms), and tetraterpenes (40 carbon atoms). IPP can also be derived from the cytosolic mevalonate pathway, which is ubiquitous in all organisms; sesquiterpenes (15 carbon atoms), triterpenes (30 carbon atoms), and sterols (derivatives of triterpenes) are the principal products of this IPP pool. There are over 25,000 terpenoids known in plants, many of which are highly toxic to herbivores [7]. Among the terpenoids in this category are the volatile resin monoterpenes limonene from citrus fruit (among others), α-pinene from pine bark (as the principal component of turpentine), and chrysanthemic and pyrethric acids from chrysanthemum flowers – both of which are precursors of the commercially popular insecticidal pyrethoids (see [9], and Figure 1.1). Though many plant terpenoids are repellent to insects, volatile terpenes are also emitted in order to attract both pollinators to the flower [10] and natural predators of attacking insects to the wounded plant [11]. Additionally, the volatile monoterpene derivative (*E*)-4,8-dimethyl-1,3,7-nonatriene (DMNT, Figure 1.1), which strongly activates expression of lima bean defense genes of the jasmonic acid signaling pathway (see below, and Figure 1.13), is also emitted by spider mite-infected lima bean leaves, suggesting a role for such volatile compounds in plant community defense from herbivores [12].

A number of terpenoid metabolites are involved in normal plant function as well as in the response of the plant to stress. Carotenoids, such as the vitamin A precursor β-carotene (Figure 1.1), are tetraterpenes that function as both antenna pigments in photosynthesis and as photoprotective agents. Also, three of the several key plant hormones are terpenoids. Abscisic acid (Figure 1.1) is a tetraterpene-derived plant hormone that generally inhibits seed germination, and is involved in the stress response of the plant to low water [7]. The gibberellins, all of which are derived from the diterpene kaurenoic acid (Figure 1.1), are hormones that promote plant growth and flowering, as well as stimulate cell division in the stems of some plants in response to flooding [7]. The brassinosteroids, of which brassinolide is the most potent and widespread (Figure 1.1), are mevalonate-derived slower-acting plant growth hormones that are especially

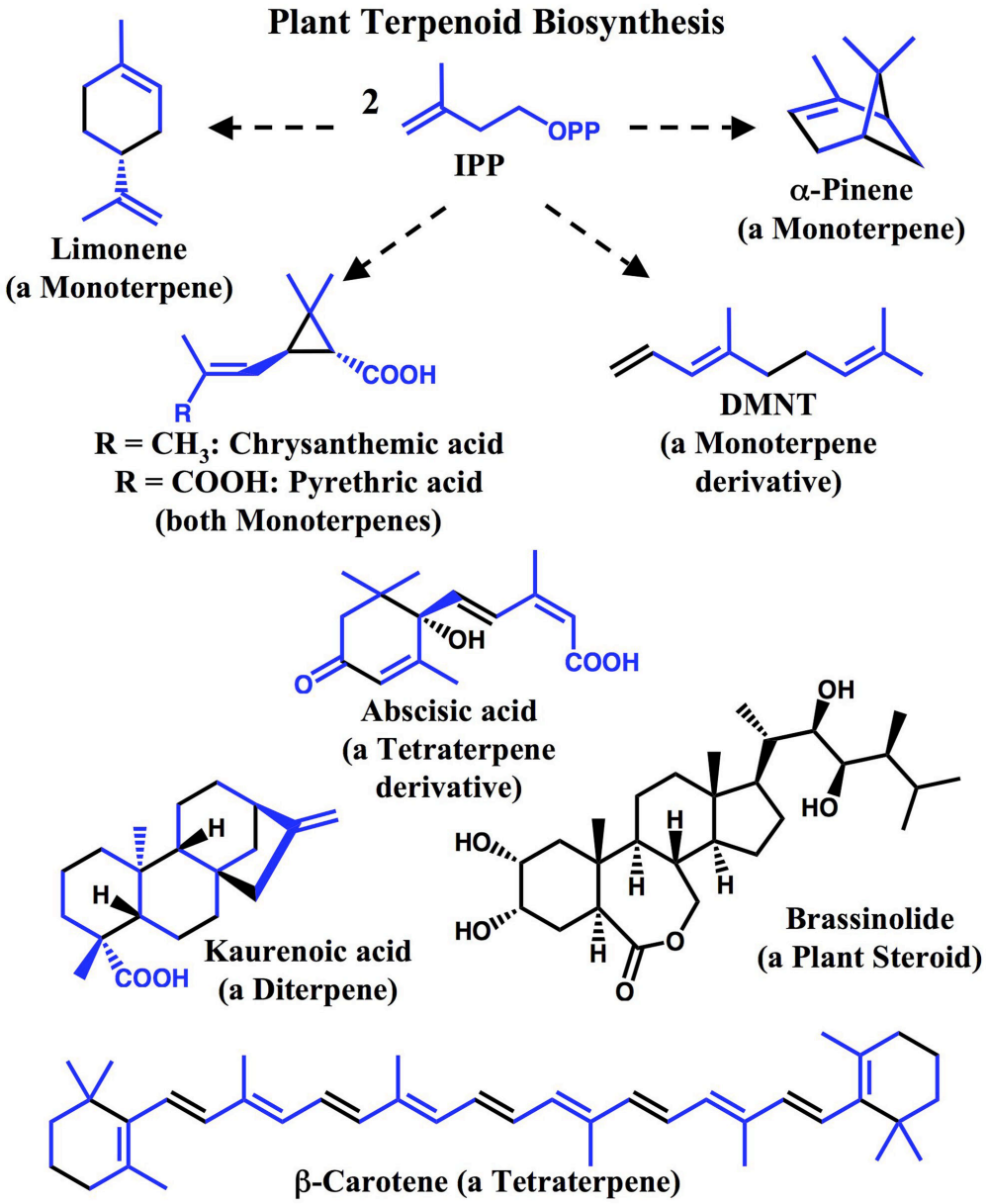

Figure 1.1 Biosynthesis of Representative Terpenoids in Plants. In this overview of the biosynthesis of terpenoids, linkage of the metabolic precursor isopentenyl diphosphate with its corresponding elaborated product is indicated by a unidirectional dotted arrow. The atoms from each IPP precursor are specified within the final terpenoid product in blue. Brassinolide is not amenable to this analysis, as a terpene precursor has been extensively modified in its production. Abbreviations used are: IPP, Isopentenyl diphosphate; DMNT, (*E*)-4,8-Dimethyl-1,3,7-nonatriene.

important in vascular development, and are essential factors in grasses in leaf bending and unrolling in response to various external stimuli [7]. Finally, one important role of terpenes is to confer additional membrane permeability to compounds that require this localization for activity. For example, the diterpenoid phytyl group (see Figure 1.11), when attached to chlorophyll molecules, helps anchor them to the membrane where they are needed to participate in photosynthesis. Chlorophyll with the phytyl group removed becomes quite water-soluble [7].

Plant Nitrogenous Amino Acid Derivatives. Nitrogenous amino acid derivatives are a second major class of plant natural products, with alkaloids being the most notable group among them. Though alkaloids are found in only about 20% of all species of flowering plants, they have approximately 15,000 known members [7]. Alkaloids are generally alkaline and water-soluble at lower pH values, and their most common function in plants is to act as anti-feedants for mammalian herbivores – nearly all alkaloids are toxic to mammals when taken in sufficient quantities [13]. Though a number of alkaloids are derived from the amino acids ornithine and lysine, the two largest groups of alkaloids by far are the tyrosine-derived isoquinoline alkaloids – with over 4000 isolated [14] – and the tyrosine-derived indole alkaloids – with over 3000 isolated [9]. The aforementioned opiate morphine is probably the best-known isoquinoline alkaloid, and the poison strychnine (from the Asian tree of the same name) is a particularly famous representative of the indole alkaloids (Figure 1.2). The class of plant hormones known as the auxins – of which indole-3-acetic acid (Figure 1.2) is the most common naturally occurring form – are important growth hormones required by all plants [10] that are derived principally from tryptophan; they are especially important in promoting stem and root elongation in response to a variety of external factors [7]. Another important derivative of tryptophan in *Arabidopsis* plants is camalexin (Figure 1.2), which has been shown to belong to a category of plant metabolites known as phytoalexins that exhibit strong anti-microbial activity and accumulate around the site of infection. Recent evidence suggests that indole-3-acetaldoxime (not shown), generated in one enzymatic step from tryptophan, is a common intermediate in the production of camalexin, indole glucosinolates (see below, and Figure 1.9), and auxins, although other pathways also exist for auxin production [15, 16]. Cyanogenic glycosides and glucosinolates are two other groups of amino acid derivatives, often derived from aromatic amino acids, which act as herbivore toxins upon exposure to glycosidase enzymes. Dhurrin from sorghum is a representative cyanogenic glycoside derived from tyrosine (Figure 1.2); when the glycosidic bond is hydrolyzed, a cyanohydrin is formed that spontaneously decomposes to an aldehyde and highly toxic hydrogen cyanide [17]. Whereas cyanogenic glycosides are known in 2500 separate plant taxa, glucosinolates are less broadly distributed in the plant kingdom [18]. Glucosinolates are found principally in the order Brassicales and their breakdown products are responsible for the pungency of mustards, radishes, horseradishes, and cabbages, among others. Sinalbin from white mustard is a glucosinolate derived from tyrosine; when it is exposed to the thioglucosidase myrosinase [19], an unstable aglycone is formed that spontaneously rearranges to (principally) a toxic isothiocyanate (Figure 1.2).

Plant Phenolics. Phenolic compounds are the third major class of plant natural products, and are arguably the most structurally diverse. Though some plant phenolics are biosynthesized wholly by the same malonic acid pathway – involving the action of polyketide synthase enzymes – utilized by microbes for production of complex aromatics, most plant phenolics are biosynthesized via the phenylpropanoid pathway. This pathway, which is unique to the plant

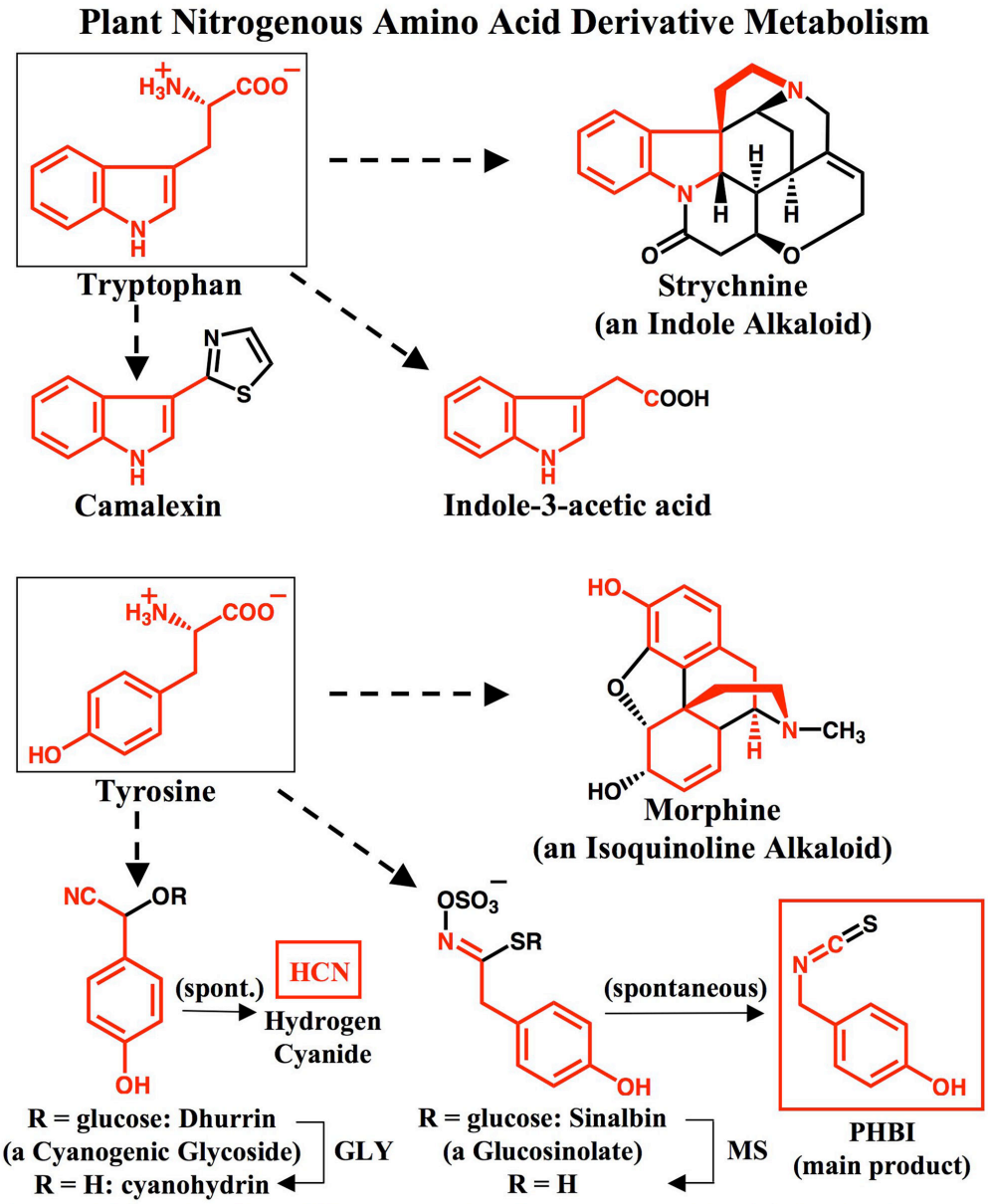

Figure 1.2 Metabolism of Representative Nitrogenous Amino Acid Derivatives in Plants. In this overview of the metabolism of nitrogenous amino acid derivatives, linkage of the amino acid precursor with its corresponding elaborated product is indicated using a unidirectional dotted arrow. The atoms from each amino acid precursor are specified within the final derivative in red. Subsequent reactions of metabolites are indicated by normal arrows, and the toxic products of those reactions are indicated by red boxes. Abbreviations used are: GLY, any operative glycosylase; MS, myrosinase; PHBI, *para*-Hydroxybenzyl isothiocyanate.

kingdom, derives a nine-carbon cinnamate skeleton from aromatic amino acid precursors (Figure 1.3). All phenylpropanoid biosynthesis (shown in Figures 1.3, 1.4, and 1.5) is made possible by the initial action of phenylalanine ammonia lyase (PAL), an enzyme that catalyzes the β-elimination of ammonium ion from both phenylalanine and tyrosine – though the latter process occurs only in monocots due to the less stringent substrate specificity of its PAL (referred to as TAL in Figure 1.3). It is believed that the evolution of PAL activity in plants was a necessary prerequisite for their colonization of land, as the critically important structural component of the cell wall – lignin – is a product of the phenylpropanoid pathway. Lignin is a hydrophobic, highly branched polymer that is generated by oxidative polymerization of *para*-coumaryl alcohol, and the related coniferyl alcohol and sinapyl alcohol – both of which are biosynthesized from *para*-coumaric acid – in a highly irregular manner according to the permutations allowed by the various resonance forms of the radical reactants (Figure 1.3). Its exceptional mechanical rigidity provides the strength and toughness to both the stems and tree trunks needed for the upward growth of the organism, and to the vascular tissue needed for water and nutrient transport. Lignin is the second most abundant carbon-based substance in plants, after cellulose, and its resistance to biodegradation is a large part of the reason that phenolic compounds account for 40% of organic carbon in the biosphere [7]. Enzymes involved in lignin biosynthesis are induced under conditions of osmotic stress [10] and in the response to fungal infection [7], consistent in both cases with the need for greater impermeability of the plant cell wall. Lignin is a primary component of the papillae that are generated at the site of infection to form a physical barrier to invasion of some pathogens, and lignification is likely enhanced by the peroxidase enzymes present in the early stages of the plant resistance response [7].

There are approximately 10,000 known phenylpropanoids [10], with a wide array of structures and functions. Simple phenylpropanoids, like caffeic acid (Figure 1.3), are frequently found to have allelopathic properties. The slightly more elaborated coumarins are lactone derivatives of cinnamic acid that play manifold roles in plant defense. Psoralen (Figure 1.3), a furanocoumarin found in abundance in celery and parsley, is highly toxic to animals by virtue of its ability to crosslink DNA upon activation by UV-A radiation (320-400 nm). Coumarin itself causes massive internal bleeding in mammals by acting as a vitamin K antagonist, a property that led to the development of 3-substituted synthetic derivatives like Warfarin for use as blood thinning therapeutic agents (Figure 1.3). The phenylpropanoid pathway also produces benzoic acid from cinnamic acid by way of a β-oxidation process similar to that seen in fatty acid degradation (see [7], and Figure 1.12 and associated text below). Simple plant phenolics such as these also contribute the fragrances and flavors unique to plants, which have indeterminate effects on plant viability. For example, eugenol in cloves and vanillin in the vanilla bean are both derivatives of caffeic acid with well-known scents (Figure 1.3).

Elaborated Plant Phenolics: The Phenylpropanoid-Acetate Pathway. The structural diversity potential of the phenylpropanoid pathway is enhanced dramatically by the biosynthetic addition of a second ring derived from acetyl groups – this is sometimes referred to as the phenylpropanoid-acetate pathway. *para*-Coumaric acid, when converted to its coenzyme A thioester (Figure 1.3), can function as a starter unit for iterative Claisen condensation of acetyl units derived from the decarboxylation of malonyl-CoA. This chain extension is followed by cyclization of the bound linear polyketide intermediate (in brackets in Figure 1.4). These transformations are all catalyzed by structurally similar plant-specific type III polyketide synthase (PKS) enzymes of the chalcone synthase superfamily [20]. Type III PKSs are

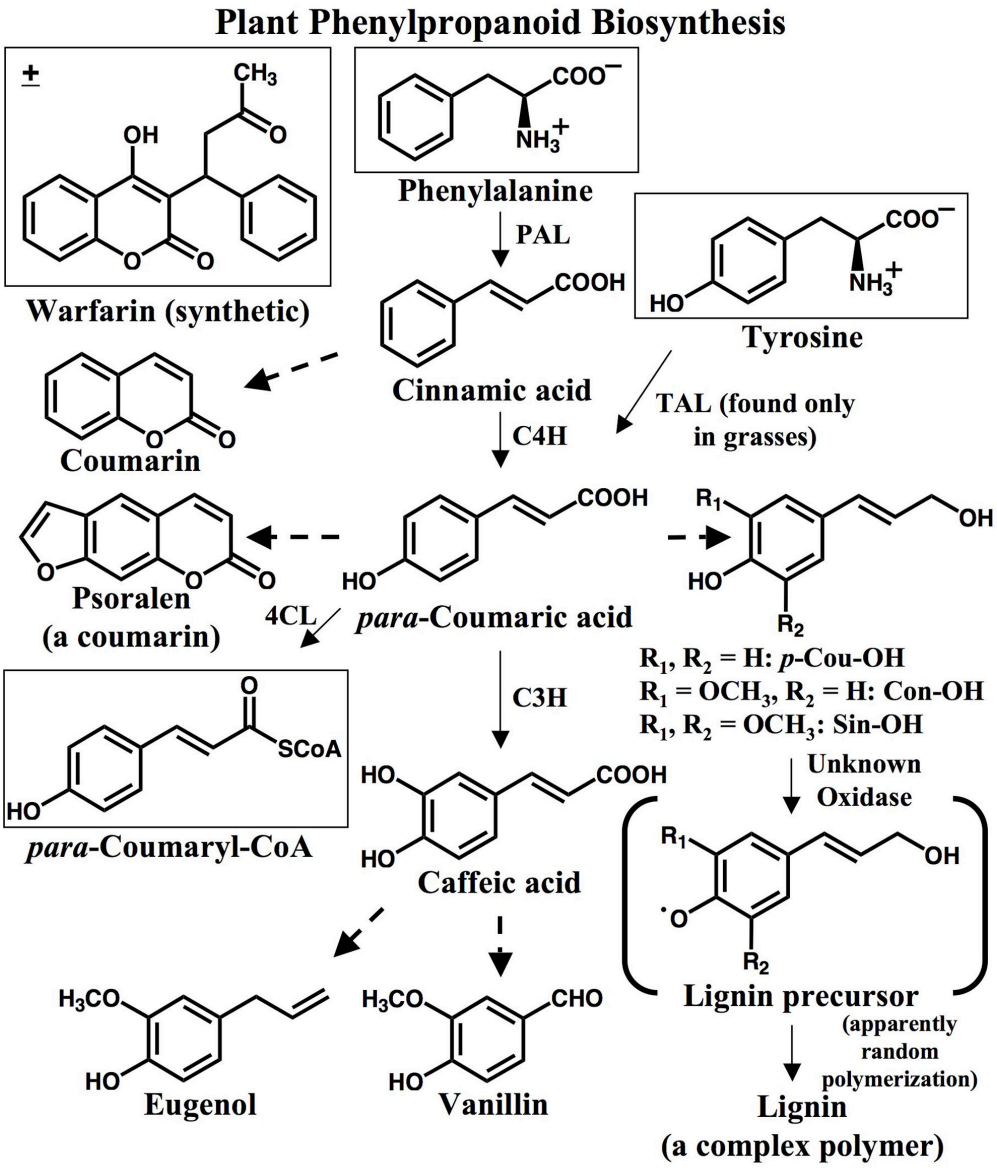

Figure 1.3 Phenylpropanoid Metabolism in Plants. In this overview of phenylpropanoid metabolism, linkage of the precursor with its corresponding elaborated product is indicated using a unidirectional dotted arrow. Simple reactions of metabolites are indicated by normal arrows, with the catalyzing enzyme shown. Brackets around the highly reactive lignin precursor suggest the many resonance forms that combine to generate lignin. Abbreviations used are: PAL, Phenylalanine ammonia lyase; TAL, Tyrosine ammonia lyase; C4H, Cinnamate 4-hydroxylase; 4CL, 4-Coumarate CoA ligase; C3H, Coumarate 3-hydroxylase; Cou-OH, *para*-Coumaryl alcohol; Con-OH, Coniferyl alcohol; Sin-OH, Sinapyl alcohol; CoA, Coenzyme A.

homodimeric iterative PKS enzymes that do not use acyl carrier protein (ACP) domains. One such PKS, arylpyrone synthase, adds a single malonyl-CoA equivalent before catalyzing sequential hydrolysis of the thioester and cyclization by conjugate addition of the carboxylate; the arylpyrone psilotinin is formed after minimal elaboration of this enzyme product (Figure 1.4). Psilotin, the O-β-D-glucopyranoside of psilotinin from the primitive vascular plant *Psilotum nudum*, has been shown to be a potent insect feeding deterrent and growth reducer in *in vitro* studies [21]. A related type III PKS, styrylpyrone synthase, adds two malonyl-CoA equivalents to *para*-coumaryl-CoA before cyclization by transesterification with a hydroxyl of the dienol tautomer of the polyketone intermediate. Enzymatic methylation of this enzyme product forms yangonin (Figure 1.4). Yangonin and related structures are the active principles of the kava plant root, which is an herbal remedy used medicinally as a treatment for anxiety [22]. More relevant biologically are structurally similar styrylpyrones and styryllactones, many of which have been shown to act as potent anti-microbial agents whose biosynthesis is activated in the plant by wounding [23-25]. Type III PKS enzymes of the chalcone synthase superfamily tolerate phenylpropanoid starter units other than *para*-coumaryl-CoA, which greatly expands the structural diversity of the arylpyrones and styrylpyrones produced in this manner, as well as that of the stilbenes and chalcones mentioned below [20].

Type III PKS enzymes that add three successive malonyl-CoA equivalents to phenylpropanoid starter units produce much more stable products. Stilbene synthase catalyzes an intramolecular C2-to-C7 aldol reaction subsequent to chain extension that produces resveratrol, a medicinally important tumor-suppressing agent found in red wine [26, 27]. This cyclization reaction involves a decarboxylation event that precedes aromatization of the new ring [28]; no stilbenecarboxylic acid byproducts of this enzymatic reaction are found (Figure 1.4). There are more than 300 stilbenoid compounds known in plants, and they are generally important as fungal growth inhibitors, though some also display toxicity to a broad range of organisms [7]. Resveratrol itself is a phytoalexin in grapes – tobacco plants transformed with the gene encoding grape stilbene synthase were shown to display greatly elevated resistance to the fungal pathogen *Botrytis cinerea* [29]. Chalcone synthase shares 90% amino acid sequence identity with stilbene synthase, though it catalyzes an alternative C6-to-C1 Dieckmann cyclization on the chain-extended polyketone (Figure 1.4). Interestingly, studies in solution of nearly identical substrates have shown that when C1 is esterified, this Dieckmann cyclization proceeds spontaneously, whereas when C1 is a free acid, styrene formation by aldol cyclization predominates [30]. This reactivity explains how the mutagenesis of active site residues designed to promote thioesterase activity effectively transforms alfalfa chalcone synthase into a functioning stilbene synthase [31]. Naringenin chalcone (boxed in Figures 1.4 and 1.5) is the product of wild type chalcone synthase action when a *para*-coumaryl-CoA starter unit is used, and it acts as the direct precursor to the flavonoids – the largest class of phenylpropanoids. This explains the ubiquity of chalcone synthase in the plant kingdom, as – unlike flavonoids – the other products of type III PKS enzymes mentioned above appear in a limited number of phylogenetically distinct plants [31].

Elaborated Plant Phenolics: The Flavonoids. There are over 4500 known flavonoids [7], the majority of which exist naturally as glycosides [10]. The synthesis of all flavonoids is initiated by the action of chalcone isomerase, which catalyzes the intramolecular conjugate addition of the *ortho*-hydroxyl group of an appropriate chalcone to its double bond to form the flavanone skeleton (Figure 1.5). The product of this reaction on naringenin chalcone –

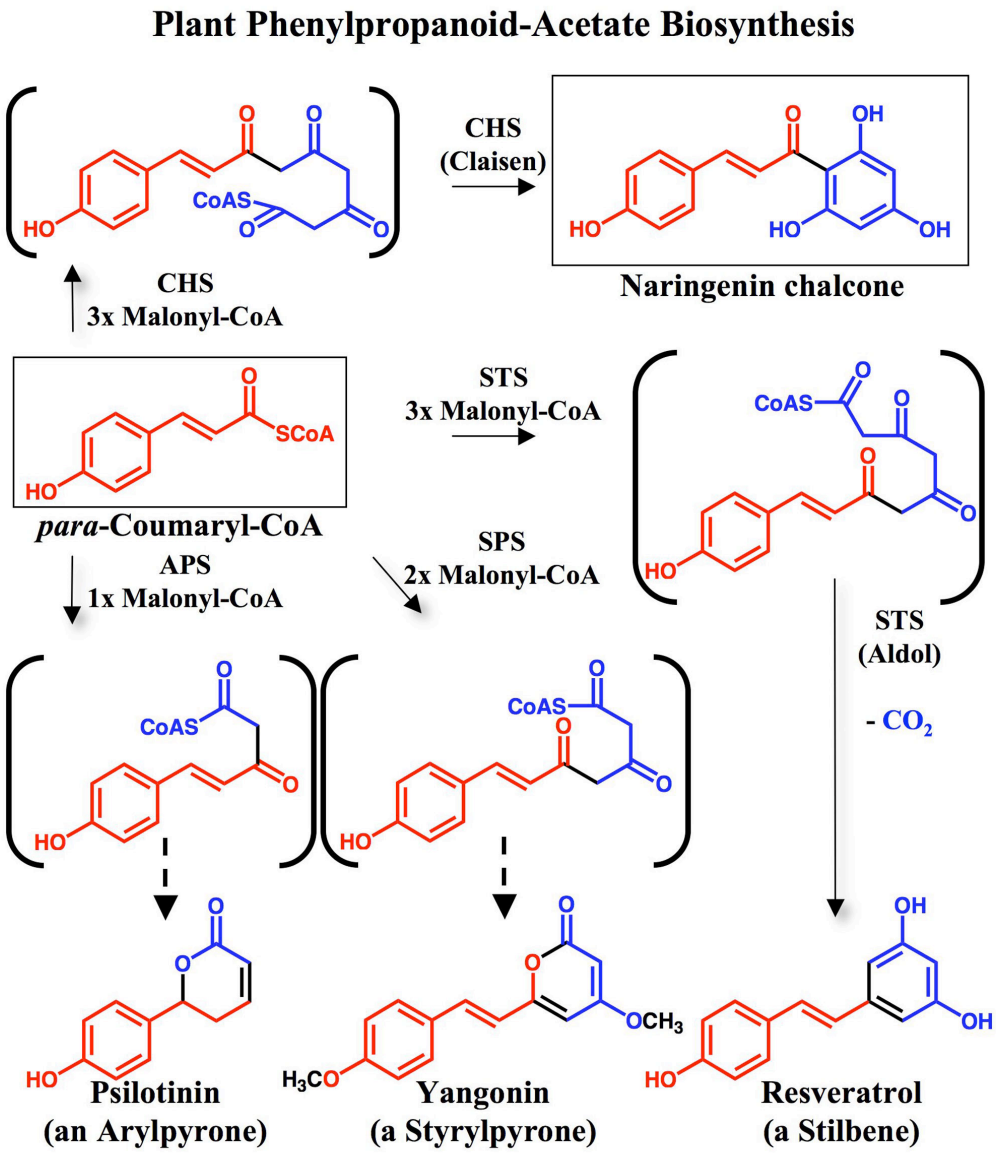

Figure 1.4 Phenylpropanoid-Acetate Biosynthesis in Plants. The phenylpropanoid-acetate biosynthetic pathway is shown to radiate out from the coenzyme A thioester of *para*-coumaric acid. Enzymatic steps are indicated by unidirectional solid arrows with the catalyzing enzyme specified, and further enzymatic elaborations are indicated by a unidirectional dotted arrow. Brackets are placed around important intermediates to which the specified number of malonyl-CoA units have been added to the coumaryl precursor. The atoms in each molecule that are contributed by the coumaryl precursor are highlighted in red, and the atoms contributed by malonyl units are highlighted in blue. Abbreviations used are: APS, Arylpyrone synthase; SPS, Styrylpyrone synthase; STS, Stilbene synthase; CHS, Chalcone synthase; CoA, Coenzyme A.

naringenin – is an important branchpoint in the biosynthesis of many flavonoids. Direct dehydrogenation of naringenin in this case generates apigenin (Figure 1.5), a flavone which in legumes acts as a signaling molecule to encourage Nod gene expression in compatible *Rhizobium* bacteria, thereby allowing formation of the root nodules that are needed for nitrogen fixation in the plant [7]. Alternatively, when hydroxylation precedes dehydrogenation, flavonols like the widely distributed kaempferol and quercetin are formed. Both of these flavonols are known to act as photoprotectants in leaves by absorbing harmful UV-B radiation (280-320 nm) [7, 32]. In addition, the many flavones and flavonols present in flowers absorb UV wavelengths that are only visible to insects, and their concentration near the plant reproductive organs enables them to act as visual attractants known as nectar guides [33]. Isoflavones, which are found almost exclusively in the legume family, are generated by the action of isoflavone synthase, an unusual cytochrome P450-dependent enzyme that catalyzes C2-to-C3 aryl migration with concomitant C2 hydroxylation (Figure 1.5). Subsequent enzymatic dehydration produces genistein (Figure 1.5), which – like many isoflavones – possesses a structural resemblance to estradiol that enables it to effect infertility in grazing animals, and that has lately motivated an increased interest in the consumption of legumes for the prevention of breast and prostate cancers [9, 34]. Isoflavonoids are best known, however, for comprising a significant segment of the phytoalexins found in legumes; for example, medicarpin in alfalfa (Figure 1.5) acts as a phytoalexin during fungal attack [7, 10]. A fourth group of flavonoids known as the anthocyanins (Figure 1.5) are responsible for most of the red, pink, purple and blue colors observed in plants – they work in combination with the complementary orange and yellow carotenoids (Figure 1.1) in the plant to act as visual attractants for potential animal carriers of pollen or seed. Their accumulation in vegetative tissues is also generally an indication of plant stress [35]. Anthocyanins are glycosylated forms of anthocyanidins, which are generated from precursor molecules like dihydrokaempferol by successive carbonyl reduction, dehydrogenation, and elimination events (Figure 1.5). Modification on the pendant phenyl group of the anthocyanin by hydroxylation and methylation is the principal determinant of the color of the molecule (Figure 1.5), though modification of the main ring and the pH present in the vacuole where they are stored are influencing factors [10]. Among the common anthocyanidins are cyanidin from rose and delphinidin from larkspur (Figure 1.5). Lastly, condensed tannins, like the proanthocyanidin shown here, are complex polymers generated from molecules like leucopelargonidin (Figure 1.5). Their bitter taste to mammals (they are common in unripe fruit), their general toxicity due to the covalent attachment of their oxidized quinone form to proteins, and their resistance to metabolism by most organisms, all make tannins potent anti-herbivoric agents. These substances are also present in high concentrations in woody plants, and they are the agents responsible for tree heartwood being so refractory to decomposition by bacteria and fungi [10].

CHORISMATE-DERIVED COMPOUNDS

The Shikimate Pathway. Because the vast majority of phenolic plant metabolites (Figures 1.3, 1.4, and 1.5) and a high percentage of nitrogenous amino acid derivatives – including nearly half of all known alkaloids (see Figure 1.2) – are derived from phenylalanine, tyrosine, and tryptophan (the source of the boxed precursors in Figures 1.2, 1.3, 1.4, and 1.5), the biosynthesis of these aromatic amino acids is of considerable importance in plants. The

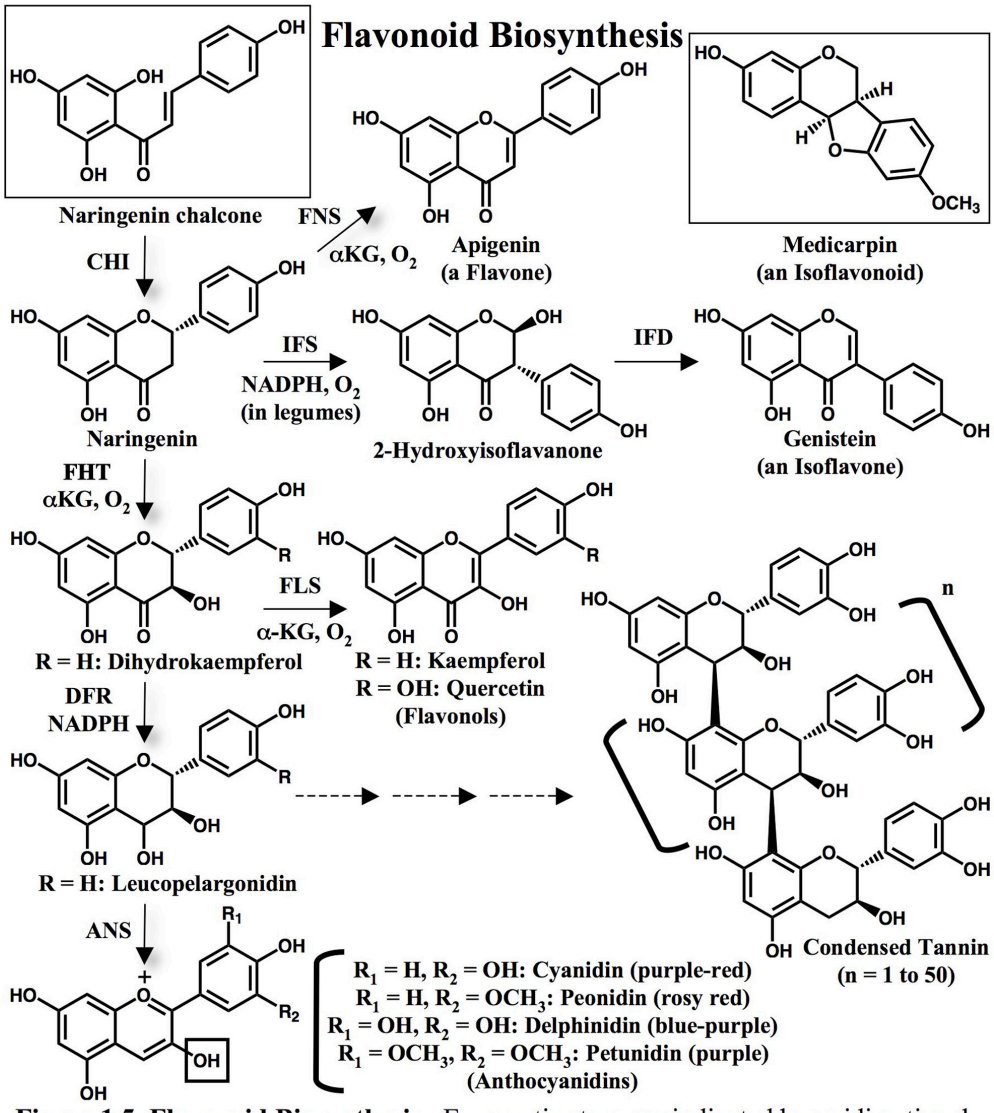

Figure 1.5 Flavonoid Biosynthesis. Enzymatic steps are indicated by unidirectional solid arrows with the catalyzing enzyme specified. Condensed tannin biosynthesis is undefined, and is indicated by dotted arrows. Many enzymes in this pathway catalyze the transformation of several substrates, and are particularly insensitive to substitution on the pendant phenyl ring of the flavonoid. Enzymatic hydroxylations of this ring can occur at many points in the pathway, and for convenience hydroxylation events and some intermediate oxidation states are not shown. The 3-hydroxy group (boxed) of the anthocyanidins is always glycosylated in the anthocyanins. Abbreviations used are: CHI, Chalcone isomerase; FNS, Flavone synthase; IFS, 2-Hydroxyisoflavanone synthase; IFD, 2-Hydroxyisoflavanone dehydratase; FHT, Flavanone 3-hydroxylase; FLS, Flavonol synthase; DFR, Dihydroflavonol 4-reductase; ANS, Anthocyanidin synthase; αKG, α-Ketoglutarate.

metabolic pathway responsible for initiating their production is known as the shikimate pathway [36], which produces the key intermediate chorismate in seven metabolic steps from D-erythrose 4-phosphate (E4P) and phosphoenolpyruvate (PEP), two intermediates of carbohydrate metabolism (Figure 1.6). The importance of the shikimate pathway in plants is emphasized by the fact that more than 20% of all the carbon fixed by plants is diverted through it [37]. The amount of carbon processed by the shikimate pathway globally has been estimated at 7×10^{15} kg per year [37], and unlike microorganisms, which invest 90% of their metabolic energy in amino acid and protein production, most of the flux through this pathway in plants is for the purpose of aromatic natural product biosynthesis – particularly of lignin [38]. Furthermore, the best-selling herbicide worldwide – at over 30% of the total market and climbing yearly [39] – is glyphosate (N-[phosphonomethyl]-glycine, marketed as "Roundup"), which acts by competitive inhibition of EPSP synthase (in red in Figure 1.6), the penultimate enzyme in the shikimate pathway [7]. All gene sequences characterized for the six enzymes in the plant shikimate pathway contain amino-terminal signal sequences for chloroplast import, which enable transport of the encoded protein from the cytosol to the chloroplast with concomitant excision of the signal peptide. Many of these shikimate pathway enzymes have been isolated from plant chloroplasts directly, indicating that chloroplasts are the exclusive site of chorismate biosynthesis [37].

Chorismate Utilization. Chorismate is the common branchpoint for the biosynthesis of most aromatic plant natural products, many of which are essential components of the animal diet (because they cannot be biosynthesized by animals). There are five pathways branching from it that have been thoroughly characterized in bacteria, each beginning with a chorismate-utilizing enzyme (see [38, 40], and Figure 1.6). Chorismate mutase (CM) catalyzes the first committed step in the biosynthesis of phenylalanine and tyrosine, a Claisen rearrangement that produces the α-keto acid prephenate. In contrast to bacterial and fungal metabolism, prephenate is typically converted to arogenate in plants before final enzymatic aromatization to tyrosine or the essential amino acid phenylalanine (see [7], and Figure 1.6). Tyrosine is also a biosynthetic precursor to the tocopherols – also known as vitamin E – essential membrane-localized anti-oxidants that are only produced by plants (Figure 1.6). A second enzyme, anthranilate synthase (AS), catalyzes the first committed step in tryptophan biosynthesis by converting chorismate to anthranilate. The four successive enzymatic manipulations that convert anthranilate to the essential amino acid tryptophan are identical in microbes and plants (Figure 1.6), though plants – particularly those from the citrus (Rutaceae) family – also use some of the anthranilate pool for the biosynthesis of acridine alkaloids [9]. A third chorismate-utilizing enzyme, isochorismate synthase (ICS), generates the isochorismate used in bacteria for the biosynthesis of iron-chelating siderophores and for the production of menaquinone, a terpenoid naphthoquinone electron acceptor (see below). Plants apparently do not use isochorismate for siderophore production, but the pathway for the biosynthesis of the essential terpenoid naphthoquinone phylloquinone (also known as vitamin K_1) is nearly identical to that of menaquinone, and the key plant hormone salicylic acid and a number of anthraquinones are biosynthesized from isochorismate as well (see [9], and Figures 1.6 and 1.11 along with their associated text below). A fourth chorismate-utilizing enzyme, 4-amino-4-deoxychorismate synthase (ADCS), generates the non-aromatic intermediate 4-amino-4-deoxychorismate (ADC). A second aromatizing enzyme present in both microbes and plants, ADC lyase, initiates production of *para*-aminobenzoic acid (PABA), a component of the essential biosynthetic cofactor dihydrofolate (also known as vitamin B_9; atoms derived from PABA are highlighted in red in Figure 1.6). A fifth chorismate-utilizing enzyme, chorismate

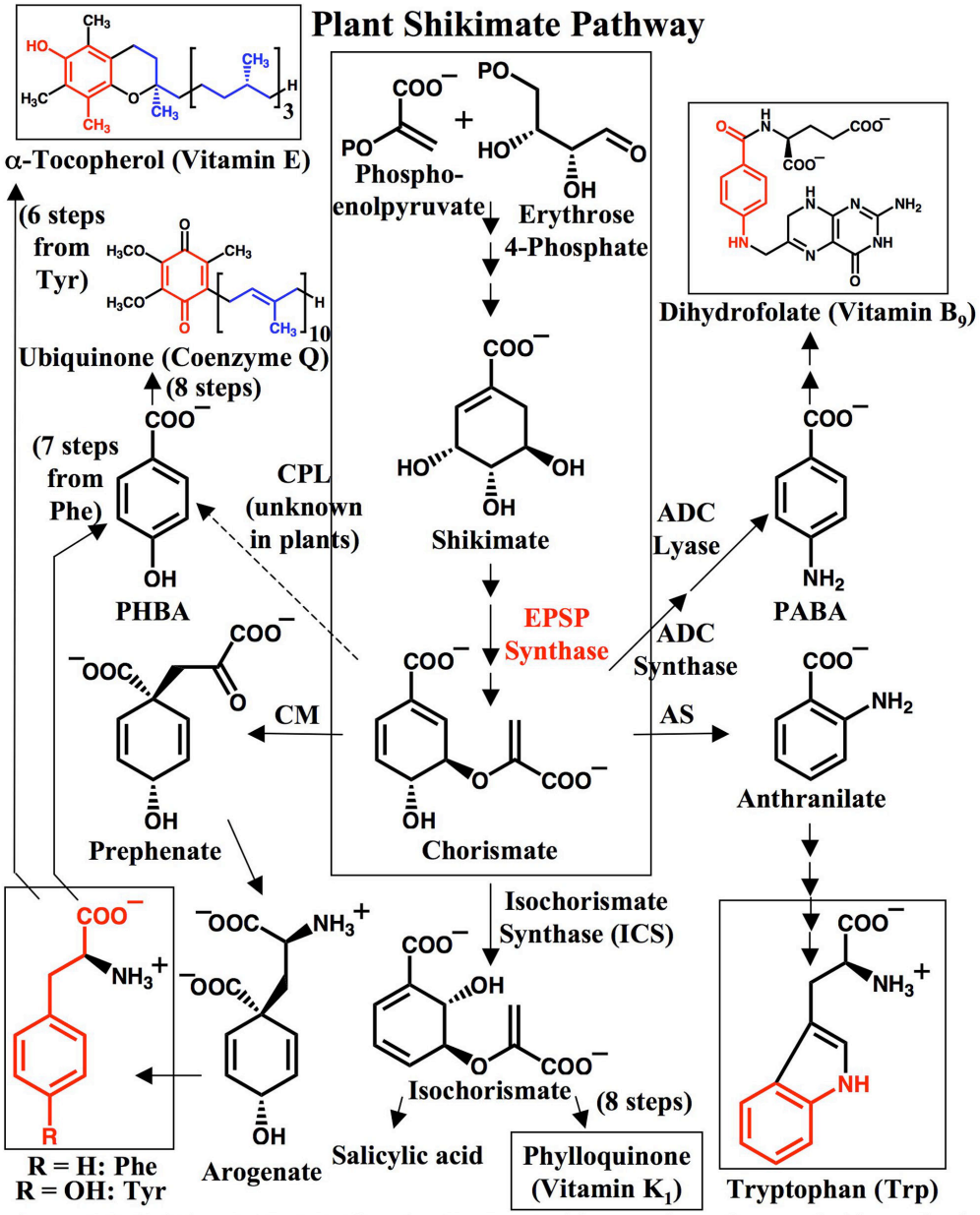

Figure 1.6 Shikimate Metabolism in Plants. In this overview of aromatic biosynthesis in plants, each enzymatic transformation is indicated by a unidirectional arrow, except where indicated. Enzymes referenced in the text are specified. Boxes indicate the shikimate pathway and the plant metabolites produced by it that are essential in the animal diet. Atoms derived from the reactions of chorismate are labeled in red. Abbreviations are: EPSP, 5-Enolpyruvylshikimate 3-phosphate; CM, Chorismate mutase; CPL, Chorismate pyruvate lyase; ADC, 4-Amino-4-deoxychorismate; AS, Anthranilate synthase; PHBA, *para*-Hydroxybenzoic acid; PABA, *para*-Aminobenzoic acid.

pyruvate lyase (CPL), is well known in bacteria for catalyzing the conversion of chorismate to *para*-hydroxybenzoic acid (PHBA). Unlike the other chorismate-utilizing enzymes above, no CPL homolog has yet been found in plants, and it has been shown in plant cell culture that the majority of PHBA is produced by β-oxidative degradation of phenylpropanoids derived from chorismate mutase-generated phenylalanine (see [41], and Figure 1.6). PHBA is a precursor for the production of the ubiquinones (also known as coenzyme Q; atoms derived from PHBA are highlighted in red in Figure 1.6), which function in eukaryotes as electron carriers in the mitochondrial electron transport chain [7], and are biosynthesized – usually from the essential amino acid phenylalanine – in almost all organisms.

The MST Family of Enzymes. The mechanisms of the five known chorismate-utilizing enzymes have been studied mainly using bacterial proteins. Though CM [42] and CPL [43] are not homologous to other chorismate-utilizing enzymes and are believed to catalyze reactions that proceed through pericyclic transition states [38, 40, 44], ICS, AS, and ADCS appear to be members of a closely related group of enzymes. This group has been labeled the MST family, for menaquinone, siderophore, and tryptophan, three of the principal products of these enzymes in bacteria [45]. The carboxy-terminal chorismate-binding domains of MST enzymes show high sequence similarity to one another (Figure 1.7). For example, *E. coli* MenF (an ICS) is 28% identical and 43% similar to *S. marcescens* TrpE (an AS) over the carboxy-terminal 254 residues, and *E. coli* PabB (an ADCS) is 26% similar to *E. coli* TrpE (an AS) over the entire protein [38]. Furthermore, all three of these enzymes likely arose from a common ancestor [46-48]. All members of the MST family require magnesium for activity and catalyze apparently related substitution reactions (Figure 1.8). X-ray crystal structures of bacterial AS [49-51], ADCS [52], and ICS enzymes [45, 53] have shown these proteins to possess a high degree of structural similarity to one another, and analysis of these structures has led to the proposal of a conserved reaction mechanism for all three of these enzymes [54]. In this proposed mechanism, each enzyme catalyzes the reversible 1,5-S_N2'' displacement of the 4-hydroxyl group of chorismate with a different nucleophile added at the C2 position (Figure 1.8). Thus, monofunctional isochorismate synthase (ICS) adds water at C2 to form isochorismate. Alternatively, bifunctional anthranilate synthase (AS) adds ammonia to form 2-amino-2-deoxyisochorismate (ADIC) as a tightly bound intermediate, before catalyzing a second irreversible aromatization by elimination of pyruvate to form anthranilate (Figure 1.8; see Chapter 4 for a discussion of the aromatization process). In the most involved reaction, monofunctional 4-amino-4-deoxychorismate synthase (ADCS) adds a lysine side chain amine to form a covalent enzyme-substrate intermediate, then catalyzes a second S_N2'' reaction, adding ammonia at C4 with concomitant elimination of the lysine side chain at C2 to form ADC (Figure 1.8). Bacterial ICS enzymes are composed of a single subunit, and add water derived from solvent [55]. Bacterial AS and ADCS enzymes each possess two different subunits, one with amidotransferase activity that generates ammonia by catalyzing the hydrolysis of glutamine, and a second MST family enzyme that accepts this ammonia and catalyzes its addition to chorismate. In the ADCS enzymes of tomato and *Arabidopsis*, however, these two subunits are fused into one [56]. All glutamine amidotransferases crystallized thus far possess molecular channels between subunits that transfer the ammonia formed from the hydrolysis of glutamine to the site where it is used as a nucleophile – this prevents leakage of ammonia into the external medium and is believed to be a general phenomenon in all glutamine amidotransferases [57].

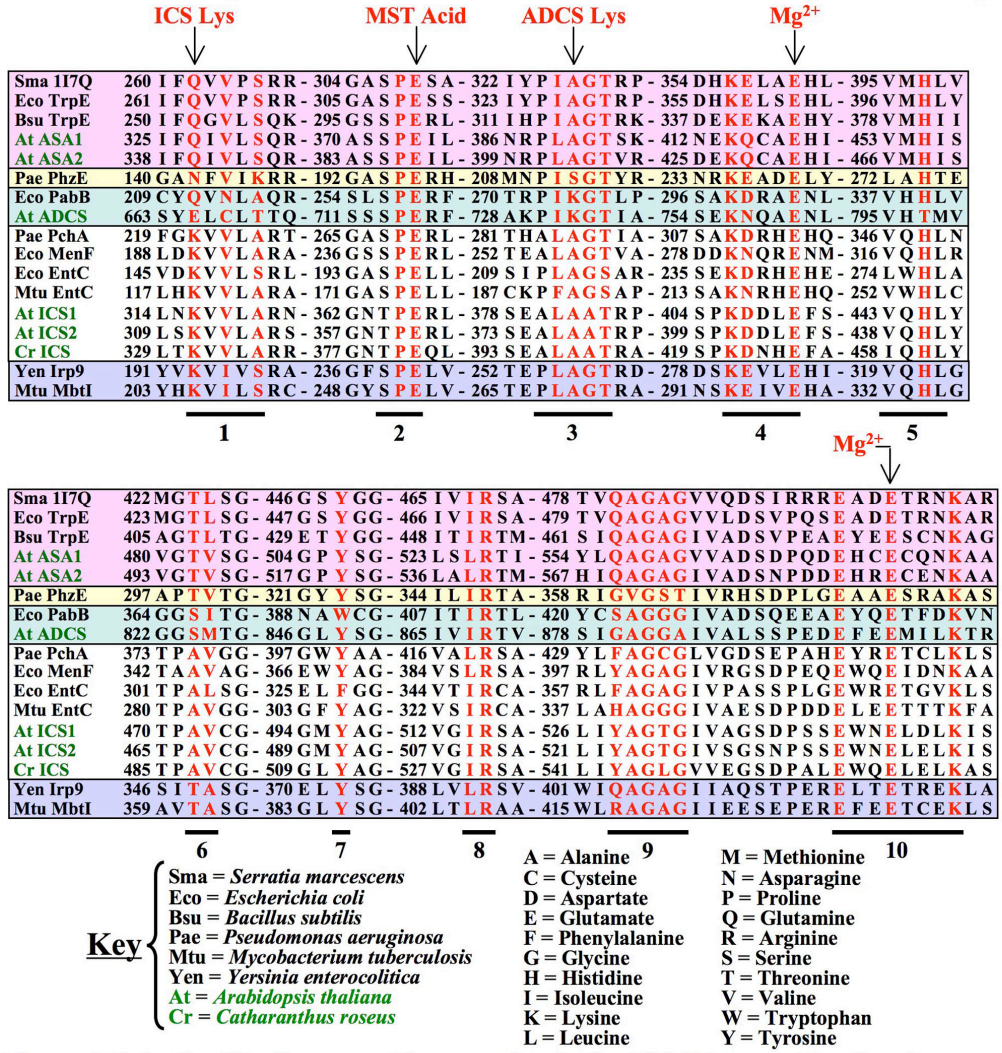

Figure 1.7 Active Site Sequence Conservation in the MST Enzyme Family. An alignment of protein sequences of the MST family is shown (top section are AS enzymes, second is an ADIC synthase, third are ADC synthases, fourth are ICS enzymes, and fifth are SAS enzymes). Bacterial enzymes are denoted by black lettering, plant enzymes by green. The underlined residues can be assigned to the 10 labeled motifs which collectively signify a MST enzyme. The 26 positions within 6 Å of the Mg^{2+}, benzoate, and pyruvate ligands bound in the Sma 1I7Q AS crystal structure are indicated in red. The positions where Lys residues are necessary for ICS and ADC synthase activities are indicated, as are the invarient Glu residues that chelate Mg^{2+} and act as a general acid catalyst. Abbreviations used are: MST, Menaquinone, Siderophore and Tryptophan; AS, Anthranilate synthase; ADIC, 2-Amino-2-deoxyisochorismate; ADC, 4-Amino-4-deoxychorismate; ICS, Isochorismate synthase; SAS, Salicylic acid synthase.

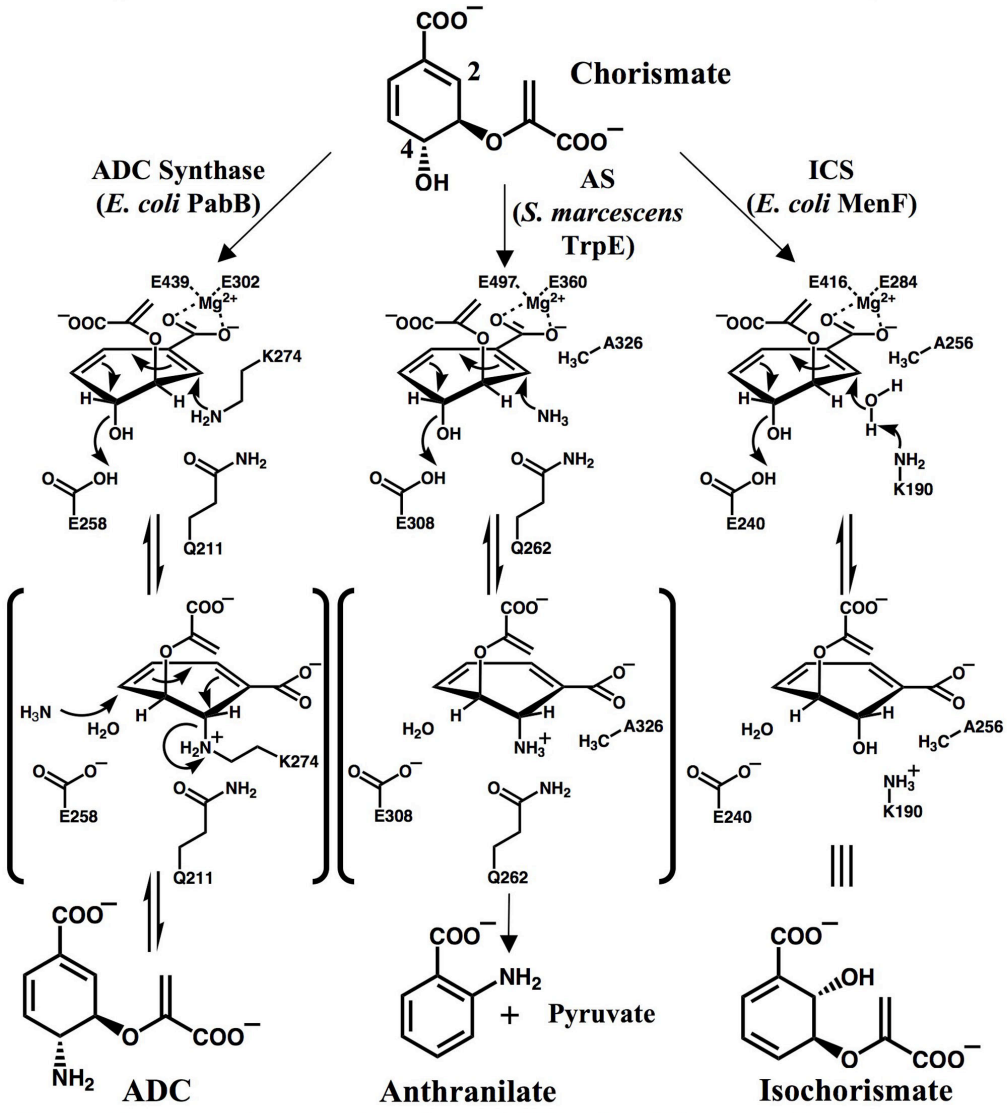

Figure 1.8 Proposed Mechanism of the MST Family of Enzymes. Enzymatic reaction mechanisms of three evolutionarily related chorismate-utilizing enzymes have been elucidated from biochemical and structural data. Each enzyme catalyzes the reversible addition of a different nucleophile to C2 of chorismate with concomitant elimination of the C4 hydroxyl group. Isochorismate synthase (ICS) adds solvent water at C2, anthranilate synthase (AS) adds ammonia and subsequently enables pyruvate elimination, and 4-amino-4-deoxychorismate (ADC) synthase adds a lysine side-chain amine and subsequently catalyzes ammonia addition to C4 with concomitant elimination of the lysine from C2. Five key homologous active site amino acid residues are labeled, though bound magnesium and two glutamate residues are not shown in the initial adduct.

A Unified Reaction Mechanism for MST Enzymes. Figure 1.8 graphically summarizes the proposed unified mechanism of these three MST enzymes using a schematic derived from structural data. ADCS enzyme *E. coli* PabB [52], AS enzyme *Serratia marcescens* TrpE [51], and ICS enzyme *E. coli* MenF [45, 53] each have superimposable active site structures in which 26 amino acid residues are within 6 Å of bound Mg^{2+}, pyruvate and benzoate ligands from the *S. marcescens* TrpE structure [51]. Five of these homologous amino acid residues are shown for each active site with pseudodiaxial chorismate placed roughly where the ring of the bound benzoate ligand from the TrpE structure is found (Figure 1.8). One clear finding of these, and related (like that of *Y. enterocolitica* Irp9 [58]; see below), structures is that two invariant glutamate residues – E284 and E416 in *E. coli* MenF – join with the ring carboxylate of chorismate to coordinate magnesium. Originally, Walsh proposed a universal concerted S_N2'' reaction mechanism with magnesium bound to both the departing C4 hydroxyl and the incoming nucleophile at C2 in the transition state of all three reactions [40]. This explained the effectiveness of the Bartlett high affinity inhibitors (shown in Figure 4.2) that preferentially mimic a pseudoaxial transition state [59], as well as NMR and EPR data that indicate that magnesium interacts with chorismate in the active site of AS [60]. However, comparison of the magnesium-bound and apo structures of MenF demonstrates that magnesium ion is a key structural element of the active site that organizes many of the amino acid side chains in a closed configuration more suitable for binding substrate [53]. It has been proposed [61] that the partial positive charge generated at the C2 position of chorismate by coordination of magnesium to the ring carboxylate is the critical feature facilitating nucleophilic attack at C2 in the MST family of enzymes (see Chapter 4 for a more thorough discussion). This proposal is reinforced by structural studies of the non-MST chorismate-utilizing enzymes *B. subtilis* CM [62] and *E. coli* CPL [63], which have no magnesium bound in the active site, showing instead non-activating arginine residues coordinating the ring carboxylate of a chorismate analog. These active site arginine residues appear to be conserved in all non-MST chorismate-utilizing enzymes (including *P. aeruginosa* PchB; see Chapter 4), and it has been proposed that they do not activate chorismate sufficiently for ring substitution to occur [61].

Several other observations made from analysis of this structural data with chorismate modeled in the active site, as well as sequence alignment of more than 1000 related sequences in the National Center for Biotechnology Information (NCBI) genomic database, enable conclusions to be drawn about a unified mechanism for these three enzymes. First, a glutamate residue – E240 in *E. coli* MenF – that is absolutely invariant in the enzymes of this family (Figure 1.7) is always positioned to interact with the C4 hydroxyl of pseudodiaxial chorismate (Figure 1.8). This glutamate side chain is likely a catalytic acid that assists in the elimination of the C4 hydroxyl by protonating it. Evidence for this proposal is provided by the inactivity of the *E. coli* MenF mutant in which E240 is replaced by a glutamine [45], and by the dramatic rotation away from substrate hydroxyl of the homologous E308 residue of inactivated *S. marcescens* AS in a structure with the allosteric regulator tryptophan bound [51]. Secondly, a lysine residue – K190 in *E. coli* MenF – in proximity to the *si* face of chorismate C2 is conserved in all enzymes of this family that hydroxylate chorismate, and is primarily glutamine in enzymes which aminate chorismate (Figure 1.7). This lysine side chain is proposed to be a catalytic base that abstracts a proton from water to generate a hydroxide nucleophile poised for attack at the C2 atom of chorismate [45]. Evidence for this is provided by the inactivity of the K190A MenF mutant [45], and by the presence of a water molecule in a MenF structure that is juxtaposed between this lysine amine and C2 of chorismate ([53], also seen in the related Irp9 structure described in

Chapter 4 [58]). Superposition of MenF and AS structures shows that this MenF lysine is positioned such that it overlaps the channel in AS where the TrpE subunit accepts ammonia from the TrpG subunit, suggesting that water pursues a similar trajectory in MenF [45]. This proposal is further supported by the placement of this lysine side chain in an extremely hydrophobic environment where it is likely to be unprotonated [45]. Thirdly, a residue – A256 in *E. coli* MenF – that is strictly conserved as alanine in ICS and AS enzymes is found to be lysine in most – but not all [64] – ADCS enzymes (Figure 1.7). This residue is positioned such that the amino group of a lysine side chain is in good position to add to C2 of chorismate, and is proposed to be the residue mentioned above that forms a covalent enzyme-substrate bond in all ADCS enzymes [54]. Strong evidence for the proposed ADCS mechanism involving a covalent enzyme-substrate intermediate is provided by the inactivity of *E. coli* PabB mutants in which K274 is replaced by other amino acid residues [54], and by the discovery that 2-fluorochorismate inactivates PabB by forming a covalent adduct with the K274 side chain amine [65].

Chorismate-Utilizing Enzymes in *Arabidopsis thaliana*. Though homologous enzymes perform many of the same transformations in both, metabolism in plants is significantly more complicated than in bacteria. Whereas bacteria are prokaryotes with relatively small genomes, plants are complex organisms that carefully control the subcellular and intercellular transport of metabolites. Plants often possess multiple genes for each transformation in a pathway; these isozymes are differentially transcribed in various cell types and in response to various stimuli. Studies of biosynthetic pathways in bacteria have historically been conducted by supplementing auxotrophic mutants with some product from the pathway under investigation, but this straightforward approach for plants is made difficult by gene redundancy due to multiple isozymes, as well as the inability of the supplemented metabolite to freely diffuse due to their high degree of compartmentalization. As a result, much of the earlier research on plant metabolism either made use of plant cells in culture or involved the feeding of radiolabeled precursors to whole plants. However, the emergence of the dicot *Arabidopsis thaliana* as a plant model organism has enabled a genetic approach to the study of metabolism in plants. *Arabidopsis* possesses a streamlined genome that is among the smallest known in the plant kingdom, being about one percent the size of the maize genome with a similar number of genes [7]. Additionally, *Arabidopsis* is physically small with a relatively short life cycle and whole-plant mutants are easily prepared by transformation or mutagenesis, allowing large numbers of mutants to be screened. The entire *Arabidopsis* genome has been sequenced, and the public availability of knockout mutants for nearly every open reading frame has made it an ideal model organism in plants. Though *Arabidopsis* is of no commercial importance, it has become the organism of choice for studies of plant gene expression, and investigation of the factors controlling transcription of *Arabidopsis* biosynthetic genes has revealed details of the metabolic response to biotic and abiotic stress that can be generalized to many other members of the plant kingdom.

Most of the genes encoding chorismate-utilizing enzymes in *Arabidopsis* possess amino-terminal signal sequences for chloroplast import, and many of their protein products have either been extracted from purified chloroplasts, or been shown to localize to the plant chloroplast (see [7], and Figure 1.9). As most *Arabidopsis* chorismate-utilizing enzymes are known to have chloroplast-localized homologs in other plant species [7], and as chorismate is also produced by the shikimate pathway in the chloroplast of all plants, knowledge of the factors determining chorismate utilization by these enzymes is the key to understanding how flux toward the various

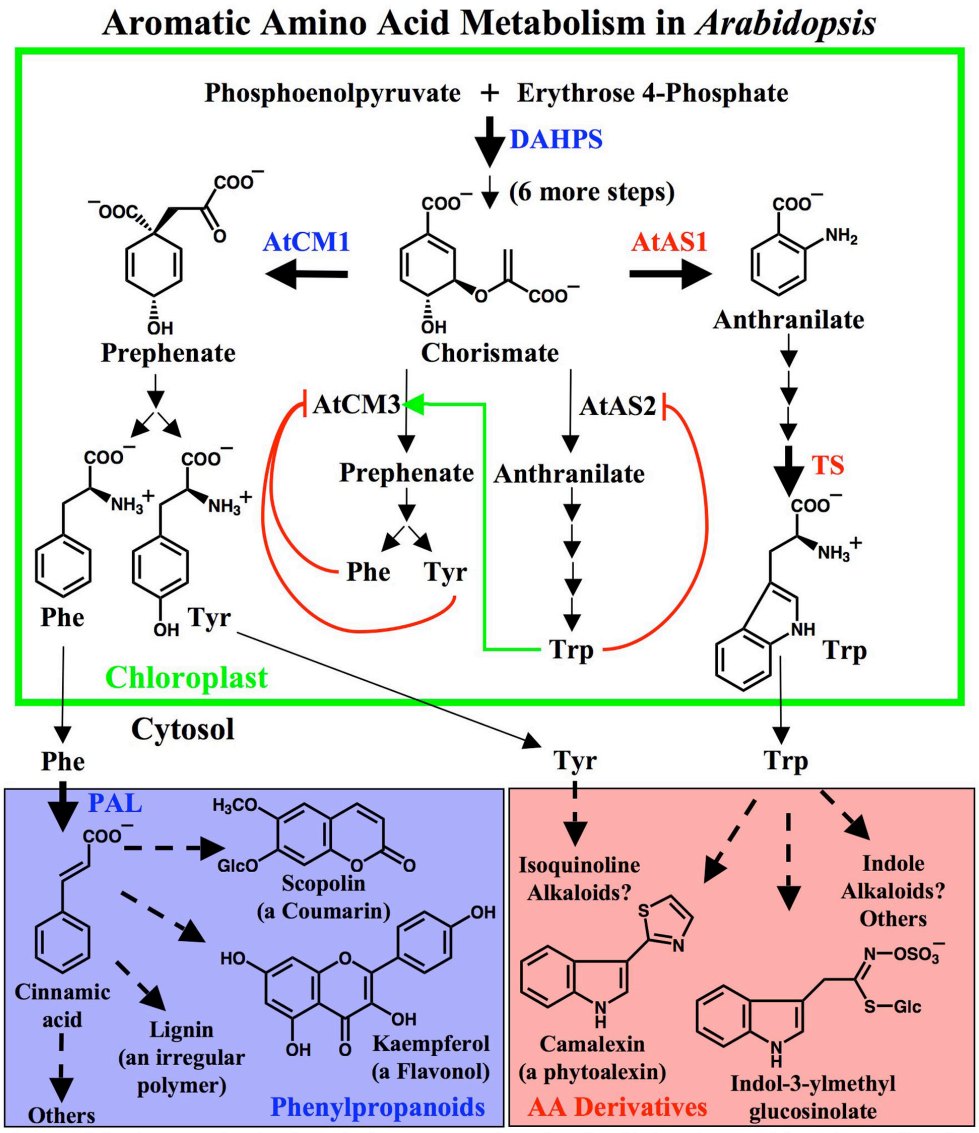

Figure 1.9 Aromatic Amino Acid Metabolism in *Arabidopsis*. In this schematic of aromatic amino acid biosynthesis, each enzymatic transformation is indicated by a solid black arrow, except where indicated, and multiple complex transformations are indicated by a dotted black arrow. All enzymes referenced in the text are specified. Thicker arrows indicate inducible upregulation of enzyme levels, and are accompanied by a color-coded enzyme name indicating which other enzymes are simultaneously induced. The chloroplast is indicated by green box. For simplicity, allosteric regulation is shown for constitutive enzymes only; red arrows indicate feedback inhibition and green arrows indicate activation. Abbreviations used are: DAHPS, 3-Deoxy-D-arabinoheptulosonate 7-phosphate synthase; CM, Chorismate mutase; PAL, Phenylalanine ammonia lyase; AS, Anthranilate synthase; TS, Tryptophan synthase; AA, Amino acids.

downstream metabolites is regulated in higher plants. Each chorismate-utilizing gene is differentially expressed, and each corresponding enzyme competes with one another for available chorismate. *Arabidopsis* cDNAs for three genes encoding chorismate mutase enzymes [66, 67] and two encoding anthranilate synthase enzymes [68] were obtained by complementing bacterial and yeast strains deficient in these respective activities, and the resultant sequences shown to be homologous to bacterial and yeast forms of these enzymes. Of the three *Arabidopsis* CM genes, only *AtCM2* ("At" indicating the form present in *Arabidopsis thaliana*) does not possess a sequence encoding an amino-terminal chloroplast transit peptide, suggesting that AtCM1 and AtCM3 are found in the chloroplast and AtCM2 is cytosolic (see [66, 67], and Figure 1.9). While levels of the gene encoding AtCM3 do not appear to change in response to wounding or treatment with the bacterial plant pathogen *Pseudomonas syringae* [67], genes encoding AtCM1, a 3-deoxy-D-arabinoheptulosonate 7-phosphate synthase (DAHPS, the first enzyme in the shikimate pathway) and a PAL are maximally and coordinately induced (Figure 1.9) within several hours of treatment of cultured cells with a *P. syringae* elicitor [66] (elicitors are molecules produced by the pathogen that elicit an immune response in the plant host). Furthermore, the inducible AtCM1 has a high K_M for chorismate (2900 μM), whereas the non-inducible AtCM3 has a much lower K_M (420 μM) [67]. These data suggest that AtCM1 plays a significant role in generating prephenate for the biosynthesis of phenylpropanoid molecules needed in plant defense and stress responses, as genes both upstream and downstream of chorismate metabolism are up-regulated, and as AtCM1 operates at relatively high concentrations of chorismate. Whereas, AtCM3 is more likely responsible for the constitutive production of prephenate for the biosynthesis of phenylalanine and tyrosine used in translation. CM1 may be an inducible enzyme in other plants, as increases in activity of CM1, DAHPS and PAL enzymes have been shown in parsley cells exposed to a fungal elicitor [69].

A similar expression pattern was observed in *Arabidopsis* for the two genes encoding the chorismate-utilizing α-subunits of AS (analogous to the TrpE subunits of bacterial AS). Both α-subunits AtASA1 and AtASA2 possess amino-terminal chloroplast transit peptides, indicating that they are localized in the chloroplast (see [68], and Figure 1.9). Whereas *AtASA1* gene expression is dramatically up-regulated following wounding of the plant or infection with *P. syringae*, *AtASA2* gene expression decreases slightly under these conditions and is generally found at a basal level [68]. The *AtASB1* gene, which encodes a chloroplast-localized glutamine-hydrolyzing AS β-subunit (analogous to the TrpG subunit of bacterial AS), has been shown to exhibit a similar expression profile upon infection with *P. syringae* [70]. The inducible AtASA1 has a relatively high K_M for chorismate (180 μM) consistent with its likely operation at elevated chorismate concentrations, and the non-inducible AtASA2 has a lower K_M (21 μM) suggesting its involvement in low-level anthranilate production [68]. Though these K_M values are significantly lower than those for the *Arabidopsis* CM enzymes, they are likely to be more accurate because they were measured using mature proteins (those without the chloroplast transit peptide), whereas the CM proteins were unprocessed; mature CM enzymes may have K_M values of a magnitude similar to these. These expression patterns and K_M values are consistent with a role for AtASA1 in the production of tryptophan pathway metabolites as part of an *Arabidopsis* defense response, and for AtASA2 in the constitutive production of tryptophan needed for protein synthesis. Evidence for this hypothesis was provided by the discovery that AtASA1 and tryptophan synthase (TS, the final enzyme of the tryptophan biosynthetic pathway) are coordinately induced in response to infection of *Arabidopsis* plants with the bacterial pathogen *P. syringae*, and by the tight correlation between the rate of tryptophan-derived camalexin

accumulation and the degree of this enzyme induction (see [71], and Figure 1.9). Differential gene expression of an inducible ASA1 and a constitutive ASA2 may be a general phenomenon in higher plants, as similar results have been reported for the acridine alkaloid-producing species *Ruta graveolens* [72]. In this case, *R. graveolens* cultured cells were exposed to an extract of the fungal pathogen *Rhodotorula*, and *ASA1* mRNA levels increased in six hours to 100-fold that of the control, with *ASA2* levels showing no change; other acridine alkaloid pathway genes were not examined to determine whether coordinate induction was occurring. Though *Arabidopsis* is known to produce camalexin, indole glucosinolates, and auxins from tryptophan [73], only recently, with the discovery of alkaloid biosynthetic gene homologs, has the prospect of alkaloid production in *Arabidopsis* been considered (see [74], and Figure 1.9).

Because they are committing branchpoint enzymes in amino acid biosynthesis, CM and AS are primary targets for allosteric regulation in the chloroplast. Both AtCM1 and AtCM3 are feedback inhibited to the same extent by phenylalanine and tyrosine, and activated to the same extent by tryptophan (see [67], and Figure 1.9). This regulates flux to CM products phenylalanine and tyrosine by suppressing their biosynthesis when their supply is adequate, and increasing their biosynthesis when AS metabolite tryptophan is plentiful. Furthermore, AtASA1 [75] and AtASA2 [76] are feedback inhibited by downstream product tryptophan (Figure 1.9), preventing overproduction of this amino acid at the expense of other metabolites of chorismate. This regulatory mechanism would be expected for enzymes – like AtCM3 and AtASA2 – that appear to be responsible for the constitutive production of amino acids, but is seemingly counterproductive in the case of inducible AtCM1 and AtASA1, which are believed to initiate the production of phenylpropanoids and indole-containing products, respectively. It is possible that inducible enzymes downstream of these amino acids ensure that they are maintained at levels below that which would inhibit their action during the biosynthesis of important metabolites. Alternatively, in the case of inducible AtCM1, it is possible that levels of tryptophan may be kept artificially high during phenylpropanoid biosynthesis in order to reverse AtCM1 inhibition by phenylalanine and tyrosine. The plant *R. graveolens* avoids the problem of feedback inhibition in downstream metabolite biosynthesis by expressing an inducible AtASA1 that is not subject to feedback inhibition by tryptophan, a strategy that may be employed in other organisms that that must engage in large-scale production of tryptophan metabolites even when free tryptophan is plentiful [77]. Indeed, when the gene encoding a feedback-insensitive AtASA1 point mutant is transformed into *Catharanthus roseus* hairy root cells, greatly elevated levels of the indole alkaloid lochnericine are generated [78]. Importantly, many plants do not possess a CM3 equivalent, suggesting that CM1 must act to produce amino acids as well as complex natural products, and thus requiring that CM1 be regulated allosterically in this instance.

Other chorismate-utilizing enzymes in *Arabidopsis* have been shown to be chloroplast-localized, and thus compete for available chorismate. The amino-terminal peptide segment of AtADCS targets other fusion proteins to the chloroplast [56], and the secondary aromatizing enzyme responsible for generating PABA from ADC (Figure 1.6) – ADC lyase (ADCL) – has been visualized in the chloroplast [79], indicating that PABA biosynthesis occurs there. Studies of the genes encoding both of these enzymes in tomato showed that extent of tomato ADCS expression in leaves and unripe fruit roughly matches levels of total folate [56] – which is produced from PABA – and that levels of tomato ADCS and ADCL gene expression are similar and follow the same general trend [79]. Furthermore, kinetic studies of overexpressed AtADCS show that the K_M for chorismate is 1.3 μM, suggesting that it typically functions when

chorismate levels are low, and the enzyme is only inhibited by dihydrofolate and related molecules, suggesting that it is the endpoint metabolic product of ADCS action [80]. These data are all consistent with a role for ADCS in the constitutive production of ADC for dihydrofolate biosynthesis.

Two ICS genes have been characterized in *Arabidopsis*, *AtICS1* and *AtICS2* [81]. Both have been shown to produce chloroplast-localized, stromal proteins by import assays ([82], and unpublished data), and by fluorescence visualization [82, 83]. These two proteins are 83% identical to each other, and AtICS1 is 57% identical to ICS from *C. roseus* and greater than 20% identical to bacterial ICS enzymes [81]. Recent studies have provided the first genetic evidence for an operational ICS pathway in plants – salicylic acid (SA) biosynthesis from isochorismate in *Arabidopsis* [81]. In this work, *AtICS1* mRNA is induced in response to infection with both bacterial pathogen *P. syringae* and fungal pathogen *Erysiphe orontii*, and its expression is shown to be correlated with total SA levels in *Erysiphe*-infected leaves [81]. In addition, induced SA synthesis in *Arabidopsis ics1* knockout mutants was essentially abrogated relative to wild type plants [81]. Importantly, no *AtICS2* mRNA is detected in either infected or uninfected *Arabidopsis* leaves under these conditions, suggesting that the gene is either constitutively expressed at extremely low levels, or is induced under conditions different from those employed [81].

Isochorismate Utilization in Prokaryotes. Knowledge of bacterial biosynthetic pathways that utilize isochorismate is much more extensive than that of plants. ICS enzymes have been associated with biosynthesis of low molecular weight iron-chelating siderophores [84], which are secreted from the cell to bind extremely insoluble ferric (Fe^{3+}) ions needed for growth, thus rendering them soluble in complexes which are more easily retrieved [85]. ICS enzymes also play an important role in the production of menaquinones, one of the two main types of membrane-bound terpenoid quinones known in bacterial electron transport [86] – the other is ubiquinone (shown in Figure 1.6) which is also found in the mitochondria of eukaryotes. For example, *E. coli* contains two ICS genes located in distinct operons encoding proteins with distinct biochemical properties: EntC is expressed under iron-limited – and often oxidative – conditions and is associated with siderophore biosynthesis, and MenF is required for menaquinone biosynthesis and is expressed under anaerobic conditions (see [55, 87-89], and Figure 1.10). The initial steps in bacterial siderophore production from isochorismate often involve the synthesis of SA or 2,3-dihydroxybenzoic acid (DHBA). SA is incorporated into siderophores such as pyochelin in *Pseudomonas aeruginosa* [90] and yersiniabactin in *Yersinia enterocolitica* [91], and three units of DHBA are incorporated into enterobactin in *E. coli* (see [92], and Figure 1.10); enterobactin is the tightest-binding siderophore known, with a $K_D = 10^{-49}$ M [85, 93]. In *P. aeruginosa*, ICS (PchA) and isochorismate pyruvate lyase (PchB) are required for the synthesis of SA from chorismate [90], whereas *Y. enterocolitica* Irp9 – a bifunctional SA synthase (SAS) [91, 94] – directly converts chorismate to SA via an isochorismate intermediate (Figure 1.10). Importantly, the monofunctional ICS enzyme Eco EntC and the bifunctional SAS Yen Irp9 exhibit a high degree of structural similarity [58], and both possess highly conserved active sites containing the lysine residue believed to act as a catalytic base in all MST enzymes known to add water to chorismate [45]. On the other hand, as shown in Figure 1.10, bacterial synthesis of menaquinones occurs via the intermediate *ortho*-succinylbenzoate (OSB) [86]. Although bifunctional or multifunctional bacterial ICS enzymes associated with the synthesis of OSB have not been reported, bacterial genomes contain conserved co-localized MenF (ICS) and

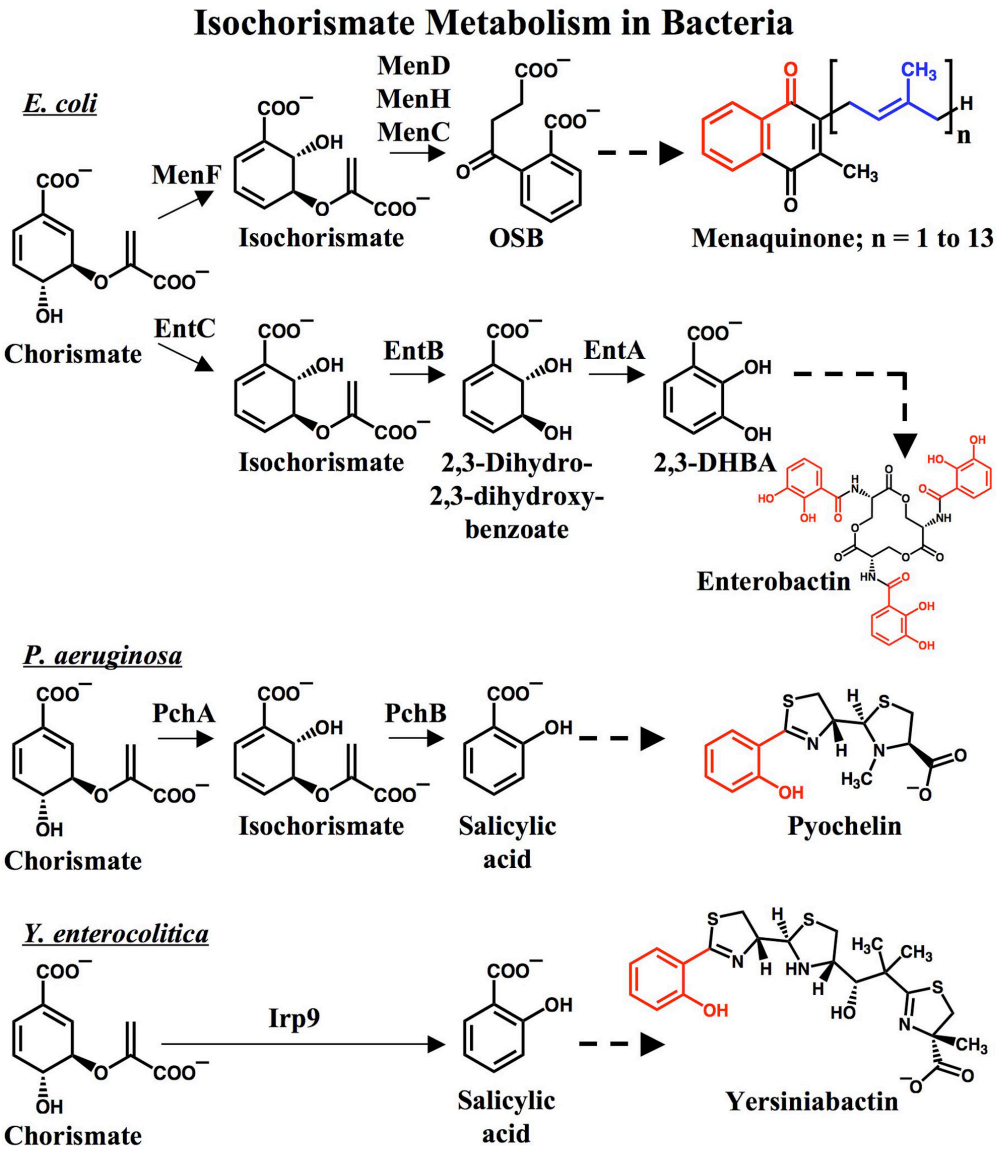

Figure 1.10 Isochorismate Metabolism in Bacteria. In this overview of bacterial isochorismate metabolism, each enzymatic transformation is indicated by a solid arrow and multiple transformations are indicated by a thick dotted arrow. All enzymes referenced in the text are specified, the atoms in each target molecule that are contributed by isochorismate are highlighted in red, and the atoms contributed by individual isopentenyl diphosphate (IPP) monomers are highlighted in blue. MenF, EntC, and PchA are all isochorismate synthase (ICS) enzymes, PchB is an isochorismate pyruvate lyase (IPL) enzyme, and Irp9 is a salicylic acid synthase (SAS) enzyme that produces a bound isochorismate intermediate. Abbreviations used are: OSB, *ortho*-Succinyl-benzoate; 2,3-DHBA, 2,3-Dihydroxybenzoic acid.

MenD (the second enzyme in menaquinone biosynthesis; see below) genes [87, 95, 96] to channel isochorismate to the menaquinone pathway (Figure 1.10).

Menaquinone biosynthesis is essential for all bacteria living in anaerobic environments, and menaquinone is the only terpenoid quinone found in many Gram-negative and all Gram-positive bacteria [86]. Menaquinone (also known as vitamin K_2) and related molecules are essential nutrients in mammals, participating as they do in the oxidative carboxylation of glutamate residues [97] in proteins involved in blood coagulation, bone metabolism, and cell cycle regulation [98-100]. Though an alternative menaquinone biosynthetic pathway involving the intermediate futalosine has recently been discovered [101], it is present in only a few prokaryotic organisms. The much more common pathway involving the intermediates isochorismate and OSB (Figure 1.11) has been thoroughly characterized genetically in *E. coli*, and most enzymes of this putative pathway have been overexpressed and assayed biochemically [86]. After the action of the menaquinone-specific ICS MenF [89], the resultant isochorismate is modified at the C2 position by conjugate addition of succinic semialdehyde derived from thiamine-dependent decarboxylation of α-ketoglutarate. This reaction is catalyzed by MenD [102, 103], a bifunctional enzyme whose true product has only recently been identified as the 2-succinyl-5-enolpyruvyl-6-hydroxy-3-cyclohexene-1-carboxylate (SEPHCHC) with the stereochemistry indicated in Figure 1.11 [104, 105]. MenH has also recently been shown to catalyze subsequent 2,5-elimination of pyruvate to form 2-succinyl-6-hydroxy-2,4-cyclohexadiene-1-carboxylate (SHCHC) with the indicated stereochemistry (Figure 1.11) – it had previously been misannotated as a thioesterase [106]. Dehydration to form the aromatic product OSB is then catalyzed by MenC [86]. MenE next catalyzes the formation of the CoA thioester OSB-CoA in an ATP-dependent process [107], and this intermediate is cyclized by MenB to the CoA ester of 1,4-dihydroxy-2-naphthoic acid (DHNA-CoA) [86, 108, 109]. The final enzyme in the naphthoquinone pathway to be discovered, DHNA-CoA thioesterase, has recently been characterized in the cyanobacterium *Synechocystis* (see below), and also shown to have homologs in many other prokaryotes, including *E. coli* [110]. This thioesterase generates 1,4-dihydroxy-2-naphthoic acid (DHNA), the substrate for decarboxylative polyprenylation by MenA [111]. The length of the polyprenyl group attached by MenA is highly variable in prokaryotes (Figure 1.11), though in *E. coli* the side chain of this demethylmenaquinol ($DMQH_2$) is generally composed of 40 carbon atoms [86]. Final S-adenosylmethionine (SAM)-dependent methylation catalyzed by UbiE [112], an enzyme also involved in the biosynthesis of ubiquinone (Figure 1.6), generates menaquinol, which is readily oxidized to menaquinone (Figure 1.11). MenG had previously been misannotated as the gene responsible for this transformation; it is now known to be a protein inhibitor of RNase E, a function unrelated to menaquinone biosynthesis [113].

Though production of menaquinone by intestinal microflora like *E. coli* provides a portion of the vitamin K needed, the principal source of vitamin K in mammals is phylloquinone (PhQ, also known as vitamin K_1), which is obtained in the diet mainly by consumption of green vegetables [114]. Phylloquinone is almost identical structurally to menaquinone, possessing the same substituted 1,4-naphthoquinone core, but with a 20-carbon partially saturated phytyl side chain replacing the menaquinone polyprenyl side chain (Figure 1.11). Phylloquinone is found in virtually all photosynthetic organisms, where it functions as the one-electron carrier at the A_1 site of photosystem I (PS I) complexes; in plants these complexes are found in the thylakoid membranes of the chloroplast [7]. Recently, the discovery that as much as 50% of PhQ in the plant is not associated with PS I [95] has led to the consideration of additional roles for PhQ as a

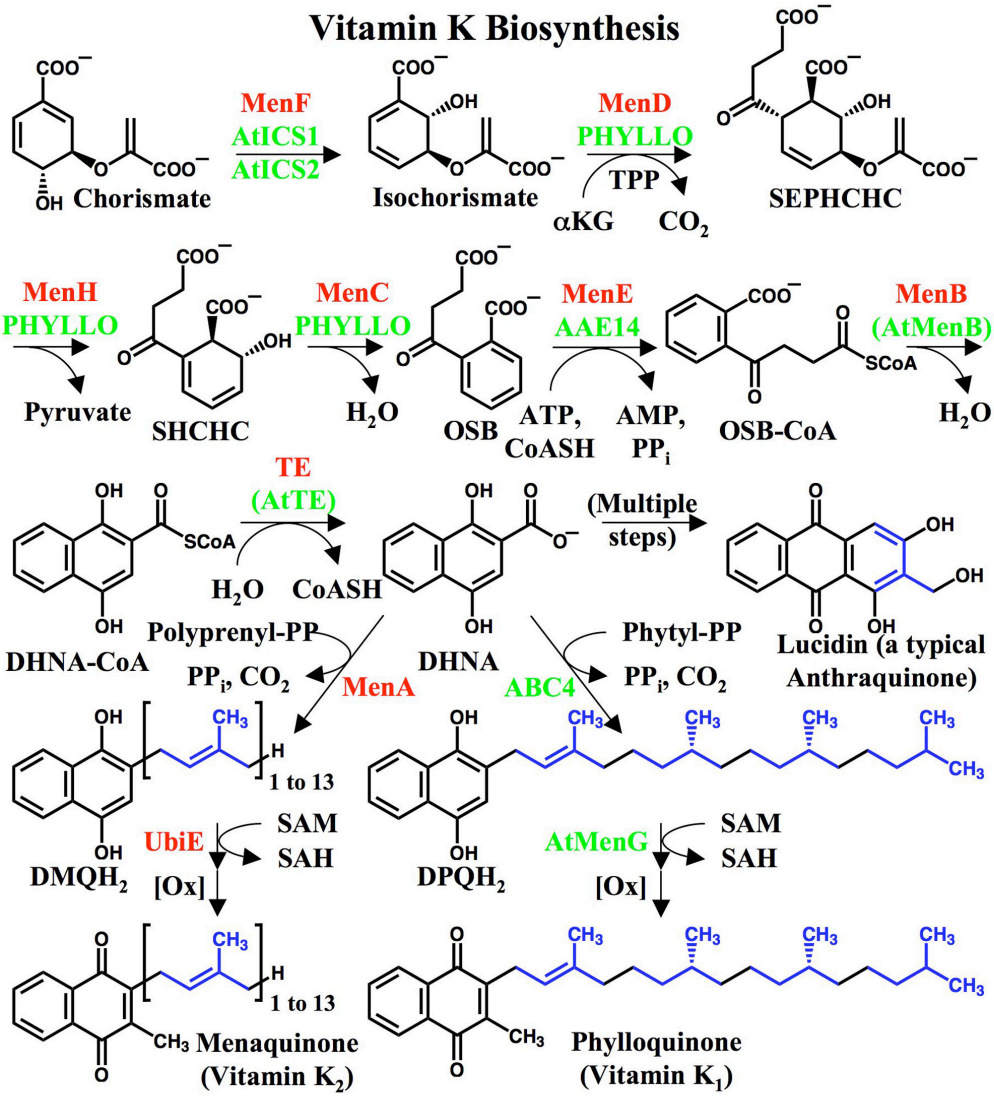

Figure 1.11 Vitamin K Biosynthesis. In this schematic of vitamin K biosynthesis, each enzymatic transformation is indicated by a solid arrow. All enzymes referenced in the text are specified, and the atoms contributed by individual isopentenyl diphosphate (IPP) monomers are highlighted in blue. Bacterial menaquinone pathway enzymes are highlighted in red, and *Arabidopsis* phylloquinone pathway enzymes are highlighted in green, with putative enzymes in parentheses. Abbreviations used are: SEPHCHC, 2-Succinyl-5-enolpyruvyl-6-hydroxy-3-cyclohexene-1-carboxylate; SHCHC, 2-Succinyl-6-hydroxy-2,4-cyclohexadiene-1-carboxylate; OSB, *ortho*-Succinylbenzoate; CoA, Coenzyme A; DHNA, 1,4-Dihydroxy-2-naphthoic acid; $DMQH_2$, Demethyl-menaquinol; $DPQH_2$, Demethylphylloquinol; αKG, α-Ketoglutarate; TPP, Thiamine pyrophosphate; TE, DHNA-CoA thioesterase; [Ox], Oxidation event; SAM, S-Adenosyl-methionine; SAH, S-Adenosylhomocysteine.

sensor or scavenger of reactive oxygen species in the plant plasma membrane [115, 116]. PhQ biosynthesis in photosynthetic organisms had been studied by feeding radiolabeled biosynthetic precursors to, and by enzyme assays of, the extracts of cells from spinach [117], *Capsicum annuum* [118], *Galium* [119], and the protist *Euglena gracilis* [120] – these determined that many of the steps in PhQ biosynthesis were identical to those of menaquinone, and that PhQ biosynthesis is localized mainly in membrane associated with the chloroplast. However, until the work described in this thesis, no purified plant enzymes of the phylloquinone pathway had been characterized biochemically, and much of what was learned initially about the proteins responsible for phylloquinone biosynthesis was gained by genetic approaches in the PhQ-producing photosynthetic cyanobacterium *Synechocystis* sp. PCC 6803, a prokaryote. Targeted mutagenesis in *Synechocystis* disrupted homologs of menaquinone biosynthesis *menA* [121], *menB* [121], *menD* [122], *menE* [122], *ubiE* [123], and the gene encoding the DHNA-CoA thioesterase [110]. All mutants lacked the ability to biosynthesize phylloquinone, and had impaired PS I activity when exposed to high light. It was determined that plastoquinone – a terpenoid benzoquinone that normally participates in photosystem II electron transfer and that is biosynthesized via the same pathway as vitamin E (see Figure 1.6) – can substitute for PhQ in the A_1 site of PS I in *Synechocystis*, allowing PS I to function with limited efficiency [121, 122], and thus preventing the appearance of a clear phenotype under conditions of normal light. This same phenomenon was observed for a *menD* domain knockout mutant in the photosynthetic model eukaryote *Chlamydomonas reinhardtii* [124].

Isochorismate Utilization in *Arabidopsis thaliana*. Candidate genes for the phylloquinone pathway in *Arabidopsis* were obtained after searching for genes with homology to those of the common menaquinone pathway (Figure 1.11) from other organisms; their protein products, and the biosynthetic pathway itself, are likely localized to the chloroplast [95, 110, 125]. All studies of plant PhQ biosynthesis undertaken to date have been genetic in nature. *Arabidopsis* genes homologous to *menD*, *menH*, and *menC*, along with a truncated and apparently non-functional *menF* homolog, were found to be part of the tetramodular monocistronic gene *PHYLLO*, encoding a chloroplast-localized polypeptide required for PhQ production [95]. The same *PHYLLO* fusion was also observed in rice and poplar, suggesting its universality in higher plants [95]. Though the phenotype of the *Arabidopsis PHYLLO* knockout mutant was not pronounced – PS I operates at an efficiency of 5-15% that of wild type – it could be abrogated by feeding the plant the downstream metabolite DHNA, confirming that PHYLLO is responsible for converting the ICS product isochorismate into OSB (see [95], and Figure 1.11). It was also discovered that AtICS1 and AtICS2 are functionally redundant in PhQ biosynthesis, as only the double knockout possessed the *PHYLLO* phenotype (see [95], and Figure 1.11). A number of other genes homologous to those of the menaquinone pathway have also been disrupted by targeted mutagenesis. *AAE14* (a *menE* homolog, [126]), *ABC4* (a *menA* homolog, [127]), and *AtMenG* (a *ubiE* homolog, despite the gene name, [128]) knockout mutants all failed to biosynthesize PhQ. All mutants were deficient in PS I activity and showed a noticeable phenotype – particularly the *ABC4* knockout, which had an albino phenotype in older leaves [127]. Fusions of each of these three gene products with green fluorescent protein (GFP) demonstrated that they, like other PhQ pathway gene products, are localized to the chloroplast [126-128]. Further evidence that *AAE14* is a *menE* homolog is provided by its ability to restore menaquinone production when expressed in an *E. coli* mutant disrupted in the *menE* gene, and by the fact that the *Arabidopsis AAE14* knockout accumulates the MenE substrate OSB and

reverts to the wild type phenotype when supplied with the downstream metabolite DHNA [126]. Likewise, *AtMenG* restores phylloquinone biosynthesis when expressed in a *Synechocystis* mutant disrupted in the *ubiE* gene, and the *Arabidopsis AtMenG* knockout accumulates demethylphylloquinone, the quinone form of the AtMenG substrate (see [128], and Figure 1.11). The final two genes involved in the pathway have not yet been confirmed by genetic analysis, but candidates in *Arabidopsis* exist. The recently discovered *Synechocystis* gene encoding a putative DHNA-CoA thioesterase has been shown to have four homologs in *Arabidopsis* (Accession numbers NP_176995, NP_564926, NP_564457, and NP_174759), each possessing amino-terminal extensions that are predicted to encode chloroplast transit peptides (CTPs), and each containing apparently conserved histidine and aspartate residues deemed essential for activity [110]. The final pathway gene candidate, a *menB* homolog (At1g60550), does not appear to contain an amino-terminal extension encoding a CTP, although it may be misannotated [125]. Nevertheless, it is clustered with *ABC4* (16.5 kb away), and in view of the fact that clustering of these and other naphthoquinone biosynthetic genes have been maintained evolutionarily across species [95], and that it is commonly the case that conservation of gene order in bacteria correlates with the proteins that those genes encode interacting physically [129, 130], it has been hypothesized that phylloquinone is biosynthesized by a multienzymatic complex possessing all of the nine biosynthetic gene products [95]. Evidence for the existence of such a complex is provided by the similarity in appearance of the punctuate patterns observed for fluorescent reporters used to confirm chloroplast localization of AAE14, AtMenG, and PHYLLO [95, 126, 128]. Metabolic channeling by multienzyme complexes is common in plants, as it promotes efficient biosynthesis by preventing diffusion of reactive and potentially toxic intermediates away from the complex [131].

Anthraquinones, as well as a number of other naphthoquinones produced by plants in addition to PhQ, are typically elicitor-induced colored compounds, reported to have anti-oxidant, anti-microbial, and cytotoxic activities [132-134]. Most of these are biosynthesized from isochorismate via the branchpoint intermediate DHNA (Figure 1.11), although some anthraquinones are generated by polyketide synthases [9]. Decarboxylative alkylation of DHNA with an isoprenyl group at either the C2 or C3 positions, followed by oxidative ring closure, generates the anthraquinone core structure [9]. Further enzymatic oxidations and alkylations of various intermediates in the anthraquinone and naphthoquinone pathways generate great molecular diversity [9]. Though *Arabidopsis* is not known to produce any anthraquinones or naphthoquinones besides PhQ, many species do, particularly those of the madder family (Rubiaceae) [135]. The highly mutagenic compound lucidin is shown in Figure 1.11 in order to emphasize that anthraquinone biosynthesis proceeds from a prenylated naphthoquinone, but probably the best-known natural product of the madder family is alizarin (1,2-dihydroxyanthraquinone, not shown), which is demethylated and differentially hydroxylated [9]. Alizarin is a bright red substance isolated from the madder root that served as one of the two leading dyestuffs throughout human history [136] – indigo being the other. Perhaps the best-known naphthoquinone, lawsone (2-hydroxy-1,4-naphthoquinone, not shown), is also a dye, being the principal component of the leaves of the henna plant [9]. The biological function of most anthraquinones and naphthoquinones is not known, though recent work has indicated a possible role for one in the induction of programmed cell death associated with pathogen defense responses [137].

Salicylic Acid Metabolism in Plants. Though it has long been known that plants produce quinones from isochorismate, it has recently been found that plants, like bacteria, use isochorismate to produce SA [81] and DHBA [138] – though DHBA is likely generated from SA (see Figure 1.15) in *C. roseus* [139] instead of 2,3-dihydro-2,3-dihydroxybenzoate (Figure 1.10). SA is a plant hormone that is best known for its role as a key regulator of plant defense against pathogens, and that is required for the induction of hundreds of defense-related genes [140]. Originally, SA biosynthesis in plants was believed to proceed entirely from the CM-initiated phenylpropanoid pathway [141]. Radiolabeling studies in uninfected and virus-infected tobacco showed conclusively that cinnamic acid and benzoic acid are intermediates in the biosynthesis of SA, and a β-oxidative process involving coenzyme A thioesters was proposed for this pathway (see [141, 142], and Figure 1.12) – this is analogous to the process whereby phenylalanine is metabolized to PHBA (indicated in Figure 1.6). This pathway relies upon the action of benzoic acid 2-hydroxylase (BA2H) to convert benzoic acid to SA [143], and the β-oxidative pathway incorporating this enzyme has been confirmed in other plant species – though a few species also make use of pathways involving retro-aldol formation of benzaldehyde in SA production (see [144, 145], and Figure 1.12). However, radiolabeling studies in both tobacco [142] and potato [146] showed that the specific activity of the SA accumulating through the β-oxidative pathway was less than predicted by total salicylate quantification, and significant SA levels were still found in pathogen-infected *Arabidopsis* [147] and elicitor-exposed potato [146] plants that had been fed the PAL inhibitor 2-aminoindan-2-phosphonic acid (AIP), indicating that SA biosynthesis was also occurring via a different pathway. In addition, no BA2H enzyme has yet been found in *Arabidopsis*, and no genetic evidence exists in this organism for conversion of benzoic acid to SA. This suggests that little, if any, SA is being biosynthesized in *Arabidopsis* via the phenylpropanoid pathway.

A second pathway for SA biosynthesis in plants was discovered in 2001 (see [81], and Figure 1.12). Forward genetic screens identified mutations in *Arabidopsis* that failed to accumulate SA and were deficient in a form of systemic resistance to pathogen infection (SAR; see below). Both *sid2* [148] and *eds16* [149] mutants possess SA levels upon infection that are 5-10% that of infected wild type, have impaired systemic defenses, and map to the same locus at the bottom of *Arabidopsis* chromosome I [81]. This gene was shown to encode a protein with homology to known ICS enzymes, and was termed *AtICS1*. The fact that RNA blot analysis shows *AtICS1* induction only in infected wild type plants, and the appearance of a strong correlation between the degree of *AtICS1* and defense gene expression and level of SA production, strongly suggest that the isochorismate pathway is the main source of the SA required for systemic defense [81]. It was not clear from this work whether the product of the *AtICS1* gene acted as a bifunctional SAS, or was a monofunctional ICS that worked in concert with a secondary isochorismate pyruvate lyase (IPL) to generate SA (Figure 1.12). Basal levels of SA found in pathogen-infected knockout mutants of *AtICS1*, and in uninfected wild type *Arabidopsis* plants, suggest that low levels of SA are being biosynthesized by the β-oxidative pathway. Nevertheless, the dominant form of SA biosynthesis in *Arabidopsis* and other plant species appears to proceed from isochorismate. Irrespective of the origin of SA biosynthesis, most cytosolic SA is glucosylated by UDP-glucosyltransferase enzymes to form non-toxic SA 2-O-β-glucoside (SAG; Figure 1.12). SAG can be hydrolyzed back to SA by glucosylase enzymes (see Figure 1.15), and is normally sequestered in the vacuole where it forms a readily available source of SA [150].

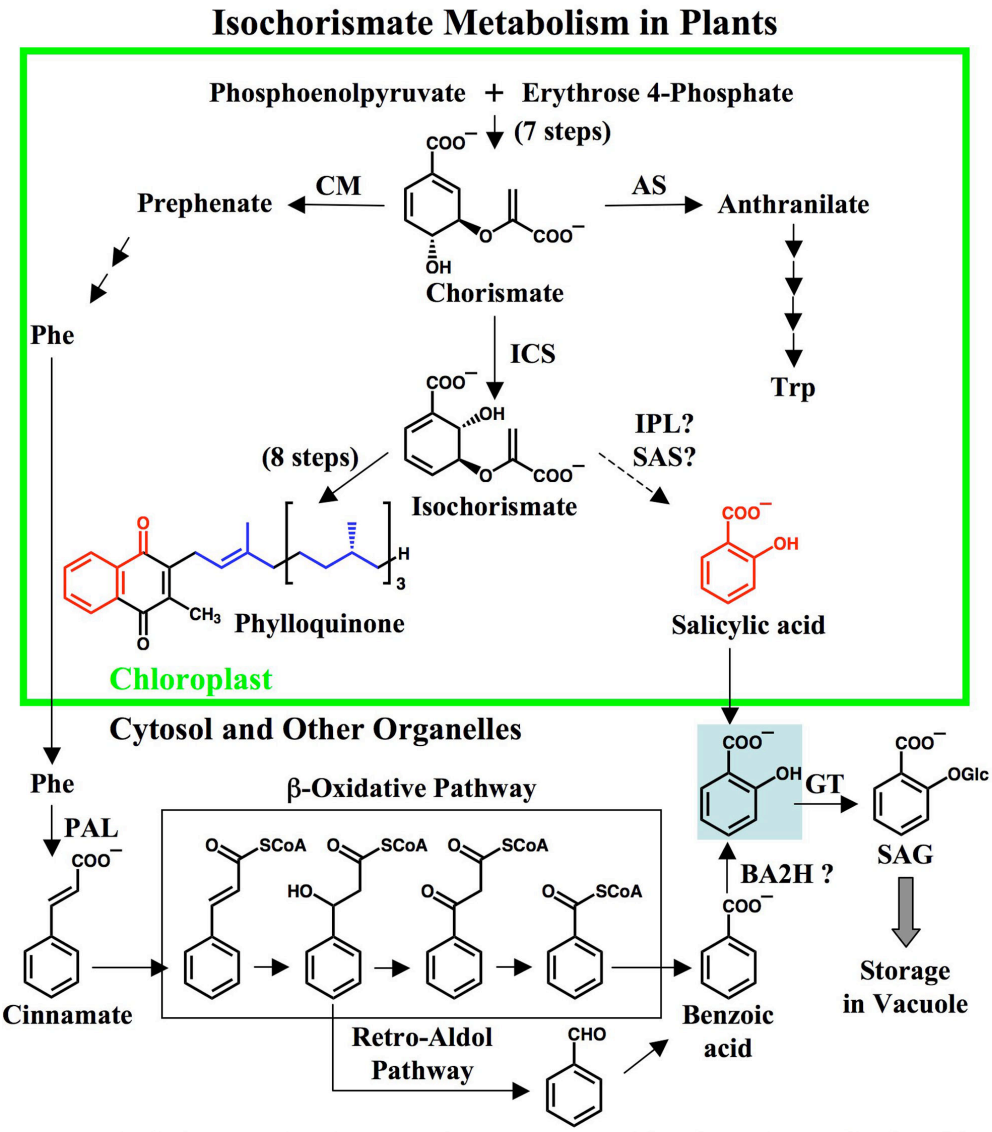

Figure 1.12 Salicylic Acid Biosynthesis in Plants. In this schematic of salicylic acid biosynthesis, each enzymatic transformation is indicated by a solid black arrow, except where indicated, and unknown transformations are indicated by a dotted black arrow. All enzymes referenced in the text are specified, and the putative β-oxidation pathway is boxed. The chloroplast is indicated by green box. The atoms in each target molecule that are contributed by isochorismate are highlighted in red, and the atoms contributed by individual isopentenyl diphosphate (IPP) monomers are highlighted in blue. Abbreviations used are: CM, Chorismate mutase; AS, Anthranilate synthase; ICS, Isochorismate synthase; IPL, Isochorismate pyruvate lyase; SAS, Salicylic acid synthase; PAL, Phenylalanine ammonia lyase; BA2H, Benzoic acid 2-hydroxylase; GT, Glucosyl-transferase; SAG, Salicylic acid 2-O-β-glucoside.

SALICYLIC ACID IN PLANT DEFENSE

Introduction to Plant Defense Against Biotic Stress. It has been known for decades that in many plant species a relationship exists between biotic stress and the accumulation of hormones like SA. Plants are hosts to thousands of infectious diseases caused by a vast number of phytopathogenic fungi, oomycetes, bacteria, viruses, and nematodes, as well as potential food sources for herbivorous insects, mammals, and other animals. Despite this, pathogens and herbivores rarely kill plants: only 13.3% of crops worldwide are lost to disease and 15.6% lost to herbivory [151]. In order to gain access to plant nutrients, all biota must first overcome preformed defenses that are constitutively maintained, like the cuticle surrounding the plant exterior (described above), the cell wall of each individual cell, and vacuole-sequestered defense compounds with broad-spectrum toxicity – like glucosinolates and cyanogenic glycosides – that exert their effects when cellular membranes are ruptured (see Figures 1.2 and 1.14). However, most resistance to biotic stress is inducible. Typically, these inducible defense responses are the result of the transcriptional activation of specific genes, and they vary according to the identity of the attacker. Necrotrophic pathogens (those that kill the host and feed on the contents), wounding induced by herbivores, and mechanical wounding all mainly activate defense mechanisms that are mediated by the plant hormones jasmonic acid (JA) and ethylene (Figure 1.13). Alternatively, biotrophic pathogens (those that require a living host to complete their life cycle) mainly activate defense mechanisms that are mediated by SA. Both types of responses involve the transcriptional activation of defense-related genes, including 17 separate classes of *Pathogenesis-Related* (*PR*) genes that are present across plant species and that encode small, mostly secreted or vacuole-targeted proteins with anti-microbial activity [152]. The SA- and JA/ethylene-dependent pathways (Figure 1.13) tend to be antagonistic to one another, with the biosynthesis and accumulation of one set of hormones preventing that of the other – though many so-called hemibiotrophic pathogens (like the bacterium *P. syringae*) are able to activate elements of both [153]. Recent work has uncovered additional complexity in these processes due to the involvement of other plant hormones – abscisic acid, gibberelic acid, the brassinosteroids (Figure 1.1), and the auxins (Figure 1.2) – in signal transduction [154].

Basal Defense in Plants. Having overcome the preformed defenses of the plant cell, an attacking organism is confronted by several tiers of defense responses [7, 18]. The primary response is known as basal (or non-host) resistance, and it initiates a number of biochemical processes that prevent nearly every type of pathogen or herbivore from destroying the plant. Without basal resistance, the plant is highly susceptible to even mild infection or small numbers of herbivores [155]. The organism is usually – though not always [156] – perceived by the plant as a result of a binding event between an elicitor produced by the attacking organism and a plant plasma membrane receptor (Figure 1.13). Elicitors generally possess common molecular features of plant pathogens and herbivores – these include oligosaccharides from partially degraded fungal and bacterial cell walls (β-glucans and chitin), non-plant polypeptides (bacterial harpins and flagellin), and non-plant lipids from insects (volicitin) and bacteria

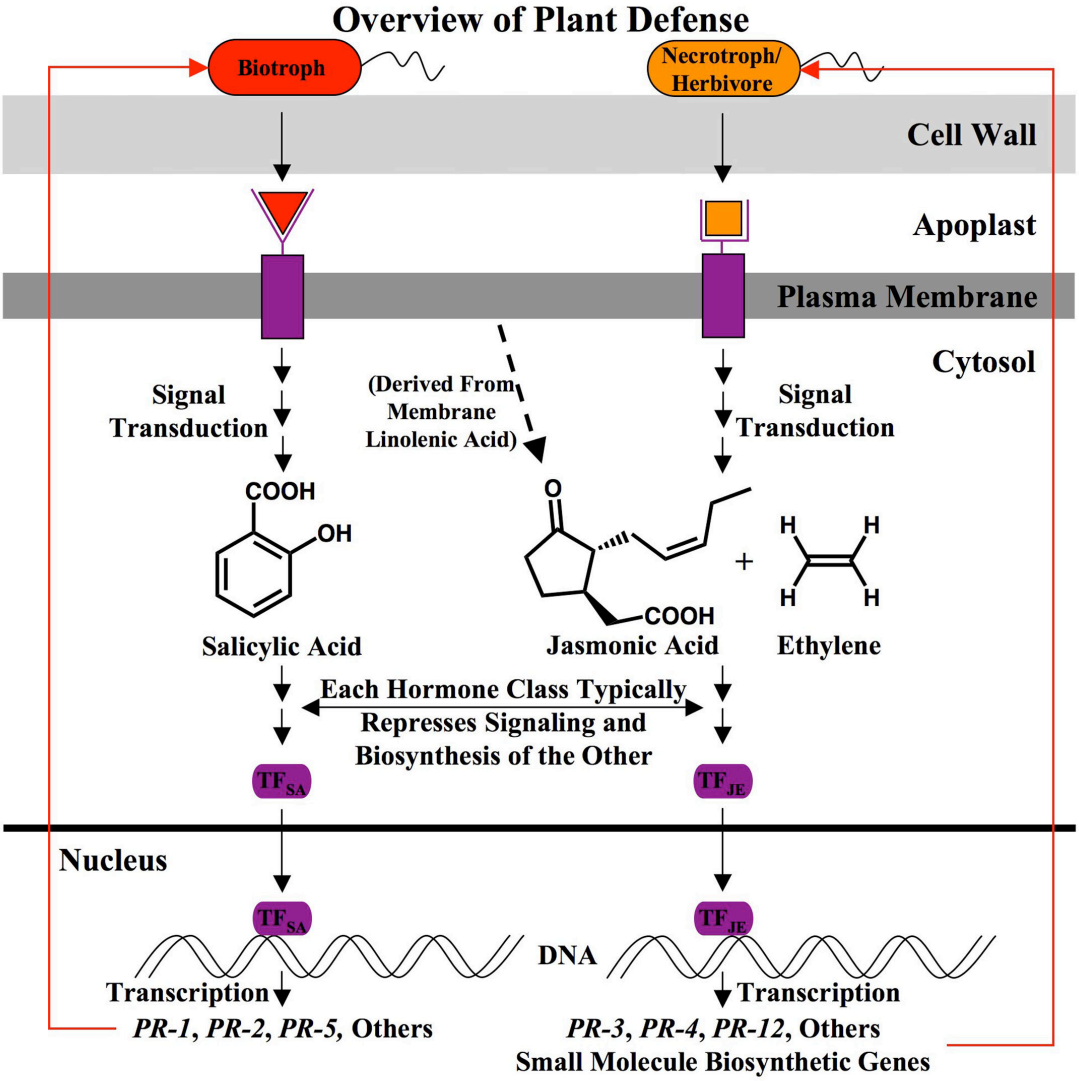

Figure 1.13 Simplified Overview of Plant Defense. An overview of plant defense against other organisms is given. Biotrophic pathogens (in red) and necrotrophic pathogens or herbivores (in orange) produce elicitors that bind to cognate receptors at the plasma membrane. This activates signal transduction pathways in the cytosol that result in hormone biosynthesis. Salicylic acid is produced in response to biotrophic pathogen attack, jasmonic acid and ethylene are produced in response to necrotrophic pathogen or herbivore attack, and typically each hormone class is mutually inhibitory to the other. Each hormone activates specific transcription factors that translocate to the nucleus and induce the transcription of defense genes. The protein products of these genes are active against the attacking organism, as indicated by the red arrows. Abbreviations used are: PR, Pathogenesis Related; TF_{SA}, Salicylic acid-responsive transcription factor; TF_{JE}, Jasmonic acid- and ethylene-responsive transcription factor.

(lipopolysaccharide) [156]. Most elicitors have been shown to bind their receptors with apparent dissociation constants in the low nanomolar to high picomolar range [157]. Receptor binding of the elicitor initiates a signal that is usually transduced by a cytoplasmic kinase, resulting in a phosphorylation cascade propagated by mitogen-activated protein kinases (MAPKs) that ultimately activates gene transcription in the nucleus (Figure 1.14). There are over 200 receptor-like kinases in the *Arabidopsis* genome – these possess kinase domains that transduce the signal directly – as well as many cytoplasmic Ca^{2+}- and GTP-dependent kinases that can interact with receptors to transduce the signal [158].

The MAPKs involved in initial defense signaling are believed to already be present in the cytosol, and they are known to induce gene transcription by phosphorylating – and thereby typically activating – specific transcription factors that can then migrate to the nucleus [158-160]. Within 30 minutes of elicitation, early defense genes are transcribed that encode plasma membrane receptors and transcription factors [18]. A complete MAPK cascade (Figure 1.14) has been elucidated in *Arabidopsis* that is activated by bacterial flagellin, and this induces genes for several WRKY transcription factors and a transmembrane receptor kinase [161]. WRKYs are a type of plant-specific zinc-finger transcription factor that are defined by the conserved amino acid sequence WRKYGQK at its amino-terminal end, and that bind specifically to a DNA sequence motif known as a W box (C/TTGACC/T) [162]. As numerous W boxes are frequently found in the promoters of genes involved in the SA-mediated defense response – including those of the *ICS1*, *NPR1*, and *PR-1* genes in *Arabidopsis* (see below) – WRKYs are believed to play a pivotal role in the regulation of these genes [163]. There are 72 genes encoding WRKYs in *Arabidopsis*, at least 49 of which are differentially regulated during the SA-dependent defense response; their combinatorial interactions with each other and with non-WRKY transcription factors can either activate or repress SA-dependent transcription, and WRKYs are known to play a key role in the antagonism between the JA- and SA-dependent defense responses [163]. However, many kinases and transcription factors are activated independently of these hormones: within 30 minutes of exposure to flagellin, no SA or JA production has yet occurred, but global transcriptional profiling indicates that at least 1100 *Arabidopsis* genes involved in basal defense have been induced, including 28 of the over 200 known receptor kinases needed for signaling the presence of increased numbers of pathogen, as well as a number of strongly expressed MAPKs and WRKYs [160, 164]. Flagellin and many other elicitors activate defense responses in both plants and animals, and the involvement of homologous receptor kinases and MAPKs in defense signal transduction suggests innate immunity in plants and animals likely evolved from a common ancestor [159].

Elevated levels of intracellular calcium, reactive oxygen species (ROS), and nitric oxide (NO) are also known to mediate defense responses in both plant and animal innate immunity, though plants possess the machinery for their defense in every cell, whereas animals generally have specialized effector cells [159]. Within 5 minutes of elicitation, changes in ion flux across the plant plasma membrane occur which are virtually simultaneous with the increase in MAPK phosphorylation activity [18, 156]. Though the mechanism for it is not well understood, elicitor binding to its cognate receptor promotes the opening of plasma membrane ion channels (Figure 1.14). These allow influx of protons and Ca^{2+} ions and efflux of K^+ and Cl^- ions, resulting in a net acidification of the cytoplasm. Ca^{2+} influx is regarded as particularly significant, as its cytoplasmic concentration spikes from a resting level of 50-100 nM to 1-5 μM upon elicitation (see [156], and Figure 1.14). Calcium is known to activate many plant kinases, and the presence of calmodulin-binding domains in one entire class of WRKY transcription factors suggests that

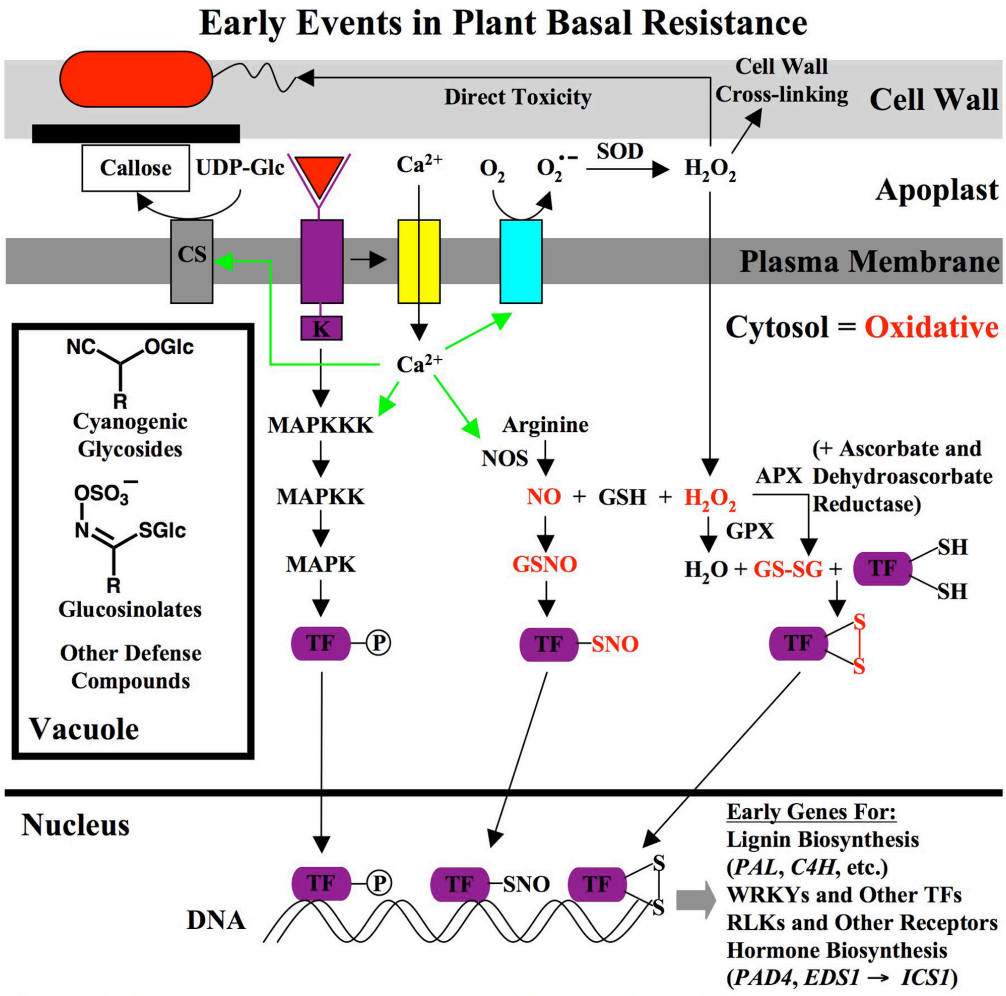

Figure 1.14 Early Events in Plant Basal Defense Against Biota. Early receptor binding, signal transduction, and gene transcription events are depicted, along with the vacuolar preformed defenses. Briefly, an invading microbe has produced an elicitor (both in red) bound to a RLK (purple) at the plasma membrane; this initiates a MAPK cascade, culminating in activation of a TF (in purple) by phosphorylation (the circled P). Receptor binding also activates Ca^{2+} import to the cytosol by ion channels (yellow); this Ca^{2+} activates (green arrows) MAPKs, NOS, NADPH oxidase (in light blue), and CS, the last of which forms a protective callose layer (black) at the site of biotic attack. TFs can also be activated by redox and nitrosylation mechanisms, both of which are mediated by GSH (oxidized molecules in red). Activated TFs translocate to the nucleus, where they bind to cognate promotors and activate specific genes. Detailed explanation of these processes is provided in the text. Abbreviations used are: RLK, Receptor-like kinase; TF, Transcription factor; MAPK, Mitogen-activated protein kinase; K, Kinase; Glc, Glucose; SOD, Superoxide dismutase; NOS, Nitric oxide synthase; GSH, Glutathione; GPX, Glutathione peroxidase; APX, Ascorbate peroxidase, CS, Callose synthase.

they may also respond to pathogen-triggered fluctuations of intracellular Ca^{2+} levels [163]. Deposition of cell wall-strengthening callose – a β-1,3-glucan – at the site of attack also commences within 30 minutes of elicitation due to activation of latent callose synthase by calcium (see [18, 165], and Figure 1.14). In addition, elevated calcium levels are required [166] for the oxidative burst, which is defined by a spike in the generation of ROS components superoxide ($O_2^{\bullet -}$) and hydrogen peroxide (H_2O_2) that is maximal at 30 minutes after elicitation [156].

The oxidative burst is initiated by plasma membrane NADPH oxidase, which forms superoxide by the one-electron reduction of O_2, and is activated by cytosolic calcium (see [167], and Figure 1.14) in the same manner as seen in vertebrate phagocytes and B-lymphocytes [168]. Superoxide dismutase (SOD) in the apoplast rapidly converts superoxide to H_2O_2 (Figure 1.14), which can reach concentrations of 1-3 μM in basal defense [169]. H_2O_2 is directly toxic to microbial invaders, and is also a substrate for the apoplastic peroxidases that catalyze oxidative cross-linking of proline-rich glycoproteins and lignin in the cell wall (Figure 1.14) beginning 2-5 minutes after elicitation [170]. However, unlike superoxide, H_2O_2 can also cross the plasma membrane and enter the cytoplasm, shifting the normal redox status of the cell to a more oxidative one. This cytosolic H_2O_2 is acted on by the enzymes glutathione peroxidase (GPX) and ascorbate peroxidase (APX), which catalyze redox reactions that increase the balance of cytosolic glutathione disulfide (GS-SG) over reduced glutathione (GSH) – APX requires a second enzyme (dehydroascorbate reductase) to replenish its ascorbate (or vitamin C) substrate – resulting in a corresponding increase in the disulfide content of specific proteins with newly-modified function [168, 171]. The activities of many proteins in plants are redox regulated in this manner [7, 171], including a number of MAPKs and transcription factors (Figure 1.14) activated by increases in cytosolic ROS [168].

Protein activity is also regulated in both plant and animal defense by reversible nitrosylation of specific cysteine thiols present in the correct sequence context, though the identity of the enzymes involved in nitroso transfer to and removal from protein targets are unknown [172]. An initial burst of NO in basal defense is stimulated by increased cytosolic Ca^{2+} [173], and reaches a maximal value of ~0.5 μM [174] at 30-45 minutes after elicitation [175]. NO is apparently synthesized in plants [176] – as in animals – from arginine by the enzyme NO synthase (NOS; Figure 1.14), though the gene originally assigned to this function has recently been found to be misannotated [177]. Reversible S-nitrosylation is another post-translational modification mediated by glutathione, which maintains an intracellular store of S-nitrosoglutathione (GSNO) that acts as an NO-donor in protein nitrosylation [173]. Consequently, GSNO reductase is an important enzyme in plant defense, as it attenuates NO signaling by reducing GSNO levels [175]; for example, loss of *Arabidopsis* GSNO reductase function compromised basal resistance against a type of powdery mildew pathogen [178]. Candidates for regulation by reversible S-nitrosylation in basal defense have been identified in *Arabidopsis*, and include an SOD, a GPX, a glutaredoxin, and number of transcription factors (see [179], and Figure 1.14). Protein kinases are also well-known targets for S-nitrosylation, and it is likely that those involved in defense-related signaling are regulated in this way [180].

Elicitation effects the transcription of defense-related genes by inducing or otherwise activating transcription factors as described above, and the identity of the specific genes activated depends upon the particular conditions of elicitation [7, 156]. Among the first genes to be induced – by all types of biotic stress – are those encoding the biosynthetic enzymes of the lignin-producing phenylpropanoid pathway (PAL, C4H, 4CL; see Figure 1.3), which usually

begin appearing 2-3 hours after the elicitation event [156, 181, 182]. However, the levels of various plant hormones determine the character of the defense response, mainly by mediating the induction of multiple *PR* genes [152]; thus, the initiation of a response appropriate to the attacking species involves varying degrees of transcriptional activation of hormone biosynthetic genes (Figure 1.13). The timing of the defense response to individual elicitors or whole organisms (which contain many different elicitors) is quite idiosyncratic among plant species, and there are as many examples of plant hormone biosynthesis being initiated in the first hour following elicitation as there are of it beginning as late as 6 hours after elicitation [183-185]. Once biosynthesis is commenced, hormone levels continue to accumulate for hours or days until threshold concentrations are reached, though these target concentrations are highly variable. For example, the hemibiotrophic pathogen *P. syringae* induces the accumulation of high levels of SA, JA, and ethylene (~2300 ng, 580 ng, and 500 nl per gram fresh weight of plant tissue, respectively) in *Arabidopsis* that are maximal about 24 hours after infection; the fungal necrotroph *Alternaria brassicicola* induces very little SA, more modest levels of JA, and far higher levels of ethylene, all of which are maximal several days after infection; and a variety of insect herbivores induce no SA, and levels of JA and ethylene that are maximal at wildly different time points – and all of these herbivore-induced hormone levels are present at levels far below those observed in pathogen infection [186]. The variable levels of each hormone determine the panel of *PR* genes that are induced, with genes encoding putative pore-forming proteins (PR-1 and PR-5) and β-1,3-glucanases (PR-2) induced readily by SA, and genes encoding chitinases (PR-3 and PR-4) and pore-forming peptides known as defensins (PR-12, which includes the well-studied defensin PDF1.2) induced mainly by JA and ethylene (see [187], and Figure 1.13). PR proteins have anti-microbial activity generally, but the various chitinases (PR-3, PR-4, PR-8, and PR-11) and protease inhibitors (PR-6) also target nematodes and herbivorous insects [152], and production of these PR proteins is known to form – in combination with elevated levels of lectins and α-amylase inhibitors – the backbone of the JA/ethylene-mediated response to insect herbivores [10]. Other important PR protein classes are proteases (PR-7), ribonucleases (PR-10), and lignin-forming peroxidases (PR-9) [152].

JA signaling is particularly important for the biosynthesis of defense-related molecules having activity against herbivores and necrotrophic pathogens (see Figure 1.13). JA-deficient *Arabidopsis* mutants fail to produce sufficient quantities of such molecules, and as a result are extremely susceptible to insect pests that do not normally consume *Arabidopsis* [188]. JA induces the transcription of genes involved in the production of well known plant natural products from many different plant species: the terpenoid insect toxins limonene, α-pinene, and pyrethric acid (Figure 1.1); other terpenoid toxins, like artemisin and taxol (not shown); the alkaloid animal toxins strychnine and morphine (Figure 1.2); other alkaloid toxins, like the indole alkaloid vinblastine, the isoquinoline alkaloid berberine, and nicotine (not shown); the indole bacterial toxin camalexin (Figure 1.2); the coumarin animal toxins coumarin, psoralen (Figure 1.3) and scopolin (Figure 1.9); the stilbene fungal toxin resveratrol (Figure 1.4); flavone signaling molecules like apigenin (Figure 1.5); isoflavone phytoestrogens like genistein (Figure 1.5); the isoflavonoid fungal toxin medicarpin (Figure 1.5); anthocyanins that act as microbial toxins (Figure 1.5); and many related compounds [156, 189-193]. Most of the molecules described above are distributed throughout the plant; some that exhibit anti-microbial activity, are lipophilic, and are localized at the site of infection are termed phytoalexins (from the above list are camalexin, resveratrol, medicarpin, and some anthocyanins). Phytoalexins have a wide range of structures [194], are concentrated to an extent proportional to their distance from the

infection site [18], and are generally believed to act – as camalexin does – by disrupting the integrity of microbial membranes [195]. It is unusual for phytoalexins – or any specialized metabolite – to be produced as part of the SA-mediated response to biotrophic pathogens, but there are examples of this [156, 194].

SA signaling activates basal defense responses that are mainly directed at biotrophic and hemibiotrophic pathogens. Though the principal function of the phenylpropanoid pathway in plant defense is to provide lignin precursors for cell wall strengthening (see Figure 1.3), it is possible that some SA is biosynthesized via this route [196, 197]. However, the majority of SA needed for plant defense against biotrophic pathogens – in *Arabidopsis*, as well as other plants (for example, tobacco and rice [183]) – is produced from isochorismate (Figure 1.12). Elevated levels of the *ICS1* transcript are observed 3 hours following either elicitation by flagellin or infection with a *P. syringae* strain that activates basal defense, and the resultant SA that begins to accumulate within 6 hours is absolutely required for basal defense [198]. The delay in the development of SA-mediated basal defense in *Arabidopsis* is caused in part by the need for accumulation of significant levels of the *EDS1* and *PAD4* gene products prior to *ICS1* induction and SA accumulation (Figure 1.14). Though the function of the *EDS1* and *PAD4* gene products is not known, they are homologous to known lipases, they physically interact with each other *in vivo*, and they are required for *ICS1* induction [155, 199].

Cytosolic SA is known to induce two waves of gene expression [200]. The first wave peaks 2-3 hours after treatment by exogenous SA (a substitute for induced SA biosynthesis, which occurs slowly when using the viral pathogen in this study; see [201]), and includes genes encoding glucosyl transferases – which glucosylate toxic small molecules like SA for vacuolar sequestration – and enzymes that protect the plant cell against oxidative stress (see [202], and Figure 1.15). SA also likely induces enzymes involved in callose deposition at this point, as SA from the isochorismate pathway is known to initiate the process during this same time frame (7-9 hours post infection; see [203]). The mechanism of this first wave of gene induction by SA is unknown, but the transient increase of ROS immediately after basal defenses are induced suggests a role for redox-regulated signaling by the formation of internal disulfide bonds in specific proteins. The activities of newly induced ROS-reducing enzymes – like SOD and catalase – are hypothesized to make the cytosol progressively more reducing over time [204], although it is believed that SA achieves a reducing redox balance partly by reacting directly – or via a transition metal-mediated process – with radical ROSs to form covalent adducts at positions *ortho-* and *para-* to the SA hydroxyl group (see [183], and Figure 1.15). Regardless of how the reducing environment is achieved, it activates a second wave of gene expression 12-16 hours after SA treatment [201]. Many defense genes – including most SA-induced *PR* genes – are induced in this wave in a process mediated by NPR1, a protein that is constitutively expressed and normally located in the cytosol as an inactive, disulfide-bound oligomer [205]. When the cytosol becomes sufficiently reducing, oligomeric NPR1 is reduced to active monomers that are able to translocate into the nucleus and activate gene expression (see [206], and Figure 1.15). Monomeric NPR1 does this by interacting with the constitutively expressed, nuclear TGA class of transcription factors to form an active complex. Several of these TGA factors have been shown to possess intramolecular disulfide bridges that must also be reduced in order to properly interact with NPR1 and fully activate transcription [207]. Redox activation of NPR1 and many TGA transcription factors is mediated by glutaredoxins and thioredoxins, at least one of which is actually induced by an NPR1-TGA complex [208]. Most SA-induced *PR* and defense-related

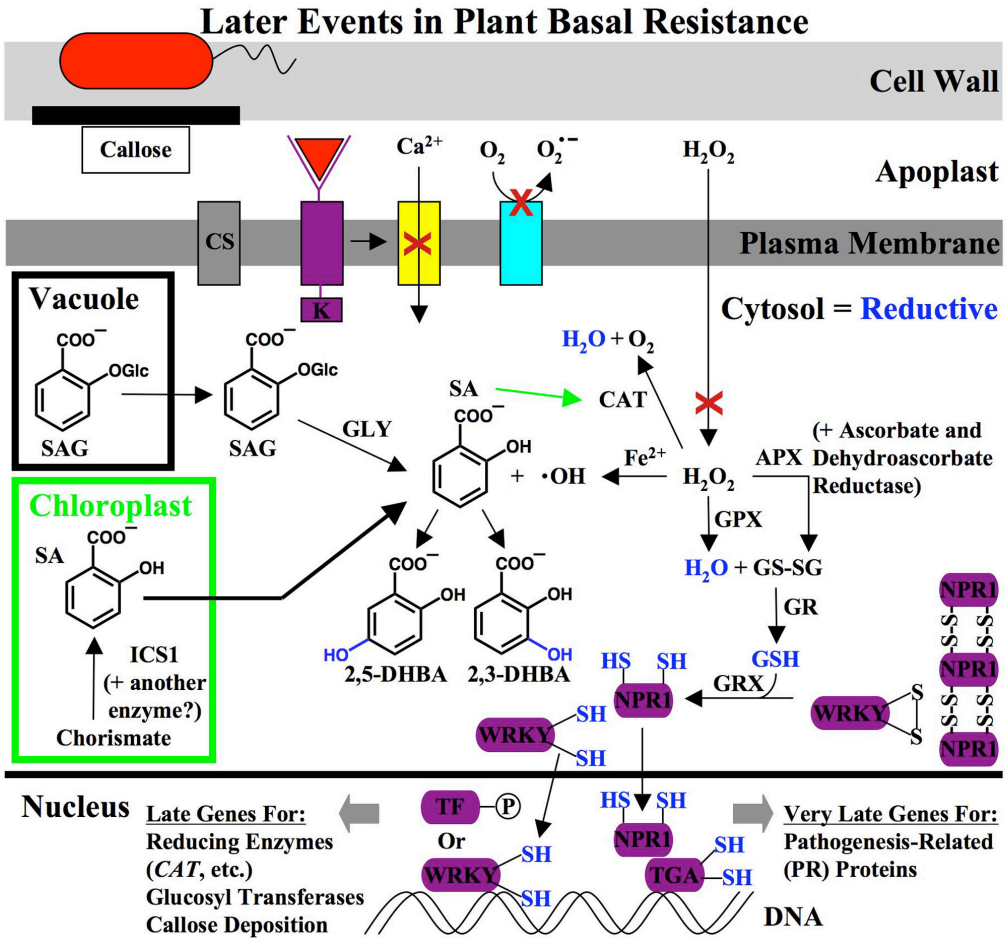

Figure 1.15 Late Events in Plant Basal Defense Against Biotrophs. Later events are depicted occurring after salicylic acid (SA) biosynthesis from SA 2-O-β-glucoside (SAG) stores in the vacuole, from the phenylpropanoid (PP) pathway in the cytosol, and from isochorismate synthse (ICS1) in the chloroplast (thick arrow indicates main pathway). The attacking biotroph and its bound elicitor (both in red) are no longer activating receptor (purple) signaling, Ca^{2+} import by ion channels (yellow), or NADPH oxidase-initiated (light blue) production of H_2O_2 (reduced molecules in dark blue). The cytosolic H_2O_2 formed during early signaling is reduced by recently-induced catalase (CAT), and the green arrow indicates CAT gene induction by SA. The enzymes ascorbate peroxidase (APX) and glutathione peroxidase (GPX) also contribute to H_2O_2 reduction, and SA itself reacts with hydroxyl radical formed via the Fenton reaction to form two different dihydroxybenzoic acids (DHBAs). Cytosolic stores of glutathione (GSH) are increased by the enzyme glutathione reductase (GR), and GSH is a substrate for glutaredoxin (GRX) reduction of transcription factors (TF). Reductively-activated TFs, including NPR1 and many WRKYs and other TFs, translocate to the nucleus, where they bind to cognate promotors and activate specific genes. Abbreviations used are: GLY, any operative glycosidase; K, Kinase; Glc, Glucose; CS, Callose synthase.

genes require NPR1 for activation (Figure 1.15), but there are examples of NPR1-independent *PR* gene activation [209].

Effector-Triggered Immunity in Plants. As plants and microbes co-evolved, certain microbes acquired the ability to deliver effector proteins – also known as avirulence (Avr) proteins – that suppress basal defenses in particular plant species, thereby easing the process of infection. Little is known about Avr proteins from fungi or oomycetes, but many bacterial Avr proteins have been characterized, including a number of proteases, transcription factors that alter resistance signaling, inhibitors of critical defense enzymes like callose synthase and MAPKs, inhibitors of elicitor recognition, and biosynthetic enzymes that produce inhibitory small molecules (see [158, 160], and Figure 1.16). A given Avr protein usually damages specific targets in only one or a few plant species. Bacterial pathogens secrete as many as 30 different Avr proteins per strain into the plant cytosol during infection, mostly via type III secretion systems [210]. In the course of plant-microbe co-evolution, plants responded by acquiring a highly specific resistance (*R*) gene for each Avr protein that threatened it, and the recognition of even one effector by its corresponding *R* gene product activates effector-triggered immunity (ETI), an accelerated and amplified form of the basal defense response [160]. Usually, *R* gene products activate ETI after the plant basal defense response is already underway [160], and pathogens that secrete an *Avr* gene product into a plant missing the complementary *R* gene continue the basal response without activating ETI, develop disease, and are referred to as virulent. *R* genes constitute one of the largest gene families in plants, and are of two main types. Some encode plasma membrane receptors from the same group as those involved in basal defense, and these activate ETI after directly sensing extracellular pathogen effectors [160]. A second, larger group encodes cytoplasmic surveillance proteins – of which there are over 150 in *Arabidopsis* – that activate ETI after detecting intracellular damage by pathogen effectors (see [160], and Figure 1.16). Both groups of R proteins signal the activation of genes by a process that is at least partly mediated by WRKY transcription factors, and at least one WRKY in *Arabidopsis* (AtWRKY52) is believed to function as an R protein [163]. The vast majority of *R* gene products are highly homologous to defense proteins from flies and mammals, possessing one of five possible domain architectures all containing carboxy-terminal leucine-rich repeats [158, 160, 211]. Though both necrotrophs and biotrophs make use of effector proteins in their pathogenesis, only biotrophs produce effectors that are recognized by R proteins and consequently activate ETI [160].

ETI involves enhanced operation of the mechanisms of basal defense, but differs from the basal response in that it also usually [160] activates the hypersensitive response (HR). HR deprives biotrophic pathogens of nutrients and restricts their spread by inducing programmed cell death in and around the infected cell, leaving the rest of the plant unaffected [10]. Though HR requires 1-2 days to effect complete cell death, its initiation must precede pathogen movement to be effective [7]. As a result, ETI is initiated by signaling agents in the cytosol immediately after R protein recognition of pathogen effector action; this usually occurs 1-3 hours after the initiation of basal defense [212]. Within several minutes of R protein activation, a second burst of intracellular Ca^{2+} takes place that is required for HR [213, 214] – it is of a similar magnitude (1-5 μM) to the first burst in basal defense (see Figure 1.14), but has a much longer duration (up to 2.5 h, indicated by thick green arrows in Figure 1.16). Elevated Ca^{2+} levels are in turn responsible for secondary bursts of ROS and NO that are also required for HR, although both must be of sustained duration to induce the transcriptional and translational events necessary for

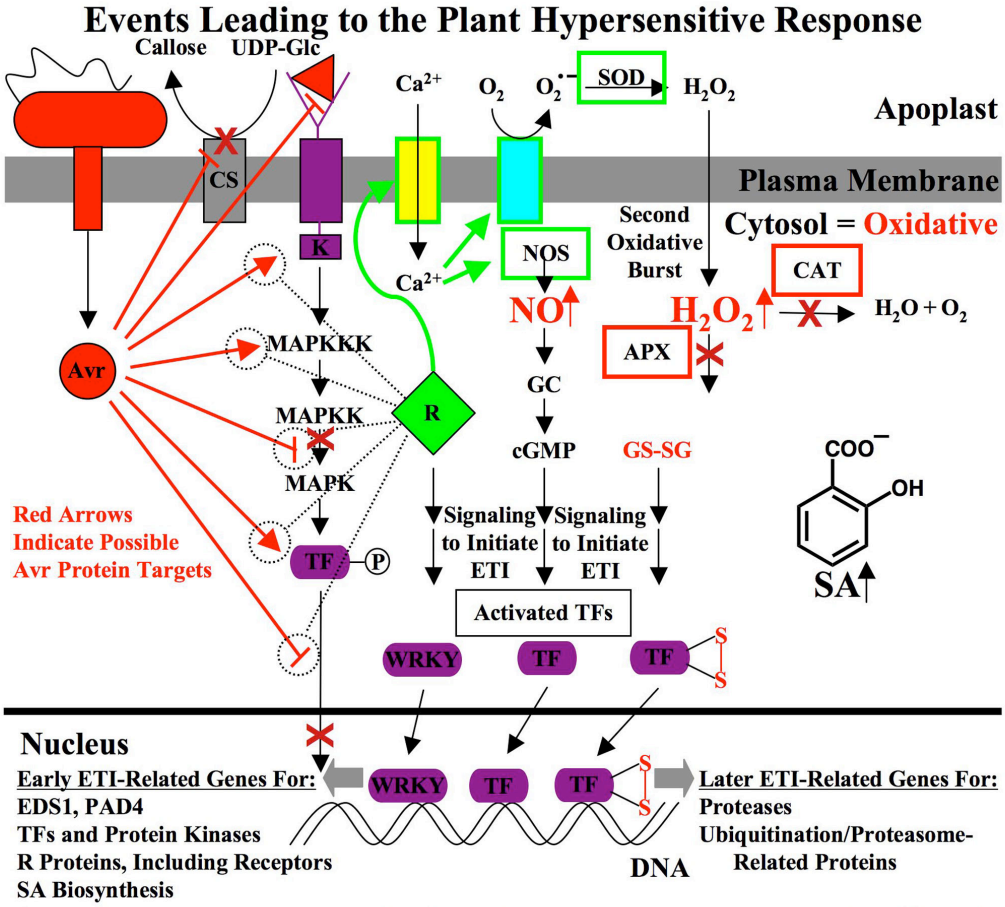

Figure 1.16 Events Leading to the Plant Hypersensitive Response. A given biotroph-secreted Avr protein (both in red) disrupts a specific basal defense process in the cytosol (possible targets indicated by dotted circles, red dashes for inhibition, red arrows for proteolysis, purple membrane protein is receptor). If a complementary R protein is present to detect Avr action (indicated by dotted line), it activates proteins involved in initiating the second burst of NO and H_2O_2 (indicated by green arrows, ion channels are yellow, NADPH oxidase is light blue). NO activates the enzyme guanylate cyclase (GC), which produces the signaling molecule cyclic GMP (cGMP). Signal transduction pathways activated by R proteins, and cGMP- and redox-dependent (oxidized molecules in red) processes, lead to early ETI-related gene induction mediated by WRKYs and various other transcription factors (TFs). SA biosynthesis (not shown) is dramatically upregulated by this signaling, and high SA levels further activate many proteins responsible for NO and H_2O_2 production (boxed in green). High NO and SA levels also directly inhibit (boxed in red) catalase (CAT) and ascorbate peroxidase (APX), elevating H_2O_2 levels and contributing to signal amplification (upward arrows indicate very high concentrations). Abbreviations used are: MAPK, Mitogen-activated protein kinase; K, Kinase; Glc, Glucose; CS, Callose synthase; SOD, Superoxide dismutase; NOS, NO synthase; GSH, Glutathione; SA, Salicylic acid; ETI, Effector-triggered immunity.

cell death [173, 215, 216]. The second oxidative burst is also NADPH oxidase-dependent, results in levels of H_2O_2 that are nearly ten-fold higher (up to 15 μM) than those observed in basal defense (Figure 1.16), and is sustained for up to 5 hours before slowly declining [168, 169]. The second burst of NO that accompanies it results in levels that are about four-fold higher (2.0 μM) than those seen in basal defense (Figure 1.16), and is also sustained at this level for hours [173, 174].

Within 15 minutes of activation of ETI, ROS and NO have induced a massive transcriptional reprogramming of the cell, with a set of new transcripts comprising 1% of the total cellular mRNA already identifiable [211]. The early ETI-related genes induced in *Arabidopsis* – which are required for HR development – are similar to the early genes induced in basal defense, and include those encoding a number of protein kinases [212], transcription factors of the WRKY family [163], EDS1 and PAD4 [155], at least one thioredoxin [217], and a GSNO reductase [218]. Another early event required for HR is the activation of guanylate cyclase by elevated NO levels (Figure 1.16) – this enzyme synthesizes the important signaling molecule cyclic GMP [219]. Direct R protein action, cyclic GMP, and kinases and transcription factors redox-activated by the highly oxidized state of the cytosol undergoing the second oxidative burst, all initiate signal transduction pathways that result in induction of genes for ubiquitination and proteasome operation, as well as a large number of proteases – these later genes are induced in *Arabidopsis* between 24 and 48 hours after initiation of ETI, and are those responsible for actually effecting cell death [220]. Though ROS and NO induce similar sets of genes in the infected cells of all plants undergoing HR, the detailed mechanisms of plant cell death are not known, and the morphology of HR development differs from one plant-pathogen interaction to another. For example, although two different *P. syringae* strains activate the same early HR-related genes within 4.5 hours of inoculation in tobacco, one strain induces plant plasma membrane discontinuity ~4.5 hours after inoculation and the other ~12 hours after inoculation; additionally, both processes proceed by different mechanisms [221]. The secondary bursts of NO and ROS also induce genes in cells adjacent to those undergoing the necrotic cell death of HR: superoxide and NO have been shown in oat to induce apoptotic cell death in bordering uninfected cells [222], and H_2O_2 is known to induce anti-oxidant proteins [7] and cell death-inhibitory signaling [223] in nearby cells not marked for death.

SA is a central component of the signal transduction pathway that leads to HR. Whereas a moderate amount of salicylate is generated in the basal defense responses to elicitation in tobacco cells (3 μg per gram fresh weight in 16 hours; see [224]) and infection with virulent (non-HR causing) bacteria in *Arabidopsis* leaves (up to 17 μg per gram fresh weight in 48 hours; see [225-227]), the total salicylate content in tobacco leaves inoculated with HR-inducing tobacco mosaic virus can reach much higher levels (up to up to 216 μg per gram fresh weight in 72 hours) – with the large majority located within 3.5 mm of the HR lesions [228]. The elevated salicylate levels associated with HR are part of several positive feedback loops that are responsible for the intensity of ETI. SA activates K^+ efflux [183], H^+ [183] and Ca^{2+} [229] influx, and ROS generation [169], by unknown mechanisms that involve interrelated plasma membrane channels and NADPH oxidase [230], as well as apoplastic SOD [231]; all signaling components activated by SA are framed in green in Figure 1.16. SA also contributes to the secondary oxidative burst by its suppression of the activity of the ROS-detoxifying enzymes APX and catalase (see [232-234], and Figure 1.16), and this suppression by SA is required for HR [235, 236]. The phenomenon of catalase inhibition by SA is one of the only effects of SA that has been biochemically characterized, and it appears to be universal in the plant kingdom,

having been observed in *Arabidopsis*, tobacco, tomato, cucumber, and many other species [183]. It has been speculated that the higher SA levels associated with R protein activation are a principal reason for ETI development, as very high concentrations of cytosolic SA are required to inhibit catalase and generate the secondary oxidative burst [183]. This then would differ markedly from the situation in the basal defense response, where much lower concentrations of SA can activate transcription of genes for ROS-detoxifying enzymes like catalase (see Figure 1.15).

The elevated levels of ROS in turn induce a dose-dependent increase in SA biosynthesis (see Figure 1.16). This in turn is responsible for the best-known type of signal amplification in ETI: progressive elevation of the levels of both H_2O_2 and SA, a condition necessary for HR development [169]. In general, the phenylpropanoid pathway is believed to produce a high proportion of the SA required for HR development (Figure 1.16), although examples exist of HR processes involving significant production of SA by AtICS1 (see [183, 197], and references therein). SA also induces NO production via NO synthase [237], and the resultant elevated NO levels initiate another signal amplification loop both indirectly – by inhibiting catalase and APX [238] – and directly – by activating cyclic GMP synthesis (see [239], and Figure 1.16). Signal amplification also results from SA enhancement of the expression of certain types of *R* genes [240], coupled with elevated SA biosynthesis resulting from action of these *R* gene products [140, 241]. EDS1 and PAD4, in addition to their role in activating SA biosynthesis in *Arabidopsis*, also activate HR by an unknown mechanism, and SA induction of the *EDS1* and *PAD4* genes has led to the proposal of a fourth signal amplification loop [155, 199].

Systemic Acquired Resistance. Most of the immediate defense response occurs where it is needed – in the infected tissue of the plant. However, within several days to a week after the initial infection by an HR-inducing pathogen, a systemic response affecting the entire plant is induced [242]. This systemic response to pathogen infection is known as systemic acquired resistance (SAR). SAR provides heightened resistance to a broad spectrum of microbial pathogens, and is long lasting – sometimes for the lifetime of the plant [243]. It is characterized in systemic tissue by elevated levels of SA and *PR* gene expression, with up-regulated *PR-1* expression in uninfected tissues serving as typical evidence of the establishment of SAR [244]. The concerted effects of all the induced *PR* gene products are believed to be principally responsible for the enhanced resistance to pathogens afforded by SAR, although about 300 other genes also exhibit altered expression during the time frame of SAR [243, 245]. Elevated SA levels in the uninfected tissue are absolutely required for SAR [246], and application of SA to uninfected tissue of many plants is sufficient to induce the *PR* genes involved in SAR [247]. The mechanism of SA activation of *PR* genes in SAR is very similar to that of basal resistance and ETI: approximately two hours after an initial oxidative burst as part of HR in pathogen-challenged *Arabidopsis* leaves, microbursts of ROS are initiated throughout the plant, AtICS1 is induced, SA is biosynthesized, and a gradual reduction in cellular redox balance takes place in uninfected tissue [248]. This leads to activation of NPR1 and transcription of the panel of *PR* genes needed for SAR (Figure 1.17; see also Figure 1.15). Though the dramatically up-regulated *PR* gene expression associated with SAR effectively protects the plant from most pathogens, it has deleterious effects on long-term plant viability. For example, some plant species undergoing SAR are much more vulnerable to insect herbivores than plants in which SAR has not been induced [249] – importantly, there is a different plant systemic defense against herbivore attack.

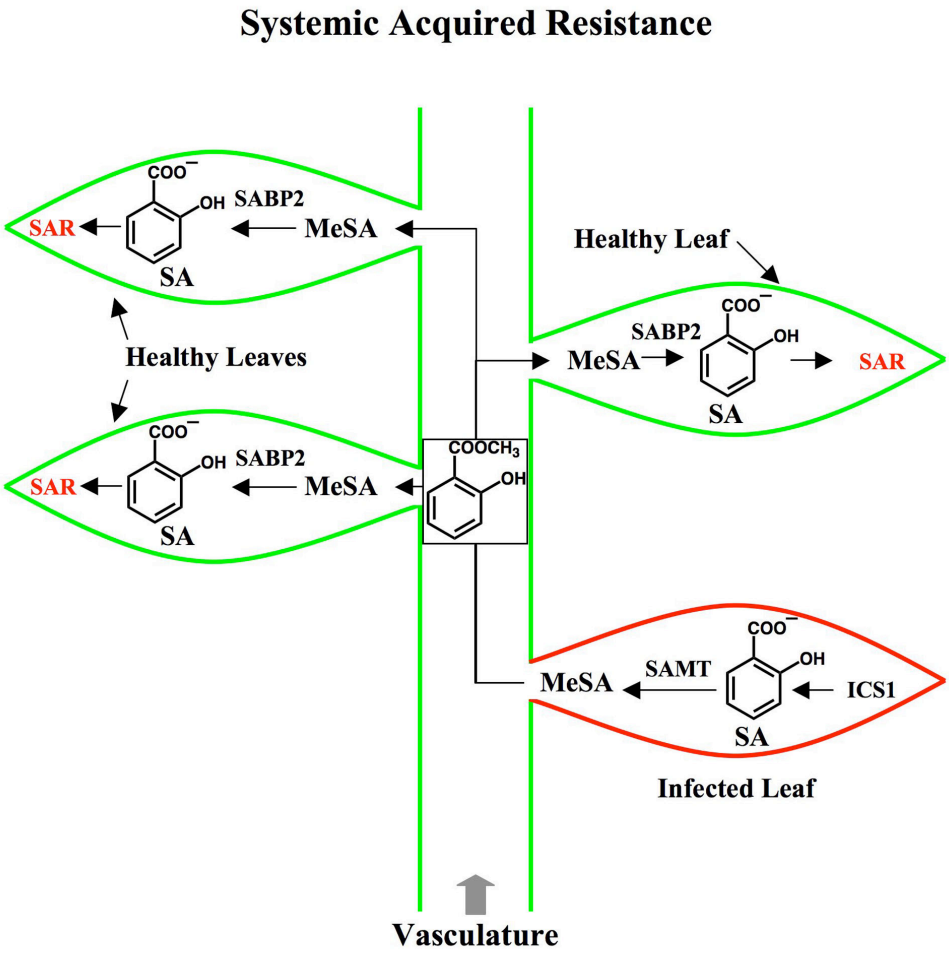

Figure 1.17 Development of Systemic Acquired Resistance. Isochorismate synthase from the chloroplast initiates the production of SA in the cells of infected leaves (in red). Cytosolic SAMT generates phloem-mobile MeSA. MeSA moves through the plant vasculature to uninfected leaves where it is taken up by healthy cells; however, to date this has only been established for tobacco [259]. Cytosolic SABP2 hydrolyzes MeSA to regenerate SA and establish SAR. Other signaling molecules are also transported through the phloem to help initiate SAR (not shown). SAR is established in healthy cells by SA in a process mediated by NPR1, and is characterized mainly by the increased production of PR proteins (not shown). Abbreviations used are: SA, Salicylic acid; MeSA, Methyl salicylate; SAMT, Salicylic acid methyl transferase; SABP2, Salicylic acid binding protein 2 (MeSA esterase); SAR, Systemic acquired resistance.

Also, SAR appears to exert a significant fitness cost due to ICS1-mediated depletion of chloroplast chorismate needed for lignin and aromatic amino acid biosyntheses.

Though it had long been known that SA induces SAR in all parts of the plant [250-252], the identity of the signal that is transported between infected and uninfected tissues – and thus activates SA production systemically – remained unknown. Within hours of the initial defense response, SAR is activated in tissues far from the site of attack by a signal that is transported at a rate of ~3 cm/h through the plant phloem [10]. Studies in tobacco mosaic virus-infected tobacco – showing that 69% of the SA accumulating systemically in plants undergoing SAR was generated by infected tissue [253], that total salicylate increased as much as 100-fold (up to 56 μM) in phloem sap prior to the development of SAR [232], and that the level of SA in infected leaves was directly proportional to the degree of SAR induction in uninfected leaves [254] – all suggested that SA was this phloem-mobile signal, but grafting studies determined that this was not the case [255]. Recently, the discovery that SAR development in tobacco requires both SA carboxyl methyl transferase (SAMT) enzyme activity [256] in the infected tissue, and MeSA esterase (known as SABP2) activity [257, 258] in the systemic tissue, led to the proposal that the SA derivative methyl salicylate (MeSA) is instead acting as this phloem-mobile signal [259]. In the proposed model for SAR development (Figure 1.17), infected plant tissue converts immobile SA into phloem-mobile MeSA by action of SAMT, the phloem transports the MeSA to uninfected tissue, and the uninfected tissue hydrolyzes biologically inert MeSA into SAR-activating SA by action of SABP2 [259]. In tobacco mosaic virus-infected tobacco, amounts of MeSA sufficient to establish SAR are generated, transmitted, and hydrolyzed between 48 and 72 hours after the primary infection [260]. Though the evidence for MeSA acting as a signal for SAR development is convincing, other phloem-mobile small molecules have also been implicated in this process, including one or more lipids [261], JA or one of its derivatives [262], a peptide [263], and azelaic acid (nonanedioic acid) [264]. The intermediacy of MeSA – as well as all these other potential components – in SAR development appears to be conserved across plant genera [265].

Plant Defense Against Abiotic Stress. Over the past few years, a more general role for SA as a mediator of diverse stress responses has been emerging. For example, in *Arabidopsis* SA is synthesized in response to abiotic stresses such as UV-C [266], ozone [267], cold [268], heat [269, 270], and osmotic stress due to high salt or other solutes [271]. SA has also been shown to play a role in stress-induced developmental transitions, including flowering [272] and senescence [273]. AtICS1 is known to be directly involved in most of these processes, and has been implicated in others – such as cold-tolerant growth. The mechanisms of SA-mediated defense against these diverse stresses are similar to those already described for defense against pathogens and herbivores [183]. Most abiotic stresses also lead to a burst of ROS that alters the cellular redox balance, and this in turn modulates transcription and protein function that is under redox control [171]. Whether the abiotic stress event initiates an oxidative burst for signaling or involves exposure of the cell to high levels of toxic ROS, ROS-detoxifying enzymes known to be inhibited by SA – like catalase and APX – are induced [183]. SA also induces heat shock proteins during heat stress, and anti-freeze proteins and small molecules during cold stress [183]. Some abiotic stresses are so damaging to the cell – for example, those associated with severe O_3 exposure – that they induce a cell death process similar to SA-mediated HR, though little is known about it [168]. Importantly, as in the case of pathogen defense, other hormones besides SA are often involved in the plant response to abiotic stress [183].

SALICYLATES IN MEDICINE

Salicylates as Human Therapeutic Agents. SA and its derivatives also display biological function in humans, most notably in the case of aspirin (2-acetoxybenzoate). SA and prodrugs that are metabolized to SA – like SAG, free and glucosylated MeSA, salicylaldehyde, and saligenin (2-hydroxybenzyl alcohol) – are the active components of willow (genus *Salix*, the root of the term salicylate), myrtle, poplar, and meadowsweet, all of which have been consumed for the relief of pain since the 15th century B.C. [7, 274]. The 19th century saw tremendous advances in the development of SA and its derivatives for medicinal use: salicin (glucosylated saligenin) was first isolated in pure form by Johann Buchner (1828), MeSA was first sold as a component of oil of wintergreen (1844), pure SA was first chemically synthesized (1858), an inexpensive synthesis of SA from phenol and CO_2 was developed by Hermann Kolbe (1860), SA was first commercially produced in pure form (1874), SA was first acetylated on a large scale by Felix Hoffman of Bayer and Co. in an attempt to minimize its bitterness and irritation to the stomach (1897), and this SA derivative was first marketed by Bayer as Aspirin and sold in tablet form (1899) [7, 275]. Aspirin has gone on to become by far the best-selling drug in history, with 100 million kg produced per year worldwide, equating to ~330 billion aspirin tablets of 300 mg each – a standard dose [276]. Aspirin is still widely used to treat colds, headaches, fevers, and rheumatoid arthritis, and as a preventative agent for heart attacks and cerebral thrombosis [7].

SA, SA derivatives like aspirin, and well-known pain medications like ibuprofin and naproxen, are all non-steroidal anti-inflammatory drugs (NSAIDs). The NSAIDs are generally planar and lipophilic small molecules, and unlike the narcotics – a group of pain medications that includes morphine and acts only on the central nervous system – NSAIDs have efficacy in all body tissues. NSAIDs act mainly by retarding the production of prostaglandins (PGs) and thromboxanes (TXs), two classes of mammalian hormones that induce inflammation, pain and fever in a variety of tissues. The treatment of inflammatory conditions like arthritis and gout requires relatively high doses of NSAIDs (4-8 g/day of aspirin) [276]. NSAIDs accumulate in the inflamed tissue of joints and tendons, where they inhibit leukocyte production of mediators of inflammation, including PGE_2, NO, ROS, cytokines like IL-1 and TNFα, and leukocyte adhesion molecules like ICAM-1; the reduced levels of these mediators prevent leukocyte adhesion to their receptors, limiting the inflammation inherent to the immune response [276]. More modest doses of NSAIDs (650-1950 mg/day of aspirin) are required for treatment of pain and fever [276]. NSAID activity for these indications is in part related to their anti-inflammatory activity in the peripheral nervous system, though they also limit production of additional inflammation and fever-promoting compounds throughout the nervous system – such as PGI_2 and neural peptides like substance P and bradykinin – as well as reduce turnover of endogenous pain-relieving compounds like noradrenaline and serotonin [276]. The restriction of PG biosynthesis in the gastrointestinal tract by high concentrations of the orally available NSAIDs is responsible for the well-known side effects of intestinal ulcers and hemorrhaging, as PGs are required for maintenance of the mucosal lining that prevents the gastrointestinal system from damage by strong stomach acid [276]. NSAIDs have also been implicated in the prevention of cancer and Alzheimer's disease, though by unknown mechanisms [276]. Aspirin alone among the NSAIDs prevents heart attacks and strokes when administered in doses of 75-100 mg/day [276]. Aspirin achieves this by retarding the thromboxane production in platelets needed for

platelet aggregation and blood clot formation [277]. Platelets are especially vulnerable to this inhibition by aspirin, as they have no nucleus and are unable to biosynthesize new protein.

A mechanism for the inhibition of platelet aggregation by aspirin – and for NSAID action in general – was elucidated in the 1970s, when it was shown that cyclooxygenases (COXs) are inhibited reversibly by most NSAIDs (see [278, 279]; Vane won the Nobel Prize in Physiology of Medicine in 1982 for this discovery), and irreversibly by aspirin acetylation of an active site serine residue [280]. COXs catalyze the first step in all PG and TX biosynthesis – the addition of two molecules of O_2 to unsaturated fatty acids like arachidonic acid. There are two main cyclooxygenases in humans: constitutively expressed COX-1, which synthesizes PGs and TXs for normal physiological functions like maintenance of the gastrointestinal mucosal lining and platelet aggregation, and inducible COX-2, which synthesizes PGs that mediate inflammation, pain, and fever [281, 282]. Though this inhibition is the only form operative on COX-1, NSAIDs were later shown to inhibit induction of the COX-2 gene as well [283], and this inhibitory mode is believed to play the greater role in the suppression of inflammation by NSAIDs. COX-2 gene transcription is mediated by NF-κB, a transcription factor that is normally sequestered in the cytoplasm by binding to the inhibitor IκB; disruption of this protein-protein interaction by targeted IκB degradation occurs normally in response to growth factors, cytokines and pathogenic elicitors, allowing NF-κB to translocate to the nucleus and activate COX-2, inducible NO synthase, and many other genes involved in inflammation and innate immunity. IκB is the principal target of NSAID action, as competitive inhibition of IκB kinase by the NSAIDs aspirin and SA [284] has been shown to prevent this enzyme from phosphorylating two specific serine residues on IκB that target it for degradation [285]. The finding that salicylates also shift the redox balance of the cytosol to a more reductive state by an unknown mechanism, coupled with the well-known activation of NF-κB by cytosolic ROS, has led to the hypothesis that salicylate-induced redox regulation of cytosolic enzymes is responsible for the maintenance of inactive cytosolic NF-κB [276].

Parallels Between Salicylate Action in Plants and Mammals. The effects of salicylates on innate immunity in plants and mammals have a number of parallels, suggesting that both immune responses may be inherited from a common ancestor [286]. Elicited plant cells and activated mammalian leukocytes both generate initial bursts of ROS. The introduction of salicylate by biosynthesis (in plants) or ingestion (in mammals) inhibits the levels of both of these defense signals. It is hypothesized that SA and its analogs react directly with the various radical ROSs to form covalent adducts [183, 276], and when ROS levels are low and SA levels relatively high, this phenomenon alone may be sufficient to restore a reductive redox balance to the cytosol in both plants and mammals. In addition, the main protein targets of salicylate action – NPR1 in plants and IκB in mammals – are homologous over a long region that includes the serine residues phosphorylated in IkB [287], though no evidence has yet been presented for NPR1 phosphorylation at these sites. Though NPR1 – unlike IκB – has long been known to translocate to the nucleus and activate gene transcription, more recent work has determined that cytosolic NPR1 plays a role in suppressing the JA response to necrotrophic pathogens and herbivores [288]. This is analogous to the situation in mammals, in which salicylates disrupt PG signaling by preventing their biosynthesis. JA and PGs are structurally quite similar, and are both derived from oxidative elaboration of unsaturated fatty acids from the plasma membrane. The evidence of a common evolutionary origin for the innate immune response in plants and

animals is to date largely circumstantial, though many of the mechanisms of their operation remain to be elucidated.

This thesis examines the function of plant ICS enzymes from a biochemical perspective. Although synthesis and regulation of the bacterial isochorismate pathways have been thoroughly investigated, there is limited knowledge regarding these enzymes, their products, and their functional roles in plants. Past biochemical characterizations of plant ICS enzymes utilized ICS (partially) purified from elicited cell suspension cultures of *Galium mollugo* L. [289, 290], *Rubia tinctorum* [291], and *Catharanthus roseus* [139], because these systems provided sufficient activity, protein, and product. Elicited cell suspension cultures have also been used to investigate the regulation of isochorismate-derived products such as anthraquinones produced by *Morinda citrifolia* [292]. However, these species were not genetically tractable, and thus detailed knowledge of the genes and enzymes involved in the synthesis of isochorismate-derived plant products has been limited. The cloning of the *ICS1* and *ICS2* genes from the model plant organism *Arabidopsis* [81] makes overexpression and isolation of these ICS enzymes much more feasible. Herein, I describe the purification of the AtICS1 and AtICS2 enzymes, as well as report characterizations designed to answer a number of questions about their functional role in plants. First, do these enzymes have the predicted enzyme activity, and if so, are they monofunctional ICSs or bifunctional SASs? If these enzymes are monofunctional, what might be the identity of the secondary IPL enzyme involved in SA production? Also, bacterial ICS enzymes achieve a rapid equilibrium between chorismate and isochorismate; if these plant enzymes are monofunctional, do they exhibit similar behavior, and what is the apparent equilibrium constant for the reaction? Can the active site residues involved in monofunctional ICS catalysis be mutagenized to generate a bifunctional SAS – or vice versa – and could this conversion be achieved post-transcriptionally or post-translationally? What are their K_M values for chorismate, and do these enzymes compete effectively with other chorismate-utilizing enzymes for available chorismate in the chloroplast? What are their K_M values for magnesium, and what biological conditions are these consistent with? Do these enzymes have any activity when other metal ions are substituted for magnesium, and if so, is the activity modulated? What pH and temperature profiles do these enzymes display, and what do they imply about the biological conditions under which they operate? It is expected that any conclusions drawn about ICS enzyme operation in *Arabidopsis* can be generalized to most – if not all – other plants. Indeed, the finding that stress-induced ICS1 is responsible for SA synthesis has already been confirmed for tomato (*Solanum lycopersicum* [293]) and *Nicotiana benthamiana* [294].

CHAPTER II

CHARACTERIZATION OF *ARABIDOPSIS* ICS1

PREFACE

The material presented herein was previously published in:

Strawn, M. A., Marr, S. K., Inoue, K., Inada, N., Zubieta, C., Wildermuth, M. C., *Arabidopsis isochorismate synthase functional in pathogen-induced salicylate biosynthesis exhibits properties consistent with a role in diverse stress responses*. Journal of Biological Chemistry, 2007. **282**(8): p. 5919-5933.

INTRODUCTION

Here, I focus on the enzymology of AtICS1 (At1g74710), a gene/enzyme required for pathogen-induced SA biosynthesis [81]. As mentioned in Chapter 1, SA is best known for its role as a key regulator of plant defense against pathogens. It accumulates primarily as a glucose conjugate (SAG) in response to viral, bacterial, and fungal pathogens [140] and is required for the induction of hundreds of defense-related genes (*e.g.* pathogenesis-related *PR-1*), and the establishment of local and systemic acquired resistance responses [140, 243]. In *A. thaliana*, null mutations in the *AtICS1* gene abrogated induced SA and SAG accumulation and associated defensive responses [81, 148, 149].

Despite the importance of SA, our understanding of the underlying enzymology of its production is very limited. As a complement to my work, other members of the Wildermuth lab showed via immunofluorescence that AtICS1 is localized to the chloroplast stroma *in planta* [82]. In addition, in collaboration with the Wildermuth lab, Dr. Kentaro Inoue (UC Davis) showed that AtICS1 is imported into the chloroplast with the mature protein residing in the stroma [82]. These results are consistent with the presence of a putative chloroplast transit peptide in the gene sequence of *AtICS1*, as well as the requirement that AtICS1 be physically present at the subcellular location where most of its substrate chorismate is biosynthesized. Here, I have undertaken experiments to fill this knowledge gap and present the first biochemical characterization of a plant ICS enzyme involved in SA biosynthesis – AtICS1 – including quantitative assessment of its kinetic parameters. This is particularly critical, because past biochemical studies neither measured nor accounted for the fact that ICS enzymes typically operate near equilibrium. Here I address this reversibility directly, and specify kinetic and thermodynamic properties for a plant ICS. Detailed knowledge of the nature of the ICS reaction and the strength of its binding to chorismate, as well as its subcellular localization, allows us to (1) examine positive selection for monofunctional ICS versus bifunctional SAS enzymes in higher plants, (2) assess the influence of environmental factors such as light and temperature on AtICS1 activity, SA biosynthesis, and function, and (3) understand controls over chorismate partitioning and utilization.

Arabidopsis contains multiple genes encoding the chorismate-utilizing enzymes chorismate mutase (including AtCM1, AtCM2, and AtCM3) [66, 67], anthranilate synthase (*e.g.* α subunits AtASA1 and AtASA2, and β subunits AtASB1 and AtASB2) [68], and ICS (AtICS1 and AtICS2) [81]. Although some of these genes are constitutively expressed, a subset, including *AtICS1*, *AtCM1*, and *AtASA1*, is induced in response to pathogen treatment [66-68, 81]; therefore, knowledge of the biochemical properties of AtICS1 allows one to assess its ability to successfully compete for available chorismate. Because it is estimated that 20% of carbon fixed by plants flows through the shikimate pathway to chorismate under normal growth conditions (see Figure 1.6), with the bulk of this carbon utilized in the synthesis of specialized metabolites [37], detailed knowledge of these controls is essential to our understanding of plant fitness.

MATERIALS AND METHODS

Materials and General Protocols

All specialty reagents and chemicals were obtained from Sigma-Aldrich unless otherwise specified. HPLC-grade solvents (EMD Biosciences) were employed in the HPLC analyses.

Chorismic acid (Sigma C-1761, ≥80% purity) was used in all assays with the following exceptions: Barium chorismate (Sigma C-1259, 60-80% purity) was used to assess recombinant AtICS1 activity during overexpression and purification, and for determining the temperature-dependence of AtICS1 activity. For selection and growth of transformed cells (described below): pBAD33 derivatives were selected with 30 μg/ml chloramphenicol; pET-28 derivatives were selected with 50 μg/ml kanamycin; and pME3368 was selected with 100 μg/ml ampicillin. Commonly utilized protein and molecular biological reagents and protocols were prepared/performed as in *Current Protocols in Molecular Biology* [295]. Independent replicate experiments were performed for all experiments described in the Results section, with similar findings.

Expression and Purification of Recombinant AtICS1

The construct pSM157-16 (obtained from Dr. Sharon Marr) is a pET-28 derivative containing a sequence encoding an amino-terminal His_6-tag fused to the sequence beginning with that encoding amino acid 48 of the *Aradibopsis thaliana* ICS1 coding region. The pSM157-16 AtICS1 coding sequence was confirmed to be identical to AtICS1 sequence AY056055 (At1g74710.1). *E. coli* Rosetta2 (DE3) cells (Novagen) were transformed with these plasmids. Crude cell extracts were prepared from a 2 L culture of transformed cells in TB media containing 0.2% glucose, 50 μg/ml kanamycin and 30 μg/ml chloramphenicol. Cultures were grown at 37 °C to mid-log phase, 0.2 mM isopropyl-β-D-thiogalactopyranoside (IPTG) was added to induce His_6-AtICS1 synthesis (hereafter referred to as AtICS1), and cells were harvested after 18 hours at 21 °C (~30 g wet weight) and resuspended in 150 ml of buffer A (20 mM sodium phosphate buffer, pH 7.4, 500 mM sodium chloride, 10% glycerol) containing 1 mM dithiothreitol (DTT), 2 mM phenylmethanesulfonyl fluoride (PMSF), 5 μM leupeptin, 10 μg/ml DNase and 1% Triton X-100. The cells, which could be stored at –20 °C, were lysed by two passages through a French press at 18000 psi. Following centrifugation, the supernatant was filtered by syringe through an HPF Millex-HV 0.45 μm filter unit attached in series to a Millex-AP prefilter (Millipore). Filtrate was applied to a 1 ml HisTrap HP nickel affinity column (Amersham Biosciences) at a flow rate of 1.0 ml/min by use of a ÄKTA fast protein liquid chromatography system (Amersham Biosciences). After washing the column with 10 ml of buffer A, AtICS1 was eluted with 40 ml of a linear gradient from 0% to 15% at a flow rate of 1.0 ml/min of buffer A containing 500 mM imidazole. Fractions containing ICS activity were pooled and concentrated using an Amicon Ultra-15 (10 kDa molecular mass cutoff) ultrafiltration device (Millipore) to a final volume of 900 μl. The pooled solution was applied to a HiPrep 16/60 Sephacryl S-200 High Resolution gel filtration column (Amersham Biosciences) previously equilibrated with 200 ml of buffer B (50 mM sodium phosphate buffer, pH 8.0, 150 mM sodium chloride, 10% glycerol and 1 mM DTT). The enzyme was eluted at a flow rate of 1.0 ml/min as a broad peak with 60 ml of buffer B. Fractions containing ICS activity were pooled and concentrated as before to a final volume of 2 ml. The concentrate was dialyzed overnight into buffer C (100 mM Tris buffer, pH 7.7, 10% glycerol and 1 mM DTT) with or without 10 mM $MgCl_2$ as desired. The protein was aliquoted and stored at –80 °C. All further characterization was performed on the mature AtICS1 (without the chloroplast transit sequence) recombinant purified protein.

Determination of Protein Concentration

Protein concentrations were determined by the method of Bradford, modified for use in a 96-well plate format with Coomassie Blue G-250 (EM Biosciences) and analyzed using a

Spectramax Plus microplate spectrophotometer (Molecular Devices). 200 µl of Coomassie stain per well [295] was mixed with 20 µl of sample and allowed to stand for 10 minutes before analysis at 595 nm with a Spectramax Plus microplate spectrophotometer (Molecular Devices), using distilled water as a cuvette reference. Bovine serum albumin was used as the standard.

Protein Molecular Mass Estimation

The subunit molecular mass of AtICS1 was estimated by SDS-PAGE in a 10% gel with Precision Plus unstained protein standards (Bio-Rad). The native molecular mass was estimated by gel filtration chromatography on a HiPrep 16/60 Sephacryl S-200 High Resolution column in buffer B (above) at a flow rate of 1.0 ml/min, using thyroglobulin (670 kDa), γ-globulin (158 kDa), ovalbumin (44 kDa), myoglobin (17 kDa), and Vitamin B-12 (1.35 kDa) as markers (Bio-Rad Gel Filtration Standards). The apparent molecular mass of AtICS1 was determined from a plot of the elution volumes against the logarithm of the molecular masses. This experiment was performed two times, each time using protein purified from two different cultures. Each set of results was similar to the other.

Isochorismate Synthase Activity Assays

An HPLC isochorismate synthase activity assay was modified from [139] as described below. 40 µl of substrate solution (2 mM chorismic acid in buffer D: 100 mM Tris, pH 7.7, 10% glycerol, 10 mM $MgCl_2$, 1 mM DTT) was added to 40 µl of a 220 µg/ml solution of AtICS1 in buffer D, incubated for 60 minutes at 30 °C, immediately filtered through a 0.2 µm Millex-LG syringe filter (Millipore), and a 50 µl aliquot was injected into a Shimadzu SCL-10AVP series HPLC system equipped with a Shimadzu SPD-10AVP photodiode array detector and a Shimadzu RF-10AXL fluorescence detector. A 5 µm, 15 cm × 4.6 mm inner diameter Supelcosil LC-ABZPlus column (Supelco) preceded by a LC-ABZPlus guard column was maintained at 27 °C, and had previously been equilibrated in 15% acetonitrile with 25 mM potassium phosphate buffer, pH 2.5. All flow rates were at 1.0 ml/min. The elution program began with an isocratic flow of 15% acetonitrile with 25 mM potassium phosphate buffer, pH 2.5, for 1 minute, followed by a linear increase to 20% acetonitrile over 7 minutes. Prior to injecting subsequent samples, a linear decrease to 15% acetonitrile over 2 minutes was undertaken, followed by reequilibration at 15% acetonitrile for at least 5 minutes. Under these conditions, isochorismic acid eluted (A_{280}) at approximately 3.4 minutes and chorismic acid (A_{280}) at 4.2 minutes. The calibration curve for chorismic acid is as follows: $y = 0.00386319\ x - 11.2600$ with $R^2 > 0.999$, where x = area units and y = chorismic acid in nanograms.

A coupled HPLC isochorismate synthase activity assay was modified from [296] as described below. 437.5 µl of a solution of AtICS1 (3.8 µg/ml) and excess recombinant PchB (218 µg/ml) in buffer E (100 mM potassium phosphate buffer, pH 7.0, 15 mM $MgCl_2$, 10% glycerol and 1 mM DTT) was mixed with 62.5 µl of substrate solution (4 mM chorismic acid in buffer E) and incubated for 60 minutes at 30 °C. The reaction was filtered as above, and a 50 µl aliquot was injected into the HPLC system equipped with column described above. All flow rates were at 1.0 ml/min. The elution program began with an isocratic flow of 15% acetonitrile with 25 mM potassium phosphate buffer, pH 2.5, for 1 minute, followed by a linear increase to 20% acetonitrile over 5 minutes, isocratic flow at 20% for 10 minutes, a linear increase from 20 to 55% acetonitrile over 17.5 minutes, a linear increase from 55 to 66% over 5 minutes, and an isocratic flow at 66% for 1.5 minutes. Prior to injecting subsequent samples, a linear decrease to 15% acetonitrile over 5 minutes was undertaken, followed by reequilibration at 15% acetonitrile

for at least 5 minutes. This program allowed for the detection of isochorismic acid (A_{280}, 3.7 min), chorismic acid (A_{280}, 4.9 min), and salicylic acid (ex 305nm/em 407nm, 22.9 min). The calibration curve was: $y = 0.000231406\ x - 2.81054$ with $R^2 = 0.999$, where x = area units and y = nanograms of salicylic acid. Salicylic acid (S-5922, Sigma ultrapure) was used for all calibrations.

A coupled continuous spectrophotometric assay for ICS activity was performed as described in Appendix 2, but substituting AtICS1 for EntC and making several modifications described below. The ICS reaction rate was measured by coupling excess amounts of isochorismate pyruvate lyase (recombinant PchB) and L-lactic dehydrogenase (LDH). Dilution series of AtICS1 were performed to establish the linear range for this assay (to ~25 μg/ml recombinant, purified AtICS1) and my standard assay conditions (10 μg/ml recombinant purified AtICS1). Velocity was linear with time (following an initial lag) for >15 min with 10 μg/ml AtICS1. Unless otherwise indicated, the 200 μl per well assay volume contained 0.2 mM NADH, 0.833 μg/ml LDH, 32.0 μg/ml recombinant PchB, 10.0 μg/ml AtICS1 and 2 mM chorismic acid in buffer D. The reaction was initiated by addition of the chorismic acid to the reaction mixture in a 96-well plate preheated to 30 °C, and analyzed using a Spectramax Plus microplate spectrophotometer (Molecular Devices). The change in absorbance at 340 nm was measured in each well in increments of 30 or 60 seconds and monitored for at least 30 minutes. The initial reaction rate in each well was assessed for a 5-10 minute period approximately 7-20 minutes after initiation of the reaction, depending upon manual confirmation of the linear range of reaction, and it was calculated using least squares fitting of each curve. An extinction coefficient for NADH of 6220 M^{-1} cm^{-1} was used for conversion of these values to units of μM/min.

Determination of the Apparent K_{eq} using ^1H NMR

My protocol is similar to that previously used with *E. coli* EntC [55]. The spectrum of the equilibrium mixture of chorismic acid and isochorismic acid was acquired as follows: 500 μl of a 220 μg solution of AtICS1 was exchanged into D_2O buffer containing 50 mM potassium phosphate, pD 7.5, and 5 mM $MgCl_2$, was incubated with 500 μl of chorismic acid solution (2 mM in the above D_2O buffer) at 30 °C for 60 minutes. HPLC analyses of successive aliquots confirmed the reaction was at equilibrium. ^1H NMR spectra for a 900 μl aliquot were recorded using a 500-MHz Bruker DRX-500 spectrometer. Spectra were scanned every 8 seconds for a total period of 9 hours each. The ratio between chorismic acid and isochorismic acid was determined by integration of the two peaks most downfield in the spectrum (the C2 protons). The chorismate spectrum was obtained with chorismic acid in the above D_2O buffer. This experiment was performed two times, each time using protein purified from two different cultures. Each set of results was similar to the other.

Apparent K_M Determination for Chorismate

The coupled continuous spectrophotometric isochorismate synthase assay was modified by using working chorismic acid concentrations of 1.5 mM, 1.0 mM, 750 μM, 500 μM, 400 μM, 300 μM, 250 μM, 225 μM, 200 μM, 180 μM, 160 μM, 133 μM, 100 μM, 80 μM, 40 μM and 20 μM. The reaction was initiated by the addition of chorismic acid. Reactions without AtICS1 were used as blanks. As per standard protocol, triplicate samples were run for each condition. Initial velocity data were fitted to the equation of Hanes to determine kinetic parameters [297]. To determine the effective chorismate concentrations in the above assay, I assessed the non-

productive conversion of chorismate to prephenate by PchB in parallel as described in Appendix 2. The correction for chorismate content after 15 minutes that was determined in Appendix 2 was used in the revised K_M determination, as kinetic data had originally been obtained from reaction progress curves at about 15 minutes elapsed reaction time. This experiment was performed two times, each time using protein purified from two different cultures. Each set of results was similar to the other.

Effect of Mg^{2+} on Isochorismate Synthase Activity

The coupled continuous spectrophotometric ICS assay was modified by using buffer C (no Mg^{2+}) supplemented with $MgCl_2$ at the following working concentrations: 15 mM, 10 mM, 5 mM, 3 mM, 2 mM, 1 mM, 800 μM, 650 μM, 500 μM, 200 μM, 100 μM, 80 μM, 50 μM, 20 μM, 10 μM, 5 μM, and 0 μM. Reactions were performed in triplicate and reactions without AtICS1 were used as blanks. Note that neither IPL [298] nor LDH activities are impacted by changes in the Mg^{2+} concentration. Initial velocity data were fitted to the equation of Hanes to determine kinetic parameters [297]. This experiment was performed two times, each time using protein purified from two different cultures. Each set of results was similar to the other.

Effect of Other Metals on Isochorismate Synthase Activity

The coupled continuous spectrophotometric ICS assay was modified by substitution of other divalent metals for Mg^{2+}. As above, buffer C was used and a working concentration of 10 mM, 1 mM and 0.1 mM of each of the following divalent metals was substituted: $CaCl_2$, $BaCl_2$, $MnCl_2$, $ZnCl_2$ and $CdCl_2$. Each reaction was performed in triplicate. Reactions without AtICS1 were used as blanks. Reactions containing no added metal ion were also included. IPL activity is reported to be unaffected by divalent cations [296]. However, L-lactic dehydrogenase (Sigma L-1254, rabbit muscle) activity may be inhibited by heavy metals such as Hg^{2+} and Pb^{2+} (Sigma-Aldrich Technical Service). Therefore, I repeated the metal experiments using 1 mM of the divalent metal ion and the HPLC ICS assay, which directly measures the conversion of chorismic acid to isochorismic acid. For metals with significant absorbance at 340 nm, I exclusively employed the HPLC ICS assay. Buffer C was substituted for buffer D and the reactions were supplemented with each of the following metals: $FeCl_2$, $FeCl_3$, $CoCl_2$, $NiCl_2$, or $CuCl_2$. Working concentrations of 10 mM, 1 mM and 0.1 mM of each of the above metals were used in the reactions. This experiment was performed two times, each time using protein purified from two different cultures. Each set of results was similar to the other.

pH Profile of Isochorismate Synthase Activity

The HPLC assay for isochorismate synthase activity was modified by alteration of the pH of the reaction buffer. 40 μl of a 100 mM buffered solution containing 220 μg/ml AtICS1 was mixed with 40 μl of a 2 mM solution of chorismic acid in the same buffer. Buffer solutions utilized 100 mM 2-(N-Morpholino)ethanesulfonic acid (MES) at pH 5.0, 5.5, 6.0, and 6.5, 3-(N-Morpholino)propanesulfonic acid (MOPS) at pH 7.0 and 7.5, 2-Amino-2-(hydroxymethyl)-1,3-propanediol (Tris) at pH 7.5, 7.7, 8.0, and 8.5, 2-(Cyclohexylamino)ethanesulfonic acid (CHES) at pH 9.0, 9.5, and 10.0, or 2-(Cyclohexylamino)propanesulfonic acid (CAPS) at pH 11.0. All of the above buffers are used as substitutes for the standard buffering agent in buffer D (100 mM Tris, pH 7.7). Reactions were performed in triplicate for 60 minutes at 30 °C, with results reported for the formation of isochorismate. Reactions without AtICS1 were used as controls (to be subtracted from results with enzyme), although I observed no non-enzymatic production of

isochorismate. This experiment was performed two times, each time using protein purified from two different cultures. Each set of results was similar to the other.

Temperature Profile of Isochorismate Synthase Activity

The HPLC assay for isochorismate synthase activity was modified by alteration of the temperature at which the reaction was incubated. Reactions were performed in triplicate incubating for 60 minutes at each of the following temperatures: 4 °C, 15 °C, 23 °C, 30 °C, 37 °C, 44 °C, 51 °C, 60 °C and 70 °C. Results are reported for the formation of isochorismate. Non-enzymatic production of isochorismate was not observed. At 51 °C and above, there was some decomposition of chorismate (to products other than isochorismate); however, the chorismate concentration was never limiting. This experiment was performed two times, each time using protein purified from two different cultures. Each set of results was similar to the other.

Non-enzymatic Synthesis of SA from Isochorismate

Isochorismate was produced enzymatically by the conversion of chorismate to isochorismate via ICS (purified recombinant Eco EntC), and purified as in [299]. Isochorismate was incubated in solution (37 μM isochorismate, pH 7.5, 3 mM $MgCl_2$, 23 °C) for 1 hour, 3 hours, and 6 hours, and chorismate, isochorismate, and salicylate were quantified by HPLC using the normal and the coupled HPLC ICS assays described above. Incubations were performed in triplicate with the conversion rate of isochorismate to salicylate (μM SA/hr) as the slope of SA production with time ($y = 0.036x + 1.40$; $R^2 = 0.999$).

ADIC Formation in the Presence of Ammonium Ion

An HPLC isochorismate synthase activity assay was modified from [59] to quantify ADIC formation as described below. 150 μl of substrate solution (2 mM chorismic acid) was added to 150 μl of a 220 μg/ml solution of AtICS1, in parallel, in several different media. All media contained 100 mM Tris, pH 7.7, 10% glycerol, and 10 mM $MgCl_2$, but one had no additives, and the others contained one each of the following reagents: 5 mM glutamate, 5 mM glutamine, or 50 mM ammonium sulfate. All four reactions were incubated for 30 minutes at 30 °C, immediately filtered through a 0.2 μm Millex-LG syringe filter (Millipore), and a 50 μl aliquot was injected into the HPLC system equipped with column described above. The elution program was the same as for the coupled HPLC ICS activity assay described above. Under these conditions, ADIC eluted at approximately 2.3 minutes (A_{280}), isochorismate (A_{280}) at 3.5 minutes, and chorismate (A_{280}) at 4.4 minutes. ADIC concentration was determined by using an extinction coefficient of 11,500 M^{-1} cm^{-1} at 280 nm [300].

RESULTS

AtICS1 was overexpressed and purified. In order to assess AtICS1 biochemical activity, I overexpressed amino-terminal His_6-tagged mature AtICS1 (without the chloroplast transit sequence) in *E. coli* and purified the soluble induced protein using Ni^{2+}-nitrilotriacetic acid (Ni^{2+}-NTA) and size-exclusion chromatographies. The gene for this recombinant protein is under the control of a T7 promoter in a pET-28 construct (Figure 2.1), and is overexpressed to up to 50% of total cellular protein when IPTG is added to initiate expression of T7 polymerase in

Composition of the pSM157-16 Construct

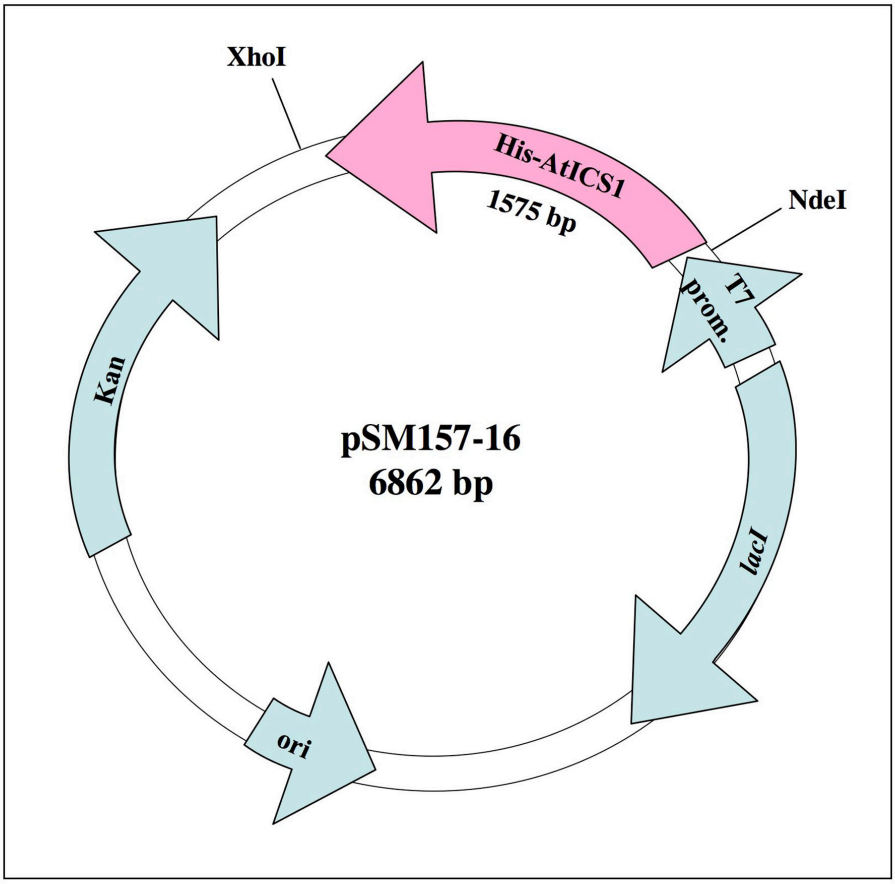

Figure 2.1. Composition of the pSM157-16 Construct. The construct is a pET-28c derivative in which AtICS1 has been inserted into the NdeI/XhoI segment of the multiple cloning sequence. Abbreviations used are: Kan, Kanamycin resistance gene, ori, origin of replication; *lacI*, *lac* repressor gene; T7 prom., the T7 promoter, His-AtICS1, the ICS enzyme being overexpressed.

the BL-21 (DE3) strain that contains it. Purification by Ni^{2+}-NTA chromatography effected 13-fold enrichment in specific activity over that found in the cell extract (Figure 2.2). Submission of the pooled samples shown in Figure 2.2 to size-exclusion chromatography (Figure 2.3) resulted in a further 5-fold enrichment in specific activity. Overall, for a typical preparation, AtICS1 was purified 69-fold from induced cell extracts to near homogeneity (Figure 2.4). The specific activity of the recombinant purified AtICS1 was 0.241 μmol/min/mg (4,010 pkat mg^{-1}), which is ~10-fold lower than the specific activity of a typical preparation of the bacterial ICS enzyme EntC. All further biochemical characterization (below) was performed on the purified, recombinant mature AtICS1 enzyme.

AtICS1 is a monofunctional isochorismate synthase, not a bifunctional SA synthase. In bacteria, the synthesis of SA via isochorismate occurs either via a bifunctional SAS – like Yen Irp9 [94] – or an enzyme complex consisting of the product of ICS and isochorismate pyruvate lyase (IPL) genes co-expressed and present in *cis* – like Pae PchBA [90, 296]. As ICS and SAS enzymes share similar global structure and have highly conserved active sites [58, 94], it was important to determine whether AtICS1 exhibits monofunctional ICS activity or bifunctional SAS activity. Because (1) AtICS1 expression and function are correlated with induced SA accumulation (see Chapter 1 and [301, 302]), (2) no other genes have been identified in mutant screens for lack of SA production or associated phenotypes, and (3) isochorismate pathways likely have been derived via bacterial endosymbiosis (for example, [95]), I thought it quite possible that AtICS1 could act as a bifunctional SAS.

My HPLC analyses show that AtICS1 converts chorismate to isochorismate (Figure 2.5A). ^{1}H NMR confirmed the presence of isochorismate. Salicylic acid was not detected as a product of this reaction (Figure 2.5B). The addition of recombinant Pae PchB (an IPL) to the AtICS1 reaction did result in the production of SA (see Appendix 2). Therefore, AtICS1 functions as a traditional monofunctional ICS and not a bifunctional SAS like Irp9 [94].

AtICS1 is an active monomer. In order to determine whether AtICS1 likely exists as a monomer, dimer or other multimer, I estimated the molecular mass of the recombinant purified enzyme by fast protein liquid chromatography (FPLC) using a calibrated Sephacryl S-200 gel filtration column. Active AtICS1 was estimated to have a molecular mass of 59.7 kDa. SDS-PAGE performed on eluted fractions indicated that the ICS monomer (calculated to be ~59 kDa; see Figure 2.3A) was exclusively enriched in the fractions with ICS activity. Therefore, similar to the bacterial ICS proteins Pae PchA [296] and Eco EntC [55], AtICS1 appears to function as a monomer, whereas the SAS Yen Irp9 appears to function as a dimer [94].

AtICS1 catalyzes a reversible reaction and exhibits an apparent K_{eq} of 0.89. The chorismate-isochorismate interconversion catalyzed by monofunctional bacterial ICS enzymes has been shown to be reversible, favoring chorismate [55, 88, 296]. However, past work on plant ICS enzymes had not examined the reversibility of the reaction, nor incorporated this reversibility when assessing apparent K_M values [139, 290, 291]. Therefore, I experimentally determined that the reaction catalyzed by AtICS1 is reversible, and also acquired an apparent K_{eq}.

To determine the apparent equilibrium constant (K_{eq}) for recombinant AtICS1, I followed the conversion of chorismate to isochorismate by HPLC to establish that the reaction was

AtICS1 Ni^{2+}-NTA Affinity Column Purification

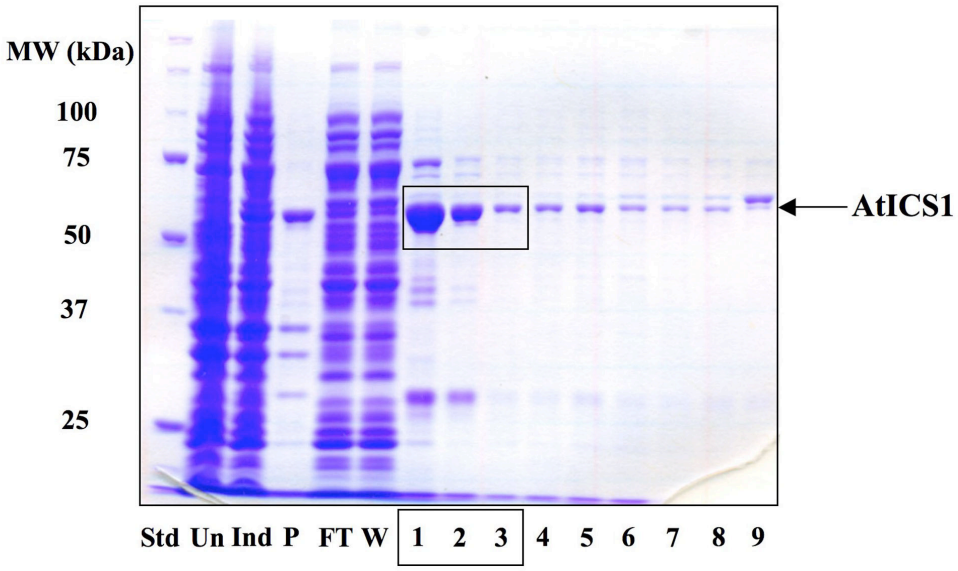

Fraction	P	SN	FT	W	1	2	3	Comb
Protein (mg/ml)	7.1	3.2	2.3	2.1	0.63	0.35	0.27	1.2
Specific Activity (nmol/min/mg)	1.08	3.50	0.06	1.82	11.9	9.9	9.9	46.0

Figure 2.2. SDS-PAGE on Ni^{2+}-NTA Fractions from the Initial Purification of AtICS1. Proteins were separated on a 10% SDS-PAGE gel and stained with Coomassie blue. Abbreviations used are: Std, Bio-Rad Precision Plus protein standards (3.6 μg protein loaded), molecular masses in kDa are indicated on left; Un, Uninduced *E. coli* cells; Ind, IPTG-induced *E. coli* cells; P, Pellet from lysed induced cells; SN, Crude extract (Supernatant) from lysed induced cells; FT, Flow-through from column loading; W, Wash of column; Comb, Combined fractions indicated by the boxes; Numbers are elution fractions.

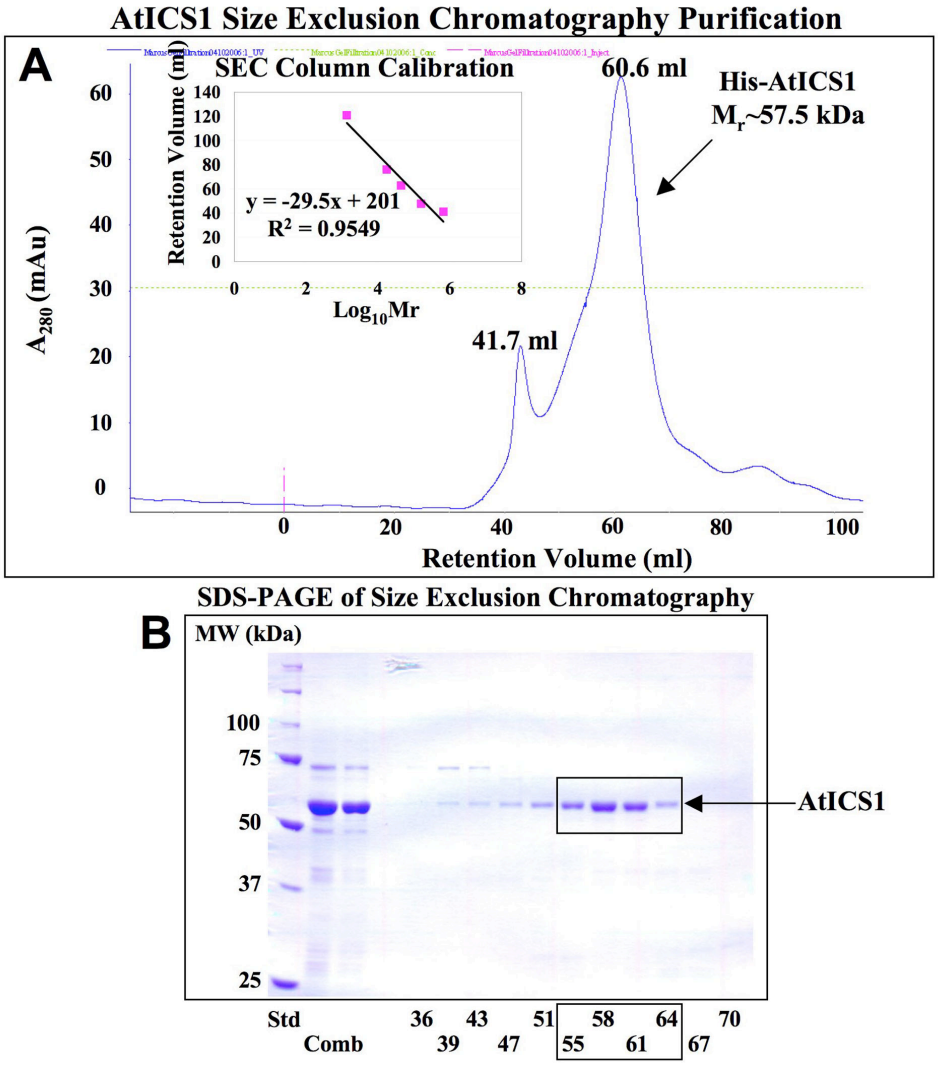

Fraction	Comb	36	39	43	47	51	55	58	61	64	67	Final
Protein (μg/ml)	1200	0	9.3	11.9	15.9	49.0	83.4	133.5	118.8	63.0	1.5	1.22
Specific Activity (μmol/min/mg)	0.046	0	2.9	2.2	1.7	0.64	0.44	0.34	0.30	0.44	16.3	0.241

Figure 2.3. Size Exclusion Chromatography Fractions of AtICS1. (A) Protein was eluted at 1.0 ml/min on a gel filtration column and fractions were collected at the minute number indicated. Active AtICS1 eluted at 60.6 min. (inset) Subsequent calibration of the column with Bio-Rad Gel Filtration Standards indicated that the peak containing active protein was a monomer of approximately 57.5 kDa. (B) Proteins were separated on a 10% SDS-PAGe gel and stained with Coomassie blue. Abbreviations used are: Std, Bio-Rad Precision Plus Protein Standards (3.6 μg protein loaded), molecular masses in kDa are indicated on left; Comb, Combined fractions from Ni^{2+}-NTA Chromatography; Final, Final pooled protein indicated by the boxes; Numbers indicate time in minutes that the fraction was eluted.

Overall AtICS1 Purification

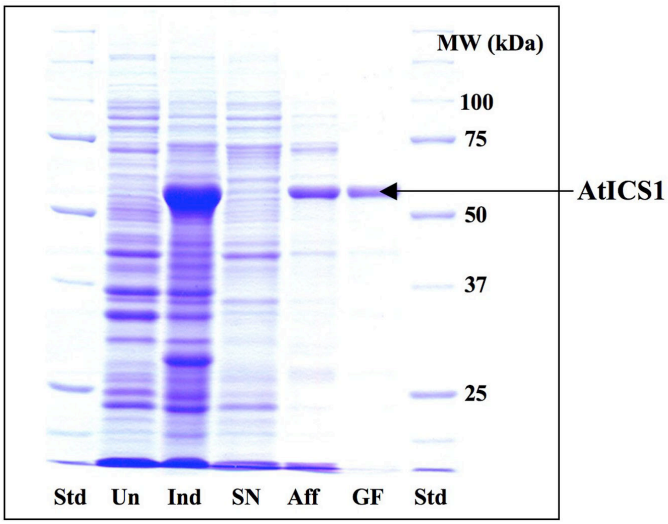

Purification Step	Total Protein (mg)	Total Activity (μmoles/ min)	Specific Activity (μmoles/ min/mg)	Purification (x-fold)	Yield (%)
Crude Extract (SN)	3,155	11.031	0.0035	1	100
Ni^{2+}-NTA Column	33.9	1.556	0.0459	13	1.07
Sephacryl S-200 GF Column	1.48	0.3569	0.2406	69	0.047

Figure 2.4. SDS-PAGE on Fractions from the Overall Purification of AtICS1. Proteins were separated on a 10% SDS-PAGE gel and stained with Coomassie blue. Abbreviations used are: Std, Bio-Rad Precision Plus Protein Standards (3.6 μg protein loaded), molecular masses in kDa are indicated on right; Un, Uninduced *E. coli* cells; Ind, IPTG-induced *E. coli* cells; SN, Crude extract (Supernatant) from lysed induced cells; Aff, Combined fractions from Ni^{2+}-NTA affinity purification; GF, Combined fractions from size exclusion chromatography. The table below shows the details of the overall purification.

complete. When successive injections 15 minutes apart showed no change in either substrate or product quantities, or in the substrate/product ratio, the reaction was judged to have reached equilibrium. I then obtained a ^{1}H NMR spectrum for the equilibrium mixture (Figure 2.6). The ratio between chorismate and isochorismate at equilibrium was calculated from the integration of the unique olefinic protons in each compound (*i.e.* the C2 protons) as shown in Figure 2.6B. I obtained a value for the apparent K_{eq} for AtICS1 = 0.89 ± 0.02, showing that a plant ICS (AtICS1) does operate near equilibrium, with the reaction slightly favoring chorismate. This value for the apparent equilibrium constant was the product of two separate experiments, each one using protein purified from a different culture.

AtICS1 has an apparent K_M of 41.5 μM for chorismate. To calculate the apparent K_M of AtICS1 for chorismate, I developed a coupled assay in which isochorismate (produced via AtICS1) is converted irreversibly to SA and pyruvate by the IPL Pae PchB (in excess), in a manner similar to that of the protocol used to assess the catalytic properties of PchA (see [296], and Figures A2.9 and A2.10). To facilitate kinetic measurements, L-lactic dehydrogenase is included (in excess) as a tertiary enzyme to convert pyruvate to lactate in a NADH-dependent reaction, and the decrease in A_{340} associated with the conversion of NADH to NAD^+ is followed spectroscopically. I found AtICS1 exhibited standard Michaelis-Menten kinetics for chorismate (Figure 2.7). The corresponding Hanes plot yielded an apparent K_M = 84.2 ± 3.9 μM for chorismate and a k_{cat} = 34.7 ± 6.8 min^{-1}. However, PchB also has chorismate mutase activity and can utilize chorismate as a substrate – producing prephenate [298] – but with less pronounced binding to chorismate (K_M = 150 μM) than to isochorismate (K_M = 14 μM). As the binding strength of PchB for chorismate at optimal conditions (pH 7.0, 37 ˚C) is similar to that of AtICS1 (above, assessed at pH 7.7 and 30 ˚C), I wanted to determine whether PchB was reducing the effective concentration of chorismate in my assay. Therefore, I assessed effective chorismate concentrations for my K_M experiment by measuring prephenate accumulation in parallel. I found significant conversion of chorismate to prephenate at concentrations below 200 μM chorismate. The adjusted kinetic parameters calculated using the effective chorismate concentrations result in an apparent K_M = 41.5 μM and k_{cat} = 38.7 min^{-1} (Figure 2.8). The apparent K_M of AtICS1 for chorismate is ~10-fold lower than past reports for plant ICS enzymes, which did not use coupled irreversible assays [139, 290, 291], and ~10-fold higher than bacterial enzymes involved in SA synthesis from chorismate via isochorismate (Pae PchA [296] and Yen Irp9 [94]).

Catalytic properties of AtICS1. I assessed the dependence of AtICS1 activity on Mg^{2+}, an array of other divalent cations, and Fe^{3+}. The presence of Mg^{2+} was found to be an absolute and specific requirement for AtICS1 activity, similar to other plant and bacterial ICS enzymes [55, 139, 290, 296, 303]. This requirement is consistent with the dominant proposed reaction mechanism for ICS: regiospecific 1,5-S_N2'' addition of a nucleophilic water to the C2 atom of chorismate via an Mg^{2+}-bound transition state with concomitant loss of the hydroxyl group at C4 [40, 59]. A typical saturation curve was obtained for AtICS1 activity as a function of Mg^{2+} concentration (assessed with 2 mM chorismate) with saturation occurring at ~2 mM $MgCl_2$ (Figure 2.9); a K_M of 193 μM for Mg^{2+} was obtained. Incubation with five other divalent cations at concentrations of 0.1, 1, or 10 mM in place of Mg^{2+} (Mn^{2+}, Ca^{2+}, Zn^{2+}, Ba^{2+}, and Cd^{2+}) did not result in significant AtICS1 activity by the coupled spectrophotometric assay (Figure 2.10). In order to test other metal ions that displayed significant absorbance at 340 nm, and thus interfered with the assay, the HPLC activity assay was employed. When Mg^{2+} was replaced with Co^{2+},

AtICS1 is Monofunctional

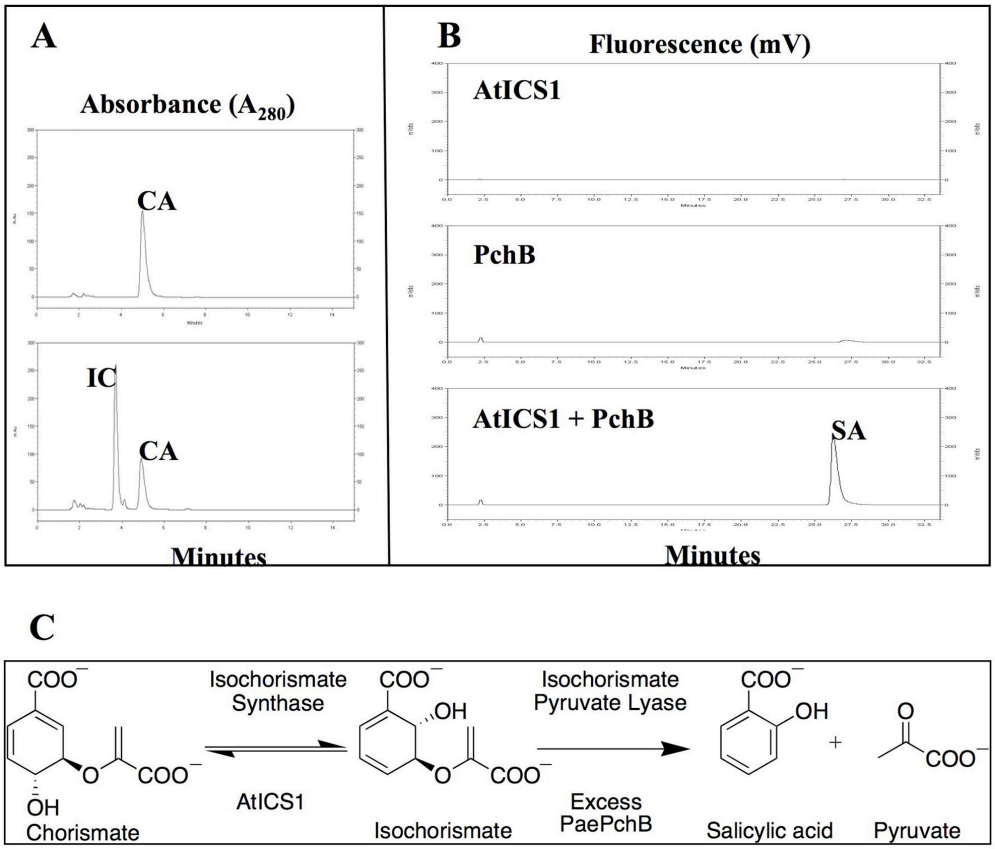

Figure 2.5. AtICS1 Exhibits Isochorismate Synthase Activity. LEFT (A) Chorismate (CA) is converted to isochorismate (IC) in the presence of enzyme (lower chromatogram) but not in the no enzyme control (above). HPLC ICS assay was employed. RIGHT (B) Salicylic acid (SA) is not a product of the ICS reaction (top chromatogram). SA is observed when AtICS1 and PchB, an IPL that converts IC to SA, are both present (bottom). A coupled HPLC ICS assay was utilized. Fluorescence was measured at ex305/em407 nm. All reactions were performed in triplicate multiple times, each using protein purified from a different culture. BOTTOM (C) Diagram of the reactions occurring above. The equilibrium on the left is the monofunctional reaction seen in (A). The overall reaction is the bifunctional process shown in the lower right of (B).

AtICS1 Effects Equilibrium Between Substrate and Product

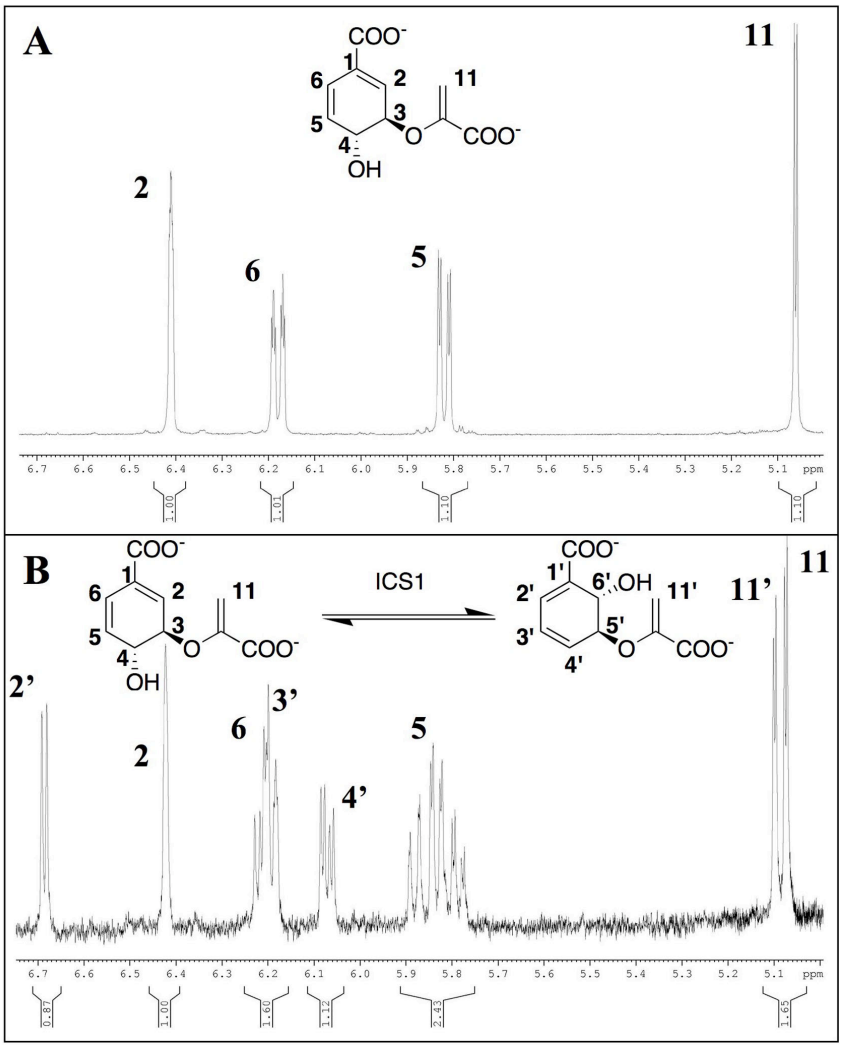

Figure 2.6. ^{1}H NMR Spectra of Chorismate (A) and the Chorismate /Isochorismate Equilibrium Mixture in the Presence of AtICS1 (B). The vinylic regions (5.0-6.75 ppm) of the NMR spectra are displayed. The four vinyl protons 2, 5, 6, and 11 for chorismate and 2', 3', 4', and 11' for isochorismate are indicated on each structure and the corresponding NMR peaks are labeled. The apparent equilibrium constant calculation used the integration of the two most downfield proton peaks (2' and 2) for determining the ratio of chorismate to isochorismate. This reaction was performed twice with two different purified samples of protein, with similar results.

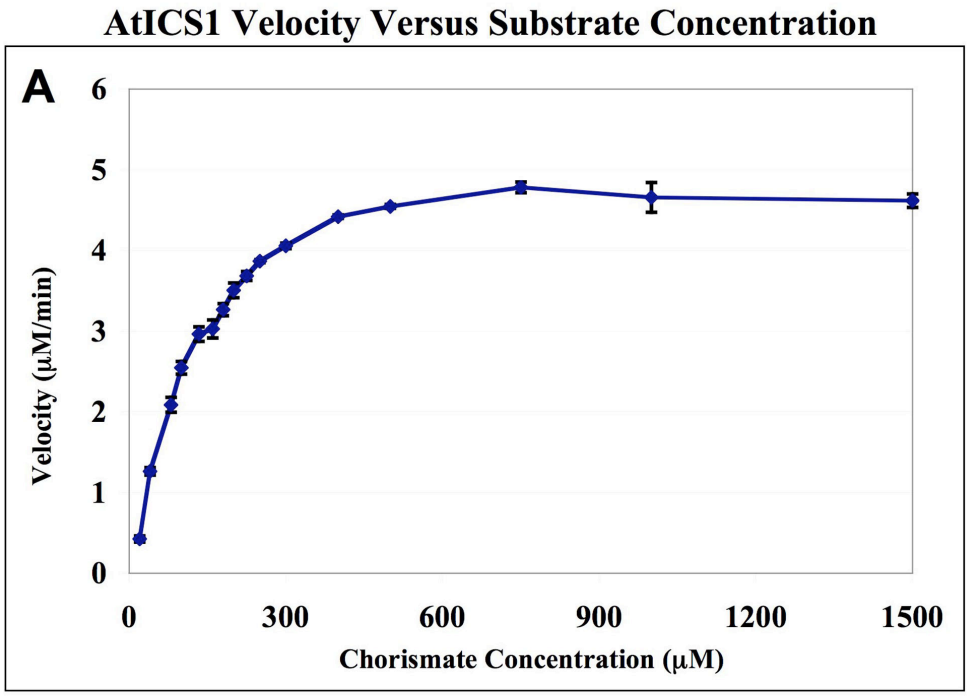

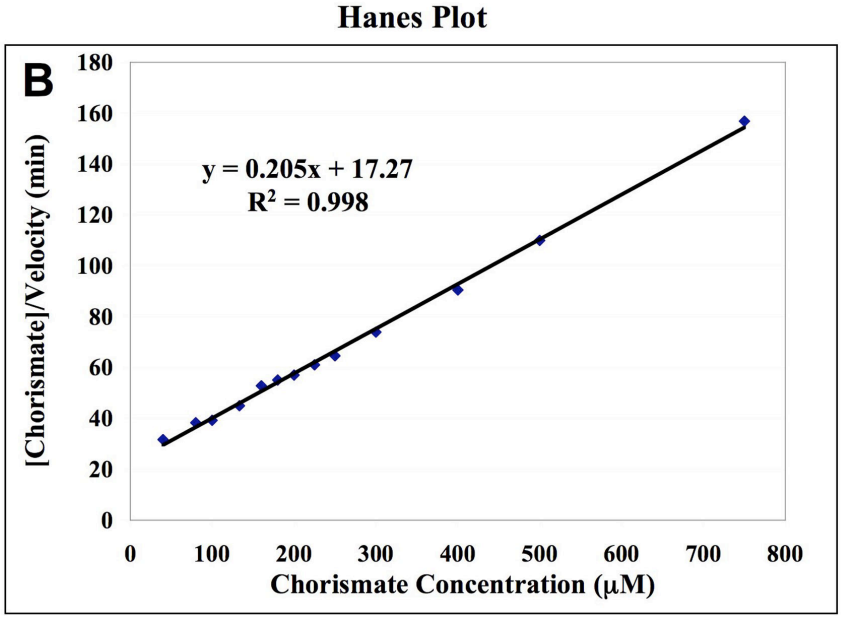

Figure 2.7. Determination of Kinetic Constants. (A) AtICS1 Velocity versus Substrate concentration determined via coupled continuous ICS activity assay. (B) Plot of same data as (A) using the formulation of Hanes to determine kinetic constants. All reactions were performed in triplicate two times, each using protein purified from a different culture.

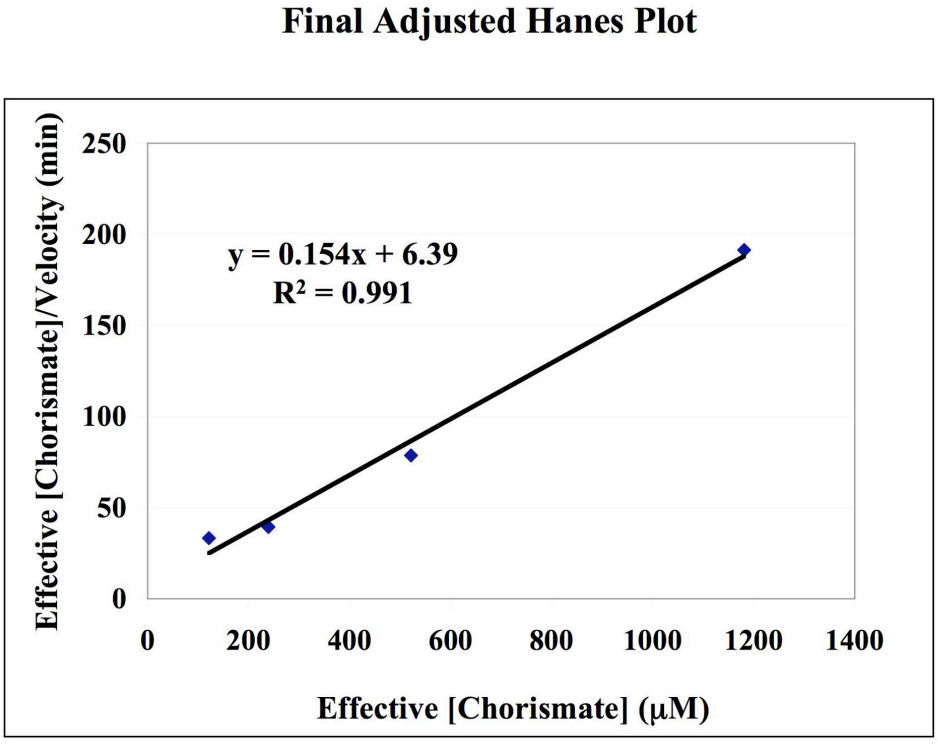

Figure 2.8. Revised AtICS1 Kinetic Constants Determined by the Method of Hanes, Using Adjusted Values for Chorismate Concentration. Effective chorismate concentration was determined as described in Appendix 2. The formulation of Hanes was used with these revised values to determine refined kinetic constants. All reactions were performed in triplicate two times, each using protein purified from a different culture.

Ni^{2+}, Cu^{2+}, Fe^{2+}, or Fe^{3+} – each at concentrations of 0.1, 1, or 10 mM – no significant isochorismate formation was observed after incubation for 60 minutes at 30 °C (Figure 2.10). The pH optimum for recombinant AtICS1 was determined using the range of pH 5 to 11. As shown in Figure 2.11, AtICS1 has a broad pH range of maximal activity from 7 to 9.5, with optimal AtICS1 activity from pH 7.5 to 8. A similar range of maximal activity was reported for other plant ICS enzymes [139, 290, 291], though values at each pH were not provided; pH optima for bacterial ICS enzymes range from 7.0 [296] to 7.5-8.0. [89].

The temperature dependence of AtICS1 activity was assessed from 4 °C to 70 °C, with maximal activity at room temperature (23 °C) and no activity at 70 °C (Figure 2.12). AtICS1 exhibited a surprisingly broad range of activity with >75% maximal activity from 4 to 44 °C, and >90% of maximal activity from 4-37 °C. Extensive temperature profiles of plant ICS enzymes had not been previously reported [139, 290, 291], although similar optima had been found (*e.g. G. mollugo*, [290]). Where reported, bacterial ICS enzymes exhibited optimal activity at 37 °C [89].

Non-enzymatic synthesis of SA from isochorismate is negligible. Non-enzymatic conversion of isochorismate to SA (~25% conversion, 100 °C, 10 minutes) has long been reported [303, 304]. Therefore, using the findings (above) regarding the subcellular localization and biochemical properties of AtICS1, I directly examined the potential for non-enzymatic formation of SA from isochorismate (produced via AtICS1) under physiological conditions. I first calculated what would be a reasonable concentration of plastidic isochorismate. It was assumed that AtICS1 operates near its K_M (41.5 μM for chorismate); therefore, the plastidic chorismate concentration is taken to be 41.5 μM and a plastidic isochorismate concentration of 37 μM is estimated ($K_{eq} = 0.89$). I then assessed non-enzymatic conversion of isochorismate to SA by HPLC, using conditions consistent with those known for the chloroplast stroma (pH 7.5, 3 mM Mg^{2+}, 23 °C) (Figure 2.13). Very little non-enzymatic conversion of isochorismate to SA was observed – 0.08% of the isochorismate was converted to SA per hour. This conversion rate is consistent with a recent isochorismate thermal decomposition study [305] (see the calculation for 30 °C, pH 7.0, and 10 mM Mg^{2+}). Furthermore, I did not detect a substantial SA signature in ^{1}H NMR spectra of AtICS1 in equilibrium (isochorismate concentration ~ 0.47 mM, pH 7.5, 5 mM Mg^{2+}, 22 °C) acquired over a 9-hour period (Figure 2.6, data not shown).

AtICS1 can catalyze the formation of ADIC. ADIC, which is made via reaction of chorismate with ammonium ion, is a transitory intermediate in the production of anthranilate by the enzyme anthranilate synthase. I wanted to see if AtICS1 also catalyzes the formation of ADIC when ammonium ion is present in the reaction medium, as does the bacterial ICS enzyme Eco EntC [59]. After 30 minutes at 30 °C in the presence of the equivalent of 100 mM ammonium, a dramatic increase occurs in the area of a peak appearing at a retention time of 2.3 minutes in the HPLC chromatogram (Figure 2.14). This peak has an absorbance spectrum and an HPLC retention time that are identical to those of the ADIC prepared under the same conditions via the action of Eco EntC [59]. Conversion to units of concentration can be carried out using an extinction coefficient of 11,500 M^{-1} cm^{-1} for ADIC [300]. This conversion indicates that 33 μM of ADIC is present in the ammonium reaction, whereas at most 6 μM ADIC is present in the control reaction undertaken without added ammonium. As the reaction began with 1 mM chorismate, this corresponds to a conversion of 3.3% of the substrate to ADIC by the enzyme AtICS1, which otherwise catalyzes chorismate to isochorismate conversion normally.

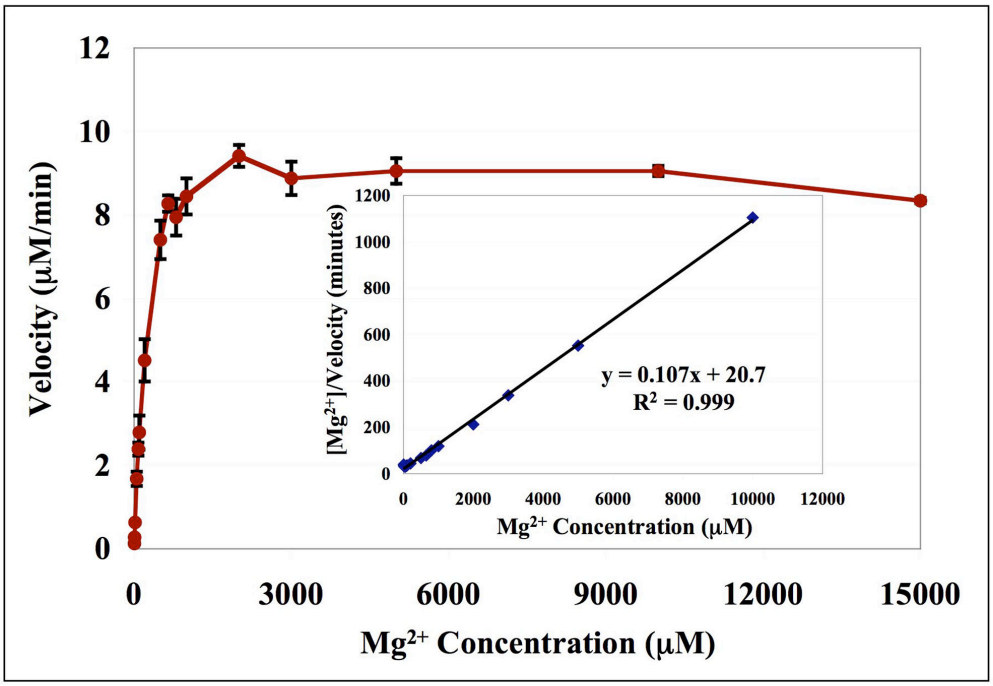

Figure 2.9. Determination of Kinetic Constants for the Effect of Mg^{2+} Ion Concentration on AtICS1 Reactivity. The main graph shows the maximal velocities for AtICS1 activity at each given concentration of Mg^{2+} ion. The inset shows the the corresponding Hanes analysis for this data and displays the trend line used to determine kinetic constants. All reactions were performed in triplicate two times, each using protein purified from a different culture.

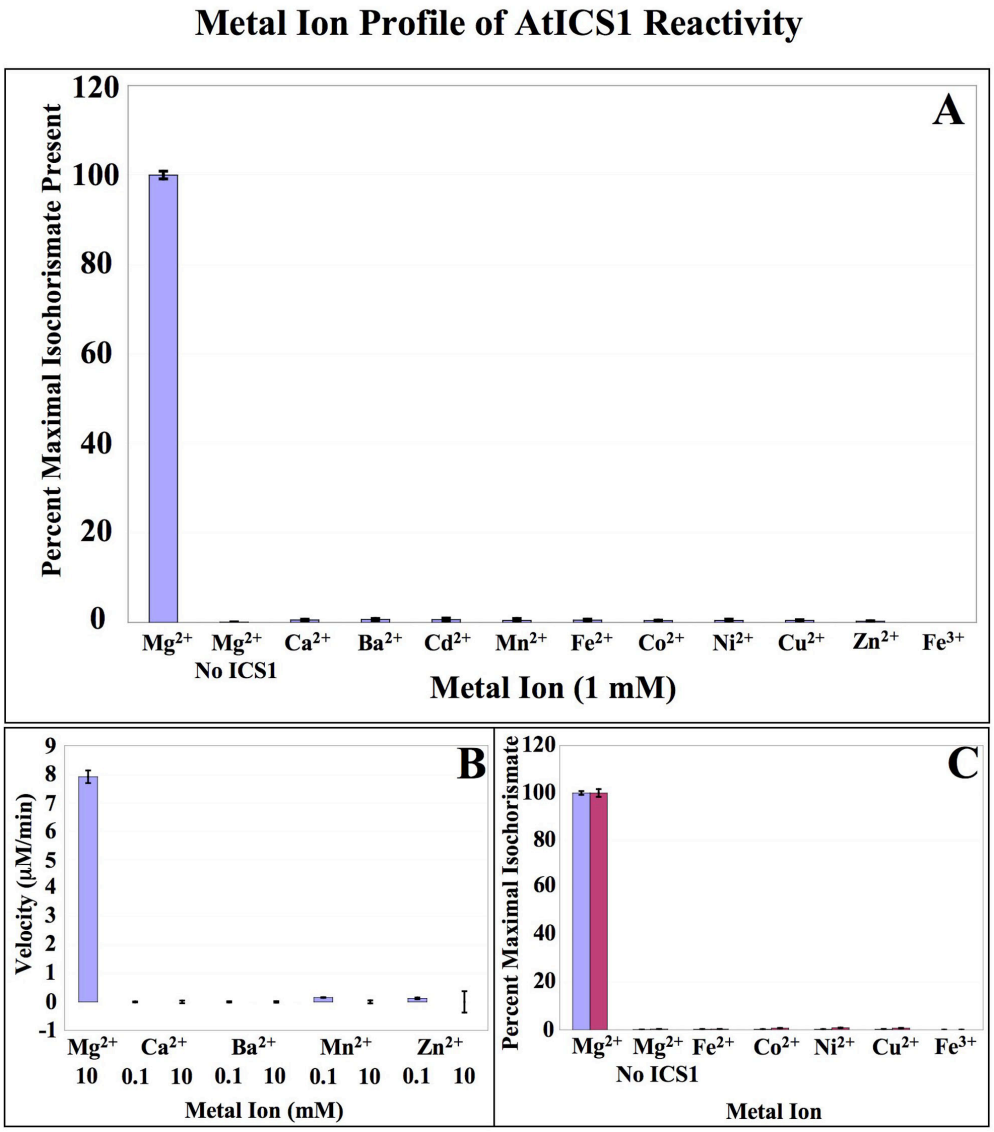

Figure 2.10. The Effect of Divalent Metal Ions on AtICS1 Reactivity. (A) Shows the extent of maximal reaction after 60 minutes incubation at 30 °C with the indicated metal ion, as assayed by HPLC. All metal ion concentrations were 1 mM. (B) Coupled spectrophotometric assay was performed using the indicated concentration of metal ion, in mM. (C) Shows extent of maximal reaction after incubation at 30 °C with the indicated metal ion, as assayed by HPLC. The left bar (blue) shows the reactivity at 0.1 mM of each metal ion. The right bar (purple) shows the reactivity at 10 mM of each metal ion. All HPLC assayed reactions (A and C) were performed in triplicate two different times, using protein isolated from separate preparations. The reactions in (B) were performed in triplicate once.

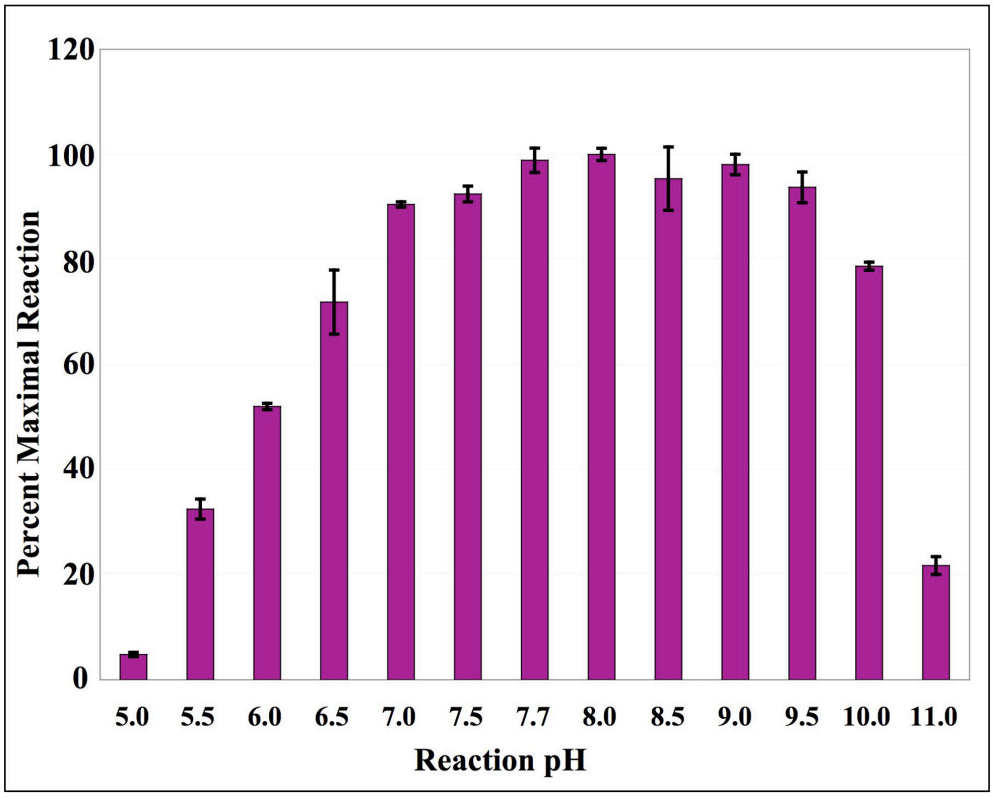

Figure 2.11. pH Profile of AtICS1 Reactivity. The top graph shows the percentage of maximal reaction after 60 minutes incubation at a variety of pH values. All reactions were performed in triplicate two different times, using protein isolated from separate preparations.

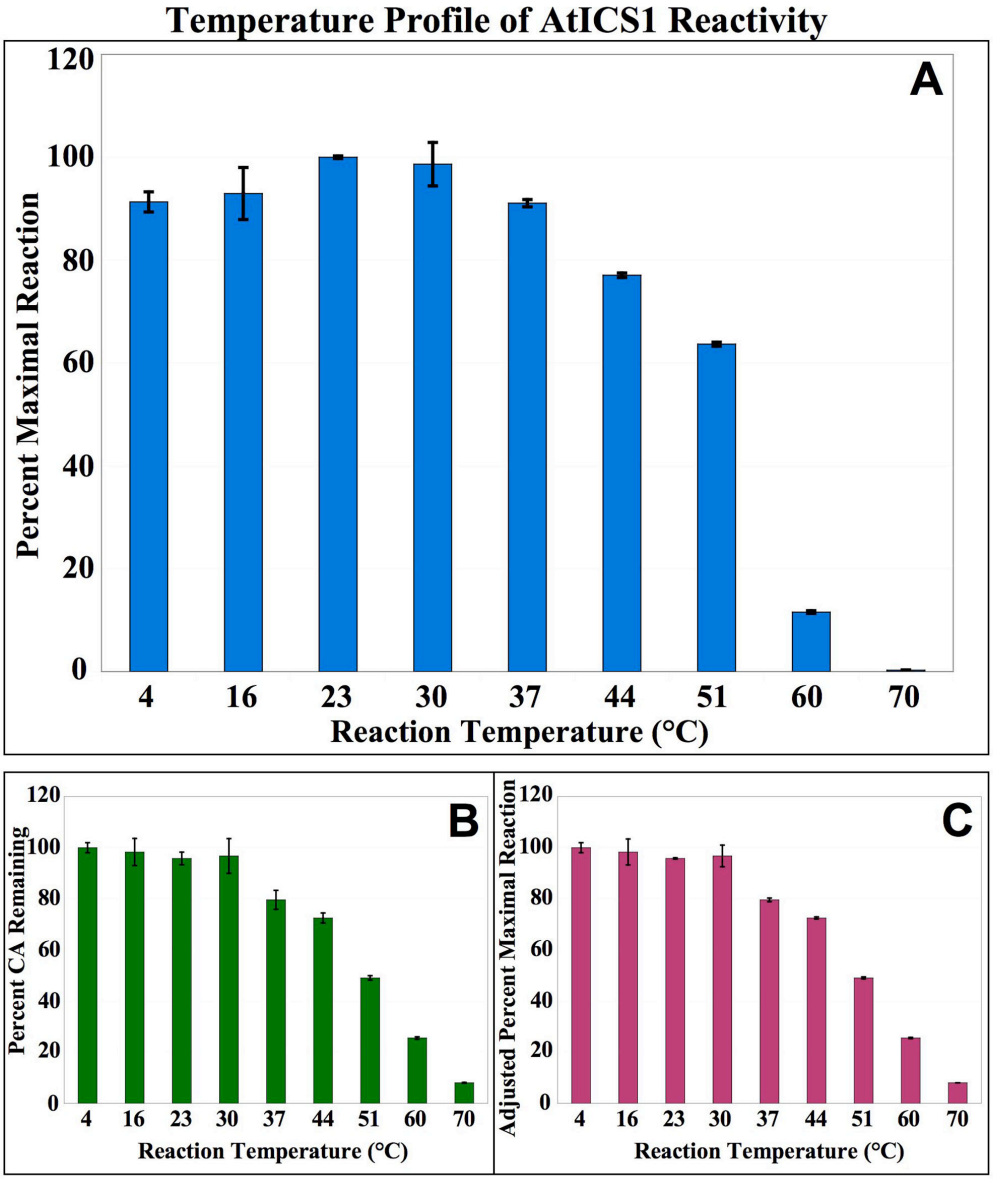

Figure 2.12. Temperature Profile of AtICS1 Reactivity. (A) Percentage of maximal reaction after 60 minutes incubation at a variety of temperatures. (B) Percent chorismate remaining after 60 minutes incubation at a variety of temperatures. (C) Above data from (A) adjusted for the non-enzymatic degradation of the isochorismate product at each given temperature, using the assumption that isochorismate degrades at a rate similar to that of chorismate. All reactions were performed in triplicate two different times, using protein isolated from separate preparations.

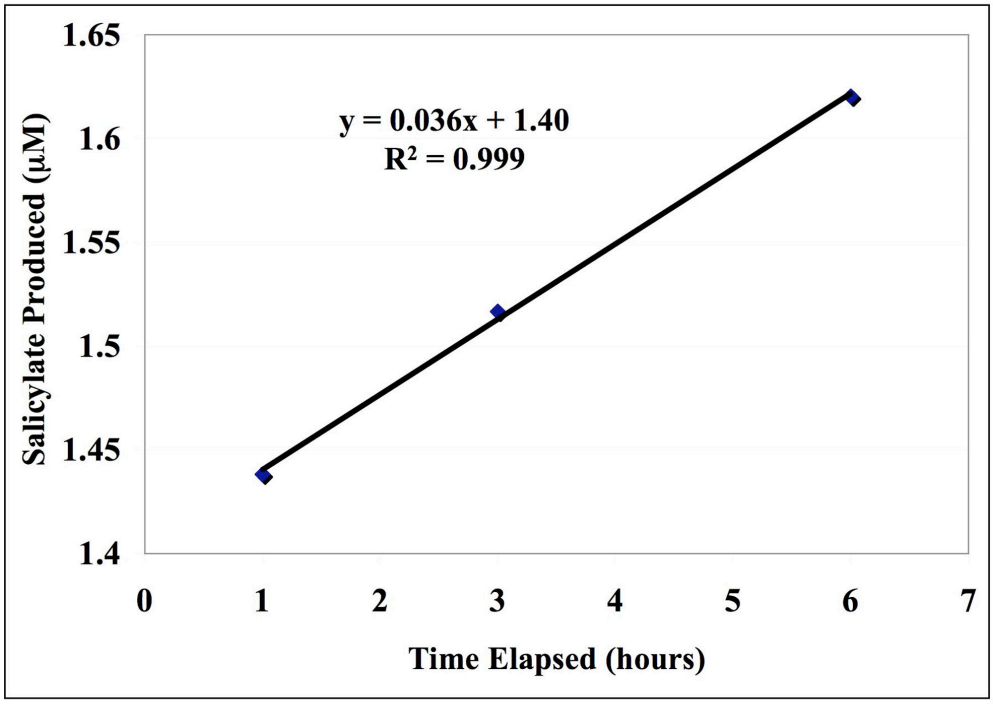

Figure 2.13. Non-enzymatic Synthesis of SA from Isochorismate. The graph shows the linear relationship between the concentration of SA generated and the time elapsed from the start of incubation at 23 °C. A starting concentration of 37 μM isochorismate was used at pH 7.5 in the presence of 3 mM $MgCl_2$, which approximate physiological conditions. All reactions were performed in triplicate two different times, with similar results.

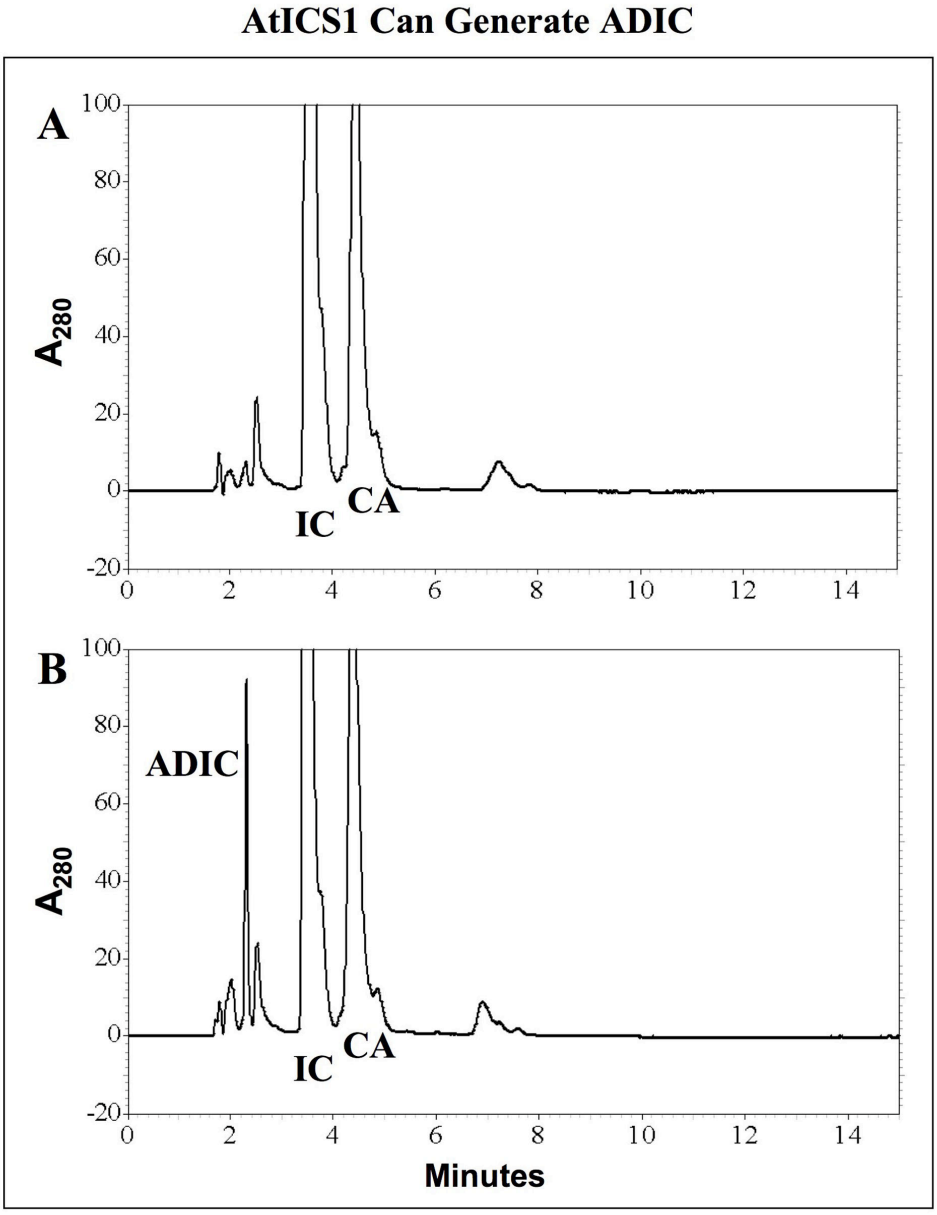

Figure 2.14. AtICS1 Can Generate ADIC. Both reactions were incubated at 30 °C for 30 minutes each. (A) Shows the HPLC chromatogram of the reaction catalyzed by AtICS1 incubated with 1 mM chorismate. (B) Shows the HPLC chromatogram of the same reaction as in (A), but with 50 mM ammonium sulfate added to the medium. The peak at ~2.15 minutes is presumed to be ADIC as its retention time and absorbance spectrum are identical to that of the ADIC produced by Eco EntC [59].

Reactions with 5 mM of the amino acids glutamate or glutamine in the media in place of ammonium produced no rise in ADIC formation (data not shown).

DISCUSSION

Herein, I have determined AtICS1 is monofunctional instead of bifunctional, and determined an apparent K_{eq} for AtICS1 (K_{eq} = 0.89), establishing that a plant ICS enzyme operates very near equilibrium. I have then provided the first kinetic data (K_M, k_{cat}) for a plant ICS using an irreversible coupled continuous assay similar to that used to obtain accurate kinetic data for bacterial ICS enzymes (for an example, see [55]). Previously, K_M (but not k_{cat}) values for plant ICS enzymes have been reported [139, 290, 291]; however, these studies employed assays that are not suitable for obtaining accurate kinetic parameters for enzymes such as ICS that operate near equilibrium (see Appendix 2 and [306]). AtICS1 is required for the induced synthesis of SA from chorismate [81]. Therefore, below, I use the detailed biochemical characterization and subcellular localization of AtICS1 to provide insights into SA biosynthesis and function as well as chorismate partitioning and utilization. Additionally, I have shown that AtICS1 converts significant (3.3%) amounts of chorismate to ADIC in the presence of ammonium ion. It is not known whether this is physiologically relevant, as tissue concentrations of ammonia range from 200 μM to 1 mM [7], far lower than the 100 mM ammonium present in solution in my test reaction. The inability of 5 mM glutamate or glutamine to catalyze the reaction to ADIC is unsurprising, as no ASB protein (the amidotransferase β-subunit needed in AS enzymes to generate ammonium from glutamate for reaction) is present. Nevertheless, given these results, it is possible that AtICS1 could act in conjunction with ASB to produce significant ADIC, and future studies will address this possibility.

AtICS1 activity and SA biosynthesis are influenced by light and temperature. A number of SA-dependent defense related processes are light dependent [307]; however, a detailed mechanistic understanding of this light-dependence is lacking. Using chloroplast import studies and immunolocalization, the Wildermuth laboratory has determined that AtICS1 is localized to the chloroplast stroma and is induced in response to pathogens in mesophyll chloroplasts of infected mature leaf tissue [82]. Light-dependent changes in pH, Mg^{2+} ion concentration, and redox status may regulate the activity of enzymes localized to the plastid stroma [308]. Therefore, I was interested in determining whether AtICS1 activity would be dramatically impacted by these changes. I found no evidence for substantial regulation of AtICS1 activity associated with reported light-dependent changes in stromal pH, which varies between 7 (dark) to 8 (light), and in Mg^{2+} ion concentration, which varies from 1-3 mM (dark) to 3-6 mM (light) [7]. Although I did not directly examine the potential for redox regulation of AtICS1, I believe redox regulation of AtICS1 is unlikely. First, the AtICS1 protein does not contain cysteine residues within sufficient distance to form a disulfide bridge, based on homology modeling with Irp9 (see Chapter 4). Also, DTT was not required to obtain active recombinant mature AtICS1. DTT (or a similar thiol reductant) is typically required throughout isolation and purification protocols to retain the activity of reduced redox-activated enzymes [309]. Taken together, these findings suggest that the light-dependent regulation of AtICS1 activity due to changes in stromal pH, Mg^{2+} ion concentration, and/or redox status do not significantly contribute to the light-dependence observed for SA-dependent defense responses.

This is in agreement with a previous report which shows that the observed light-dependence of *PR-1* expression occurs downstream of SA [307].

Initially, it seemed surprising that the temperature range of AtICS1 activity (>90% of maximal activity from 4 °C to 37 °C; see Figure 2.12) was so broad. However, from a defense perspective, it could benefit the plant to synthesize SA and induce plant defense responses over a wide range of naturally occurring temperature [310]. Furthermore, a more general role for SA as a mediator of temperature-dependent stress is emerging [268, 270]. *A. thaliana* Col-0 accumulates SA (SAG ~30 μg/g fresh weight of tissue) in response to extended growth at chilling temperatures (5 °C) [268] at levels similar to that found in strong induction by pathogens. Because AtICS1 is active at these temperatures *in planta*, it suggests that SA made via AtICS1 plays a role in cold acclimation or cold-tolerant growth. *Arabidopsis* is a chilling-resistant species, able to fully mature and produce seed at 4 °C. It will be interesting to ascertain whether ICS enzymes isolated from chilling-sensitive plant species are also highly active at 4 °C, and to explore the potential selection for and mechanism of this cold-adapted catalysis. For example, enzymatic rates can be dramatically enhanced over non-enzymatic rates (k_{cat}/k_{non}) with decreasing temperature [311]. The extent of AtICS1 activity and SAG accumulation at 4 °C (or 5 °C) also suggests that SA – and SAG in particular – may play an unexplored role in cold-tolerant growth.

Stress-induced SA biosynthesis from isochorismate is likely enzymatic and plastidic. The localization of monofunctional AtICS1, and thus isochorismate production to the plastid, strongly suggests stress-induced SA biosynthesis is plastidic. Results from two overexpression studies support this hypothesis. In the first, studies with transgenic tobacco plants overexpressing bacterial monofunctional ICS and IPL enzymes, targeted to either the plastid or cytosol singly or in combination, found that only transgenic plants in which both ICS and IPL were targeted to the plastid exhibited an SA overexpression functional phenotype. The phenotype showed SAG levels similar to those of local tobacco mosaic virus-infected leaves, the constitutive expression of pathogenesis-related genes, and a reduction in tobacco mosaic virus-induced lesion size [312]. In the other study, conducted in *Arabidopsis*, a PchBA fusion protein possessing both ICS and IPL activities was constitutively expressed in either the plastid or the cytosol [313]. Here also, a true SA overexpression phenotype (SAG ~20 μg/g fresh weight of tissue, with *PR-1* expression) was only observed when the fusion protein was targeted to the plastid, implying that SA synthesis occurs in the plastid in *Arabidopsis*.

The evidence supports enzymatic synthesis of SA from isochorismate. I found non-enzymatic conversion of isochorismate to SA under physiological conditions to be negligible. Furthermore, total SA accumulates to levels similar to those induced by pathogen in *Arabidopsis* grown at 5 °C [268], a temperature at which non-enzymatic conversion of isochorismate to SA should be insignificant. In *P. aeruginosa,* a direct comparison of the enzymatic [298] rate of SA formation from isochorismate with that recently determined for the non-enzymatic rate of the same reaction indicates that the enzyme accelerates SA formation ~4×10^5-fold [305]. Therefore, it appears that *Arabidopsis* requires one or more enzymes in addition to AtICS1 in order to convert isochorismate to SA.

In conclusion, AtICS1 is required for the pathogen-induced accumulation of SA, a key phytohormone mediating plant response to pathogens, abiotic stress, and stress-induced developmental transitions. The biochemical properties of AtICS1 described herein suggest that (1) its activity is not regulated by light-dependent changes in the chloroplast stroma, (2) it can

effectively compete with other stress-induced and constitutive plastidic chorismate-utilizing enzymes, and (3) it is active at both low and high physiologically relevant temperatures supporting its proposed role mediating temperature-dependent stress. Finally, I argue that stress-induced SA biosynthesis occurs in the plastid and requires AtICS1 and an additional enzyme(s).

CHAPTER III

CHARACTERIZATION OF *ARABIDOPSIS* ICS2

INTRODUCTION

As discussed in Chapter 1, ICS enzymes are well known in *E. coli*: EntC generates isochorismate for the production of 2,3-dihydroxybenzoic acid (2,3-DHBA, used in the biosynthesis of enterobactin), and MenF generates isochorismate for the production of the OSB used to generate menaquinone (see Figure 1.10 for both). The expression of these two enzymes is highly regulated, and they are rarely operative at the same time. It is typical in plants as well for multiple genes encoding homologous enzymes to be differentially expressed. To further understand *Arabidopsis* ICS function, it is critical to know the expression patterns of these genes.

Whereas *AtICS1* expression is induced in a variety of plant tissues after infection by fungal and bacterial pathogens, there is no evidence of *AtICS2* induction under these conditions ([81]; and Wildermuth, unpublished). For example, *AtICS2* expression is shown by global mRNA profiling with Affymetrix ATH1 GeneChips to remain low in *Arabidopsis* leaves over the course of 7 days in response to fungal infection [314], while *AtICS1* expression rises dramatically as expected. In response to powdery mildew, in the *ics1* mutant, *AtICS2* is not expressed to any greater degree than it is in wild type, and induced SA synthesis is severely compromised [81, 314]. This indicates that AtICS2 cannot compensate for AtICS1 under conditions of plant stress ([81]; and Wildermuth, unpublished). In addition, examination of the NASCArray *Arabidopsis* Affymetrix GeneChip (ATH1) expression database also shows no induction of *AtICS2* expression in response to biotic stress [302].

The function of AtICS2 is not known. It may be that AtICS1 is involved in large-scale SA biosynthesis needed for SAR (see Chapter 1 and Figure 1.17), whereas AtICS2 – which is constitutively expressed at very low levels – generates low levels of SA for other purposes. While fungal-infected *Arabidopsis ics1* mutant plants have been shown by HPLC analysis to have dramatically lower levels of SA 7 days post infection than do similarly infected wild type plants, basal amounts of uninduced SA are still present in the mutant [81]. It is possible that AtICS2 is responsible for the production of this low level of SA. However, recent work shows that AtICS2 does not make a significant contribution to SA levels regardless of whether or not the plant is under stress, confirming that AtICS1 is responsible for stress-induced SA production and suggesting that basal SA is produced via the phenylpyruvate pathway [83].

The aforementioned recent work also suggests that AtICS1, and not AtICS2, is the enzyme principally responsible for generating the isochorismate used in phylloquinone production under standard conditions [83]. However, it may be that one ICS enzyme is responsible for thylakoid-associated phylloquinone production and the other is responsible for production of the phylloquinone found in other membranes. To gain insight into the potential role of AtICS2, we examined expression of the corresponding gene using the NASCArray database [302]. The vast majority of experiments in the NASCArray showed little or no *AtICS2* induction; however, experiments conducted by Dr. Lutz Nover showed *AtICS2* expression of a singularly high value in wild type seedlings in response to sudden dark to white light transition. In this work, seedlings were grown on agar plates in the dark for four days and then moved into high light; global RNA expression was analyzed by microarray at 1 and 4 hours after high light exposure. Further examination showed that *Arabidopsis MenA* and *MenB* homolog expression was strongly correlated to that of *ICS2* in this experiment, as all three genes are up-regulated two- to three-fold over control 4 hours after high light treatment. As genes in the same pathway are likely to be coordinately regulated (see Figure 1.11), the similar expression patterns of *AtICS2* and other genes in the putative phylloquinone biosynthetic pathway strongly suggest that

AtICS2 is involved in phylloquinone biosynthesis associated with plastid development during the dark-light transition. This gene and its corresponding protein product could also be associated more generally with the response to high light exposure.

As discussed in Chapter 1, phylloquinone is an important component of the electron transfer machinery of PS I that is present in all plants. Phylloquinone does not appear to be as effectively replaced by plastoquinones in *Arabidopsis* as it is in cyanobacteria [127]. However, the albino phenotype of *menA Arabidopsis* plants (see Chapter 1) is not present in *ics2* plants (Isabel Chon, unpublished), suggesting that PS I function is not dramatically affected and that phylloquinone is likely present. One potential explanation for this is that the presence of AtICS1 compensates for the absence of AtICS2; this sort of functional redundancy is common in higher plants (see [95] and Chapter 1). This would provide an explanation for the different (albino) phenotype of the *menA* mutant: there is no other *MenA* homolog apparent in the *Arabidopsis* genome to compensate for its absence in the *menA* knockout mutant, whereas there are two *ICS* genes present in *Arabidopsis*. Functional redundancy exists in this same system in *E. coli*, as the *menF* mutant makes trace amounts of menaquinone, although the *entC* mutant makes no enterobactin. The possibility of functional redundancy is supported by the fact that the *ics1ics2* homozygous double knockout plant has limited viability (Wildermuth lab, unpublished), similar to the work of Gross [95].

However, it cannot be ruled out that plastoquinones are substituting for phylloquinone in the case of the *ics2* mutant, for reasons that are unclear. *AtICS1* and *AtICS2* are both believed to have arisen from a duplication of the *menF* module of *PHYLLO* [95], which is a sound evolutionary strategy for the development of differentially regulated pathways. This gene duplication enables the differential induction of *AtICS1* and *AtICS2*, and the accompanying coordinate expression of their downstream enzymes channels chorismate to SA or phylloquinone. Little is known about the organization of this gene circuitry, however, and there are many forms of metabolic regulation. The Gross findings are not inconsistent with AtICS2 primarily acting in phylloquinone biosynthesis. Experiments under the specific conditions of transition to light or continuous exposure to high light could resolve this issue. Indeed, preliminary data in the Wildermuth lab indicates that the *ics2* knockout mutant exhibits compromised PS II efficiency after high light exposure (Isabel Chon, Gi, unpublished). The *ics1* mutant behaves similarly to wild type in these experiments, suggesting that *ics2* may play a dominant role in synthesizing phylloquinone associated with the photosystems. In contrast to the *ics1* mutant, *ics2* does not display any defect in stress-induced activation of SA-dependent gene expression (Isabel Chon, unpublished).

The most likely function of AtICS2 is to act as the first committed enzyme in phylloquinone biosynthesis. Further study of the cellular localization and enzymology of AtICS2 allows us to more accurately speculate about its potential role in phylloquinone synthesis, as well as to refine our thinking about the nature of the phylloquinone biosynthetic pathway in *Arabidopsis*. Recently, our collaborator Dr. Kentaro Inoue (UC Davis) determined – using chloroplast import assays similar to those previously described [82] – that AtICS2 is imported into the chloroplast stroma and processed to its mature form. This is consistent with a role for AtICS2 in the production of phylloquinone, as the stroma provides access to the phylloquinone biosynthetic enzymes as well as PS I, the destination of the phylloquinone product. As important as determining its subcellular localization is obtaining knowledge of whether AtICS2 is able to effectively compete for chorismate with other constitutively expressed chorismate-utilizing enzymes in the chloroplast. Also, knowledge of the magnesium ion

concentration, pH and temperature activity profiles of this enzyme provides insight into the cellular conditions in which AtICS2 is most active. If the hypothesis that AtICS2 is primarily involved in the biosynthesis of phylloquinone associated with the photosystems is correct, then this enzyme should be maximally active under conditions in which phylloquinone is likely to be synthesized.

MATERIALS AND METHODS

Materials and General Protocols

All reagents and chemicals were obtained from Sigma-Aldrich unless otherwise specified. HPLC grade solvents (EMD Biosciences) were employed in the HPLC analyses. Chorismic acid (Sigma C-1761) was used in all analyses except during the analysis of sample activity during ICS2 purification, for which barium chorismate was used (Sigma C-1259). For selection and growth of transformed cells, pET-28 derivatives were selected with 50 μg/ml kanamycin. Commonly utilized protein and molecular biological protocols were prepared and performed as described in [295]. Independent replicate experiments were performed for all experiments described in the Results section, with similar findings.

Typical Purification of Recombinant AtICS2

pSM159-8 (obtained from Dr. Sharon Marr) is a pET-28 derivative containing a sequence encoding an amino-terminal His_6-tag fused to the sequence beginning with that encoding amino acid 51 of the *Aradibopsis thaliana* ICS2 coding region, in a manner identical to pSM157-16 from Chapter 2. These two plasmids are identical in all other respects (see Figure 2.1 for the organization of plasmid pSM157-16). The pSM159-8 AtICS2 coding sequence was confirmed to be identical to AtICS2 sequence NM_101744 (At1g18870). *E. coli* Rosetta2 (DE3) cells (Novagen) were transformed with plasmid pSM159-8. A crude cell extract was prepared from a 2 L culture of transformed cells grown in TB media containing 0.2% glucose, 50 μg/ml kanamycin and 30 μg/ml chloramphenicol. The culture was grown at 37 °C with agitation in baffled flasks until an OD_{600} of approximately 0.7 was reached, at which point IPTG was added to a final concentration of 1.0 mM to induce protein synthesis. Shaking was continued at 21 °C for 19 hours. All subsequent operations were carried out at 4 °C. The cells (wet weight approximately 26 g) were harvested and resuspended in 100 ml of Binding Buffer (50 mM sodium phosphate buffer, pH 7.4, 300 mM sodium chloride) containing 2 mM PMSF, 5 μM leupeptin, and 10 μg/ml DNase. The cells, which could be stored at –20 °C, were lysed by two passages through a French press at 18,000 psi at the orifice. Following centrifugation, the supernatant was filtered by syringe through an HPF Millex-HV 0.45 μm filter unit attached in series to a Millex-AP prefilter (Millipore). Filtrate was allowed to bind to 4 ml of Ni^{2+}-NTA His-Bind Resin (Novagen) by mixing with mild agitation on a rotary shaker for 3 hours. The resin had been pretreated according to the manufacturer's directions. The slurry was then poured into a column, and the flow-through was collected in two portions. After washing the column with 2 portions of 20 ml each of Binding Buffer, His_6-AtICS2 (hereafter referred to as AtICS2) was eluted with 20 ml of Elution Buffer (components as Binding Buffer, but including 250 mM imidazole). Fractions containing isochorismate synthase activity were pooled and concentrated by an Amicon Ultra-15 (10 kDa molecular mass cutoff) ultrafiltration device (Millipore) to a final volume of 500 μl. The pooled solution was applied by use of a ÄKTA FPLC system to a

HiPrep 16/60 Sephacryl S-200 High Resolution gel filtration column (Amersham Biosciences) that had been previously equilibrated with 200 ml of Gel Filtration Buffer (100 mM Tris buffer, pH 7.7, 150 mM sodium chloride, 10% glycerol and 1 mM DTT). The enzyme was eluted at a flow rate of 1.0 ml/min as a broad peak with ~70 ml of Gel Filtration Buffer. Fractions containing isochorismate synthase activity were pooled and concentrated as before to a final volume of 2 ml. The protein was then aliquoted and stored at –80 °C.

Enzyme Activity and Protein Quantification Assays

These assays were performed as described in Chapter 2.

Protein Molecular Mass Estimation

This experiment was performed as described in Chapter 2.

Determination of Apparent K_{eq} Using ^1H NMR

^1H NMR spectra were recorded on a 500-MHz Bruker DRX-500 spectrometer. Spectra were taken in a buffer of 50 mM potassium phosphate, pH 7.5, containing 5 mM $MgCl_2$ in D_2O. Both spectra shown are from reactions containing 4 mM chorismic acid in a total volume of 900 µl. A spectra was scanned every 8 seconds for a total period of 70 minutes each. The spectrum of the equilibrium mixture of chorismic acid and isochorismic acid was acquired with AtICS2 that had been exchanged into D_2O by 5 successive cycles of dilution with 4 ml of the above buffer, followed by ultrafiltration with Amicon Ultra-4 centrifugal filter devices (Millipore) to a final volume of about 100 µl. The final concentrate was diluted with D_2O buffer to a protein concentration of ~10.2 mg/ml by Bradford analysis. 30 µl of this solution was mixed with 970 µl of chorismic acid solution (4.12 mM in D_2O buffer) and incubated at 30 °C for 70 minutes. Quantification of the relative amounts of materials present was performed as in Chapter 2. This experiment was performed two times, each time using protein purified from two different cultures. Each set of results was similar to the other.

Determination of Kinetic Constants

The coupled spectrophotometric ICS assay (see Appendix 2) was modified by performing each reaction in triplicate using working chorismic acid concentrations of 15.0 mM, 10.0 mM, 5.0 mM, 2.0 mM, 1.0 mM, 800 µM, 650 µM, 500 µM, 400 µM, 300 µM, 250 µM, 200 µM, 180 µM, 160 µM, 140 µM, 120 µM, 100 µM, 80 µM, 60 µM, 40 µM, 20 µM, 10 µM, 5 µM and 0 µM. These were achieved by initiating the reactions by addition of 20 µl of a 10× solution of each of the above concentrations to 180 µl of a mixture containing uniform amounts of the other reaction components. Reactions containing no AtICS2 were run as blanks. Initial velocity data were fitted to the equation of Hanes to determine kinetic parameters. This experiment was performed two times, each time using protein purified from two different cultures. Each set of results was similar to the other.

Revision of Kinetic Constants

The spectrophotometric endpoint assay for phenylpyruvate formation was undertaken as in Appendix 2, using working chorismic acid concentrations of 400 µM, 300 µM, 200 µM, 160 µM, 120 µM, 80 µM, 40 µM, and 20 µM. After calculating effective chorismate concentrations as previously, the values for velocity at each of the eight chorismate concentrations shown here were used to calculate the revised kinetic constants via the method of Hanes.

Effect of Mg^{2+} on Isochorismate Synthase Activity

The coupled spectrophotometric ICS assay was modified for measurement of the effect of magnesium ion concentration on enzyme activity as in Chapter 2. The following working concentrations of $MgCl_2$ were assayed in triplicate: 15 mM, 10 mM, 5.0 mM, 3.0 mM, 2.0 mM, 1.0 mM, 800 μM, 650 μM, 500 μM, 200 μM, 100 μM, 80 μM, 50 μM, 20 μM, 10 μM, 5 μM. Reactions containing no $MgCl_2$ were run as blanks. Initial velocity data were fitted to the equation of Hanes to determine kinetic parameters. This experiment was performed two times, each time using protein purified from two different cultures. Each set of results was similar to the other.

Effect of Other Metals on Isochorismate Synthase Activity

The HPLC assay for ICS activity (Chapter 2) was modified by substituting the following divalent metals for Mg^{2+} at a working concentration of 10 mM each: $CaCl_2$, $BaCl_2$, $CdCl_2$, $MnCl_2$, $FeCl_2$, $CoCl_2$, $NiCl_2$, $CuCl_2$, and $ZnCl_2$. The reaction and HPLC analysis were performed as described above. This experiment was performed two times, each time using protein purified from two different cultures. Each set of results was similar to the other.

pH Profile of Isochorismate Synthase Activity

The HPLC assay for ICS activity was modified using reaction buffers with a variety of pH values. A 4.2 mg/ml solution of AtICS2 was diluted 26-fold into the buffers listed in Chapter 2. 60 μl of each of these solutions (220 μg/ml AtICS2) was mixed with 60 μl of a 2 mM solution of chorismic acid in the corresponding buffer. These reactions were performed in triplicate and incubated at 30 °C for 60 minutes each. They were analyzed by HPLC as described above. This experiment was performed two times, each time using protein purified from two different cultures. Each set of results was similar to the other.

Temperature Profile of Isochorismate Synthase Activity

The HPLC assay for ICS activity was modified and executed at various temperatures as described above in Chapter 2. This experiment was performed two times, each time using protein purified from two different cultures. Each set of results was similar to the other.

ADIC Formation in the Presence of Ammonium Ion

An HPLC isochorismate synthase activity assay was used to determine ADIC as described in Chapter 2.

RESULTS

AtICS2 was overexpressed and purified. In order to assess AtICS2 biochemical activity, I overexpressed amino-terminal His_6-tagged mature AtICS2 (without the chloroplast transit sequence) in *E. coli* and purified the soluble induced protein using Ni^{2+}-NTA and size-exclusion chromatographies. The gene for this recombinant protein is under the control of a T7 promoter as for that of ICS1 in Chapter 2, and it is overexpressed to up to 50% of total cellular protein when IPTG is added to initiate expression of T7 polymerase in the BL-21 (DE3) strain that contains it. Purification by Ni^{2+}-NTA chromatography effected 8.4-fold enrichment in

specific activity over that found in the cell extract (Figure 3.1). Submission of the pooled samples shown in Figure 3.2 to size-exclusion chromatography (Figure 3.2) resulted in a further 1.4-fold enrichment in specific activity. Overall, for a typical preparation, AtICS2 was purified 11.4-fold from induced cell extracts to near homogeneity (Figure 3.3). The specific activity of the recombinant purified AtICS2 was 0.217 μmol min^{-1} mg^{-1} (3,620 pkat mg^{-1}), which is similar to that of recombinant purified AtICS1. All further biochemical characterization (below) was performed on this or similarly purified, recombinant mature AtICS2 enzyme, with the same order of specific activity.

AtICS2 exhibits isochorismate synthase activity, not SA synthase activity. My HPLC analyses show that AtICS2 converts chorismate to isochorismate until an equilibrium distribution of the two is achieved (Figure 3.4). Isochorismate was confirmed by its ^{1}H NMR spectrum, and by similarity of its absorbance spectrum to a purified standard. Salicylic acid was not detected as a product of this reaction (Figure 3.4, inset), indicating that AtICS2 functions as a monofunctional ICS similar to AtICS1 and not a bifunctional SAS like Irp9.

AtICS2 is an active monomer. In order to determine the oligomerization status of AtICS2, the molecular mass of the recombinant purified enzyme was estimated by fast protein liquid chromatography using a calibrated Sephacryl S-200 gel filtration column (Figure 3.2). The peak maximum which elutes at a retention volume of 65.2 ml was estimated to have a molecular mass of 55 kDa, which matches closely the monomer molecular mass estimated by SDS-PAGE analysis of eluted fractions (~57 kDa). Furthermore, the eluted fractions that correspond to this major peak are enriched in ICS activity. This suggests strongly that AtICS2 exists in solution as a monomer. A second peak, which is ubiquitously present in solution without regard to the apparent purity by SDS-PAGE analysis of the gel filtration precursor sample, does have some ICS activity. It elutes at a retention time of 43.7 ml, which correspond to an estimated molecular mass of ~247 kDa. This is approximately 4.5 times the mass determined for a monomer, suggesting a possible AtICS2 oligomer, although one with limited activity, and one that is probably not relevant physiologically. That AtICS2 functions as a monomer is a reasonable conclusion in light of the fact that many known ICS enzymes (including AtICS1) exist as monomers. It should be pointed out that this gel filtration data is part of an AtICS2 purification step, not of a previously purified protein. Additionally, it is likely that the loaded sample in this case (labeled "Pre-GF") experienced some kind of decomposition prior to SDS-PAGE analysis. Nevertheless, these results are quite similar in character to others performed on the same protein, but not shown here.

AtICS2 catalyzes a reversible reaction and exhibits an apparent K_M of 17.2 μM for chorismate. To determine the apparent equilibrium constant (K_{eq}) for recombinant AtICS2, I followed the conversion of chorismate to isochorismate by HPLC and obtained ^{1}H NMR spectra for the equilibrium mixture (Figure 3.5). The ratio between chorismate and isochorismate at equilibrium was calculated from the integration of unique olefinic protons as in Chapter 2. I obtained a value of 0.76 ± 0.01 for the apparent K_{eq} for AtICS2, which differs slightly from that of AtICS1 calculated in Chapter 2 (apparent K_{eq} = 0.89). Both are similar to the apparent K_{eq} of 0.83 found using microcalorimetry for the reaction catalyzed by EntC [315]. Salicylic acid (a breakdown product of isochorismate) was not observed. *para*-Hydroxybenzoic acid was present

AtICS2 Ni^{2+}-NTA Affinity Column Purification

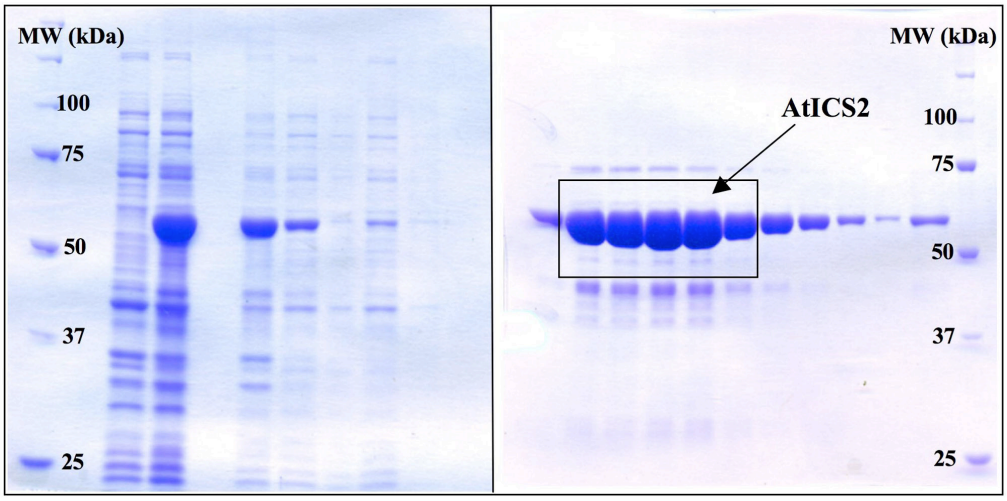

Protein (mg/ml)	15.3	12.1	12.3	12.2	2.1	0.4	4.3	28.6	31.7	39.0	34.0	14.4	9.2	4.8	1.8	0.5	0.1
Specific Activity (μmol/min/mg)	0.20	0.19	0.06	0.07	0.13	0.70	0.37	0.22	0.20	0.17	0.16	0.26	0.2	0.2	0.3	0.59	0

Figure 3.1. SDS-PAGE on Ni^{2+}-NTA Fractions from the Initial Purification of AtICS2. Proteins were separated on a 10% SDS-PAGE gel and stained with Coomassie blue. Abbreviations used are: Std, Bio-Rad Precision Plus protein standards (3.6 μg protein loaded), molecular masses in kDa are indicated both sides; Un, Uninduced *E. coli* cells; Ind, IPTG-induced *E. coli* cells; P, Pellet from lysed induced cells; SN, Crude extract (Supernatant) from lysed induced cells; FT, Flow-through from column loading; W, Wash of column; Numbers are elution fractions. Fractions that are pooled and combined are indicated by the boxes.

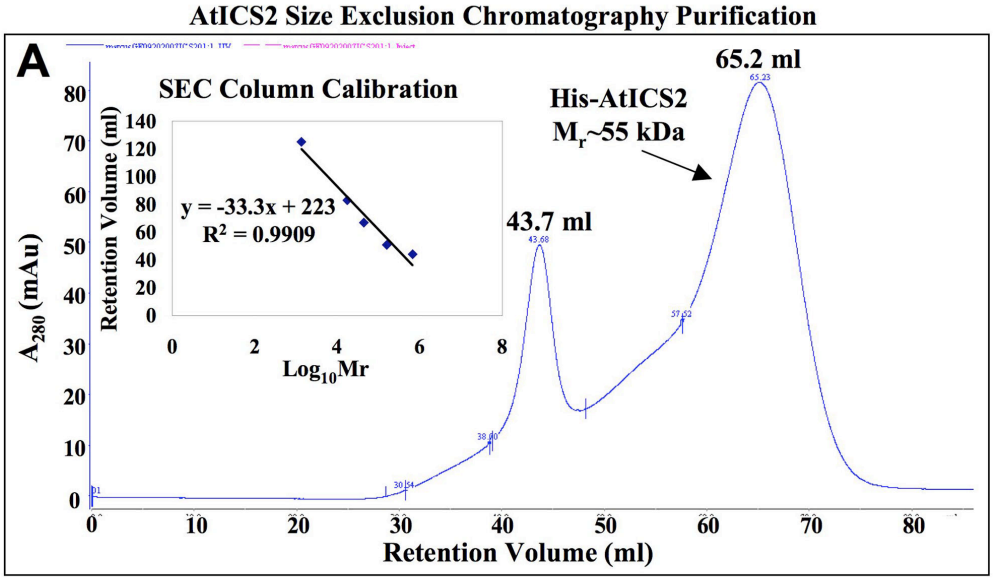

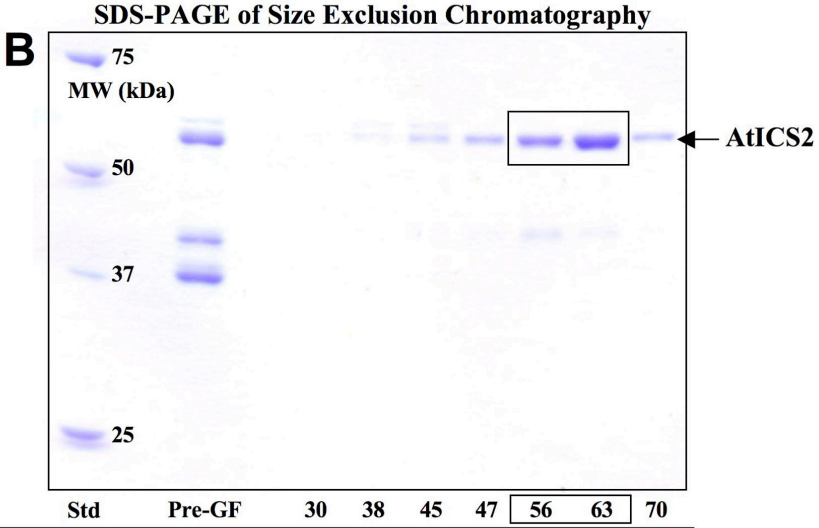

	Std	Pre-GF	30	38	45	47	56	63	70
Protein (μg/ml)		2767	0	8.3	60.7	51.5	141.0	265.5	5.0
Specific Activity (μmol/min/mg)		0.02	0	0.08	0.11	0.35	0.22	0.24	2.89

Figure 3.2. Size Exclusion Chromatography Fractions of AtICS2. (A) Protein was eluted at 1.0 ml/min on a gel filtration column and fractions were collected at the minute number indicated. Active AtICS2 eluted at 65.2 min. (inset) Subsequent calibration of the column with Bio-Rad Gel Filtration Standards indicated that the peak containing active protein was a monomer of approximately 55 kDa. (B) Proteins were separated on a 10% SDS-PAGE gel and stained with Coomassie blue. Abbreviations used are: Std, Bio-Rad Precision Plus Protein Standards (3.6 μg protein loaded), molecular masses in kDa are indicated on left; Pre-GF, Concentrated Ni^{2+}-Affinity Purified Protein; Numbers correspond to time in minutes at which the fraction was eluted. Fractions that were collected and pooled are indicated by the boxes.

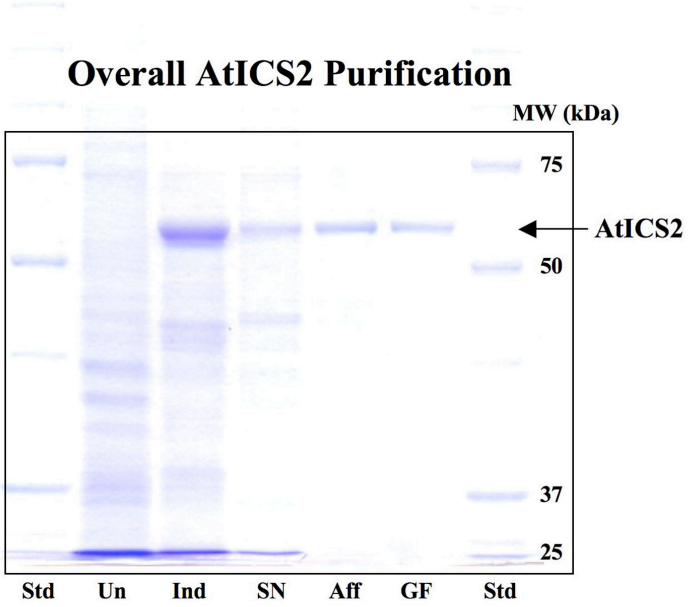

Purification Step	Total Protein (mg)	Total Activity (μmoles/ min)	Specific Activity (μmoles/ min/mg)	Purification (x-fold)	Yield (%)
Crude Extract (SN)	12,110	230.1	0.019	1	100
Ni^{2+}-NTA Column	484	77.0	0.159	8.4	33
Sephacryl S-200 GF Column	80	17.3	0.217	11.4	7.5

Figure 3.3. SDS-PAGE on Fractions from the Overall Purification of AtICS2. Proteins were separated on a 10% SDS-PAGE gel and stained with Coomassie blue. Abbreviations used are: Std, Bio-Rad Precision Plus Protein Standards (3.6 μg protein loaded), molecular masses in kDa are indicated on right; Un, Uninduced *E. coli* cells; Ind, IPTG-induced *E. coli* cells; SN, Crude extract (Supernatant) from lysed induced cells; Aff, Combined fractions from Ni^{2+}-NTA affinity purification; GF, Combined fractions from size exclusion chromatography. The table below shows the details of the overall purification.

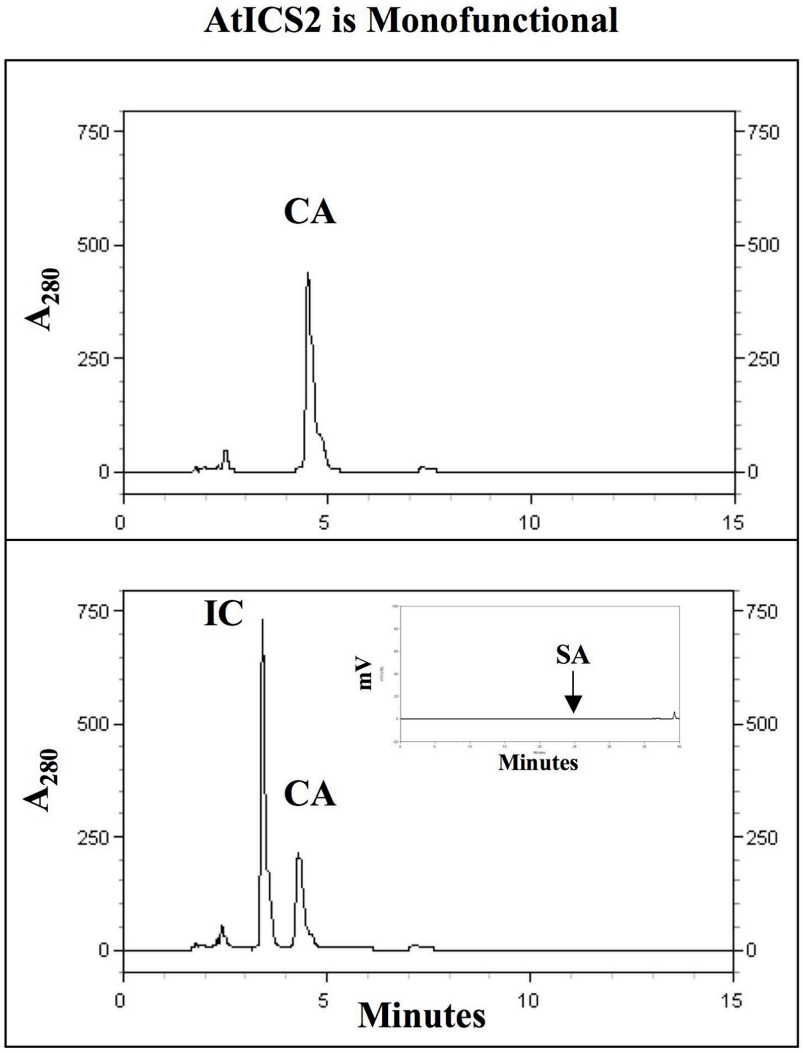

Figure 3.4. AtICS2 Exhibits Isochorismate Synthase Activity. Chorismate (CA) is converted to isochorismate (IC) in the presence of enzyme (lower chromatogram) but not in the no enzyme control (above). HPLC ICS assay was employed. (Inset) Salicylic acid (SA) is not a product of the AtICS2 reaction. Fluorescence was measured at ex305/em407 nm. All reactions were performed in triplicate multiple times, each using protein purified from a different culture.

AtICS2 Effects Equilibrium Between Substrate and Product

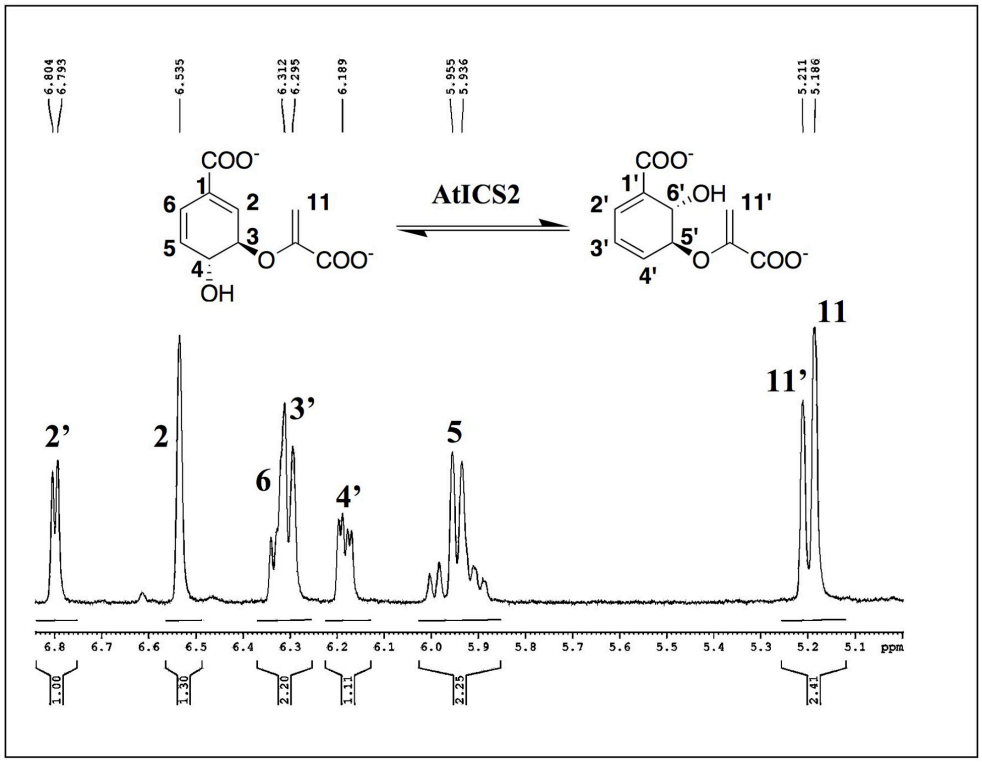

Figure 3.5. ^{1}H NMR Spectra of the Chorismate /Isochorismate Equilibrium Mixture in the Presence of AtICS2. The vinylic region (5.0-6.75 ppm) of the NMR spectrum is displayed. The four vinyl protons 2, 5, 6, and 11 for chorismate and 2', 3', 4', and 11' for isochorismate are indicated on each structure and the corresponding NMR peaks are labeled. The apparent equilibrium constant calculation used the integration of the two most downfield proton peaks (2' and 2) for determining the ratio of chorismate to isochorismate. This reaction was performed twice with two different purified samples of protein, with similar results.

in trace amounts (data not shown), but it is a known impurity in commercial preparations of chorismic acid. This, combined with all existing HPLC data, suggests that neither substrate nor product is undergoing decomposition in the course of the reaction under observation, and that the values obtained for the apparent K_{eq} of AtICS2 are relatively accurate. Presumably, slight irregularities in the automated integration of the C2 peaks in ^{1}H NMR spectra are responsible for the small disparities in the three apparent K_{eq} values specified above, all of which should be identical in theory.

To calculate the apparent K_M of AtICS2 for chorismate, I took advantage of the coupled continuous assay described in Appendix 2 and employed in Chapter 2. I found AtICS2 showed kinetics similar to those of AtICS1. The corresponding Hanes plot yielded an apparent K_M = 39.1 ± 4.1 μM for chorismate, with an apparent k_{cat} = 17.5 ± 0.2 min^{-1} (Figure 3.6). However, as for any chorismate-utilizing enzyme, it is necessary to determine the actual chorismate concentration present in solution, given its instability and relatively high rate of decomposition. In particular, we have demonstrated above that PchB, the secondary enzyme in our coupled assay, converts chorismate to prephenate at a substantial rate under these conditions (see Appendix 2). Also substantial is the spontaneous rate of decomposition of chorismate, though it is not measured under the conditions of the enzyme assay used here ($t_{1/2}$ ~30 min at 60 °C) [316]. Furthermore, because spontaneous Claisen rearrangement of chorismate to form prephenate occurs at a rate roughly 9-fold faster than that of elimination (forming 4-hydroxybenzoate and pyruvate; also measured at 60 °C) [44], mere subtraction of the control rate of reaction without enzyme will not account for most non-enzymatic decomposition (as no pyruvate will be formed to detect). The decomposition due to factors other than AtICS2 is especially a problem in low concentration regimes of chorismate, where the effective chorismate concentrations (when decomposition is considered) are likely to be dramatically lower than the initial chorismate concentrations used to calculate kinetic constants. This will tend to underestimate the extent of binding of enzyme to substrate (or, rather, overestimate the apparent K_M). Eight chorismate concentrations were selected for which values for initial velocity have been obtained above, and their corresponding effective chorismate concentrations were calculated by subtracting phenylpyruvate formed as in Appendix 2 and Chapter 2 (Figure 3.7). Again, we found significant conversion of chorismate to prephenate at concentrations below 200 μM chorismate. The adjusted kinetic parameters calculated using the effective chorismate concentrations are: K_M = 17.2 μM and k_{cat} = 18.0 min^{-1}. The K_M of AtICS2 for chorismate is over 2-fold lower than that for AtICS1 (41.5 μM), as is the value for k_{cat}.

Catalytic properties of AtICS2. As many of the enzymes previously characterized [38], including AtICS1, absolutely required Mg^{2+} for ICS activity, it was expected that AtICS2 would as well. The dependence upon Mg^{2+} for activity was originally proposed to stem from the oxophilicity of the ion: it can effectively stabilize partial negative charge on both nucleophilic and exiting water molecules (or hydroxide ions) in the transition state for a synchronous 1,5-S_N2'' reaction [40]. However, recent crystallographic data [58] suggests an enzyme reaction mechanism involving instead activation of the C2 position of chorismate by Mg^{2+} ion-binding to the ring carboxylate (see Chapter 1 and Figure 1.8). Activity was measured as a function of Mg^{2+} concentration at a saturating concentration of chorismate (2 mM), using the coupled continuous spectrophotometric ICS assay (Appendix 2). Saturation was achieved at Mg^{2+} concentrations of approximately 4 mM (Figure 3.8), and Hanes analysis determined the K_M for Mg^{2+} to be 573 μM. In addition, when Mg^{2+} was replaced by a variety of divalent cations (Ca^{2+},

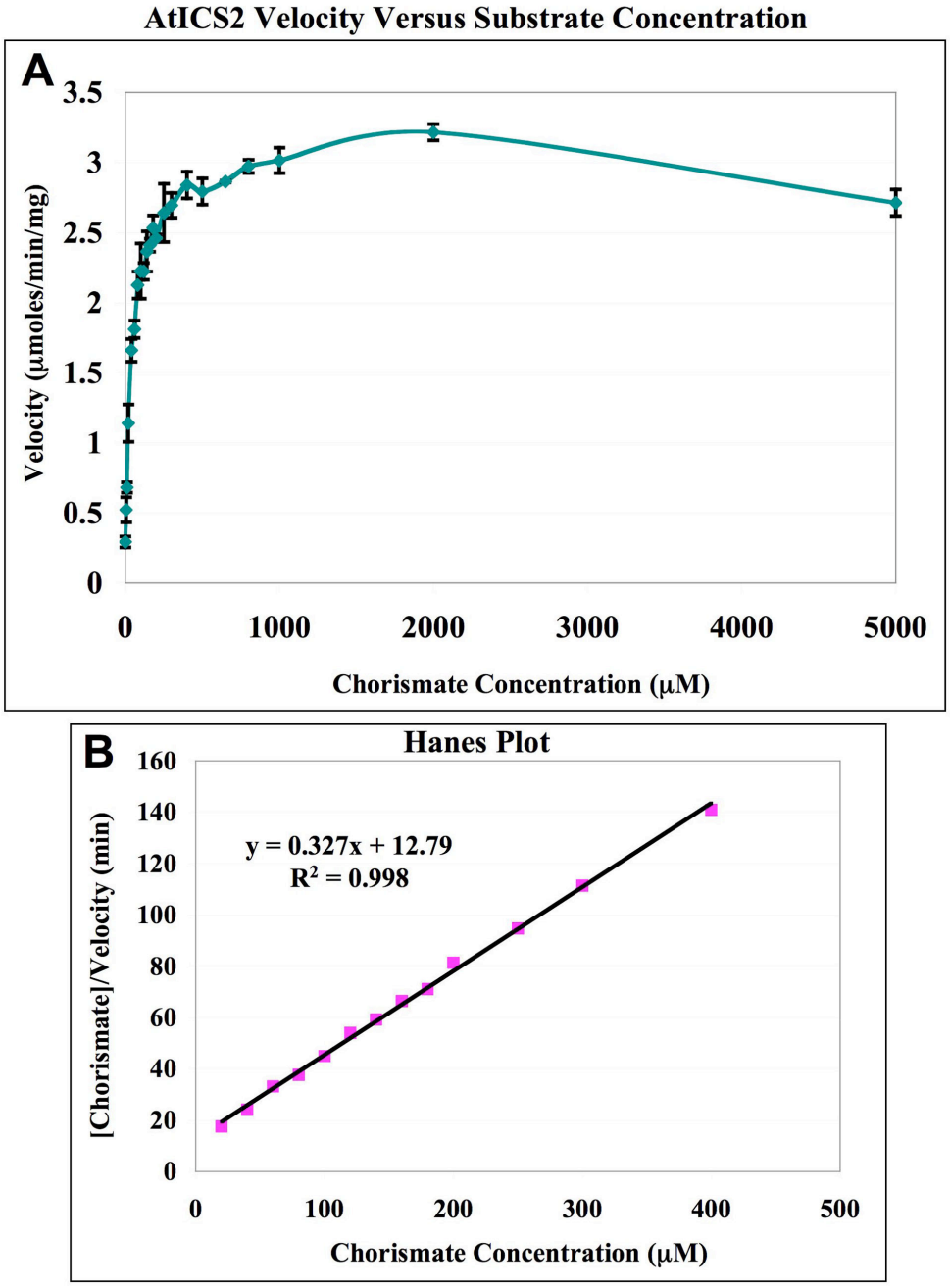

Figure 3.6. Determination of Kinetic Constants. (A) AtICS2 Velocity versus Substrate concentration determined via coupled continuous ICS activity assay. (B) Plot of same data as (A) using the formulation of Hanes to determine kinetic constants. All reactions were performed in triplicate two times, each using protein purified from a different culture.

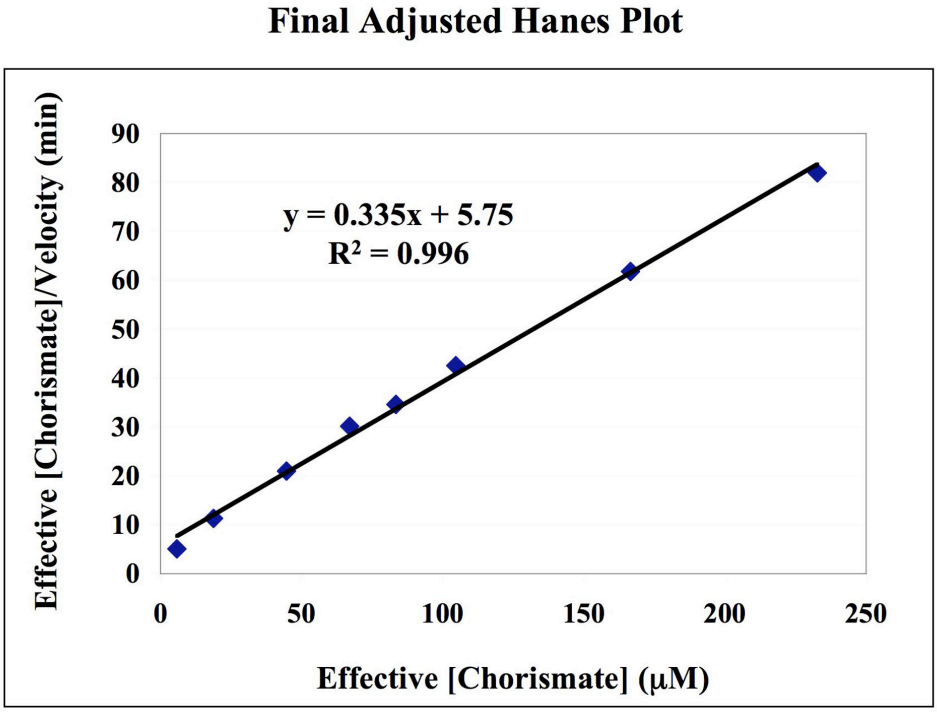

Figure 3.7. Revised AtICS2 Kinetic Constants Determined by the Method of Hanes, Using Adjusted Values for Chorismate Concentration. Effective chorismate concentration was determined as described in Appendix 2. The formulation of Hanes was used with these revised values to determine refined kinetic constants. All reactions were performed in triplicate two times, each using protein purified from a different culture.

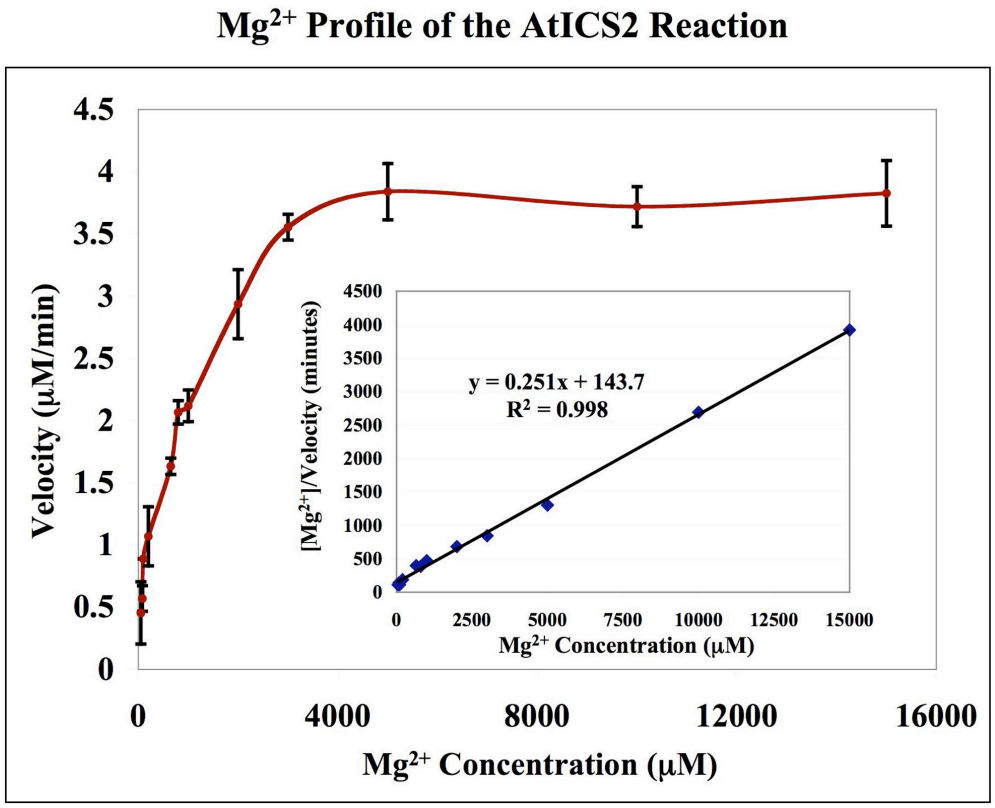

Figure 3.8. Determination of Kinetic Constants for the Effect of Mg^{2+} Ion Concentration on AtICS2 Reactivity. The main graph shows the maximal velocities for AtICS2 activity at each given concentration of Mg^{2+} ion. The inset shows the the corresponding Hanes analysis for this data and displays the trend line used to determine kinetic constants. All reactions were performed in triplicate two times, each using protein purified from a different culture.

Ba^{2+}, Mn^{2+}, Fe^{2+}, Co^{2+}, Ni^{2+}, Cu^{2+}, Zn^{2+}, and Cd^{2+}) – all at concentrations of 10 mM under otherwise standard reaction conditions – no activity whatsoever was found. This was determined by measuring both isochorismate appearance (Figure 3.9) and chorismate disappearance (data not shown) by HPLC.

The pH optimum for recombinant AtICS2 was determined using a pH range of 5 to 11. As shown in Figure 3.10, AtICS2 has a broad pH range of maximal activity from 6.5 to 8.0, with optimal AtICS2 activity at a pH of 7.7. This is similar to AtICS1, although the pH maximum in this case is less broad. This pH range is also quite similar to those of many other ICS enzymes [89, 139, 290, 291, 296].

The temperature dependence of AtICS2 activity was assessed from 4 °C to 70 °C with maximal activity at 16-23 °C and no activity at 70 °C (Figure 3.11). AtICS2 exhibited a surprisingly broad range of activity with >80% maximal activity from 4 to 37 °C, and ~100% maximal activity from 16-23 °C. These optima are similar to those of AtICS1, although less broad. As with AtICS1, this enzyme possesses exceptional maximal activity at 4 °C (~80%).

AtICS2 can catalyze the formation of ADIC. I wanted to see if AtICS2 catalyzes the formation of ADIC when ammonium is present in the reaction medium, as do Eco EntC [59] and AtICS1 (Chapter 2). After 30 minutes at 30 °C in the presence of the equivalent of 100 mM ammonium, a dramatic increase occurs in the area of a peak appearing at a retention time of 2.3 minutes in the HPLC chromatogram (Figure 3.12). This peak has an absorbance spectrum and an HPLC retention time that are identical to those of the ADIC prepared under the same conditions via the action of Eco EntC [59]. Conversion to units of concentration was carried out using an extinction coefficient of 11,500 M^{-1} cm^{-1} [300]. This conversion indicates that 49 μM of ADIC is present in the ammonium reaction, whereas at most 8 μM ADIC is present in the control reaction undertaken without added ammonium. As the reaction was initiated with 1 mM chorismate, this corresponds to a conversion of about 5% of the substrate to ADIC by the enzyme AtICS2 – this amount is similar to that produced by AtICS1. Reactions with 5 mM of the amino acids glutamate or glutamine in the media in place of ammonium produced no rise in ADIC formation, similar to AtICS1 (data not shown).

DISCUSSION

Herein is presented a characterization of the enzymology of AtICS2. I determined thermodynamic and kinetic parameters for the overexpressed recombinant enzyme using assays for isochorismate synthase enzymes that we had previously developed. My studies support a role for AtICS2 in phylloquinone biosynthesis, but do not rule out a role for AtICS1 in this pathway as well.

Precedent exists for enzymes that are highly homologous to bacterial enzymes to act as salicylic acid synthases [94, 317]. Though previous characterization of AtICS1 had determined that it was a monofunctional ICS, and not a bifunctional SAS, I needed to rule out this possibility for AtICS2. Isochorismate has been detected by ^{1}H NMR spectroscopy to be a short-lived intermediate in SA synthase enzymes [61]. Therefore, I tested whether AtICS2 could act as an SAS. It could not; AtICS2 shows monofunctional activity very similar to that of AtICS1.

It was shown by the work of Johnson [121] that the *menA* mutant in cyanobacteria grows well at low light, but does not grow at all when submitted to strong light. In the work of Gross,

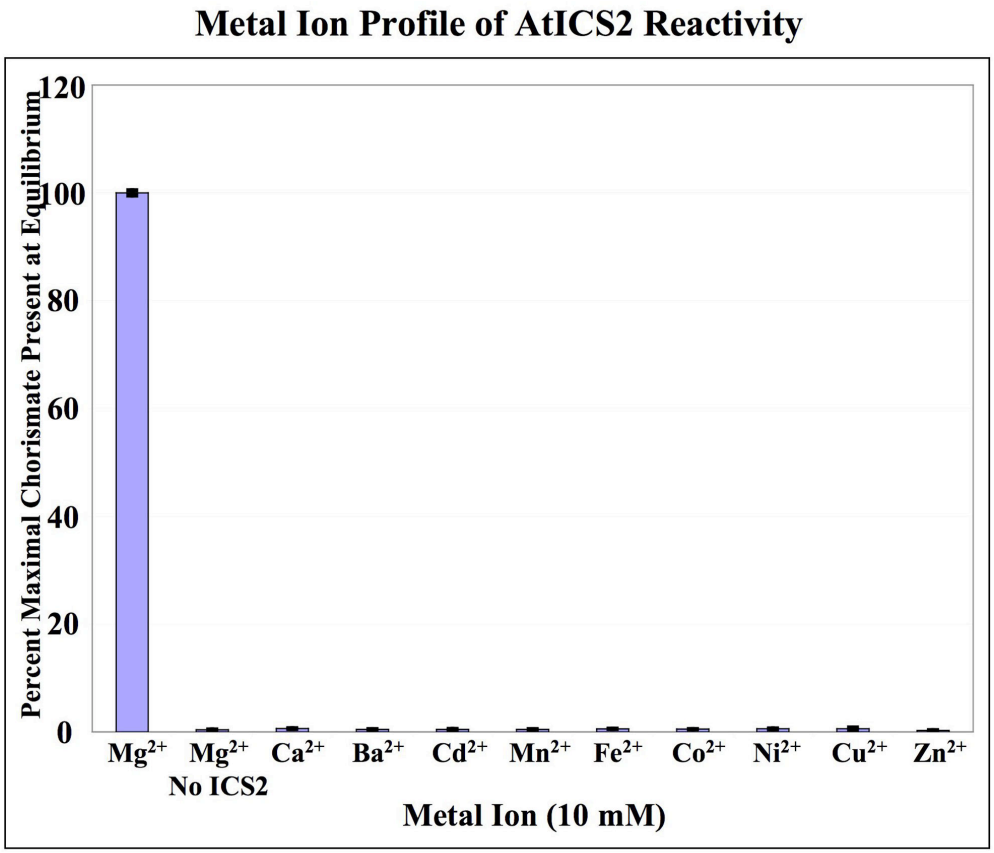

Figure 3.9. The Effect of Divalent Metal Ions on AtICS2 Reactivity. Shows the extent of maximal reaction after 60 minutes incubation at 30 °C with the indicated metal ion, as assayed by HPLC. All metal ion concentrations were 10 mM. All HPLC assayed reactions were performed in triplicate two different times, using protein isolated from separate preparations.

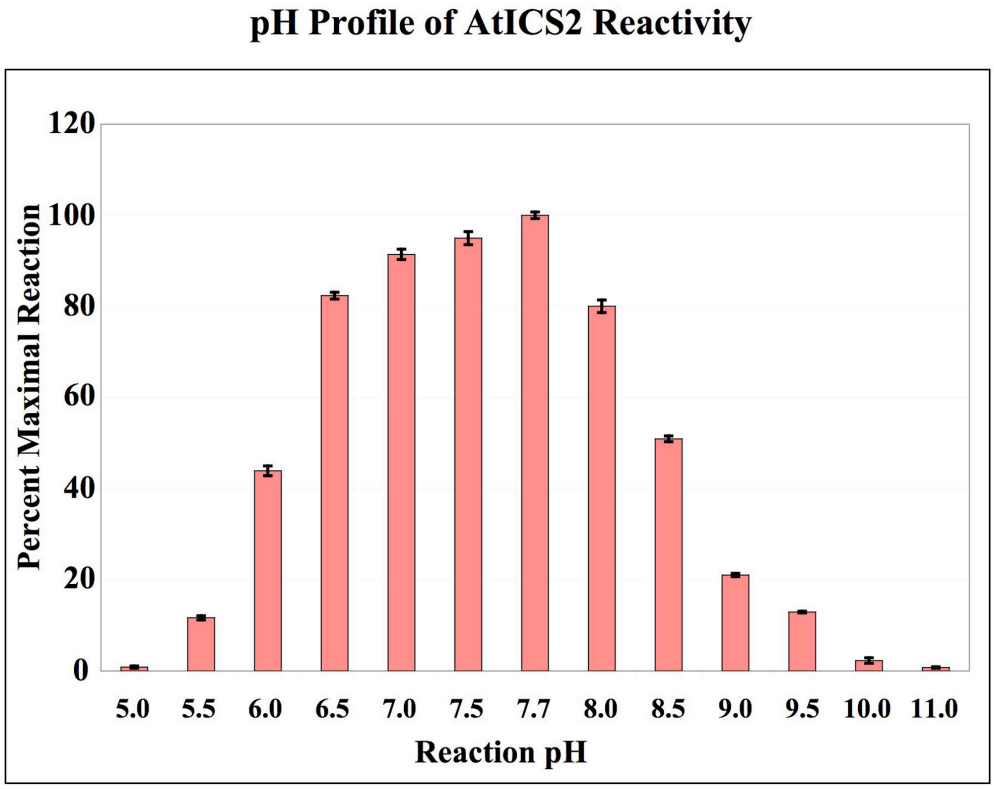

Figure 3.10. pH Profile of AtICS2 Reactivity. The top graph shows the percentage of maximal reaction after 60 minutes incubation at a variety of pH values. All reactions were performed in triplicate two different times, using protein isolated from separate preparations.

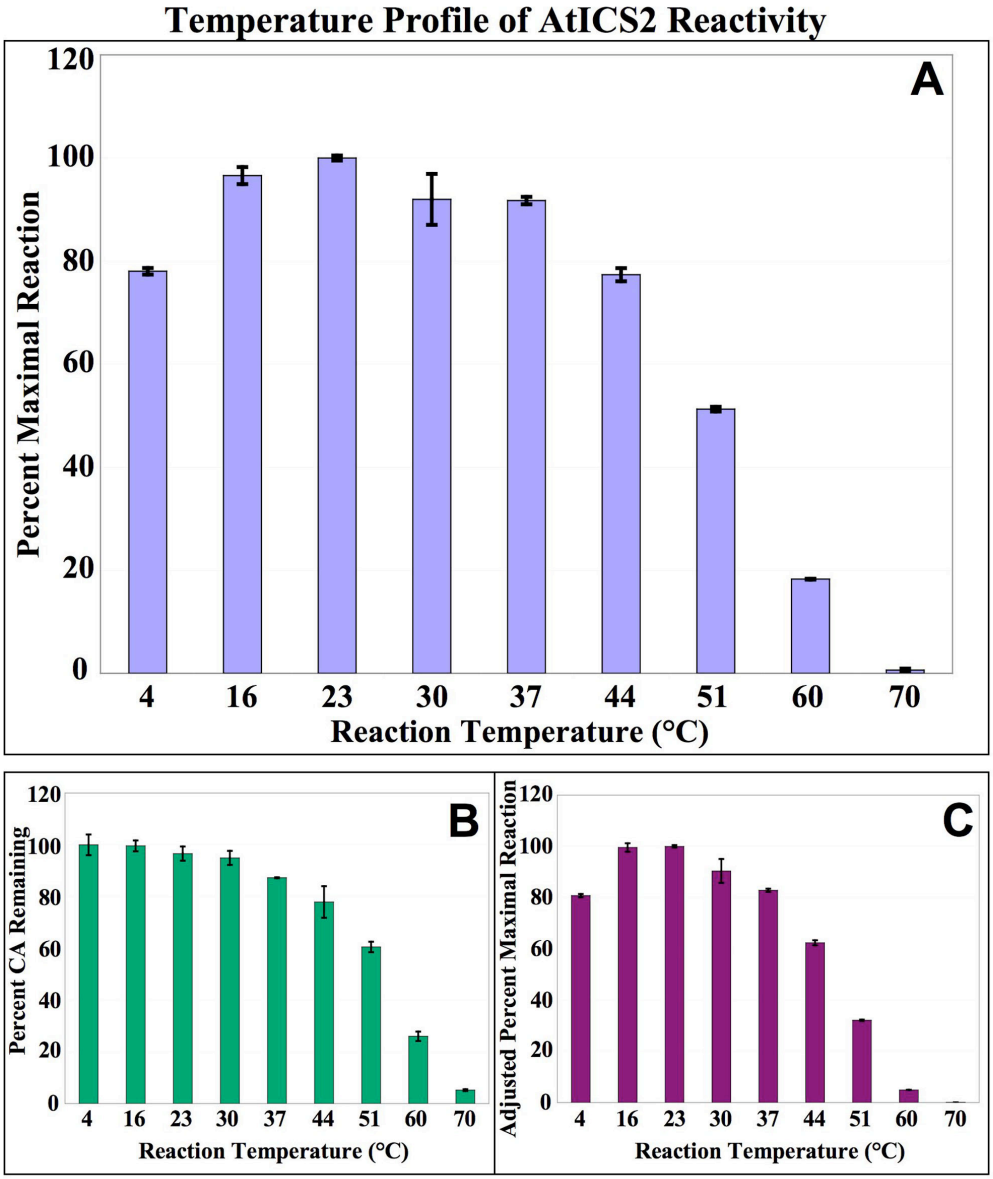

Figure 3.11. Temperature Profile of AtICS2 Reactivity. (A) Percentage of maximal reaction after 60 minutes incubation at a variety of temperatures. (B) Percent chorismate remaining after 60 minutes incubation at a variety of temperatures. (C) Above data from (A) adjusted for the non-enzymatic degradation of the isochorismate product at each given temperature, using the assumption that isochorismate degrades at a rate similar to that of chorismate. All reactions were performed in triplicate two different times, using protein isolated from separate preparations.

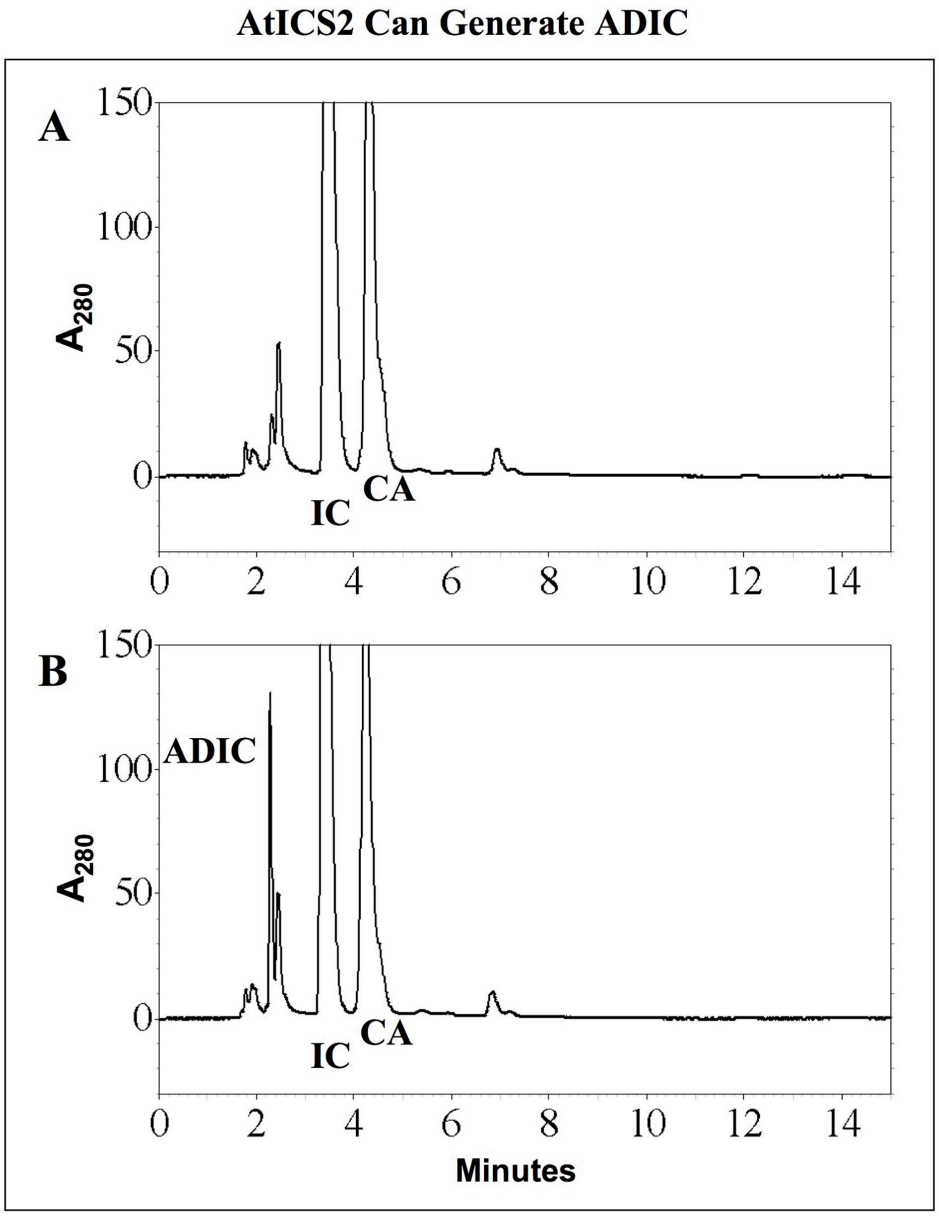

Figure 3.12. AtICS2 Can Generate ADIC. Both reactions were incubated at 30 °C for 30 minutes each. (A) Shows the HPLC chromatogram of the reaction catalyzed by AtICS2 incubated with 1 mM chorismate. (B) Shows the HPLC chromatogram of the same reaction as in (A), but with 50 mM ammonium sulfate added to the medium. The peak at ~2.15 minutes is presumed to be ADIC as its retention time and absorbance spectrum are identical to that of the ADIC produced by Eco EntC [59].

the *pha* mutants and the *ics1* and *ics2* mutants were grown under normal light [95]. It is possible that a phenotype would emerge for the *ics2* mutant when dark-grown seedlings experience a sudden switch to light, or when low light grown plants are exposed to high light. The data demonstrating localization of AtICS2 in the chloroplast stroma specifies the conditions under which AtICS2 must operate. Under dark conditions, the stroma is reported to be at pH 7, with a compartmental Mg^{2+} concentration of 1-3 mM. Under light conditions, these increase to pH 8 and an Mg^{2+} concentration of 3-6 mM, respectively [7]. Though the pH optimum of AtICS2 does not change significantly from 7-8, an increase in Mg^{2+} concentration due to light could make a significant difference in this AtICS2 activity: we have calculated the K_M for Mg^{2+} to be 573 μM, and the saturating Mg^{2+} concentration to be approximately 4 mM. Specifically, when the concentration of Mg^{2+} ions is 1 mM, the AtICS2 activity is approximately 2 μM/min, whereas when the Mg^{2+} concentration is 4 mM, the AtICS2 activity is at the V_{max} (at this concentration of enzyme) of ~3.8 μM/min. AtICS2 activity could be impaired under dark conditions, because it cannot operate at maximal velocity, but under light conditions, it would be fully saturated with Mg^{2+} and active.

I have calculated the K_M for chorismate of AtICS2 to be 17.2 μM and the k_{cat} to be 18.0 min^{-1}. The K_M for this enzyme is over 2-fold lower than that for AtICS1, and significantly lower than that for other plant chorismate-utilizing enzymes (see Discussion in Chapter 2). This suggests that AtICS2 binds the chorismate available from the shikimate pathway in preference to the other enzymes with which it is forced to compete. As the K_M of an enzyme also often matches the physiological concentration of that substrate, the low value of the AtICS2 K_M suggests that the protein has evolved to operate at a relatively low concentration of chorismate. This makes it likely that AtICS2 in leaves works in a constitutive manner, consistent with its low-level constitutive expression. This same scenario is observed for another set of *Arabidopsis* chorismate-utilizing enzymes, the anthranilate synthases: the *AtASA1* gene is induced in response to pathogen treatment, whereas *AtASA2* is constitutively expressed for the production of basal levels of anthranilate (see [68] and Chapter 1). It appears that AtICS2 may preferentially generate phylloquinone, an important biological factor that is required in photosynthesis. This stands in contrast to AtICS1, which is operative mainly under conditions of phytopathogen attack when it is required for induced SA production. Because phytopathogens up-regulate the genes in the shikimate pathway as well [36], the concentration of chorismate under these conditions is likely to be higher, and AtICS1 would not likely need the binding affinity required by a constitutive enzyme like AtICS2.

CHAPTER IV

CANDIDATES FOR ISOCHORISMATE PYRUVATE LYASE ENZYMES IN *ARABIDOPSIS*

INTRODUCTION

Arabidopsis ICS1 is known to be required for SA accumulation in response to pathogen [81], and this enzyme has been shown to possess an activity that converts chorismate to isochorismate (Chapter 2). However, the biochemical pathway from isochorismate to SA in *Arabidopsis* and other plants has not been defined. Furthermore, I have shown (Chapter 2, and see Figure 2.13) that there is little non-enzymatic conversion of isochorismate to SA – specifically, that 0.08% isochorismate is converted to SA per hour at 23 °C. Clearly, this reaction rate is insufficient to generate the large burst of SA seen in plant defense phenomena.

It is likely that an enzyme with isochorismate pyruvate lyase (IPL) activity converts isochorismate to SA. This is a pathway that is known in the bacterium *Pseudomonas aeruginosa*, in which a gene encoding the enzymatic capacity of an IPL evolved from a gene encoding a chorismate mutase (CM) enzyme [298]. Pae PchB possesses both IPL and CM activities (see Appendix 2 and Figure A2.8) – though it has a 12-fold lower K_M for chorismate than isochorismate – and is predicted to have the all α-helical structural organization of the AroQ class of CM enzymes [298]. In addition, it has been suggested that SA is also synthesized from phenylalanine in plants, via a phenylalanine ammonia lyase (PAL) pathway that has not yet been completely defined in *Arabidopsis* or any plant (see Chapter 1 and Figure 1.12). As CM enzymes are responsible for the conversion of chorismate to prephenate – a precursor of phenylalanine – CM enzymes in this case could act to control flux through this proposed SA biosynthetic pathway by competing with ICS enzymes for available chorismate. As shown in Figure 1.9, CM proteins also provide precursors for the synthesis of phenylalanine, tyrosine, and specialized metabolites such as phenylpropanoids. One of the three CM genes in *Arabidopsis* – that encoding the putative chloroplast-localized protein AtCM1 – is induced by pathogen [67]. Additionally, both AtCM1 and AtCM3 are allosterically regulated [67] by tryptophan (positively), and by tyrosine and phenylalanine (negatively), allowing for integrated chorismate utilization and partitioning in the chloroplast (see Figure 1.9).

Arabidopsis CM1 (At3g29200) and CM3 (At1g69370) are likely targeted to the chloroplast, whereas CM2 (At5g10870) appears to be cytosolic [66, 67]. Analysis of these proteins by ChloroP, PCLR, and PSORT protein localization prediction programs supports these predictions. However, chloroplast transit peptides (CTPs) can be missed in annotation and may also be missed in clones identified as being full length. Neither AtICS1 nor AtICS2 were originally annotated to include the putative chloroplast transit sequence, though it is present. Manual examination of the genomic region upstream of AtCM2 for missed open reading frames, an extensive survey conducted in the RARGE database [318] containing the full set of RIKEN full length cDNA clones and ESTs, and analysis of the *Arabidopsis* expression tiling data [319], all revealed no *AtCM2* chloroplast transit sequence [66, 67] or likely *AtCM2* differential transcript. These analyses support cytoplasmic localization for AtCM2, though it had originally been assumed that all plant chorismate mutases would be found in the chloroplast as their substrate – chorismate – is synthesized therein, and as all subsequent enzymes of the tyrosine and phenylalanine biosynthetic pathways are known to be localized to the chloroplast (see Figure 1.9). Previous studies indicated that the apparent K_M for chorismate of AtCM1 is 2900 μM, whereas AtCM2 and AtCM3 exhibit K_M values for chorismate of 230 μM and 420 μM, respectively [67]. The *Pseudomonas aeruginosa* IPL PchB also exhibits CM activity [298], and its K_M value for chorismate (150 μM) is higher than that known for *P. aeruginosa* CM (98 μM) [320]. Given the remarkably high K_M of AtCM1 for chorismate, its chloroplast localization, and

its pathogen-induced expression, AtCM1 appeared to be a top candidate to act as an *Arabidopsis* IPL enzyme. To ascertain whether any of the *Arabidopsis* CM enzymes could act as IPL enzymes in SA biosynthesis, *in vitro* analysis of the heterologously expressed recombinant enzymes needed to be performed.

Alternative possibilities are that a bifunctional SAS enzyme – possessing both ICS and IPL activities – may be responsible for SA generation, or that a SAS-like enzyme from which only the IPL activity has been retained acts to generate SA from the isochorismate produced by AtICS1. Perhaps AtICS1, due to its induction in the plant defense response, could be undergoing an alternative transcriptional event that generates a product with SAS rather than ICS activity, thereby enabling large-scale production of SA directly from chorismate. Two SAS enzymes have been characterized to date, both of which are involved in the production of SA for siderophore biosynthesis in bacteria: *Yersinia enterocolitica* Irp9 [58, 91, 94] and *Mycobacterium tuberculosis* MbtI [61, 317, 321]. Like other enzymes of the evolutionarily-related MST family – a group that includes the chorismate-utilizing enzymes AS, ADCS, and ICS (see Chapter 1 and Figure 1.7) – these SAS enzymes possess a complex α/β fold with a highly conserved deep cleft that contains binding sites for chorismate and the Mg^{2+} atom required for catalysis. In fact, the active sites of Irp9 [58] and MbtI [61, 317] are almost identical to those of the MST enzymes *S. marcescens* TrpE [51], *E. coli* PabB [52], and *E. coli* MenF [45, 53] – an AS, an ADCS, and an ICS, respectively – each of which is represented in Figure 1.8. The presence of putative general base (Lys190 in *E. coli* MenF) and general acid (Glu240 in *E. coli* MenF) amino acid residues in identical orientations in the active sites of Irp9, MbtI, and MenF strongly suggests that all of these enzymes – a group that includes the plant homologs AtICS1 and AtICS2 – convert chorismate to isochorismate via an identical mechanism (see Figure 1.8).

As both SAS and AS enzymes are bifunctional enzymes that also catalyze secondary aromatization of the initial chorismate adducts by elimination of pyruvate, it was believed that unique amino acid residues from these two classes of MST enzymes could be identified that were responsible for the aromatization. Biochemical studies involving chemical modification [322] and mutagenesis [300] of bacterial AS enzymes led to the initial conclusion [51] that a catalytic histidine residue (His397 of the Sma 1I7Q AS sequence in Figure 1.7) acts as a general base that abstracts the C2 ADIC proton as part of a bimolecular *syn*-elimination of pyruvate. However, this histidine residue is present in virtually all MST enzyme sequences regardless of whether they catalyze pyruvate elimination, and structural [58] and modeling [323] studies of the SAS Irp9 show that this residue is located on the side of the substrate molecule opposite that from which C2 proton abstraction must occur. Furthermore, the ^1H NMR studies on the reaction catalyzed by the SAS MbtI show that the proton acquired by the pyruvate methyl group in the elimination reaction is derived from the substrate and not the D_2O medium [61], suggesting that general base catalysis cannot be taking place. Finally, an analysis of several available MST crystal structures [45, 49-52] and more than 1000 MST sequences [61] indicates that there are no active site residues unique to AS and SAS enzymes that both directly contact the ligand and are capable of proton abstraction. These data all suggest that the mechanism for pyruvate elimination in AS and SAS enzymes does not involve general base catalysis.

Investigation of the uncatalyzed reactivity of chorismate and isochorismate suggests an alternative mechanism for the pyruvate lyase reaction catalyzed by SAS and AS. Work by the Hilvert laboratory has demonstrated that the orientation of the enolpyruvyl side chains of chorismate [44] and isochorismate [305] controls the reactivity of the respective compound in solution (Figure 4.1). Hybrid density functional theory calculations and experimentally

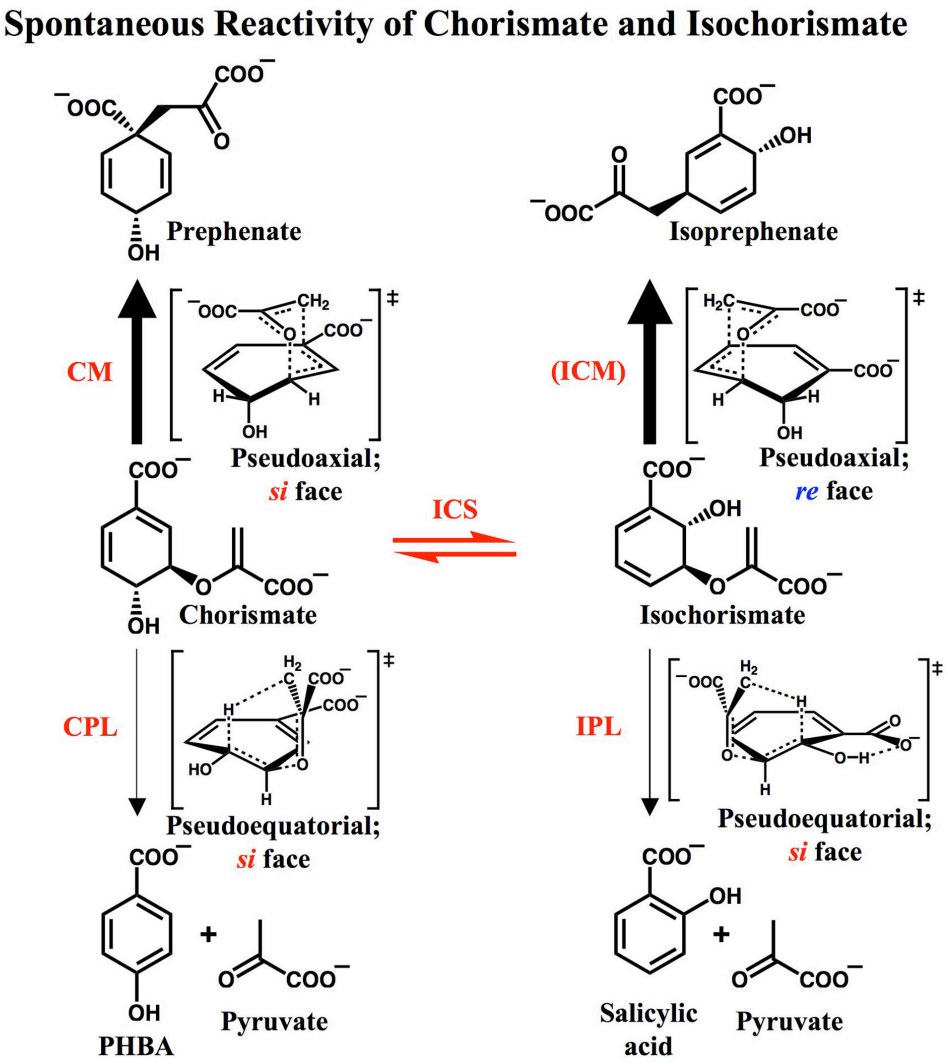

Figure 4.1. Spontaneous Reactivity of Chorismate and Isochorismate. The uncatalyzed reactions of chorismate and isochorismate that proceed in solution are shown above, with the computationally-derived transition state structures of each boxed and indicated by a double dagger symbol. The size of each black arrow is correlated with the relative rate of the spontaneous reaction in solution at 60 °C and pD 7.5 (see text). Enzymes that catalyze these reactions - likely by the same mechanisms - are specified in red, with the parentheses indicating that the enzyme ICM is uncharacterized, and the red arrows indicating that the ICS reaction is nonspontaneous. The predicted substrate conformations and facial selectivity of the reactive enolpyruvate moiety are indicated below each mechanism. Abbreviations used are: ICS, Isochorismate synthase; CM, Chorismate mutase; ICM, Isochorismate synthase; CPL, Chorismate pyruvate lyase; IPL, Isochorismate pyruvate lyase; PHBA, *para*-Hydroxybenzoic acid.

determined kinetic isotope effects show that, in the absence of catalyst, both chorismate and isochorismate undergo spontaneous rearrangement – to prephenate and isoprephenate, respectively – via concerted, asynchronous pericyclic processes in which carbon-carbon bond formation lags behind carbon-oxygen bond cleavage [44, 305]. Each of these spontaneous reactions is predicted by calculation to proceed via a chair-like transition state with the molecule positioned in a pseudoaxial conformation, and these transition states place the enolpyruvate carboxylate group over the ring, with the *si* face of this group oriented toward the ring in the case of chorismate and the *re* face oriented toward the ring in the case of isochorismate [44, 305]. These calculations are consistent with previous work using stereospecifically-labeled chorismate that showed the uncatalyzed [324] and CM-catalyzed [325, 326] reactions both proceed via chair-like transition states; however, these studies have not been performed for isochorismate and the enzyme isochorismate mutase has not been thoroughly characterized [327].

Chorismate and isochorismate have also been shown to decompose via concerted, asynchronous pericyclic mechanisms that result in the elimination of pyruvate – to *para*-hydroxybenzoic acid (PHBA) and SA, respectively [44, 305]. These uncatalyzed elimination reactions occur at rates that are 8- to 9-fold slower (at 60 °C and pD 7.5; see [44, 305]) than those of the corresponding rearrangements (Figure 4.1), in spite of the fact that elevated temperatures favor elimination, and despite each molecule being predicted by calculation [44, 305] to undergo elimination from its energetically more favorable – and more highly populated [328] – pseudoequatorial conformation. This suggests that these transition states are more strained; indeed, the structure determined computationally for pyruvate elimination in chorismate has a twist-boat conformation with the *si* face of enolpyruvate oriented toward the ring [44], and the structure determined for pyruvate elimination in isochorismate has an asymmetric chair-like conformation with the *si* face of enolpyruvate oriented toward the ring [305]. More recently, it has been established that pyruvate elimination catalyzed by the IPL enzyme Pae PchB occurs via a pericyclic mechanism that is identical to that of the uncatalyzed isochorismate elimination [329, 330], and structural evidence has been provided that the pyruvate elimination catalyzed by *E. coli* chorismate pyruvate lyase proceeds via a mechanism with the same enolpyruvate facial selectivity as that found for the uncatalyzed chorismate elimination [331].

The putative CM and IPL transition states of the reactions catalyzed by the enzyme Pae PchB are structurally and electrostatically similar, though this is not obvious in Figure 4.1. Evidence for this similarity has been provided by structural studies on PchB [332, 333], and by the ability of an *endo*-oxabicyclic diacid CM transition state analog prepared by Bartlett and coworkers [334, 335] to inhibit both the CM and IPL activities of PchB [298]. The enolpyruvate side chains of chorismate and isochorismate are oriented in a similar manner with respect to the ring carbons – with their *si* face positioned above the ring and toward it – in the putative CM and IPL transition states, respectively. These transition states differ mainly in the nature and orientation of the substituent at the ring position *ortho*- to the C1 carboxylate: there is none in the chorismate undergoing the CM reaction, and there is a pseudoequatorial hydroxyl group hydrogen bonding to the ring carboxylate in the isochorismate undergoing the IPL reaction (Figure 4.1). The discovery that a PchB point mutant with threonine replacing isoleucine at position 87 – located near the ring position *ortho*- to the C1 carboxylate – has dramatically reduced IPL activity but nearly wild type CM activity, led to the suggestion that hydrogen bonding between the threonine side chain hydroxyl and the C2 hydroxyl of isochorismate effects an isochorismate conformation that cannot undergo pyruvate elimination [298]. It is possible that such a hydrogen bond to a threonine residue is able to disrupt the intramolecular hydrogen

bond of pseudoequatorial isochorismate (shown in Figure 4.1), allowing the molecule to adopt a pseudoaxial conformation from which elimination of the enolpyruvate – positioned by active site residues to present its *si* face to the ring – is disfavored. The structure of the PchB I87T mutant was too disordered to confirm this hypothesis [332].

The IPL PchB evolved from a CM enzyme, and is not homologous to the MST family of enzymes. Nevertheless, SAS enzymes also appear to catalyze the IPL reaction via a pericyclic mechanism, as evidenced by the complete lack of deuterium incorporation into the pyruvate product when the enzymatic reaction is carried out in D_2O [61]. As 25 of the 26 active site residues are conserved in AS and SAS enzymes, and as the active site structures determined for AS [51] and SAS [58] enzymes position the bound Mg^{2+}, pyruvate and benzoate (salicylate in the SAS) ligands in identical orientations, it is highly likely that both enzymes catalyze pyruvate lyase reactions via identical mechanisms. Among the 26 amino acid residues that are located within 6 Å of the bound ligands in the *S. marcescens* TrpE AS [51] or *Y. enterocolitica* Irp9 SAS [58] structures are superimposable threonines that are within hydrogen bonding distance of the C2 of the benzoate or salicylate ligand, respectively (Figure 4.2). A threonine residue is conserved at this position in all SAS and AS enzymes, but is replaced by alanine in all ICS enzymes, and serine in most ADCS enzymes (see Figure 1.7); importantly, neither ICS nor ADCS have pyruvate lyase activity. One possibility is that the residue at this position controls the ability of the enzyme to act as a pyruvate lyase by influencing the conformation of the initial chorismate adduct. Though the Sma TrpE AS and Yen Irp9 SAS structures have only planar aromatic products bound in their active sites, high affinity MST enzyme inhibitors prepared by Bartlett and coworkers [59] provide strong evidence that MST-catalyzed reactions proceed via transition states that are nearly pseudoaxial (Figure 4.2). These compounds are believed to act as transition state analogs due to the high population in solution of their all-axial conformers, and related molecules that do not achieve this all-axial conformation as readily (or at all) are far worse inhibitors of AS [336-338], ICS [337], and SAS [323, 337] enzymes. Furthermore, the rapid reversibility of the reactions catalyzed by MST enzymes, and the results obtained from structural studies with pseudoaxial chorismate [45] and isochorismate [61] modeled onto several MST enzyme active sites, suggest that pseudoaxial substrates and intermediates are preferentially bound by MST enzymes. The threonine residue in the active sites of AS and SAS enzymes could be acting to minimize the reversion back to chorismate by altering the conformation of the ADIC and isochorismate intermediates, respectively, to one that is not purely pseudoaxial (Figure 4.2).

Another reason the pseudoaxial conformer of the initial chorismate adduct might be disfavored by bifunctional MST enzymes is that pericyclic elimination of the kind catalyzed by SAS appears to favor conformations that are pseudoequatorial [305]. The asymmetric chair-like transition states predicted for the spontaneous [305] and PchB-catalyzed [329] isochorismate pyruvate lyase reactions occur from an almost purely pseudoequatorial conformation of isochorismate in which the *si* face of the enolpyruvate side chain is directed toward the ring (see Figure 4.1). However, several structural studies [51, 58, 317] show that pyruvate is bound in the active site of MST enzymes in an orientation that presents its *re* face to the ring carbons of the product, suggesting that the enolpyruvate moiety of isochorismate bound in SAS – or of ADIC bound in AS – will also be oriented in this manner. Likewise, investigation of the steric course of the AS pyruvate lyase reaction using selectively deuterated and tritiated chorismate has determined that the pyruvate produced is stereospecifically protonated on its *re* face [326], suggesting that any pericyclic elimination catalyzed by AS or the highly homologous SAS is not

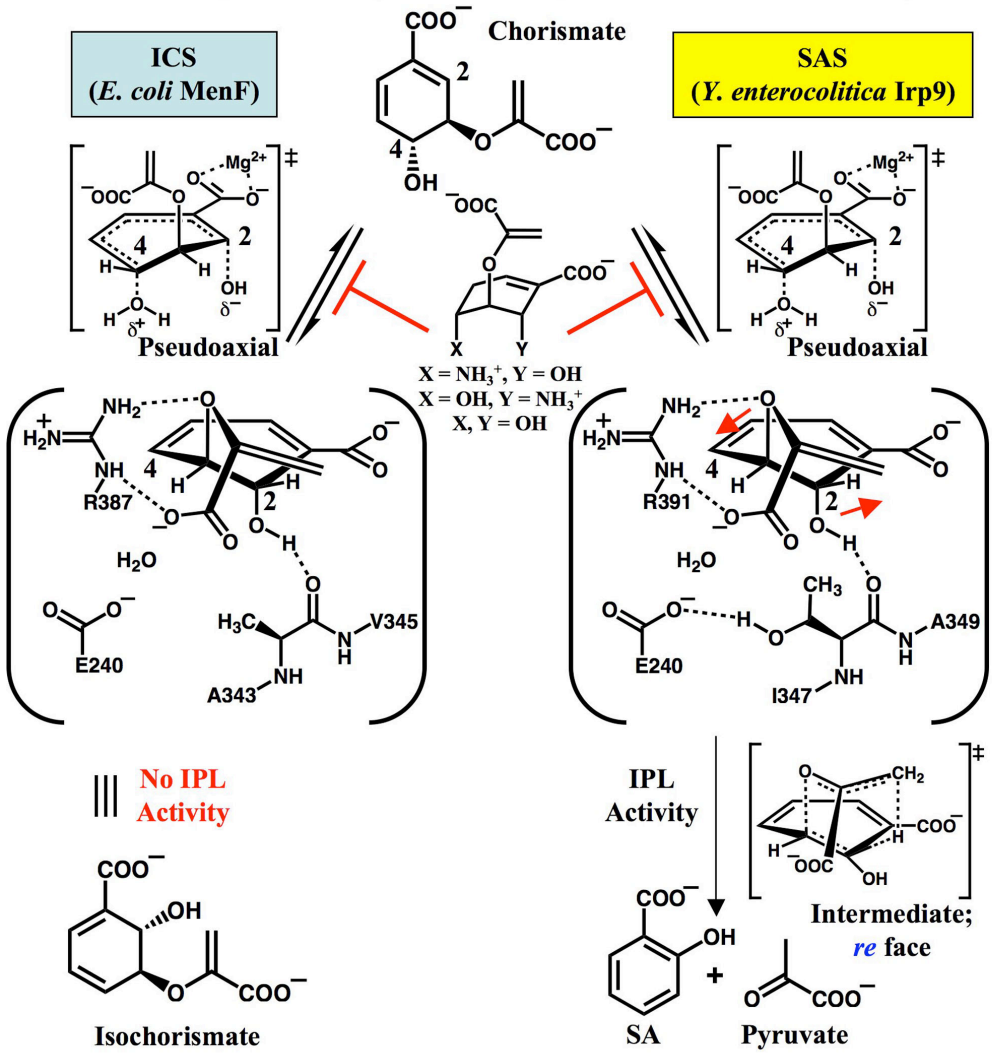

Figure 4.2 Pyruvate Lyase Activity in SAS Enzymes. The reaction course is shown for representative ICS and SAS enzymes whose structures have been solved. Both perform the ICS reaction, for which the putative pseudoaxial enzyme-catalyzed transition state is indicated. The Bartlett inhibitors are shown to inhibit the ICS reactions in their all-axial conformations. Five homologous active site residues are labeled, including the putative general acid glutamate (E240 in Irp9), the arginine (R391 in Irp9) believed to orient the enolpyruvate with its *re* face toward the ring carbons, and the threonine (T348 in Irp9, Ala in MenF) that may play a role in the pyruvate lyase reaction. Red arrows suggest a shift in the bound isochorismate intermediate to a more pseudoequatorial conformation. The putative transition state of the IPL reaction in Irp9 is shown to proceed from a partly pseudoequatorial conformation. Abbreviations used as in text.

proceeding through the chair-like transition state shown in Figure 4.1. A second asymmetric twist-boat transition state of slightly higher-energy is also predicted for the spontaneous IPL reaction [305], and it occurs from a conformation that is intermediate between purely pseudoequatorial and purely pseudoaxial (Figure 4.2). This transition state directs the *re* face of the enolpyruvate side chain toward the isochorismate C2 carbon, and it has been proposed that all pyruvate elimination in the MST family of enzymes takes place via such a transition state [61]. It could be the case that a hydrogen bond between the aforementioned active site threonine residue (Thr424 in the *S. marcescens* TrpE AS and Thr348 in the *Y. enterocolitica* Irp9 SAS) and the C2 substituent on the initial chorismate adduct aids the process of pyruvate elimination by inducing a substrate conformation with more pseudoequatorial character (shown in Figure 4.2).

In the interest of determining how the active site residues of AtICS1 could contribute to SAS activity – particularly at the site of the alanine residue that is homologous to Irp9 Thr348 – homology modeling of Irp9 and AtICS1 was undertaken. Irp9 was chosen for homology modeling because its crystal structure [58] has SA, pyruvate and Mg^{2+} ligands bound in the active site. Subsequently, single, double and triple point mutants of *AtICS1* and *AtICS2* were overexpressed in *E. coli* and purified. These could then be assayed for SAS, ICS and IPL activity using previously described procedures. In the process of this work it was hoped that light could be shed on two issues regarding the roles of ICS and CM genes in *Arabidopsis*. First, does a CM act as an IPL in the biosynthesis of SA? Second, are there specific residues in the active site of an ICS that, when mutated, will establish IPL activity in the enzyme?

MATERIALS AND METHODS

Materials and General Protocols

All specialty reagents and chemicals were obtained from Sigma-Aldrich unless otherwise specified. HPLC-grade solvents (EMD Biosciences) were employed in the HPLC analyses. Barium chorismate (Sigma C-1259, 60-80% purity) was used in all assays requiring chorismate. For selection and growth of transformed cells (described below), all pET-28 derivatives were selected with 50 μg/ml kanamycin. Commonly utilized protein and molecular biological reagents and protocols were prepared/performed as in *Current Protocols in Molecular Biology* [295].

Purification of Recombinant AtCM1

pSM157-4 (obtained from Dr. Sharon Marr) is a pET-28 derivative containing a sequence encoding an amino-terminal His_6-tag fused to the sequence beginning with that encoding amino acid 58 of the *Aradibopsis thaliana* CM1 coding region, in a manner identical to pSM157-16 from Chapter 2. These two plasmids are identical in all other respects (see Figure 2.1 for the organization of plasmid pSM157-16). The pSM157-4 AtCM1 coding sequence was confirmed to be identical to AtCM1 sequence NC_003074.5 (At3g29200). *E. coli* Rosetta2 (DE3) cells (Novagen) were transformed with plasmid pSM157-4. A crude cell extract was prepared from a 2 L culture of transformed cells grown in TB media containing 0.2% glucose, 50 μg/ml kanamycin and 30 μg/ml chloramphenicol. The culture was grown at 37 °C with agitation in baffled flasks until an OD_{600} of approximately 0.6 was reached, at which point IPTG was added to a final concentration of 0.5 mM to induce protein synthesis. Shaking was continued at 18 °C for 17 hours. All subsequent operations were carried out at 4 °C. The cells (wet weight

approximately 10.6 g) were harvested and resuspended in 40 ml of Binding Buffer (50 mM sodium phosphate buffer, pH 8.0, 300 mM sodium chloride, 10 mM imidazole) containing 2 mM PMSF and 10 μM leupeptin. The cells, which could be stored at –20 °C, were lysed by two passages through a French press at 18,000 psi at the orifice. Following centrifugation, the supernatant was filtered by syringe through an HPF Millex-HV 0.45 μm filter unit attached in series to a Millex-AP prefilter (Millipore). Filtrate was allowed to bind to 5 ml of Ni^{2+}-NTA His-Bind Resin (Novagen) by mixing with mild agitation on a rotary shaker for 3 hours. The resin had been pretreated according to the manufacturer's directions. The slurry was then poured into a column, and the flow-through was collected in one portion. After washing the column with 2 portions of 10 ml each of Binding Buffer, His_6-AtCM1 was eluted with 20 ml of Elution Buffer (components as Binding Buffer, but including 250 mM imidazole). The first 10 fractions of 1 ml each were separately dialyzed into a buffer containing 100 mM Tris, pH 7.7, 10% glycerol, and 1 mM DTT. The protein fractions were then stored at –80 °C. Similarly purified AtCM2 and AtCM3 proteins were obtained from Dr. Sharon Marr.

Chorismate mutase activity of the three above enzymes was determined via an assay based on the method of Gilchrist and Connelly [339]. A dilution of CM enzyme was prepared in 400 μl of buffer containing 100 mM Tris, pH 7.7, 10% glycerol, and 1 mM DTT, and this was mixed with 100 μl of 5 mM chorismate to initiate the reaction. This mixture was incubated at 30 °C for 10 minutes before the reaction was quenched by addition of 100 μl 6 N HCl. After 10 minutes of gentle agitation at room temperature, 400 μl of 6 N NaOH was added to neutralize the solution, and absorbance was measured spectrophotometrically at 320 nm. The value for absorbance was converted to units of phenylpyruvate concentration using an extinction coefficient of 17,500 M^{-1} cm^{-1}. A blank reaction containing no CM enzyme was performed as a control, and the phenylpyruvate produced was subtracted from the value determined with enzyme for the purpose of obtaining a value for chorismate mutase enzyme activity.

Protein Quantification Assays

These assays were performed as described in Chapter 2.

HPLC IPL Activity Assay for CM Enzymes

This assay was modified from a previous study [298]. The incubation mixture contained, in a final volume of 200 μl, 100 mM Tris, pH 7.7, 1 mM isochorismate (purified as described in Chapter 2), 10% glycerol, 10 mM $MgCl_2$, and 110 μg/ml enzyme. Controls without enzyme were also carried out. The reaction was incubated for 60 minutes at 30 °C after having been initiated with isochorismate. The mixture was then filtered through a 0.2 μm Millex-LG syringe filter (Millipore), and a 50 μl aliquot was injected into an HPLC under the same conditions as that described for the "Coupled HPLC Assay for ICS Activity" in Chapter 2.

Homology Modeling of ICS Enzymes

Homology modeling was performed in collaboration with Dr. Chloe Zubieta. The primary sequences for *A. thaliana* AtICS1 (AAL17715) and *Y. enterocolitica* Irp9 (CAB46570) were aligned with CLUSTAL W [340] using the default parameters. Due to poor alignment of the amino-terminal portion of the proteins, residues 1-198 and 1-92 of AtICS1 and Yen Irp9 respectively were not used in model generation. Note that AtICS1 contains an amino-terminal chloroplast transit sequence of ~45 amino acids as predicted by ChloroP [341] and confirmed via chloroplast import assays [82]. Homology modeling was performed with Modeller 8v2 [342]

using the Yen Irp9 crystal structure in complex with its reaction products SA and pyruvate (Protein Data Bank identification code 2FN1) [58]. Five models were generated and the lowest energy model selected. The AtICS1 model and Yen Irp9 were superimposed in COOT [343]. All figures were generated using PyMOL (DeLano, W. L. The PyMOL Molecular Graphics System (2002) on the World Wide Web http://www.pymol.org). Homology modeling of additional ICS enzymes including *M. tuberculosis* MbtI (CAE55483), Pae PchA (CAA57969), Eco EntC (POAEJ2), AtICS2 (NP_173321), *Catharanthus roseus* ICS (CAA06837), and *Capsicum annum* ICS (AAW66457) was performed in a similar manner.

Cloning and Purification of Recombinant AtICS1 A472T Mutant

The AtICS1 A472T mutant vector was generated from pSM157-16 (obtained from Dr. Sharon Marr), a pET-28 derivative, using the QuikChange II Site-Directed Mutagenesis Kit (Stratagene). The protocols accompanying the kit were followed, with the following modifications. 50 ng of pSM157-16 were PCR-amplified with 125 ng each of ultrapure primers (forward primer: 5'-tctgcatccaactccaactgtttgtgggcttcc-3', reverse primer: 5'-ggaagcccacaaacagttggagttggatgcaga-3') by undergoing 12 cycles of amplification with the designated parameters. Following Dpn I digestion of the parent plasmids and transformation of the mixture into XLI-Blue cells, the entire cell suspension was spread onto LB-kanamycin plates containing 80 μg/ml X-gal and 20 mM IPTG. Plasmids were isolated from subsequent white-colored colonies and coding sequences were confirmed to be correct for the desired point mutant.

E. coli Rosetta2 (DE3) cells (Novagen) were transformed with the above plasmid. A crude cell extract was prepared from a 2 L culture of transformed cells grown in TB media containing 0.2% glucose, 50 μg/ml kanamycin and 30 μg/ml chloramphenicol. The culture was grown at 37 °C with agitation in baffled flasks until an OD_{600} of approximately 0.7 was reached, at which point IPTG was added to a final concentration of 0.2 mM to induce protein synthesis. Shaking was continued at 18 °C for 17 hours. All subsequent operations were carried out at 4 °C. The cells (wet weight approximately 17 g) were harvested and resuspended in 50 ml of Binding Buffer (50 mM sodium phosphate buffer, pH 7.4, 300 mM sodium chloride) containing 2 mM PMSF and 10 μM leupeptin. The cells, which could be stored at –20 °C, were lysed by two passages through a French press at 18,000 psi at the orifice. Following centrifugation, the supernatant was filtered by syringe through an HPF Millex-HV 0.45 μm filter unit attached in series to a Millex-AP prefilter (Millipore). Filtrate was applied to a 1 ml HisTrap HP nickel affinity column (Amersham Biosciences) at a flow rate of 1.0 ml/min by use of a ÄKTA fast protein liquid chromatography system (Amersham Biosciences). The remainder of the FPLC purification was carried out in a manner identical to that of AtICS1 in Chapter 2. Fractions were aliquoted and stored at –80 °C without dialysis.

HPLC SAS Activity Assay

These assays were performed as described in the "HPLC ICS Activity Assay" detailed in Chapter 2, substituting mutant ICS enzyme for AtICS1. The elution program used for HPLC analysis was identical to that used in the "Coupled HPLC ICS Activity Assay" described in Chapter 2. This program allowed for the detection of prephenic acid (A_{215}, 3.2 min), chorismic acid (A_{280}, 4.2 min), *para*-hydroxybenzoic acid (A_{255}, 6.8 min), phenylpyruvic acid (A_{215}, 13.5 min), and salicylic acid (ex 305 nm/em 407 nm, 23.3 min). The calibration curve for prephenic acid was $y = 0.000353175x - 10.4660$ with $R^2 = 0.999$, the calibration curve for chorismic acid was $y = 0.0170786x - 45.3581$ with $R^2 = 0.999$, the calibration curve for *para*-hydroxybenzoic

acid was y = 0.0000292540x – 3.40260 with R^2 = 0.999, the calibration curve for phenylpyruvic acid was y = 0.000102164x – 1.04072 with R^2 = 0.998, and the calibration curve for salicylic acid was y = 0.0000193487x – 1.03132 with R^2 = 0.999, where for each of the above x = area units and y = μmoles of the molecule being quantified. For the time course assay of AtICS2 A467T activity, a volume of 300 μl was employed, incorporating standard working concentrations of all components, and using 110 μg/ml of enzyme. The reaction was incubated at 30 °C, and 50 μl aliquots were removed at intervals of 15 minutes, filtered as performed previously, and frozen at a temperature of –80 °C before injection into the SAS Activity Assay method described above. For the assay of multiple AtICS2 variants, a volume of 100 μl was employed, incorporating standard working concentrations of all components, and using 220 μg/ml of enzyme. These reactions were incubated at 30 °C for 1 hour each and analyzed as above. Each of these reactions was performed in duplicate.

Purification of Recombinant AtICS2 A467T Mutant

E. coli BL21-CodonPlus(DE3)-RIL cells (Stratagene) were transformed with plasmid pCZ101-Red (obtained from Dr. Chloe Zubieta), a pET-28 derivative containing the gene encoding the A467T point mutant of AtICS2. A crude cell extract was prepared from a 500 ml culture of transformed cells grown in TB media containing 0.2% glucose, 50 μg/ml kanamycin and 30 μg/ml chloramphenicol. The culture was grown at 37 °C with agitation in a 1 L baffled flask until an OD_{600} of approximately 0.6 was reached, at which point IPTG was added to a final concentration of 1.0 mM to induce protein synthesis. Shaking was continued at 18 °C for 19 hours. All subsequent operations were carried out at 4 °C. The cells (wet weight approximately 6.8 g) were harvested and resuspended in 40 ml of Binding Buffer (50 mM sodium phosphate buffer, pH 8.0, 300 mM sodium chloride) containing 2 mM PMSF, 2 μg/ml leupeptin, 10 μg/ml DNase, and 0.2 mg/ml lysozyme. The cells, which could be stored at –20 °C, were lysed by six successive 30 s periods of exposure to sonication, using a 90% duty cycle at 25% power. Following centrifugation, the supernatant was filtered by syringe through an HPF Millex-HV 0.45 μm filter unit attached in series to a Millex-AP prefilter (Millipore). Filtrate was allowed to bind to 3 ml of Ni^{2+}-NTA His-Bind Resin (Novagen) by mixing with mild agitation on a rotary shaker for 11 hours. The resin had been pretreated according to the manufacturer's directions. The slurry was then poured into a column, and the flow-through was collected in one portion. After washing the column with 15 ml of Binding Buffer, protein was eluted with 20 ml of Elution Buffer (components as Binding Buffer, but including 250 mM imidazole). The first 10 fractions of 1 ml each were separately dialyzed into a buffer containing 100 mM Tris, pH 7.7, 10% glycerol, and 1 mM DTT. The protein fractions were then stored at –80 °C.

Purification of Recombinant AtICS2 T526A Mutant

E. coli BL21-CodonPlus(DE3)-RIL cells (Stratagene) were transformed with plasmid pCZ101-Green (obtained from Dr. Chloe Zubieta), a pET-28 derivative containing the gene encoding the T526A point mutant of AtICS2. A crude cell extract was prepared from a 500 ml culture of transformed cells grown in TB media containing 0.2% glucose, 50 μg/ml kanamycin and 30 μg/ml chloramphenicol, and purified according to the same protocol as that of AtICS2 A467T above, with the following modifications. Cells were incubated at 18 °C for 17 hours after induction. The wet weight of the cells after harvesting was approximately 7.2 g. The filtrate after cell lysis and centrifugation was allowed to bind to 3 ml of Ni^{2+}-NTA His-Bind Resin (Novagen) by mixing with mild agitation on a rotary shaker for 3 hours.

Purification of Recombinant AtICS2 A467T T526A Double Mutant

E. coli BL21-CodonPlus(DE3)-RIL cells (Stratagene) were transformed with plasmid pCZ102-Blue (obtained from Dr. Chloe Zubieta), a pET-28 derivative containing the gene encoding the A467T T526A double mutant of AtICS2. A crude cell extract was prepared from a 500 ml culture of transformed cells grown in TB media containing 0.2% glucose, 50 μg/ml kanamycin and 30 μg/ml chloramphenicol, and purified according to the same protocol as that of AtICS2 A467T above, with the following modifications. Cells were incubated at 18 °C for 21 hours after induction. The wet weight of the cells after harvesting was approximately 2.6 g. The filtrate after cell lysis and centrifugation was allowed to bind to 3 ml of Ni^{2+}-NTA His-Bind Resin (Novagen) by mixing with mild agitation on a rotary shaker for 4 hours.

Purification of Recombinant AtICS2 A467T V468A T526A Triple Mutant

E. coli BL21-CodonPlus(DE3)-RIL cells (Stratagene) were transformed with plasmid pCZ103-Black (obtained from Dr. Chloe Zubieta), a pET-28 derivative containing the gene encoding the A467T V468A T526A triple mutant of AtICS2. A crude cell extract was prepared from a 500 ml culture of transformed cells grown in TB media containing 0.2% glucose, 50 μg/ml kanamycin and 30 μg/ml chloramphenicol, and purified according to the same protocol as that of AtICS2 A467T above, with the following modifications. Cells were incubated at 18 °C for 18 hours after induction. The wet weight of the cells after harvesting was approximately 4.5 g. The filtrate after cell lysis and centrifugation was allowed to bind to 3 ml of Ni^{2+}-NTA His-Bind Resin (Novagen) by mixing with mild agitation on a rotary shaker for 7 hours.

RESULTS

AtCM1 exhibits limited isochorismate pyruvate lyase activity. Experiments were undertaken to determine whether any of the three known *Arabidopsis* chorismate mutase enzymes could be acting as an IPL *in vivo*, as they possess homology to the known IPL Pae PchB. In order to perform biochemical characterization of the *Arabidopsis* CM proteins, purified active enzyme was required. Dr. Sharon Marr cloned the *Arabidopsis CM1*, *CM2*, and *CM3* full-length (precursor) and mature (with the chloroplast transit peptide removed) genes, and created transformed *E. coli* strains to overexpress these proteins. As shown in Figure 4.3, I overexpressed mature AtCM1 as an amino-terminal His_6-tagged protein in *E. coli* and affinity-purified it using Ni^{2+}-NTA affinity chromatography. Similarly purified AtCM2 and mature AtCM3 protein samples were obtained from Dr. Sharon Marr. Expression of mature forms of AtCM1 and AtCM3 resulted in significantly more soluble protein than those containing the predicted CTP (data for overexpression and purification of precursor AtCM1, AtCM2, and precursor and mature AtCM3 not shown), consistent with the expectation that the mature protein would be most likely to fold properly in *E. coli*. AtCM2, which has no CTP, was expressed as its full-length form in abundant quantities.

All three of the recombinant mature CM proteins were shown to be fully active as chorismate mutases (data not shown) using an assay based on the method of Gilchrist and Connelly [339]. The purified enzymes display specific activities (in units of μmoles prephenate min^{-1} mg $protein^{-1}$) of 0.165 for AtCM1, 0.098 for AtCM2, and 0.073 for AtCM3. The specific activities for these recombinant CM proteins were up to 10-fold greater than those previously

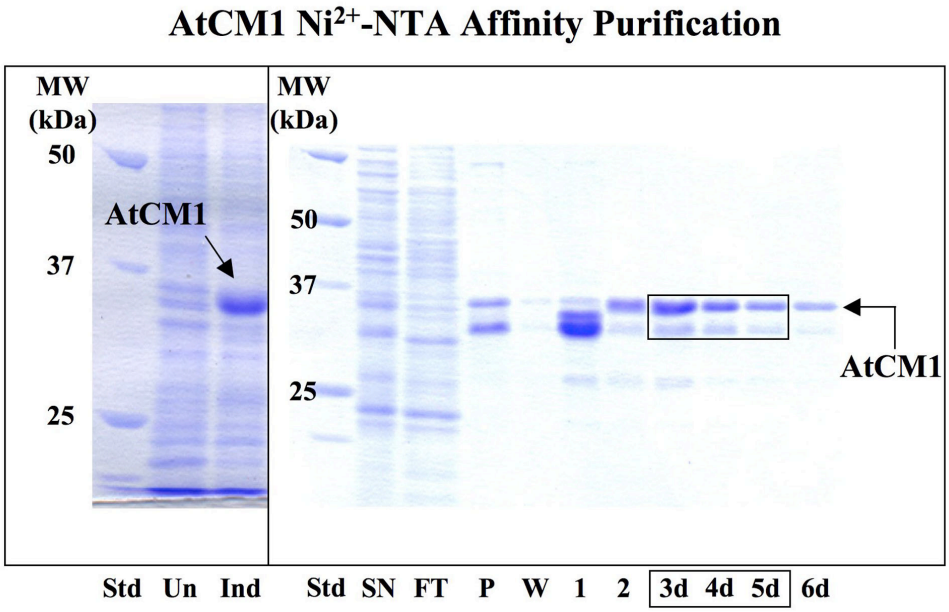

Fraction	SN	FT	P	W	1	2	Comb	6
Protein (mg/ml)	5.1	7.5	2.7	0.5	65.2	14.3	31.5	6.5
Specific Activity (μmol/min/mg)							0.165	

Figure 4.3. SDS-PAGE on Ni^{2+}-NTA Fractions from the Initial Purification of AtCM1. Proteins were separated on a 10% SDS-PAGE gel and stained with Coomassie blue. Abbreviations used are: Std, Bio-Rad Precision Plus protein standards (3.6 μg protein loaded), molecular masses in kDa are indicated on left; Un, Uninduced *E. coli* cells; Ind, IPTG-induced *E. coli* cells; SN, Crude extract (Supernatant) from lysed induced cells; P, Pellet from lysed induced cells; FT, Flow-through from column loading; W, Wash of column; Numbers are elution fractions, with a small "d" indicating that the fraction has been diluted for analysis by SDS-PAGE; Comb, Combined fractions indicated by the boxes.

reported for plant CMs, though none of these specific activities were assessed for overexpressed, affinity-purified proteins [66, 67, 339, 344-347]. The precursor AtCM1 and AtCM3 proteins did not exhibit significant CM activity (data not shown).

Isochorismate (purified as described in Chapter 2) was incubated with each of these proteins to directly measure its conversion to SA, using a modified version of the IPL activity assay in [298]. Though no SA above background was produced from isochorismate for the reactions incorporating AtCM2 or AtCM3 (data not shown), AtCM1 generated 39.1 ng of SA above background by HPLC analysis in one hour of incubation time (Figure 4.4). This corresponds to 5.7 μM of SA generated from 1 mM isochorismate (yield of 0.57%), indicating an apparent IPL specific activity for AtCM1 of 0.864 nmoles SA min^{-1} mg $protein^{-1}$.

A key threonine residue in the Irp9 active site may be required for its IPL activity. Because the amino acid residues essential to SAS IPL activity are not known, homology modeling was performed of known monofunctional ICS enzymes (AtICS1 and Pae PchA, both involved in SA biosynthesis) and a bifunctional SAS enzyme (*Mycobacterium tuberculosis* MbtI; see [61, 317]) using the crystal structure of the SAS enzyme Yen Irp9 in complex with its reaction products SA and pyruvate [58]. As expected, the homology modeling of AtICS1 with Yen Irp9 indicates a high degree of structural conservation across the full length of the proteins and within the active site (Figure 4.5). Comparison of aforementioned active sites leads us to speculate that Thr348 is important for the IPL activity of Irp9, with the apparent hydrogen bonding indicated in the Irp9 structure between the Thr348 main chain carbonyl and the 2-hydroxyl group of SA suggesting a similar hydrogen bond between the carbonyl and the 2-hydroxyl group of the isochorismate intermediate of the SAS reaction. The side chain hydroxyl of Thr348 in Irp9 apparently participates in a hydrogen bond with the side chain carboxylate of Glu241 (not shown in Figure 4.5), the active site residue proposed as the general acid involved in C4 hydroxyl protonation in all MST enzymes (see Figure 1.8). This second hydrogen bond between the Thr348 side chain and Glu241 is necessarily absent in AtICS1, which has an alanine residue at this position instead of a threonine. Furthermore, Thr348 is conserved in the SAS MbtI, and is an alanine in all known ICS enzymes, including AtICS2, Pae PchA, Eco EntC and MenF, and many other known bacterial and plant ICS enzymes (Figure 4.6, and see Figure 1.7). This led to an effort to perform site-directed mutagenesis of AtICS1 in order to potentially convert it to an SAS enzyme.

Standard QuikChange II (Stratagene) technology was employed to prepare the pET-28 construct containing the *AtICS1* gene with a point mutation coding for a threonine at Ala472 of AtICS1. AtICS1 A472T was overexpressed and purified in a manner very similar to that of AtICS1 itself (Figure 4.7). All told, less than 300 μg of this protein was isolated in a relatively impure state – an exceptionally poor yield. Furthermore, the protein had much lower specific activity by spectrophotometric assay than did wild type AtICS1. HPLC analysis of the product of incubation of 110 μg/ml of this protein with 1 mM chorismate (Figure 4.8) shows that, although negligible isochorismate or salicylate was formed after 1 hour, approximately 270 μmoles of phenylpyruvate were generated per 1000 μmoles chorismate originally present. This suggests that the AtICS1 A472T protein is catalyzing formation of significant amounts of prephenate from chorismate, and then subsequently catalyzing its decomposition to phenylpyruvate. A lack of pure enzyme motivated the overexpression and purification of a number of AtICS2 mutants, as AtICS2 is dramatically more soluble and easily purified than

AtCM1 Possesses Limited IPL Activity With Isochorismate

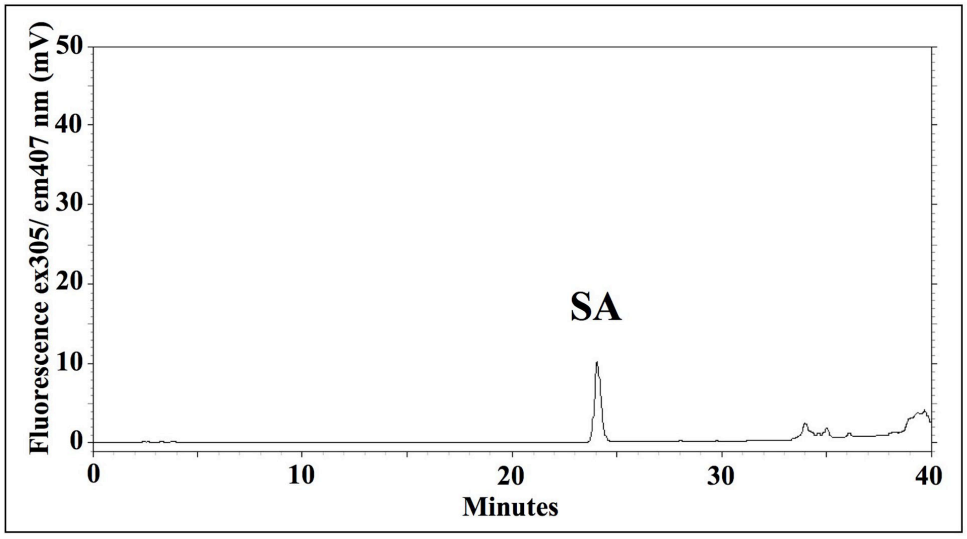

Figure 4.4. AtCM1 Exhibits Limited Isochorismate Pyruvate Lyase Activity. Isochorismate is converted to salicylate (SA) in the presence of enzyme, but only slightly above the background of the no enzyme control (not shown). HPLC IPL activity assay was employed. Fluorescence was measured at ex305/em407 nm.

Homology Modeling of AtICS1

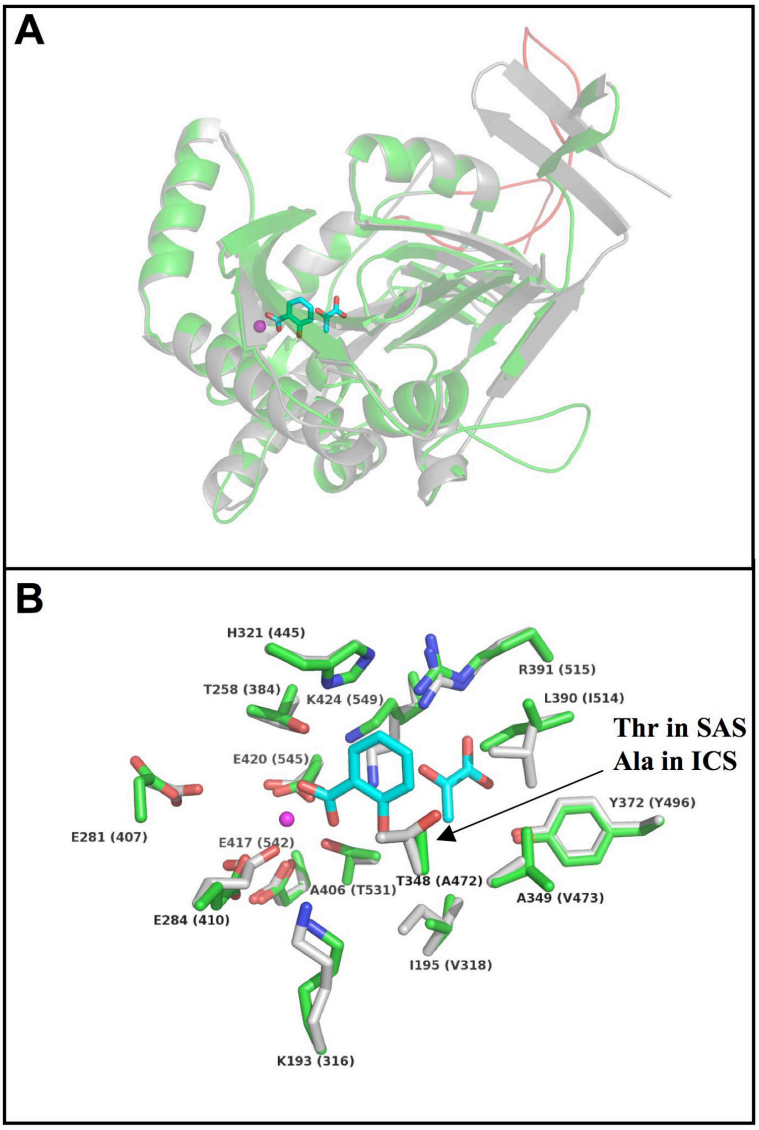

Figure 4.5. Homology Modeling of AtICS1. (A) AtICS1 (green) overlayed on the Yen Irp9 crystal structure (gray) in complex with its reaction products SA and pyruvate colored by atom with carbons in cyan and oxygens in red (PDB code 2fn1) . Mg^{2+} is shown as a magenta sphere. Insertion regions of AtICS1 are colored in red. (B) Close up view of the active site with Irp9 side chains in gray and AtICS1 side chains in green. Irp9 residues are labeled with one letter amino acid code and number for position in the protein. AtICS1 residues are given in parentheses, with the amino acid specified if different. The active site of Irp9 is completely conserved in Mtu MbtI (CAE55483). AtICS1 (AAL17715), Pae PchA (CAA57969), and Eco EntC (POAEJ2) contain an Ala at Thr348 (marked with arrow). Thr348 in Irp9 is predicted to H-bond with the 2-OH of SA.

ICS and SAS Enzyme Sequence Alignment

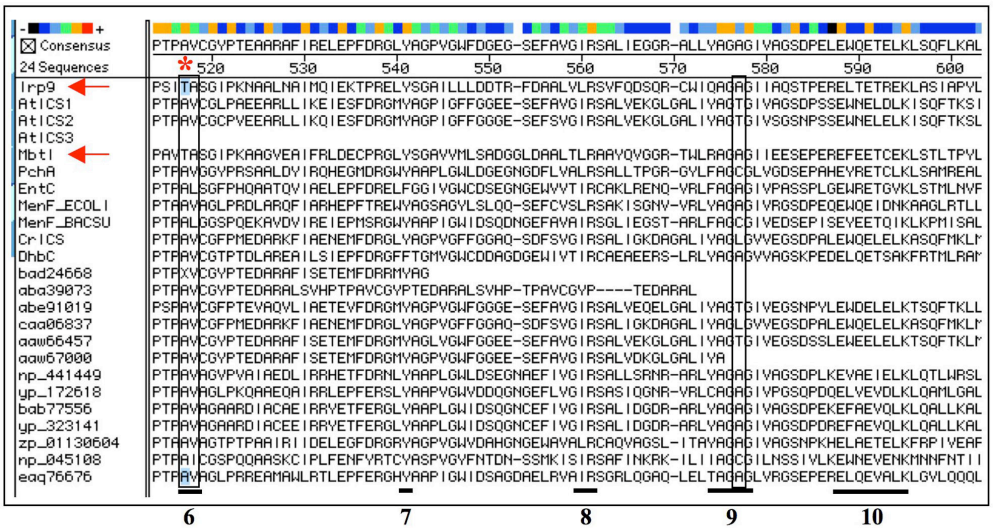

Key

A = Alanine	M = Methionine
C = Cysteine	N = Asparagine
D = Aspartate	P = Proline
E = Glutamate	Q = Glutamine
F = Phenylalanine	R = Arginine
G = Glycine	S = Serine
H = Histidine	T = Threonine
I = Isoleucine	V = Valine
K = Lysine	W = Tryptophan
L = Leucine	Y = Tyrosine

Figure 4.6. Comparison of the Amino Acid Sequences of 24 Known ICS and SAS Enzymes. An alignment of a segment of overlapping sequence in the chorismate-binding domain of 24 plant and bacterial ICS and SAS enzymes is shown. The only two SAS enzymes known are indicated by red arrows; the remainder are putatively ICS enzymes. The underlined residues can be assigned to the last 5 labeled motifs which collectively signify a MST enzyme, first shown in Figure 1.7. The threonine residue that appears to be essential for IPL activity in SAS enzymes is indicated by a red asterix. The three residues that are mutated in this chapter are boxed. AtICS3, a tomato ICS (aba39073), and two tobacco ICS enzymes (bad24668 and aaw67000) are truncated and likely nonfunctional, as they do not contain the chorismate-binding domain and active site. Abbreviations used are: MST, Menaquinone, Siderophore and Tryptophan; ICS, Isochorismate synthase; SAS, Salicylic acid synthase.

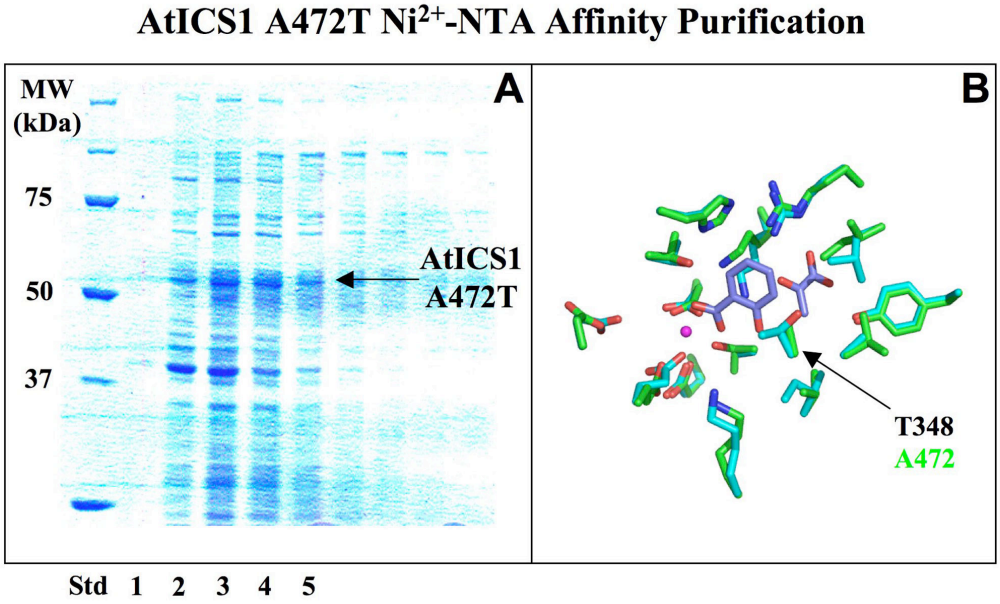

Fraction	SN	FT	W	1	2	3	4	5
Protein (μg/ml)	113	80	2.0	4.0	31	96	33	29
Specific Activity (nmol/min/mg)	25.1	2.8	3.0	15.5	27.6	30.9	25.3	13.8

Figure 4.7. SDS-PAGE on Ni^{2+}-NTA Fractions from the Initial Purification of AtICS1 A472T Mutant. (A) Proteins were separated on a 10% SDS-PAGE gel and stained with Coomassie blue. Abbreviations used are: Std, Bio-Rad Precision Plus protein standards (3.6 μg protein loaded), molecular masses in kDa are indicated on left; Numbers are elution fractions. (B) Close up view highlighting the mutation made in the active site of AtICS1, with Irp9 side chains in cyan and AtICS1 side chains in green. Irp9 residues are labeled in black using the one letter amino acid code and number for the position in the protein. The AtICS1 residue is similarly labeled in green.

AtICS1 A472T Generates Phenylpyruvate Exclusively

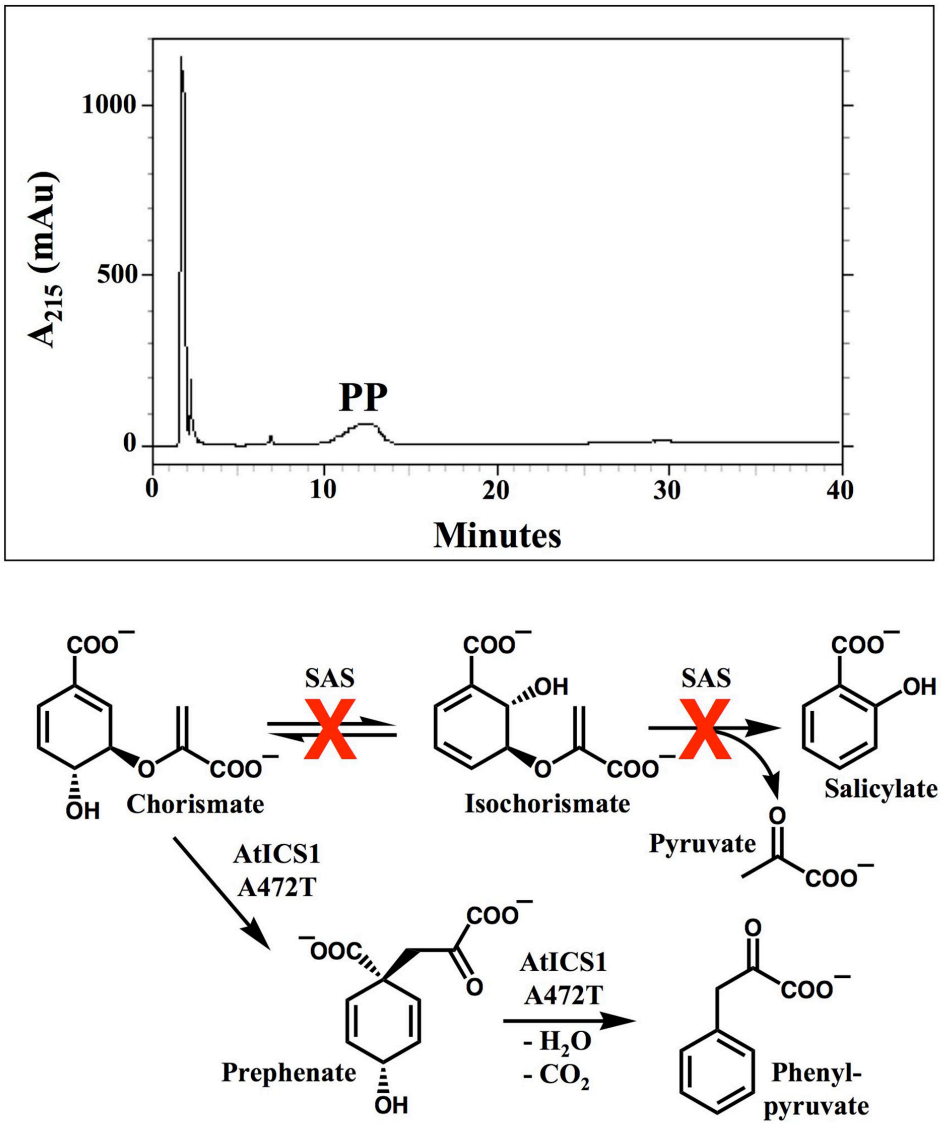

Figure 4.8. AtICS1 A472T Catalyzes the Formation of Phenylpyruvate From Chorismate. Chorismate is converted to phenylpyruvate (PP) rather than isochorismate in the presence of mutant AtICS1 enzyme. HPLC SAS activity assay was employed. Absorbance is measured at 215 nm. The HPLC SAS Activity Assay was calibrated for phenylpyruvate content, and a curve with the equation $y = 0.000102164x - 1.04072$ with $R^2 = 0.998$ was obtained. A schematic of the reactions of interest is shown below.

AtICS1 in spite of the fact that these protein sequences are 83% identical to each other with all 26 active site residues absolutely conserved (see Figure 1.7).

Active site mutations in AtICS2 entirely eliminated ICS activity, and transformed the protein into a bifunctional chorismate mutase-prephenate dehydratase. Figure 4.9 shows three amino acid residues that come into close contact with C2 of the salicylate ligand in the Irp9 crystal structure, and are therefore likely to come into contact in a similar manner with the analogous position of the chorismate substrate and the isochorismate intermediate of Irp9. Because these Irp9 residues – T348, A349, and A406 – are also largely substituted for in ICS enzymes (see Figure 4.6), it was believed that transformation of the corresponding residues in AtICS2 to their Irp9 counterparts might convert AtICS2 into a SAS. To this end, Dr. Chloe Zubieta prepared four separate AtICS2 mutant pET-28 constructs, and I overexpressed and purified each of them in a manner similar to that of AtICS2. The AtICS2 A467T mutant was targeted because of the absolute conservation of the alanine residue at this position in ICS enzymes and the apparent conservation of threonine in SAS enzymes; it was considered a strong possibility that switching AtICS2 at this position from alanine to threonine might result in an enzyme with SAS activity. AtICS2 A467T was overexpressed and purified as shown (Figure 4.10). It was isolated in high quantities with very low specific activity for isochorismate formation.

HPLC analysis of the reaction products following 45 minutes of incubation of AtICS2 A467T with 1 mM chorismate under standard conditions showed that large quantities of phenylpyruvate (758 μM) – but no isochorismate or salicylate – were produced (Figure 4.11). In addition, significant amounts of prephenate (207 μM) were observed. PHBA was detected also, but in roughly the same concentration (42 μM) as that found in the initial chorismate solution (*para*-hydroxybenzoate is a known impurity in commercially available chorismate preparations). A time course assay was conducted to survey the progress of product formation at 15-minute intervals (Figure 4.12). It indicates that phenylpyruvate is formed gradually at approximately the same rate that chorismate is consumed. Furthermore, there is an initial buildup of prephenate at 15 minutes that gradually dissipates over time with concomitant phenylpyruvate formation. This behavior is what one would expect for a protein that has CM-prephenate dehydratase activity: prephenate is formed initially, and then converted to phenylpyruvate by synchronous decarboxylation and dehydration (see the schematics in Figures 4.8 and 4.11). This is very likely enzymatic, as spontaneous conversion of prephenate to phenylpyruvate is rapid only at pH values below 6 (at 25 °C and pH 7.0, $t_{1/2}$ = 130 hours; see [348]), and in the presence of mutant enzyme in 100 mM Tris buffer, pH 7.7, ~60% of the initial chorismate has been converted to phenylpyruvate via prephenate in 45 minutes (Figure 4.12). The data shown indicate the presence of more than 1 mM of combined substrate and product at various intermediate time points – this is due to the errors introduced by the relatively weak absorbance of prephenate and the uneven peak shape of phenylpyruvate at 215 nm (Figure 4.12).

Three other AtICS2 mutants were overexpressed and purified as described below. The AtICS2 T526A mutant was targeted because this residue is close to the C2 atom of the substrate (Figure 4.9), although it is not well conserved as a threonine in ICS enzymes, and alanine residues at this position are not unique to SAS enzymes (Figure 4.4). It was considered possible that alanine at this position may be the appropriate size to orient the adjacent Irp9 Thr348 residue into the position necessary for it to promote IPL activity. AtICS2 T526A was overexpressed and purified as shown (Figure 4.13). It was isolated in large quantities with very low specific activity

AtICS2 Mutations Targeted

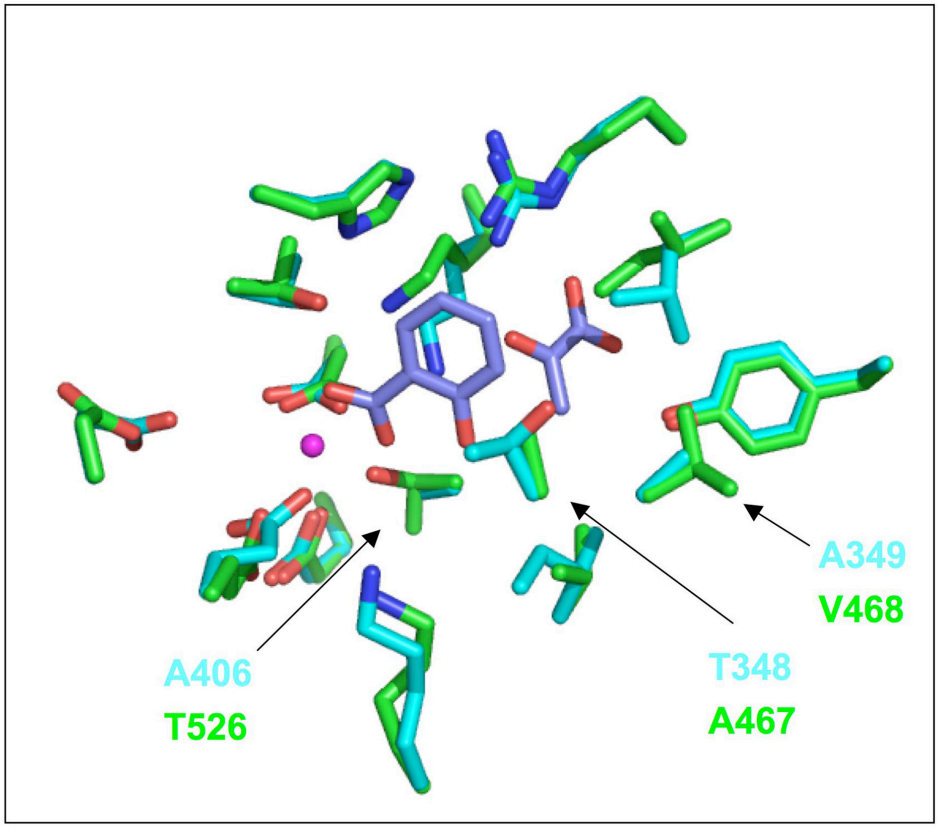

Figure 4.9. Irp9 Active Site with Bound Products Indicating the Amino Acid Residues that are Targeted for Mutation. Close up view of the active site with Irp9 side chains in cyan, AtICS1 side chains in green, and reaction products in purple. Irp9 residues are labeled with the one letter amino acid code and a number for the position in the protein. The equivalent AtICS2 residues are labeled in green in a similar manner. The active site of Irp9 is completely conserved in Mtu MbtI (CAE55483). AtICS1 and AtICS2 have identical residues at the positions indicated in green.

AtICS2 A467T Ni^{2+}-NTA Affinity Purification

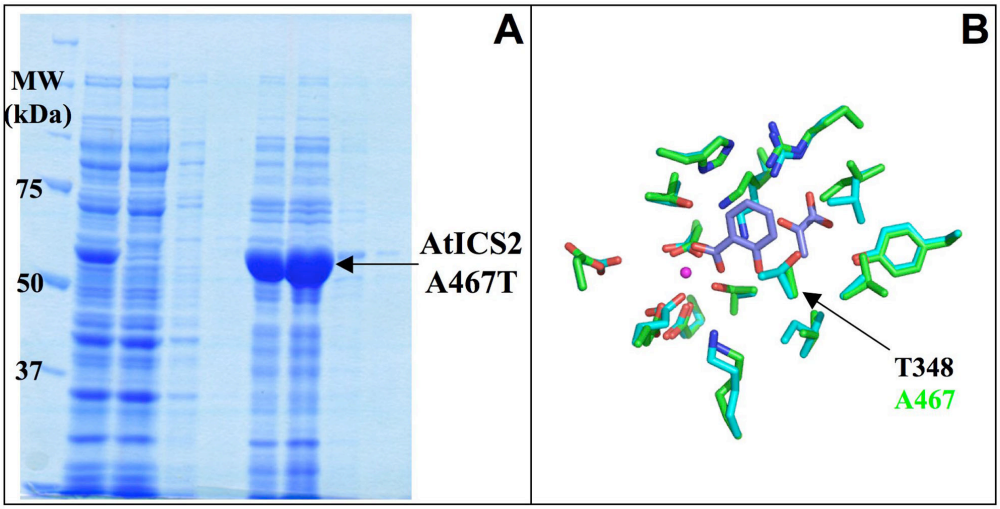

Fraction	SN	FT	W	1	2	3	4	5	AtICS2
Protein (mg/ml)	8.3	7.1	1.0	0.3	17.2	15.0	0.9	0.2	
Specific Activity (nmol/min/mg)	4.1	1.2	2.9	0	11.1	11.3	3.3	0	217

Figure 4.10. SDS-PAGE on Ni^{2+}-NTA Fractions from the Initial Purification of AtICS2 A467T Mutant. (A) Proteins were separated on a 10% SDS-PAGE gel and stained with Coomassie blue. Abbreviations used are: Std, Bio-Rad Precision Plus protein standards (3.6 µg protein loaded), molecular masses in kDa are indicated on left; SN, Crude extract (Supernatant) from lysed induced cells; FT, Flow-through from column loading; W, Wash of column; Numbers are elution fractions. (B) Close up view highlighting the mutation made in the active site of AtICS2, with Irp9 side chains in cyan and AtICS2 side chains in green. Irp9 residues are labeled in black using the one letter amino acid code and number for the position in the protein. The AtICS2 residue is similarly labeled in green. The box shows protein quantification and ICS enzyme specific activity data for each fraction indicated. A value for the specific activity of the AtICS2 wild type protein used in Chapter 3 is given in red as a reference.

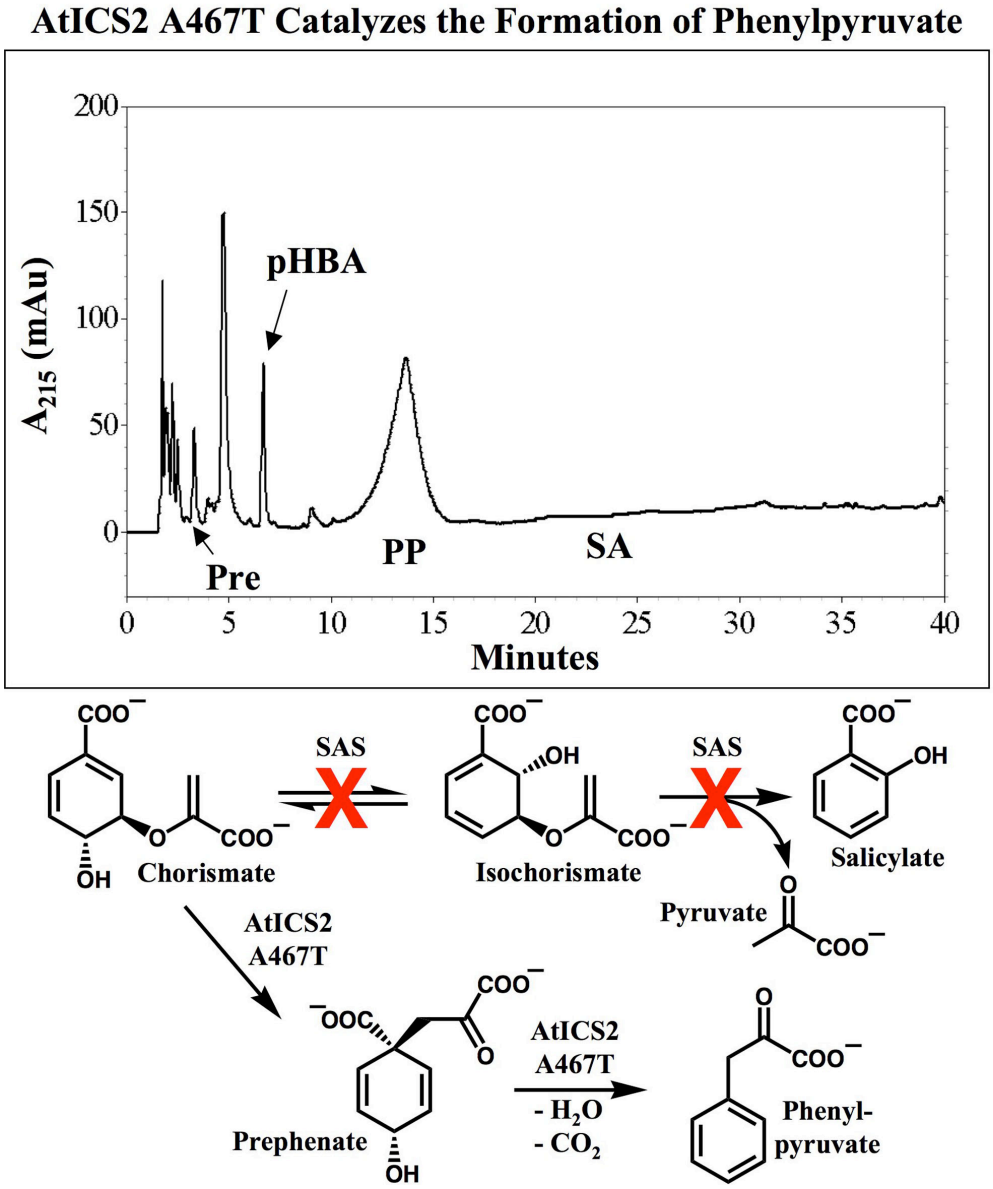

Figure 4.11. AtICS2 A467T Catalyzes the Formation of Phenylpyruvate From Chorismate. Chorismate is converted to phenylpyruvate (PP) rather than isochorismate in the presence of mutant AtICS2 enzyme after 45 minutes of incubation. HPLC SAS activity assay was employed. Absorbance is measured at 215 nm. Molecules detected by this method are: Pre, prephenic acid, 3.2 min; CA, chorismic acid, 4.2 min (not seen here); pHBA, *para*-hydroxybenzoic acid, 6.8 min; PP, phenylpyruvic acid, 13.5 min; SA, salicylic acid, 23.3 min (also not seen here). The peak at ~5.0 minutes is associated with the protein. A schematic of the reactions of interest is shown below.

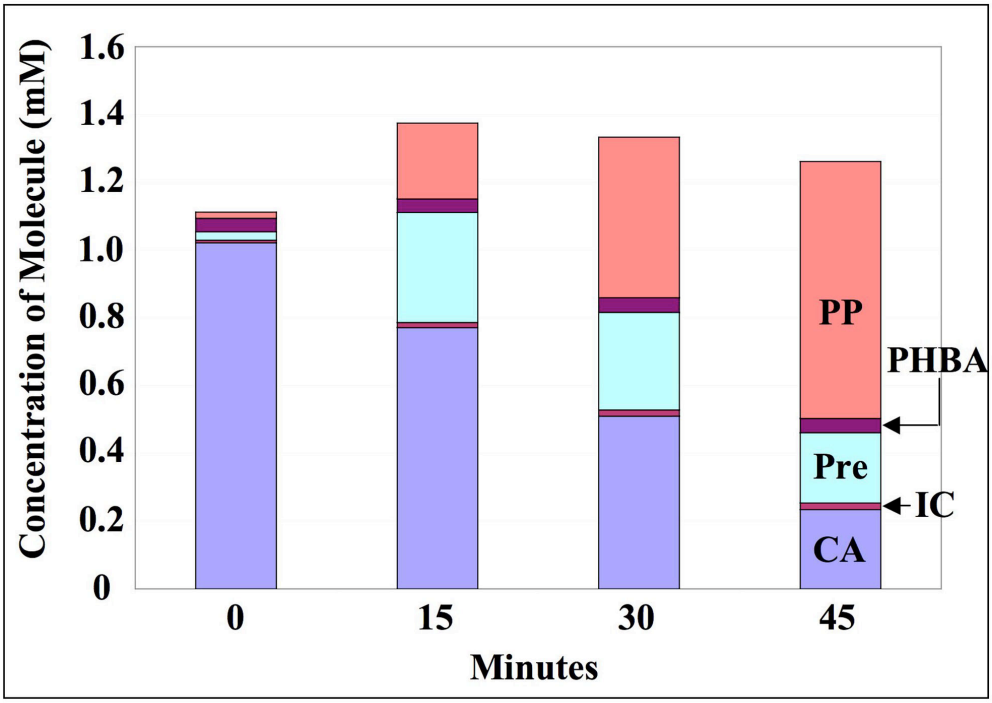

Figure 4.12. Time Course of AtICS2 A467T Catalysis of Phenylpyruvate Formation from Chorismate. Chorismate is converted to phenylpyruvate rather than isochorismate progressively over time in the presence of mutant AtICS2 enzyme. HPLC SAS activity assay was employed. The colored bars indicate the concentration of each molecule in mM. Molecules specified here are: Blue, bottom bar, chorismic acid (CA); Dark Red, second bar from bottom, isochorismate (IC); Turquiose, third bar from bottom, prephenic acid (Pre); Purple, second bar from the top, *para*-hydroxybenzoic acid (PHBA); Orange-Red, top bar, phenylpyruvic acid (PP). Salicylic acid was also measured by this method, but none was formed in the assay, so none is visible here. The errors introduced by the relatively weak absorbance of prephenate and the uneven peak shape of phenylpyruvate at 215 nm are responsible for the data shown indicating the presence of more than 1 mM of combined substrate and products.

AtICS2 T526A Ni^{2+}-NTA Affinity Purification

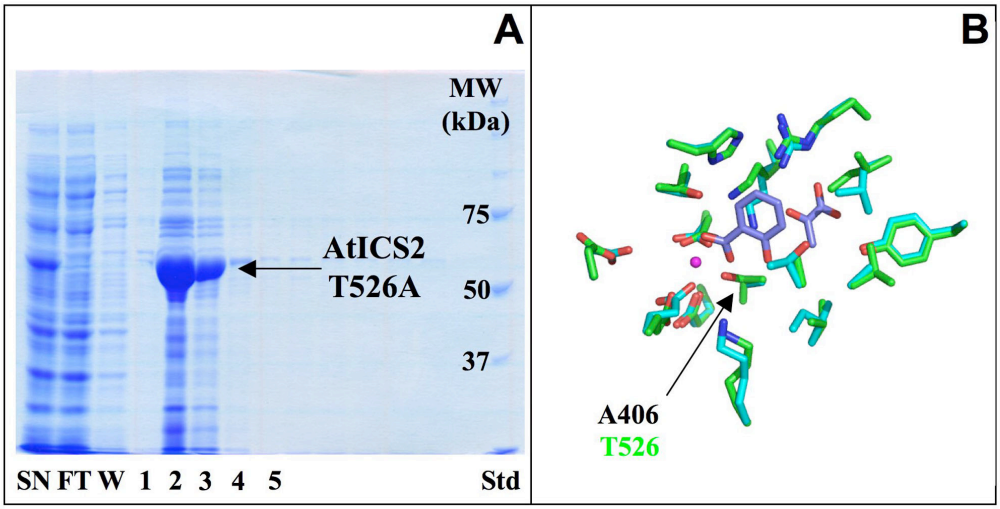

Fraction	SN	FT	W	1	2	3	4	5	AtICS2
Protein (mg/ml)	8.3	7.7	1.1	0.5	26.1	5.9	0.8	0.3	
Specific Activity (nmol/min/mg)	3.7	1.4	0.7	15.1	16.6	10.8	8.3	0	217

Figure 4.13. SDS-PAGE on Ni^{2+}-NTA Fractions from the Initial Purification of AtICS2 T526A Mutant. (A) Proteins were separated on a 10% SDS-PAGE gel and stained with Coomassie blue. Abbreviations used are: Std, Bio-Rad Precision Plus protein standards (3.6 μg protein loaded), molecular masses in kDa are indicated on left; SN, Crude extract (Supernatant) from lysed induced cells; FT, Flow-through from column loading; W, Wash of column; Numbers are elution fractions. (B) Close up view highlighting the mutation made in the active site of AtICS2, with Irp9 side chains in cyan and AtICS2 side chains in green. Irp9 residues are labeled in black using the one letter amino acid code and number for the position in the protein. The AtICS2 residue is similarly labeled in green. The box shows protein quantification and ICS enzyme specific activity data for each fraction indicated. A value for the specific activity of the AtICS2 wild type protein used in Chapter 3 is given in red as a reference.

for isochorismate formation. Additionally, the AtICS2 A467T T526A double mutant was targeted in order to determine whether the Ala406-Thr348 interaction in Irp9 was responsible for its SAS activity. AtICS2 A467T T526A was overexpressed and purified as shown (Figure 4.14). It was isolated in large quantities with very low specific activity for isochorismate formation. Lastly, a fourth mutant, AtICS2 A467T V468A T526A, was targeted because the V468 residue in AtICS2 – which is highly conserved at this position in ICS enzymes – is replaced by an alanine in the two SAS enzymes investigated. Though this valine residue is further from the substrate than the other two residues that have been mutated, it is proximal to the Ala467 residue that forms a likely hydrogen bond with the C2 of substrate. A valine residue at this position (Val468 in AtICS2) in ICS enzymes may be necessary to fill the space that a threonine would fill at the adjacent position in an SAS enzyme (Ala467 in AtICS2 and Thr348 in the SAS Irp9; see Figure 4.9). This triple mutant was prepared to investigate whether the Ala406-Thr348-Ala349 side chain alignment in Irp9 acts as a well-ordered triad that promotes the active site isochorismate orientation responsible for the IPL activity inherent in SAS enzymes. AtICS2 A467T V468A T526A was overexpressed and purified as shown (Figure 4.15). It was isolated in large quantities and, as with all above AtICS2 mutants, had low specific activity for isochorismate formation.

Subsequently, all four mutant proteins were analyzed by incubation at 30 °C for 1 hour each (Figure 4.16), using a more concentrated amount of enzyme than previously in the time course assay (220 μg/ml vs. 110 μg/ml). Each reaction was performed in duplicate, and controls with wild type AtICS2, as well as without any enzyme, were also conducted. As expected, little degradation of chorismate occurred in the no enzyme control, and a typical equilibrium distribution of chorismate and isochorismate was seen when AtICS2 was present (~60% chorismate to 40% isochorismate, adding up to 1 mM total substrate and product). However, when each of the four mutants was substituted for AtICS2, virtually all of the chorismate substrate was transformed in 1 hour to phenylpyruvate (all reactions show ~1 mM phenylpyruvate after 1 hour of reaction time). Very little prephenate remains in the reaction mixtures, indicating that it has largely been processed to phenylpyruvate. However, no SA was formed.

DISCUSSION

Does *Arabidopsis* contain a gene encoding a protein with IPL activity similar to Pae PchB? Pae PchB – a bacterial IPL – is a small 101-amino acid protein that appears to have evolved from a chorismate mutase, as it retains residual CM activity and exhibits 10-fold stronger binding of chorismate than isochorismate [298]. It structurally resembles CM enzymes of the AroQ class in both its similarity in size to the AroQ domain, and in overall α-helical structural organization. The existence of two separate activities on these alternative substrates is reasonable given that both of the molecules in question – chorismate and isochorismate – possess most of the same binding elements in roughly similar orientations. Gaille and coworkers [298] suggested that only one CM residue needed to be altered (Glu52 in Eco CM, but Val55 at the homologous site in the IPL PchB) to alter the specificity of binding from chorismate to isochorismate. Nevertheless, PchB binds both substrates – chorismate and isochorismate – and catalyzes both reactions – CM and IPL, respectively – with great facility (discussed extensively in Appendix 2). Conclusive evidence has been provided that the IPL and CM reactions both

AtICS2 A467T T526A Ni^{2+}-NTA Affinity Purification

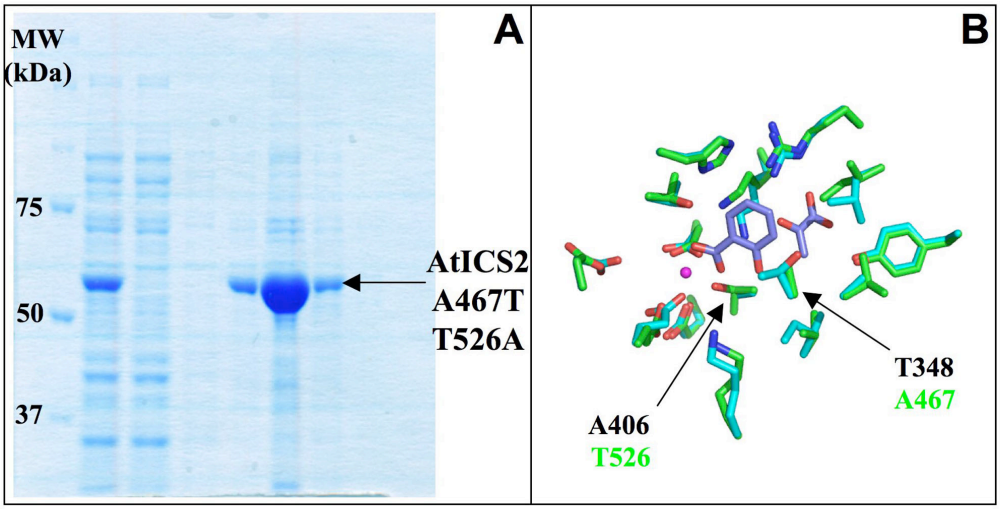

Fraction	SN	FT	W	1	2	3	4	5	AtICS2
Protein (mg/ml)	2.7	1.9	0.3	2.0	11.0	2.3	0.3	0.1	
Specific Activity (nmol/min/mg)	6.5	8.4	0	21.1	5.3	8.8	0	0	217

Figure 4.14. SDS-PAGE on Ni^{2+}-NTA Fractions from the Initial Purification of AtICS2 A467T T526A Double Mutant. (A) Proteins were separated on a 10% SDS-PAGE gel and stained with Coomassie blue. Abbreviations used are: Std, Bio-Rad Precision Plus protein standards (3.6 μg protein loaded), molecular masses in kDa are indicated on left; SN, Crude extract (Supernatant) from lysed induced cells FT, Flow-through from column loading; W, Wash of column; Numbers are elution fractions. (B) Close up view highlighting the mutations made in the active site of AtICS2, with Irp9 side chains in cyan and AtICS2 side chains in green. Irp9 residues are labeled in black using the one letter amino acid code and number for the position in the protein. The AtICS2 residues are similarly labeled in green. The box shows protein quantification and ICS enzyme specific activity data for each fraction indicated. A value for the specific activity of the AtICS2 wild type protein used in Chapter 3 is given in red as a reference.

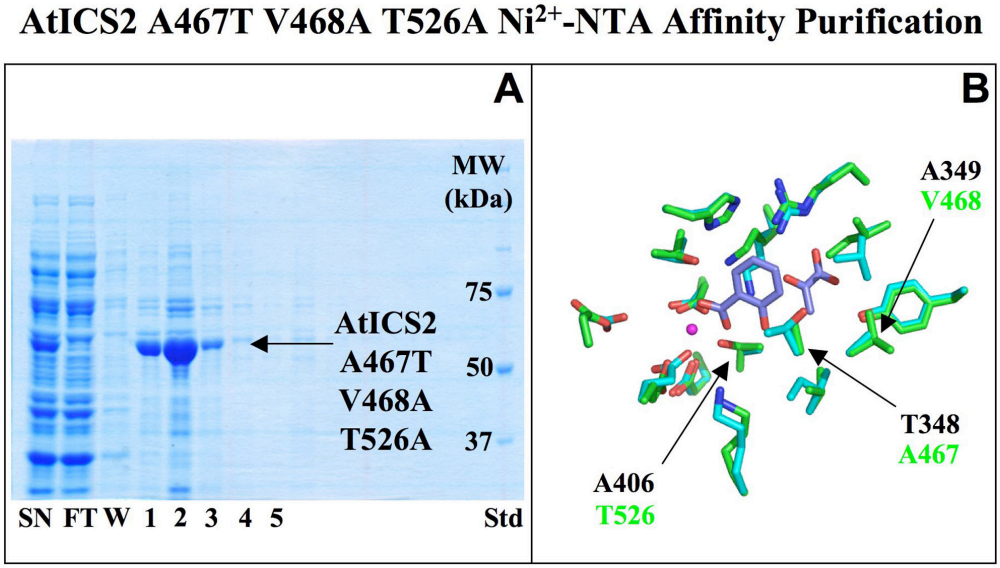

Fraction	SN	FT	W	1	2	3	4	5	AtICS2
Protein (mg/ml)	7.5	6.6	0.6	3.3	15.0	2.2	0.5	0.2	
Specific Activity (nmol/min/mg)	13.2	2.4	6.8	9.8	4.1	9.8	0	0	217

Figure 4.15. SDS-PAGE on Ni^{2+}-NTA Fractions from the Initial Purification of AtICS2 A467T V468A T526A Triple Mutant. (A) Proteins were separated on a 10% SDS-PAGE gel and stained with Coomassie blue. Abbreviations used are: Std, Bio-Rad Precision Plus protein standards (3.6 µg protein loaded), molecular masses in kDa are indicated on left; SN, Crude extract (Supernatant) from lysed induced cells FT, Flow-through from column loading; W, Wash of column; Numbers are elution fractions. (B) Close up view highlighting the mutations made in the active site of AtICS2, with Irp9 side chains in cyan and AtICS2 side chains in green. Irp9 residues are labeled in black using the one letter amino acid code and number for the position in the protein. The AtICS2 residues are similarly labeled in green. The box shows protein quantification and ICS enzyme specific activity data for each fraction indicated. A value for the specific activity of the AtICS2 wild type protein used in Chapter 3 is given in red as a reference.

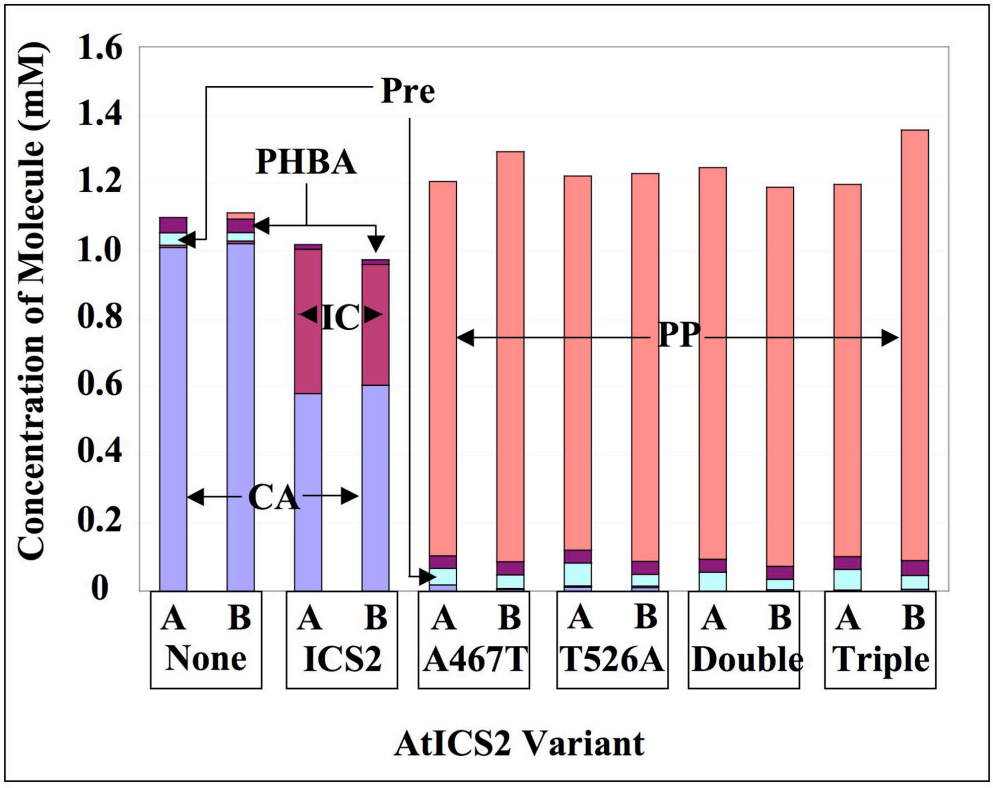

Figure 4.16. Catalysis of Chorismate Reactivity by AtICS2 Variants. Chorismate is converted to phenylpyruvate rather than isochorismate progressively over time in the presence of all mutant AtICS2 enzymes studied. HPLC SAS activity assay was employed with elevated levels of enzyme (220 μg/ml) after incubation of substrate with protein for 1 hour. All reactions were performed in duplicate. The colored bars indicate the concentration of each molecule in mM. Molecules specified here are: Blue, bottom bar, chorismic acid (CA); Dark Red, second bar from bottom, isochorismate (IC); Turquiose, third bar from bottom, prephenic acid (Pre); Purple, second bar from the top, *para*-hydroxybenzoic acid (PHBA); Orange-Red, top bar, phenylpyruvic acid (PP). Salicylic acid was also measured by this method, but none was formed in any of these assays, so none is visible here. The errors introduced by the relatively weak absorbance of prephenate and the uneven peak shape of phenylpyruvate at 215 nm are responsible for the data shown indicating the presence of more than 1 mM of combined substrate and products.

occur via pericyclic mechanisms that are structurally and electrostatically similar [305, 324, 325, 329], though they use different substrates. Both reactions proceed through transition states that place the *si* face of the enolpyruvyl group toward the ring carbons, with the terminal carbon of the enoylpyruvyl double bond positioned near the C1 and C2 ring carbons of substrate and the enolpyruvyl carboxylate positioned inward toward the ring (Figure 4.1). This active site enolpyruvyl orientation is likely the reason that PchB does not catalyze the CPL or kinetically favorable isochorismate mutase reactions, both of which require the terminal carbon of the enoylpyruvyl double bond to be positioned near the C4 and C5 ring carbons of substrate (Figure 4.1).

Whether or not CM enzymes have IPL activity when exposed to isochorismate has not previously been investigated, though this is a reasonable proposition since the terminal carbon of the enoylpyruvyl double bond of both potential substrates is appropriately positioned over the C1 and C2 position of their rings (see Figure 4.1). The *Arabidopsis* CM proteins share as much as 15% protein sequence identity with their bacterial counterparts and ~36% protein sequence identity with the yeast CM Aro7p. As the CM and IPL reactions are related mechanistically, and given that the IPL PchB also performs the CM reaction, we proposed that an *Arabidopsis* CM enzyme could similarly act as an IPL. This is an especially important consideration in the cases of AtCM1 and AtCM3, as they are chloroplast-localized and therefore present at the subcellular location of isochorismate synthesis. However, though these data show AtCM1 to have modest IPL activity, they are not consistent with AtCM1 acting as an IPL in the biosynthesis of SA. The rate of conversion of isochorismate to salicylate seen here is approximately 0.095 μM/min; the rate of isochorismate formation by AtICS1 under the same conditions would be about 71 μM/min. The IPL activity of AtCM1 would not be equal to the demands of the organism for salicylate under conditions of the plant defense response. I have shown in Chapter 2 that the spontaneous rate of SA formation from isochorismate under similar conditions to these is about 0.006 μM/min. Therefore, recombinant CM1 is responsible for a rate of isochorismate to SA conversion that is 15.8-fold higher than the non-enzymatic rate. Perhaps the recombinant enzyme activity is not reflective of its rate *in planta* – for example, association with ICS may improve the catalytic efficiency of the AtCM1 enzyme for isochorismate utilization. Furthermore, to accurately assess the ability of AtCM1 to function as an IPL, values of K_M and k_{cat} for isochorismate would need to be determined. The Wildermuth lab is also assessing *Arabidopsis* mutants with these genes knocked out in order to determine whether any are compromised in their ability to synthesize SA in response to pathogen attack.

An alternative means of forming SA from isochorismate could involve a bifunctional SAS enzyme with ICS and IPL activities. As shown in Chapters 2 and 3, AtICS1 and AtICS2 exhibit ICS – and not SAS – activity. However, there is the possibility that an alternative transcript could encode a protein that functions as an SAS enzyme. An alternative *AtICS1* transcript is expressed in low abundance (Dr. Sharon Marr, unpublished); however, it has a pattern of expression that is similar to the dominant *AtICS1* transcript. This suggests that the alternative transcript is unlikely to play a unique functional role.

I sought to determine whether an AtICS enzyme could be converted by mutation into an SAS. Though preliminary investigations of the AtICS1 A472T point mutant indicated that it produced significant amounts of phenylpyruvate when incubated with chorismate, these studies were hampered by the extremely low yields of these protein purifications. As AtICS2 is 83% identical to AtICS1 but far more soluble, the decision was made to pursue more thorough studies with mutants of AtICS2 instead. Therefore, an attempt was made to determine whether specific

residues in the active site might establish bifunctional SAS activity, as opposed to native monofunctional ICS activity.

AtICS2 A467T was the most straightforward mutant, possessing the active site threonine present in all known SAS and AS enzymes. It had virtually no ICS activity and no SAS activity, acting instead as a CM-prephenate dehydratase bifunctional enzyme like the $AroQ_p$ class of CM enzymes common in bacteria [38]. About one-third of all available chorismate (325 μM) was converted to prephenate after just 15 minutes of incubation of 1 mM chorismate with this enzyme, though this prephenate level was not maintained as time elapsed. Ultimately, the product of this bifunctional enzyme activity is phenylpyruvate, and its formation was found to be linear with time – 110 μg/ml of protein produces 16.5 μM/min of phenylpyruvate, consistent with a specific activity of ~0.150 μmoles phenylpyruvate min^{-1} mg $protein^{-1}$. This specific activity for CM-prephenate dehydratase activity of AtICS2 A467T is comparable to those for CM activity of the recombinant *Arabidopsis* CM enzymes expressed earlier in this chapter (AtCM1 has a specific activity of 0.165 μmoles prephenate min^{-1} mg $protein^{-1}$), and accomplishes the transformation of chorismate to phenylpyruvate at a rate that is over 10-fold faster than takes place non-enzymatically under far more favorable conditions (~1.55 μM/min of phenylpyruvate would be produced from a 1 mM starting concentration of chorismate at 60 °C and pH 7.5; see [44]). These data indicate that the mutant AtICS2 protein is catalyzing the chorismate mutase and prephenate dehydratase reactions taking place above. The fact that, simultaneously, chorismate is disappearing at a linear rate of 17.5 μM/min suggests that this protein quickly rearranges chorismate to achieve a steady-state concentration of the prephenate intermediate, which decomposes to phenylpyruvate more slowly. This reactivity appeared to be dose dependent in this enzyme, as two-fold higher concentrations of this protein completely converted the chorismate substrate to phenylpyruvate within 30 minutes, leaving little prephenate intermediate behind. All the other mutants prepared (AtICS2 T526A, AtICS2 A467T T526A, and AtICS2 A467T V468A T526A) showed behavior similar to that of AtICS2 A467T and likely have similar specific activities, though no time course was taken for the CM-prephenate dehydratase reaction that they catalyze (Figure 4.16).

The reasons for the changes in enzyme catalysis brought about by these mutations are unclear. None of the mutants described here display dramatic changes in solubility, suggesting that they are still able to fold properly. Six different point mutants made in the homologous *E. coli* MenF protein possessed circular dichroism spectra that were identical to that of the wild type protein, suggesting that mutation does not perturb ICS protein structure greatly [45]. Nevertheless, AtICS1 and AtICS2 point mutants cannot be properly configured to catalyze the rearrangement of chorismate to isochorismate that functional ICS enzymes do, as they all have particularly low specific activities for the ICS reaction. Nevertheless, a measurement of 0.150 μmoles phenylpyruvate min^{-1} mg $protein^{-1}$ for the specific activity of phenylpyruvate formation is quite high, comparable to the specific activity of 0.217 μmoles isochorismate min^{-1} mg $protein^{-1}$ for ICS activity of the parent AtICS2 protein. This suggests that the mutant proteins are binding and turning over substrate in the same manner as wild type protein, but that a different reaction is being catalyzed. A very precisely arranged active site would be required for catalysis of the ICS reaction, as its putative transition state is highly organized (Figure 4.2, and see Figure 1.8). Thus, it is possible that any active site mutation perturbs the structure of ICS and SAS enzymes sufficiently to prevent the 1,5-S_N2'' displacement performed by all MST enzymes from being catalyzed. Five of the six active site residue point mutations made in the ICS *E. coli* MenF rendered the protein totally inactive, and the sixth (L255A) had ICS activity that was greatly

impaired [45]. Similarly, three of the four active site residue point mutations made in the SAS Irp9 [58, 349] and all of the five active site residue point mutations made in the SAS MbtI [61] resulted in totally inactive protein; only Irp9 Y372W and Y372F had very low SAS activity. Apparently, only active site mutations abolish normal activity in MST enzymes: assay of a large number of point mutants in the AS enzymes *S. marcescens* TrpE [349] and rice ASA2 [350] showed that active site mutants had little or no AS activity, whereas most other mutants had normal or even increased activity.

Among the many MST enzyme point mutants that lacked their native activity was *E. coli* MenF A344T, a homolog of the AtICS1 A472T and AtICS2 A467T mutants shown above to be functional CM enzymes. MenF A344T and all the other ICS-inactive MenF point mutants [45] were not assayed for CM activity, nor were a number of otherwise inactive SAS [58] and AS [350] enzyme point mutants. However, all of the five active site residue point mutations made in the SAS enzyme MbtI have been shown to act as chorismate mutases [61] by spectroscopic measurement of the phenylpyruvate generated by the exposure of the putative product prephenate to strong acid (see Appendix 2 for the description of an identical assay). Furthermore, though all five of these mutations altered wildly different functionalities in the MbtI active site, they all catalyzed the chorismate mutase reaction with similar catalytic efficiencies (k_{cat}/K_M = 0.022-0.05 μM^{-1} min^{-1}; see [61]). These results are consistent with those obtained for the several AtICS2 mutants, which appear to catalyze the chorismate mutase reaction at similar rates without regard to the nature of the point mutation. However, the AtICS2 mutants have also been shown to catalyze a second, slower dehydratase reaction on the prephenate product of the initial CM reaction (see the schematics in Figures 4.8 and 4.11). Assaying inactive point mutants in the SAS Irp9 and the AS TrpE directly by ^1H NMR showed that most of the substrate chorismate is converted over 4 hours to phenylpyruvate instead of prephenate, and the realization that the prephenate dehydratase reaction was enzyme-catalyzed led to the proposal that Irp9 Glu240 – the putative active site general acid in MST enzymes (Glu308 in the AS *S. marcescens* TrpE and Glu361 in AtICS2; see Figure 1.8) – is also assisting prephenate dehydration in these mutants [349]. As phenylpyruvate formation was not assayed in any other study, it is entirely possible that all of the other active site point mutants in MST enzymes mentioned above are actually functional CM-prephenate dehydratase enzymes, provided that they possess the putative general acid glutamate residues in their active sites.

There are several possible explanations for why mutations in active site residues would inactive the 1,5-S_N2'' displacement activity of MST enzymes in general, and transform AtICS2, TrpE, and Irp9 – and possibly many other MST enzymes – into chorismate mutases in particular. Larger side chains in the mutant enzymes – like in AtICS2 A467T – could sterically hinder the approach of the nucleophile in the displacement (though this does not explain the CM activity). However, the fact that most of the point mutants characterized possess residues that are smaller than those they replace, and given that virtually no MST enzymes mutated in the active site have any displacement activity at all, suggests the existence of a more complex phenomenon. Another possibility is that a single active site mutation – or several, as in the case of the AtICS2 mutants – deforms the active site structure so much that the enolpyruvate moiety of chorismate can flip from the position with its *re* face presented to the ring (see Figure 4.2) – as seen in wild type MST enzymes – to the position with its *si* face presented to the ring (see Figure 4.1) – a conformation found in the transitions states of the uncatalyzed and CM-catalyzed rearrangements [44]. However, several pieces of evidence suggest that the active sites of these mutants are still highly ordered, likely preventing the lowest energy chair-like transition state for the CM reaction

shown in Figure 4.1 from being achieved. First, the similarity in the (relatively high) CM specific activities of AtICS2 A467T and wild type AtCM1, as well as the similarity in the catalytic efficiencies of CM activity in the various MbtI point mutants [61], all suggest that these various enzyme active sites remain similarly ordered. As the enolpyruvate group is held in place in MST enzymes by hydrogen bonds to as many as four amino acid residues – specifically, Irp9 Arg391 (shown in Figure 4.2), as well as the side chains of its Tyr372 and Lys424 residues [317] (not shown) and the main chain nitrogen of its Gly405 residue [61] (not shown) – flipping of the enolpyruvate moiety would require a massive reorganization of the active site. The various different MST enzyme point mutants indicated above would not likely all reorganize their respective active sites in the same manner. Second, a relatively disorganized active site would not be able to bias the substrate against spontaneous elimination to form PHBA (shown in Figure 4.1), but no significant PHBA production was observed for any of the AtICS2 mutants (Figure 4.16). Third, some Irp9 and TrpE mutants catalyze 1,5-S_N2'' displacement reactions and CM-prephenate dehydratase reactions simultaneously [349]. This strongly suggests that the conformation of the active site chorismate in these mutant enzymes does not change regardless of whether it is undergoing the displacement or the chorismate mutase reactions.

There is also evidence from wild type MST enzymes that conventionally-bound chorismate is able to rearrange to prephenate. Wild type TrpE – an AS – was shown to convert 30% of its chorismate substrate to prephenate over 4 hours when no ammonium is present, and wild type Irp9 – an SAS – converts 12% of its chorismate to phenylpyruvate over the same time span [349]. This result suggests that the chorismate mutase reaction is catalyzed at a significant rate by MST enzymes operating under standard conditions, though only the SAS enzyme in this case is able to then catalyze the prephenate dehydratase reaction. In addition, wild type MbtI – an SAS – has no displacement activity in the absence of Mg^{2+}, but has a value for CM catalytic efficiency that is only three-fold lower than its value for SAS catalytic efficiency in the presence of Mg^{2+} [61]. As structural studies of the closely related ICS enzyme *E. coli* MenF show active site residues being similarly positioned in the presence and absence of Mg^{2+} [53], the above result also suggests that whatever active site reorganization has occurred in the absence of Mg^{2+} does not permit the enolpyruvate moiety to significantly change its orientation. As a result, the chair-like mechanism for the chorismate mutase reaction shown in Figure 4.1 cannot be achieved. A more strained boat transition state for the enzymatic CM reaction of chorismate would present the *re* face of the enolpyruvate to the substrate ring and is consistent with all the above data (see Figure 4.17), though its existence could only be confirmed by the use of stereospecifically labeled chorismate. Computational studies indicate that the boat transition state for the Claisen rearrangement is 5-6 kcal/mol higher in energy than the chair-like transition state [351], though the reaction could possibly proceed via a lower energy twist-boat transition state.

All of the above data raise the possibility that the chorismate mutase reaction is catalyzed by all MST enzymes that are binding substrate normally, and that it proceeds at a rate that is competitive with the 1,5-S_N2'' displacement reaction. Thus, when the displacement reaction cannot proceed due to the absence of the Mg^{2+} required for chorismate ring activation, or because the required ammonia nucleophile is not present (as in the case of the wild type AS described above), or because the enzyme is mutated in a key catalytic residue, the MST enzyme could function exclusively as a CM enzyme, usually – though not always – with a secondary prephenate dehydratase activity provided by general acid catalysis from an active site glutamate (AtICS2 Glu361 in Figure 4.17). This phenomenon may be general for all MST enzymes,

although as mentioned above, CM activity has been assayed for only a very few of their mutants. Consideration of the fact that the amino acid residues mutated in the four AtICS2 mutants above – as well as those of several of the other SAS enzyme mutants shown to have CM activity [61] – are not likely involved in ICS catalysis raises the issue of why altering these residues abolishes displacement activity. The reason could be due to increased flexibility in the active site. Though, as discussed above, the unchanged active site amino acids likely interact with chorismate in the same manner in both mutant and wild type enzymes, all of these mutants have necessarily undergone realignment. This could prevent ring activation by failing to bring the magnesium-binding site in perfect alignment with the C1 carboxylate of chorismate. Alternatively, this could permit the entry of solvent water, which would be problematic for displacement catalysis in MST enzymes as every residue proposed [45] to be involved in this catalysis requires a non-polar environment in order to attain the proper protonation state: ICS and SAS enzymes would require a deprotonated lysine residue to activate water for nucleophilic attack, AS, ADCS and ADICS enzymes require deprotonated ammonium ion to act as a nucleophile, and all MST enzymes would require a protonated glutamate residue to activate the C4 hydroxyl group of chorismate for ring substitution (see Chapter 1 and Figure 1.8 for this proposed mechanism). The protonation states required for the active site residues in this putative mechanism can only be achieved in a non-polar active site environment, and any active site mutation that caused water to be admitted would tend to polarize the active site, alter these protonation states, and abolish displacement catalysis, leaving the enzyme only its residual CM activity.

The inability of the various AtICS2 mutants to catalyze ring displacement made it impossible to draw any conclusions about the effects of these particular MST active site residues on secondary pyruvate lyase catalysis. However, the ubiquity of the specific active site threonine that hydrogen bonds to the C2 substituent (Thr348 in Irp9; see Figure 4.2) in MST enzymes that have pyruvate lyase activity strongly suggests that it plays a key role in this process. It is likely that elements of the protein outside the active site influence catalysis – possibly by ensuring a non-polar environment within the active site – and that a full complement of mutations compensatory to the presumably key AtICS2 A467T mutation would involve residues not indicated in Figure 1.7. A set of mutations throughout the protein that permits the ring displacement reaction of wild type MST enzymes would deplete chorismate, thus preventing the undesirable CM reaction. A set of mutations that accomplishes this, while simultaneously preventing the disappearance of the intermediate, should favor the elimination of pyruvate to form aromatic product. This could be accomplished by reduction of the off rate of the intermediate by a transient bond across the active site cleft [53], or by minimization of the back reaction to chorismate. Though the active site threonine residue may facilitate the pyruvate lyase reaction by altering the conformation of the intermediate (see Figure 4.2), another possibility is that the hydrogen bond it forms to the putative general acid glutamate slows the back reaction to chorismate by stabilizing the carboxylate, making it less basic.

A comprehensive proposal for the enzymatic mechanisms of the actual and ideal mutant AtICS2 activities is detailed in Figure 4.17. None of the AtICS2 mutants has the 1,5-S_N2'' displacement activity common to all MST enzymes, and I propose here that this is due to the absence of ring activation by Mg^{2+} and/or protonated Lys311 being unable to activate water for nucleophilic attack. All of the AtICS2 mutants have chorismate mutase activity, however, and I propose that this irreversible rearrangement proceeds via a boat or a twist-boat transition state with the *re* face of the enolpyruvate oriented toward the substrate ring. I further propose that the

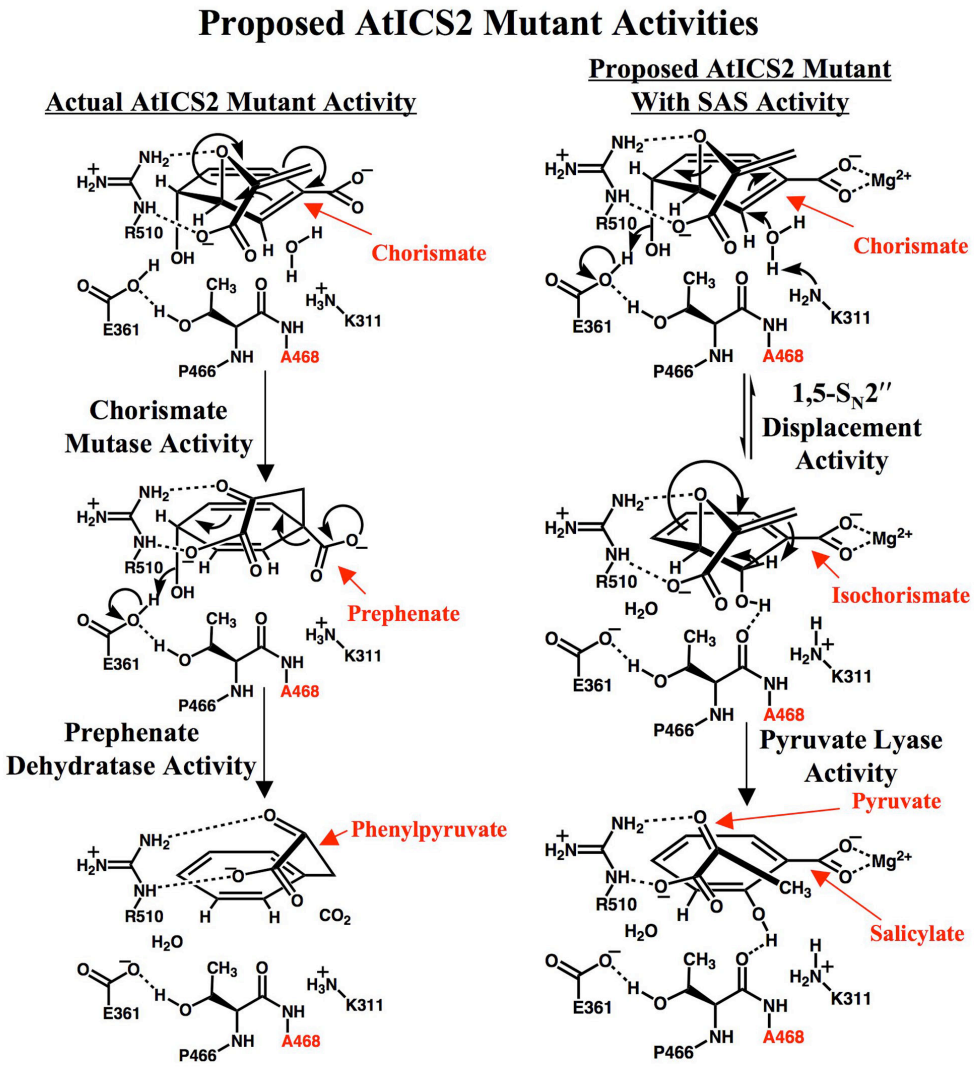

Figure 4.17 Proposed Enzyme Reaction Mechanisms for AtICS2 Mutants. Schematics are shown above of the enzyme active site of the AtICS2 A467T V468A T526A triple mutant (second mutation indicated by red lettering), which replaces three amino acid residues (two shown here) with those conserved in salicylic acid synthase (SAS) enzymes. A proposal for the mechanism of the actual activity of this mutant is shown on the left, and a proposal for the mechanism of the ideal activity of functional SAS enzymes is shown on the right. Black arrows indicate movement of electron pairs. The mechanism for the actual activity shows no Mg^{2+} bound to the substrate ring carboxylate and a prematurely protonated active site lysine side chain, although it is not known whether these are the correct reaction parameters.

prephenate so generated is quantitatively converted to phenylpyruvate by a secondary prephenate dehydratase activity: Glu361 protonates the 4-hydroxyl group, neutral water leaves, and the ring undergoes irreversible decarboxylative aromatization. The hydrogen bond between the carboxylate of Glu361 and the side chain hydroxyl of Thr467 is likely not necessary for this process to occur. I also propose that mutation at additional positions could permit Mg^{2+} to bind substrate properly and allow the active site to maintain its non-polar status – though these positions likely lie outside the active site – and that this these AtICS2 mutants would act as SAS enzymes. Properly bound Mg^{2+} and a deprotonated Lys311 side chain can convert chorismate to isochorismate with the assistance of the general acid Glu361. This reaction is reversible in ICS enzymes, though in the ideal SAS described here the back reaction to chorismate is likely suppressed. This suppression could be due to some combination of a conformational change in isochorismate like that predicted in Figure 4.2, and the inability of Glu361 to deprotonate water for attack at C4 due to stabilization of its side chain carboxylate by a hydrogen bond with Thr467. The bound isochorismate intermediate is then able to undergo an irreversible pyruvate lyase reaction via the transition state shown in Figure 4.2, producing SA and pyruvate.

It is clear that these mutant enzymes are not performing the ICS reaction, and that consequently, isochorismate is not being formed. In addition, they do not form SA and thus have not been converted to functional SAS enzymes. Instead, they convert chorismate to phenylpyruvate via mechanisms (shown in Figure 4.17) that may be general for all MST enzymes, as every member of this enzyme class possesses an active site structure that is suited to catalysis of the CM and prephenate dehydratase reaction. Indeed, it appears that the default activity of MST enzymes may be CM activity, and that specific constraints are required for ICS, IPL, or SAS activities. Therefore, my work elucidates plasticity residues associated with this evolved specificity.

CHAPTER V

FINAL DISCUSSION

Detailed biochemical data for AtICS1 and AtICS2, as well as multiple mutants of both, has been provided in this thesis. Both proteins are shown to be monofunctional ICS enzymes with similar biochemical characteristics (Figure 5.1). AtICS1 and AtICS2 catalyze the transformation of chorismate to isochorismate with apparent equilibrium constants of 0.89 and 0.76, respectively, both of which are in excellent agreement with the apparent equilibrium constant calculated (0.83) for this reaction under approximately physiological conditions [315]. Like all other known MST enzymes, AtICS1 and AtICS2 activity depends absolutely upon the presence of magnesium ion, and they have K_M values for Mg^{2+} of 193 μM and 573 μM, respectively. Both of these values are far below the lowest estimated value for chloroplast magnesium concentration (1 mM in dark conditions; see [7]), suggesting that any enzyme present in the chloroplast will not have its activity limited by magnesium deficiency. AtICS1 (≥80% maximal activity from pH 6.5-10.0) possesses a much broader tolerance of pH change than does AtICS2, consistent with a role for AtICS1 in stress-induced biosynthesis of the defense hormone SA. AtICS2 is more sensitive to changes in pH (≥80% maximal activity from pH 6.5-8.0), which is consistent with its involvement in the biosynthesis under high light (the chloroplast pH = ~8 in light; see [7]) of phylloquinone associated with the photosystems. Both of these enzymes retain activity at a broad range of temperatures (≥80% maximal activity from 4 °C – 44 °C, equivalent to 39 °F – 111 °F), consistent with their ability to operate at every possible ambient temperature. AtICS1, however, has an exceptionally high activity (≥90% maximal activity) at 4 °C, validating the proposal for its role in SA biosynthesis, particularly as SA is known to be involved in cold acclimation and cold-tolerant growth (see Chapter 2). All of these data are consistent with the involvement of AtICS1 in inducible SA biosynthesis under conditions of plant stress, and with the involvement of AtICS2 in low-level biosynthesis of phylloquinone associated with plastid development.

The K_M values for chorismate of each of these enzymes suggest that they can compete effectively with other chorismate-utilizing enzymes in the chloroplast of *Arabidopsis*. Using the coupled continuous spectrophotometric assay, I determined that mature AtICS1 and mature AtICS2 have apparent K_M values for chorismate of 41.5 μM and 17.2 μM, respectively. Under plant stress conditions, AtICS1 – but not the uninduced AtICS2 – must compete with other stress-induced, chloroplast-localized chorismate-utilizing enzymes. For example, *AtICS1* and *AtASA1* are induced in response to bacterial pathogens [68, 81], and defense-related products of these pathways – camalexin, made via anthranilate (see Figure 1.9), and SA, made via isochorismate (see Figure 1.12) – are detected in parallel (data not shown). AtASA1 (At5g05730) has an apparent K_M for chorismate of 180 μM [75] and thus competes poorly with AtICS1 for available chorismate (Figure 5.2). In contrast, past comparison of apparent K_M values for chorismate of elicitor-induced *C. roseus* ICS isoforms (558 and 319 μM; see [139]) with AS (67 μM; see [352]) did not favor ICS. *AtCM1* (At3g29200) is also induced in response to bacterial pathogens [66, 67] but has an apparent K_M of 2900 μM (2.9 mM) for chorismate [67]. However, it is possible that this K_M for chorismate is artificially high due to the presence of the chloroplast transit sequence, or because it actually functions as an IPL enzyme. Alternatively, because phenylpropanoids typically dominate other chorismate-derived pathogen-induced products, this higher K_M may be physiologically relevant, resulting in increased flux only when sufficient chorismate is available. In addition, both AtASA1 and AtCM1 activities are allosterically modulated by the aromatic amino acids of the shikimate pathway [66, 67, 75], whereas there has been no evidence for allosteric regulation of a plant or bacterial ICS enzyme

Comparison of the *Arabidopsis* ICS Enzymes

	AtICS1	AtICS2
Number of Amino Acid Residues, Precursor Polypeptide	569	562
Number of Amino Acid Residues, Mature Protein	522	512
Molecular Weight, Mature Protein	57.30 kDa	56.62 kDa
Adjusted K_M For Chorismate	41.5 μM	17.2 μM
Adjusted k_{cat}	38.7 min^{-1}	18.0 min^{-1}
Adjusted k_{cat}/K_M	0.933 μM^{-1} min^{-1}	1.05 μM^{-1} min^{-1}
Apparent K_{eq}	0.89	0.76
K_M For Magnesium	193 μM	573 μM
pH Optimum For Activity	pH 6.5 - pH 10.0	pH 6.5 - pH 8.0
Temperature Optimum For Activity	4 °C - 44 °C	4 °C - 44 °C

Figure 5.1 Comparison of the Two *Arabidopsis* ICS Enzymes. A comparison of the properties of AtICS1 and AtICS2 is made in the above table.

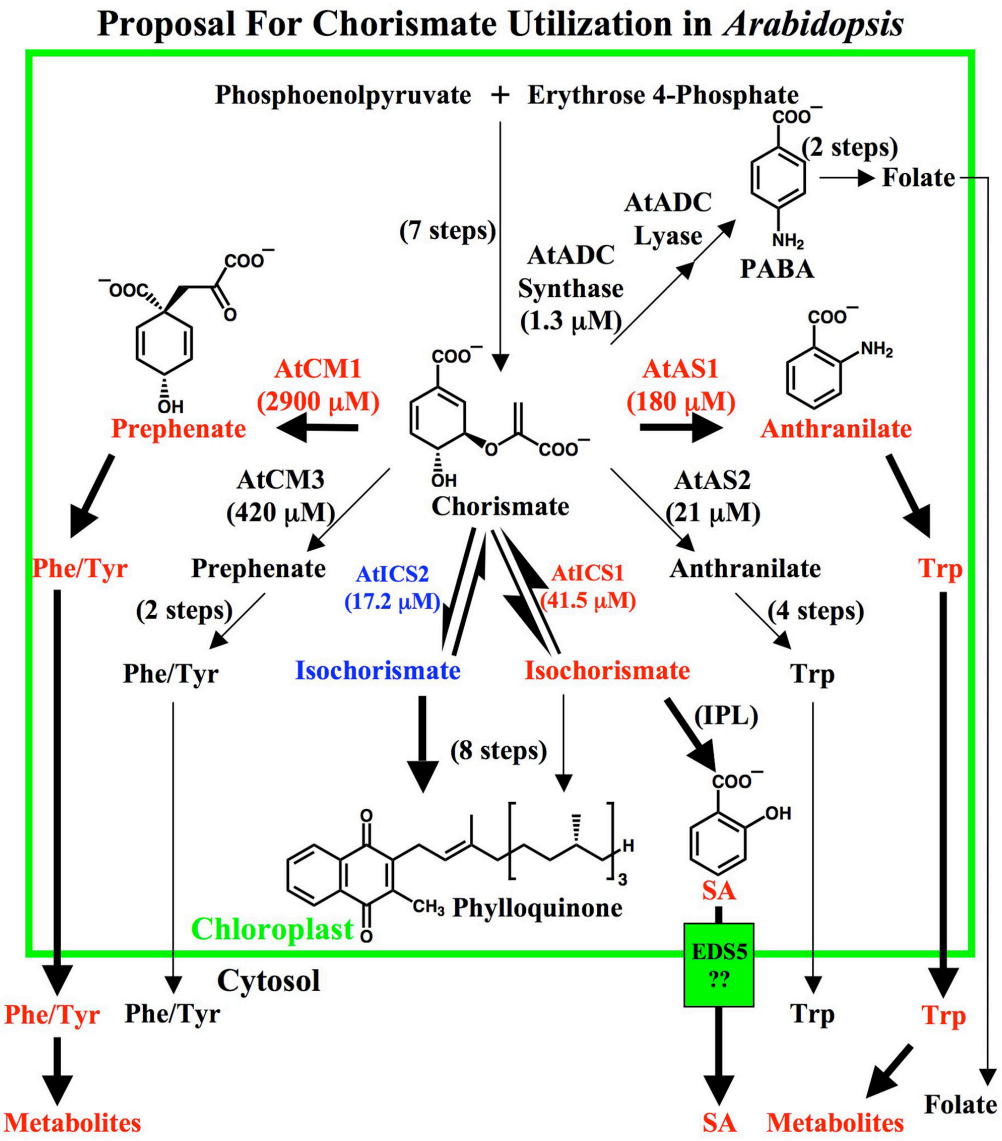

Figure 5.2 Chorismate Utilization in *Arabidopsis*. In this schematic of chorismate utilization in the *Arabidopsis* chloroplast, biosynthesis, each enzymatic transformation is indicated by a solid black arrow, except where indicated. All enzymes referenced in the text are specified, and K_M values for each chorismate-utilizing enzyme are given in parentheses. Enzymes and the compounds they produce are color-coded as follows: red for pathogen-induced, blue for light-induced, and black for constitutive. Thicker arrows indicate higher metabolic flux. EDS5, the putative SA efflux transporter, is indicated by a green box. Abbreviations used are: CM, Chorismate mutase; AS, Anthranilate synthase; ICS, Isochorismate synthase; IPL, Isochorismate pyruvate lyase; SA, Salicylic acid; ADC, 4-Amino-4-deoxychorismate; PABA, *para*-Aminobenzoic acid.

[139, 296]. Therefore, should these enzymes be expressed in the same cells, it appears that AtICS1 could successfully direct available chorismate to the production of SA.

The strong binding of AtICS1 and AtICS2 to chorismate implied by their low K_M values also suggests the possibility that they can compete with a subset of chorismate-utilizing enzymes involved in constitutive aromatic amino acid and folate production (see cytoplasmic compounds in black text in Figure 5.2). For example, both AtICS1 and AtICS2 could successfully compete for chorismate with both characterized chloroplast *Arabidopsis* chorismate mutases [66, 67], as implied by their over 10-fold lower and over 40-fold lower K_M values for chorismate, respectively, and this would allow *Arabidopsis* ICS enzymes to easily divert chorismate away from phenylalanine and tyrosine production (AtCM3 K_M for chorismate is 420 μM, whereas AtCM2 is not predicted to be chloroplast-localized). Similarly, AtICS1 has a two-fold higher K_M value for chorismate than AtASA2, and AtICS2 has a two-fold lower K_M value for chorismate than AtASA2 (chloroplast-localized AtASA2 has a K_M for chorismate of 21 μM; see [76]). This suggests that both can divert chorismate from AtASA2-mediated production of tryptophan with some success. Also, AtICS1 has a 33-fold higher K_M value for chorismate than does the recently characterized *Arabidopsis* aminodeoxychorismate synthase (ADCS), and AtICS2 has an eight-fold higher K_M value for chorismate than does AtADCS (AtADCS K_M for chorismate = 1.3 μM; see [80]). This suggests that AtADCS-mediated flux toward folate production will continue in the presence of either ICS enzyme, highlighting the importance of this cofactor. However, as folate is not produced in large amounts by the plant (1.0 nmol/ g fresh weight of plant tissue; see [353]), chloroplast chorismate is not depleted by AtADCS, and ample chorismate is available for diversion to SA or phylloquinone production by ICS enzymes.

For AtICS2 to be involved in phylloquinone biosynthesis, it would need to act as a monofunctional ICS enzyme. On the other hand, because *AtICS1* expression is highly coordinated with SA accumulation (see Chapter 1 and [301, 302]), it was surprising to find that AtICS1 was also a monofunctional ICS instead of a bifunctional SAS. Residues essential to SAS IPL activity have yet to be determined ([94, 139, 323], and see Chapter 4); therefore, homology modeling was performed on known monofunctional ICS enzymes involved in SA biosynthesis (AtICS1 and Pae PchA) – as well as the only other confirmed SAS *M. tuberculosis* MbtI [317] – using the crystal structure of the SAS *Y. enterocolitica* Irp9 in complex with its reaction products SA and pyruvate [58]. As expected, the homology modeling of AtICS1 with Irp9 indicated that the active site is highly conserved – except that an Irp9 threonine residue whose side chain hydroxyl is within hydrogen bonding distance to the putative general acid glutamate is an alanine in AtICS1 (see Chapter 4 and Figure 4.5). This threonine is conserved in all MST enzymes known to have pyruvate lyase activity – namely, the SAS MbtI and all AS enzymes – and is an alanine in all known ICS enzymes, and modeling studies suggest that the orientation of this threonine allows its backbone carbonyl to hydrogen bond to the C2 substituent of isochorismate in SAS [323] and aminodeoxyisochorismate (ADIC) in AS [338]. However, mutation of the homologous alanine residue to a threonine in several ICS enzymes – namely, AtICS1 and AtICS2 (Chapter 4), as well as *E. coli* MenF [45] – abolished ICS activity, hampering any study of the factors involved in SAS activity. It is still entirely possible that this active site threonine plays a key role in the pyruvate lyase reaction in both SAS and AS enzymes, but it is clearly the case that other factors are necessary for this activity. For example, the two ADIC synthases characterized to date – PhzE [354, 355] and SgcD [356] both catalyze the first half reaction of AS – also have a threonine at this position. Perhaps other amino acid residues outside the active

site, or global protein conformational changes due to a binding event with a small molecule effector or other protein, help activate pyruvate lyase activity (see Chapter 4).

Given that monofunctional ICS and bifunctional SAS enzymes exhibit a high degree of overall structural similarity and a highly conserved active site in which only a few residues are likely responsible for ICS versus SAS activity (see Chapter 4), we would expect to observe positive selection for either monofunctional ICS or bifunctional SAS enzymes in plants. To date, only monofunctional plant ICS activities have been reported (herein and [139, 290, 291]). It should be noted, however, that previous studies characterizing plant ICS enzymes did not examine those associated with SA biosynthesis and did not specifically look for a product other than isochorismate. Recently, *PHYLLO*, a fusion of a non-functional, 5′-truncated ICS and three full-length individual bacterial genes involved in bacterial menaquinone biosynthesis, was reported to be required for phylloquinone production in *Arabidopsis* ([95]; see Chapter 1 and Figure 1.11). The architecture of the fused *PHYLLO* locus is conserved in the nuclear genomes of plants and green algae, with gene fission and inactivation of the ICS module of *PHYLLO* occurring in higher plants. Therefore, whereas green algae encode a multifunctional enzyme involved in the conversion of chorismate to a naphthoquinone or anthraquinone intermediate (such as 1,4-dihydroxy-2-napthoate), higher plants require an independent ICS for initial production of isochorismate from chorismate (see [95], and Figure 5.1) providing strong support for positive selection for multiple monofunctional ICS enzymes in plants.

What would be the advantage of monofunctional plant ICS enzymes? First, as monofunctional ICS enzymes catalyze the reversible conversion of chorismate to isochorismate, expression of a monofunctional ICS would not drain chorismate from other plastid-localized chorismate-utilizing pathways such as aromatic acid biosynthesis or phenylpropanoid production (see Figure 5.2). This is a valid concern, as our kinetic measurements suggest that AtICS1 could potentially compete for chorismate with constitutively expressed, chorismate-utilizing enzymes associated with aromatic acid biosynthesis (for example, [67]). Furthermore, constitutive expression of a PchBA SAS fusion protein in *Arabidopsis* resulted both in a >20-fold increase in SA levels and in severe dwarfism/infertility [313]. The severity of the dwarfism/infertility phenotype compared with mutants constitutively overexpressing SA is most likely due to the channeling of chorismate to SA at the expense of other essential chorismate- and isochorismate-derived products (for example, aromatic amino acids, and phylloquinone, respectively), as the K_M of PchA for chorismate [296] is 10-fold higher than that of AtICS1.

Second, expression of multiple monofunctional ICS enzymes could allow for isochorismate to be channeled to different products (for example, SA, induced naphthoquinones or anthraquinones, and phylloquinone) depending upon co-expression of downstream enzymes (see Figure 5.2). For example, though AtICS1 expression and function is associated with induced SA biosynthesis, it may also contribute to the synthesis of other isochorismate-derived products (for example, [95, 137]). Indeed, examinations of phylloquinone biosynthesis have found that only the *ics1ics2* double mutant – but not single *ics1* or *ics2* mutants – result in phylloquinone deficient phenotypes [83, 95], suggesting that either both *Arabidopsis* ICS enzymes contribute isochorismate for phylloquinone biosynthesis in wild type plants, or that one ICS compensates for a deficiency in the other. In the case of SA biosynthesis, the *Arabidopsis ics1* single mutant was sufficient to abolish pathogen-induced SA accumulation; however, low-level endogenous SA production was unaffected [81, 149]. As *AtICS2* is not significantly induced in response to pathogens, its expression may be insufficient to functionally complement induced SA biosynthesis. To determine whether AtICS1 can channel isochorismate to different

products, it would be useful to examine whether AtICS1 can form complexes with different enzyme partners depending upon the developmental stage or biotic/abiotic stressor.

Third, multiple monofunctional ICS enzymes could provide partial functional redundancy for the robust synthesis of essential compounds – such as phylloquinone – from isochorismate. Gene duplication is a common means of facilitating the robustness of metabolic pathways [357, 358]. Robustness is typically defined as a measure of the ability of a biochemical network to withstand perturbations. Indeed, as mentioned above, the *ics1ics2* double mutant exclusively displayed the *phyllo* phenotype: no phylloquinone, 5-15% of wild type PSI activity, bleached leaves, and seedling lethality [95].

As both AtICS1 and AtICS2 are shown here to be monofunctional enzymes, the identity of the IPL enzyme involved in SA production remains unknown. What might be the identity of the secondary IPL enzyme involved in SA production? Chapter 4 shows that of the *Arabidopsis* CM1, CM2, and CM3 enzymes, only CM1 had IPL activity, despite the fact that all are homologous to the known IPL *P. aeruginosa* PchB [298]. Though the *in vitro* rate of the IPL reaction catalyzed by AtCM1 is not sufficient to produce the SA required for plant defense, the *in planta* rate of this reaction could be far higher; this is being further investigated. However, a putative fourth CM enzyme (At3g07630) has yet to be characterized, and may possess this activity. Another possibility is that the *AtICS1* transcript could experience an alternative splicing event that confers IPL activity to it in addition to the ICS activity. Any such alternative transcript must necessarily produce a protein with only a few changes to its amino acid sequence, as MST enzymes possess highly conserved active sites that tolerate substitution poorly (see Chapter 4). As discussed above, an alanine to threonine mutation at position 472 in the amino acid sequence of AtICS1 would be one promising candidate, though other mutations must accompany it to preserve the ICS activity of the enzyme (see Chapter 4). Alanine-to-threonine mutations have precedence in human biology, as the most common mutation in prostatic steroid 5α-reductase – a protein whose inactivation often leads to prostate cancer – involves this point mutation at position 49 of its amino acid sequence (via a G888A missense mutation in the nucleotide sequence; see [359]). A third possibility for the source of the required IPL activity would be induction of IPL activity in AtICS1 by a conformational shift in the protein. For example, AtICS1 could function as an ICS enzyme normally, but as an SAS enzyme in complex with another chloroplast protein. AtICS1 is relatively insoluble compared to the nearly identical AtICS2 (see Chapters 2 and 3), and could be associating with the chloroplast transmembrane protein EDS5 [266]; this could have the twin advantages of channeling chorismate to SA by the induction of IPL activity in AtICS1, and of routing the newly synthesized SA immediately to the cytoplasm where it has efficacy. A requirement for EDS5 association in effecting SAS activity would prevent chorismate depletion by AtICS1 when no transporter is available for SA export from the chloroplast.

Knowledge of chorismate utilization in plants is critical to our understanding of fundamental plant biochemistry in the context of aromatic amino acid and vitamin biosyntheses (see Figure 1.6). SA is another chorismate-derived product that mediates the plant defense response, and there are many anti-microbial and anti-herbivory agents biosynthesized from chorismate in plants (see Chapter 1). In addition, awareness of the functional evolution and diversity of the isochorismate synthase and chorismate mutase enzymes in one tractable plant system (*Arabidopsis thaliana*) allows insight into mechanisms and means by which new or alternate reactions evolve. This is especially true for chorismate mutases, as genes encoding enzymes that catalyze new reactions – in particular, the IPL enzymatic reaction catalyzed by

PchB – have evolved from genes encoding CM enzymes. In fact, chorismate mutases have been frequently engineered to display novel protein function [360]. By coupling biochemical analyses, subcellular localization studies, active site modeling, and analysis of ICS and CM *Arabidopsis* knockout lines, a detailed understanding of the enzymatic capacity and *in vivo* function of these enzymes could be elucidated.

APPENDIX I

CLONING AND EXPRESSION OF ICS1 CONSTRUCTS

INTRODUCTION

AtICS1 is the first enzyme of the SA biosynthetic pathway required for both local and systemic acquired resistance in the plant *Arabidopsis thaliana* [81]. This discovery was made by thorough characterization of the of the *ics1* knockout mutant phenotype. *AtICS1* expression was induced in wild type plants infected with the pathogenic bacterium *Pseudomonas syringae*, and the time course of its expression correlated with that of *PR-1*, a molecular marker of systemic acquired resistance [81]. These genes were not expressed in the *ics1* mutant plant, making it far more susceptible to pathogen attack. Unlike wild type plants, *ics1* does not develop SAR, a phenomenon for which SA is known to be required [81]. This SA deficiency, and the known homology between AtICS1 and biochemically characterized bacterial ICS enzymes, strongly suggested that AtICS1 was an ICS enzyme. Nevertheless, this biochemical activity had to be characterized directly to further define AtICS1 protein function.

E. coli protein overexpression strategies are extremely popular, as *E. coli* is cheap to grow, its genetics and physiology are well known to the scientific community, and strains producing 30% or more of their total protein as the overexpressed gene product can be obtained [295]. There are two principal drawbacks, however, to using *E. coli* expression systems. The first is that plant and other eukaryotic proteins do not receive proper post-translational modification in prokaryotic organisms like *E. coli*. The second is that proteins overexpressed in *E. coli* often form so-called "inclusion bodies", or insoluble aggregates of the protein – these are generally misfolded and not easily purified by conventional means, being found in the pelleted fraction of the cell extract and not the supernatant. Both of these factors can contribute to low yields of active protein from the purification. The formation of inclusion bodies can be partly ameliorated by reducing the rate of protein induction, which keeps the concentration of newly formed protein low, allowing it to fold properly before any aggregation event has a chance to occur. There are two ways of doing this: by reducing IPTG levels (*e.g.* from 1.0 mM to 0.1 mM) and by lowering the temperature used during induction (*e.g.* 37 °C to 18 °C) [361]. Though these strategies were employed with great success in the overexpression and purification of His_6-tagged AtICS2 (see Chapter 3), His_6-tagged AtICS1 was still purified in relatively small quantities (though successfully; see Chapter 2). This was somewhat surprising, as the sequences of the two proteins are 83% identical [81].

The His_6-tag is undeniably the most popular affinity tag used in the purification of recombinant proteins. However, overexpression and purification of proteins containing this tag is complicated by the fact that the process requires somewhat unfavorable conditions: 500 mM imidazole is required to elute the protein, and the resin can tolerate only very little protein-stabilizing reductant. Furthermore, the His_6-tag does not confer additional solubility to the recombinant protein. Many other affinity tags have been developed and are in widespread use for the overexpression and purification of fusion proteins. The calmodulin-binding peptide (CBP) is a 26-amino acid peptide encoded by the pCAL-n-FLAG plasmid (produced by Stratagene), and a protein sequence that is inserted in register with the tag sequence at its amino-terminus produces a CBP-protein fusion that can bind calmodulin in the presence of calcium ion. The remarkable affinity of calmodulin for CBP ($K_D = 10^{-9}$ M) in the presence of calcium allows for an extremely sensitive and mild chromatographic purification by immobilized calmodulin resin [362]. Addition of a chelating agent like ethylene glycol tetraacetic acid (EGTA) effectively removes the calcium from solution, disrupting the CBP-calmodulin interaction and allowing the recombinant protein to elute from the column. Another attractive feature of fusion

proteins generated by constructs in the pCAL-n-FLAG vector is that the 41-amino acid tag possesses an eight-amino acid FLAG epitope that abuts the CBP. A commercially available anti-FLAG antibody allows the researcher to perform Western blots on the target protein.

The maltose-binding protein (MBP), on the other hand, is a 42.5 kDa protein that is encoded by the pMAL-c2X plasmid (produced by New England Biolabs), and a protein sequence that is inserted in register with this tag sequence at its amino-terminus produces a MBP-protein fusion that can bind maltose. MBP has a K_D for maltose of 3.5 μM [363], and can be purified by chromatography with amylose (a polymer of maltose) resin. Though this affinity purification process is also quite mild, it is not as sensitive as that for the purification of CBP fusion proteins. Additionally, this fusion has no FLAG peptide, and the tag itself is a large protein that may interfere with the activity of the fusion. Nevertheless, this construct possesses the major advantage of conferring unusually high solubility on the fusion product. This is particularly useful for the production of proteins that tend to form inclusion bodies, as the greater solubility provided by the MBP tag minimizes the oligomerization rate, thereby allowing the protein to fold properly. There are a number of other affinity tags that have been designed to perform the same function, among them thioredoxin (TRX) and glutathione S-transferase (GST), but several studies have shown the maltose-binding fusion proteins to be the most soluble of this class [364, 365]. For the reasons described previously, I concluded that both the CBP-AtICS1 and the MBP-AtICS1 fusions were likely to provide a higher yield of protein after overexpression and purification of than would the His_6-AtICS1 fusion described in Chapter 2.

MATERIALS AND METHODS

Materials and General Protocols

All specialty reagents and chemicals were obtained from Sigma-Aldrich unless otherwise specified. HPLC-grade solvents (EMD Biosciences) were employed in the HPLC analyses. Barium chorismate (Sigma C-1259, 60-80% purity) was used in all assays. For selection and growth of transformed cells (described below): pCAL-n-FLAG and pMAL-c2X derivatives were selected with 100 μg/ml ampicillin; *E. coli* BL21-CodonPlus(DE3)-RIL cells were selected with 30 μg/ml chloramphenicol. Commonly utilized protein and molecular biological reagents and protocols were prepared/performed as in *Current Protocols in Molecular Biology* [295].

Cloning, Expression and Attempted Purification of Recombinant CBP-AtICS1

The AtICS1 coding region (without the chloroplast transit sequence) was PCR amplified from *Aradibopsis thaliana* ecotype Columbia-O cDNA isolated from induced leaves (forward primer: 5'-gacgacgacaagatgtctatgaatggttgtgat-3'; reverse primer: 5'-ggaacaagacccgttcaattaatcgcctgtagag-3') and inserted as an AlwNI/DraIII fragment into the AlwNI/DraIII sites of a pCAL-n-FLAG (Stratagene) construct already containing a point mutant of mature AtICS1 (obtained from Dr. Mary Wildermuth). The resulting construct, pMAS-I-110-2, contains an amino-terminal calmodulin-binding peptide tag in sequence with a FLAG epitope tag, fused to amino acid 45 of the AtICS1 coding region. The pMAS110-2 AtICS1 coding sequence was confirmed to be identical to AtICS1 sequence AY056055 (At1g74710.1).

E. coli BL21-CodonPlus(DE3)-RIL cells (Stratagene) were transformed with this plasmid. Crude cell extracts were prepared from a 5 L culture of transformed cells in LB media containing 100 μg/ml ampicillin and 30 μg/ml chloramphenicol. Cultures were grown at 37 °C

to mid-log phase, 0.1 mM IPTG was added to induce CBP-AtICS1 synthesis, and cells were harvested after 16 hours at 19 °C (~48 g wet weight) and stored at –20 °C. Upon thawing, the cells were resuspended in 50 ml of cold Ca^{2+} binding buffer (50 mM Tris-HCl, pH 8.0, 150 mM sodium chloride, 1 mM magnesium acetate, 1 mM imidazole, and 2 mM $CaCl_2$) containing 1 mM DTT, 2 μM leupeptin, and 5 μg/ml DNase. All subsequent operations were carried out at 4 °C. The cells were lysed by two passages through a French press at 18000 psi. Following centrifugation, the supernatant was allowed to bind to 5 ml calmodulin affinity resin (Stratagene) by mixing with mild agitation on a rotary shaker for 12 hours. The resin had been pretreated with Ca^{2+} binding buffer according to the manufacturer's directions. The slurry was then poured into a column, and the flow-through was collected in two portions. After washing the column with 25 ml of Binding Buffer, protein was eluted with 30 ml of elution buffer (50 mM Tris-HCl, pH 8.0, 150 mM sodium chloride, 2 mM EGTA) containing 1 mM DTT. Fractions were dialyzed into 50 mM potassium phosphate, pH 7.5, 10 mM $MgCl_2$, 10% glycerol, 1 mM DTT, and then aliquoted and stored at –80°C.

Determination of Protein Concentration

Protein concentrations were determined by the method of Bradford, modified as described in *Current Protocols in Molecular Biology* [295].

Isochorismate Synthase Activity Assays

The HPLC isochorismate synthase activity assay was performed as described in Chapter 2.

Immunoblot Analysis of CPB-ICS1

Proteins were analyzed by SDS-PAGE using standard protocols [295], and stained with Coomassie Blue R-250 after transfer of protein to the nitrocellulose membrane. Transfer to the membrane was conducted in 1× Tris-Glycine buffer containing 20% methanol for 90 minutes with a constant voltage of at 25 V. All successive steps were carried out at room temperature using mild agitation. The membrane was suspended overnight in 40 ml of 10% milk protein in 1× TTBS (0.1% Tween-20 in 1× TBS). The membrane was then incubated for 4 hours with 10 μg/ml of mouse anti-FLAG antibody (Stratagene) in 10 ml of 1× TTBS containing 5% milk protein. After washing the membrane 4 times in 200 ml of 1× TTBS for 10 minutes each to remove non-specifically bound primary antibody, incubation with a 1:3000 dilution of secondary goat anti-mouse antibody (conjugated to horseradish peroxidase; Bio-Rad) was carried out for one hour. The membrane was again washed 4 times with 200 ml of 1× TTBS for 10 minutes each, and then was developed by applying one ml of ECL reagent (from Pierce, made according to the manufacturer's directions) to the protein-bearing membrane surface. The membrane was then wrapped in plastic wrap and exposed in the dark room using Biomax XAR film (Kodak).

Cloning, Expression and Purification of Recombinant MBP-AtICS1

The AtICS1 coding region (without the chloroplast transit sequence), including an amino-terminal 34-base pair sequence containing the FLAG epitope from the pCAL-n-FLAG vector, was inserted as a BstUI/SalI fragment into the XmnI/SalI (BstUI and XmnI leave blunt ends) sites of pMAL-c2X (New England Biolabs). The resulting construct, pMAS-II-58-7, contains an amino-terminal maltose-binding protein tag in sequence with a FLAG epitope tag, fused to

amino acid 45 of the AtICS1 coding region. The pMAS-II-58-7 AtICS1 coding sequence was confirmed to be identical to AtICS1 sequence AY056055 (At1g74710.1).

E. coli BL21-CodonPlus(DE3)-RIL cells (Stratagene) were transformed with this plasmid. Crude cell extracts were prepared from a 4 L culture of transformed cells in LB media containing 100 μg/ml ampicillin and 30 μg/ml chloramphenicol. Cultures were grown at 37 °C to mid-log phase, 0.3 mM IPTG was added to induce MBP-AtICS1 synthesis, and cells were harvested after 23 hours at 18 °C (~40 g wet weight). After resuspending the cells in 80 ml of cold column buffer (20 mM Tris-HCl, pH 7.4, 200 mM sodium chloride, 1 mM EDTA), the cells were stored at –20 °C. Upon thawing, amounts of stock solution were added appropriate to effect the following working concentrations: 1 mM DTT, 2 μM leupeptin, and 5 μg/ml DNase. All subsequent operations were carried out at 4 °C. The cells were lysed by two passages through a French press at 18000 psi. Following centrifugation, the supernatant was diluted to a final volume of 400 ml with column buffer, and allowed to bind overnight for 12 hours with mild agitation to 10 ml amylose affinity resin (New England Biolabs) that had been pretreated according to the manufacturer's instructions. The slurry was then poured into a column, and the flow-through was collected in three portions. After washing the column with 120 ml of column buffer, protein was eluted with 30 ml of elution buffer (above column buffer containing 10 mM maltose). Fractions 3 through 9 (1 ml each) were concentrated using an Amicon Ultra-15 (10 kDa molecular mass cutoff) ultrafiltration device (Millipore) to a final volume of ~1 ml, and then dialyzed into enterokinase cleavage buffer (50 mM Tris-HCl, pH 8.0, 50 mM sodium chloride, 2 mM $CaCl_2$, 0.1% Tween-20).

Five separate enterokinase reactions were conducted on the MBP-AtICS1 fusion protein isolated above. Each reaction was performed in 30 μl volumes in which MBP-AtICS1 has a working concentration of 1.2 mg/ml in enterokinase cleavage buffer. Four separate reactions were carried out with varying amounts of enterokinase (Stratagene): 0.5 units, 1 unit, 2 units, and 5 units. A fifth control reaction was carried out simultaneously with no enterokinase. Two other reactions were undertaken in 5 μl volumes of enterokinase cleavage buffer in which enterokinase Cleavage Control Protein (Novagen) was present at a working concentration of 0.6 mg/ml. One of these reactions was incubated with 1 unit of enterokinase, the other with no enterokinase. All seven reactions were incubated at room temperature for 4 hours.

RESULTS

CBP-AtICS1 is not soluble and forms inclusion bodies. Dr. Mary Wildermuth had previously used ligation independent cloning to construct a number of unsequenced pCAL-n-FLAG constructs that encoded all but the first 44 amino acids of AtICS1 (this is the bulk of the chloroplast transit sequence). Upon sequencing, one was found to contain a single point mutation. The authentic sequence was amplified from a cDNA library, and this fragment and the original construct were cut with the same restriction enzymes and gel purified. Though this led to three separate fragments instead of two, all were ligated successfully to form the desired wild type AtICS1 pCAL-n-FLAG construct, as revealed by sequencing and restriction analysis.

Expression and purification of CBP-ICS1 proceeded as described above. As shown in the SDS-PAGE gel of the fractions from the purification (Figure A1.1), very little soluble protein was present in the supernatant, although the protein expressed normally. Nevertheless, a protein of the same size as that predicted for CBP-AtICS1 (~62 kDa) eluted from the column after

CBP-ICS1 Calmodulin Affinity Column Purification

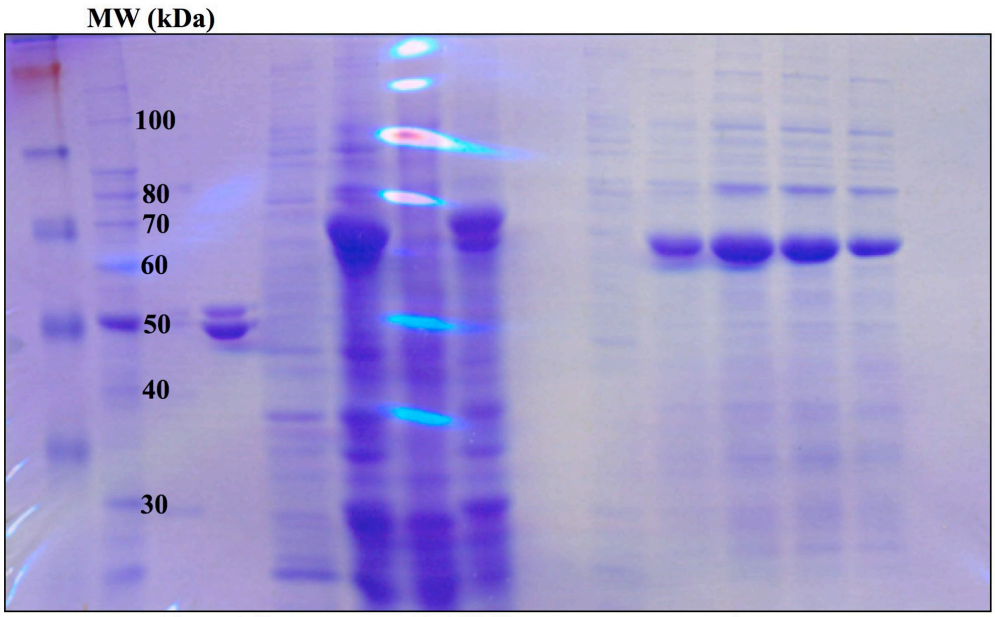

Std	FP	Un	Ind	SN	P	FT1	FT2	2	3	4	5	12
Protein (mg/ml)								2.2	6.7	4.9	1.9	0

Fraction	P	SN	FT	W	1	2	3	Comb
Protein (mg/ml)	7.1	3.2	2.3	2.1	0.63	0.35	0.27	1.2
Specific Activity (nmol/min/mg)	1.08	3.50	0.06	1.82	11.9	9.9	9.9	46.0

Figure A1.1. SDS-PAGE on Calmodulin Affinity Column Fractions from the Purification of CBP-AtICS1. Proteins were separated on a 10% SDS-PAGE gel and stained with Coomassie blue. Abbreviations used are: Std, Invitrogen BenchMark protein standards, molecular masses in kDa are indicated on left; FP, Control FLAG protein; Un, Uninduced *E. coli* total protein; Ind, IPTG-induced *E. coli* total protein; SN, Supernatant (crude extract) from lysed induced cells; P, Pellet from lysed induced cells; FT, Flow-through from column loading; Numbers are elution fractions; CPB, Calmodulin-binding peptide.

exposure of the bound protein to EGTA. Approximately 18 mg of this protein was isolated, but assay by HPLC showed that the protein had no ICS activity. It was not clear whether this protein was inactive CBP-AtICS1 or a different protein whose binding to the calmodulin affinity resin was also Ca^{2+}-dependent.

In order to determine whether this eluted protein was CBP-AtICS1, immunoblot analysis was performed on dilutions of many of the purification fractions from the initial purification (Figure A1.2). Though the eluted fractions are transferred to the membrane in this process, antibody specific to the FLAG peptide did not bind to any protein in the fractions. This strongly suggests that the protein in question is not the one desired. Moreover, identical bands in the IPTG-induced protein faction and in the pellet fraction – but not the supernatant fraction – bound antibody, confirming that the CBP-AtICS1 was present entirely in the form of inclusion bodies. That the antibody was specific for the FLAG peptide was demonstrated by the strong signal in the immunoblot lane abbreviated FP, which contained a FLAG-containing control protein.

MBP-AtICS1 is soluble, but does not produce a protein with ICS activity. The entirety of the AtICS1 coding region from the previously described pCAL-n-FLAG vector – also containing a short sequence at the amino-terminus of ICS1 that includes the coding region for an 8-amino acid FLAG epitope – was cloned in register with the maltose-binding protein tag encoded in pMAL-c2X. As shown in the SDS-PAGE gel of the fractions from the purification (Figure A1.3), the MBP-AtICS1 protein product is highly soluble – in fact, the supernatant fraction possesses relatively more fusion protein than the pellet fraction (data not shown). MBP-AtICS1 elutes cleanly over several fractions when maltose is added to the pre-loaded column. This purification also provides an exceptionally high yield of target protein (~17 mg/4 L culture). However, none of the fractions has ICS activity by HPLC assay.

To judge whether the inactivity of MBP-AtICS1 was due to the presence of the relatively large MBP domain, cleavage of the fusion by exposure to the highly specific protease enterokinase to form the native AtICS1 protein was attempted. The SDS-PAGE gel of this cleavage reaction (Figure A1.4) carried out at low concentrations of enterokinase (Lane R4) showed visible cleavage product (~57 kDa), as well as some uncleaved fusion and a very substantial amount of native protein degradation product. The MBP domain was present (~42 kDa), and appeared to suffer no additional cleavage. In addition, a control protein (Lane Rb, 48 kDa) was cleaved at its known enterokinase cleavage site to form two fragments of the expected molecular mass (Lane Ra, 32 kDa band is visible and 16 kDa band is not), demonstrating that enterokinase has the proper activity. Though the evidence is strong that native AtICS1 is present in the mixture after cleavage, none of the fractions had ICS activity by HPLC assay.

DISCUSSION

Initial attempts at overexpressing and purifying active AtICS1 made use of a CBP tag. Ideally, I would have been able to take advantage of the ease of use and stringency of purification of the calmodulin affinity column. A gene encoding an active fusion protein could have been introduced into *Arabidopsis* mutants missing the ICS1 gene; the presence of the FLAG epitope would have enabled *in vivo* immunofluorescence studies. However, no active protein was obtained. The insolubility of the AtICS1 target protein was a continual problem in this purification. Though an outstanding amount of protein was eluted from the column (18 mg),

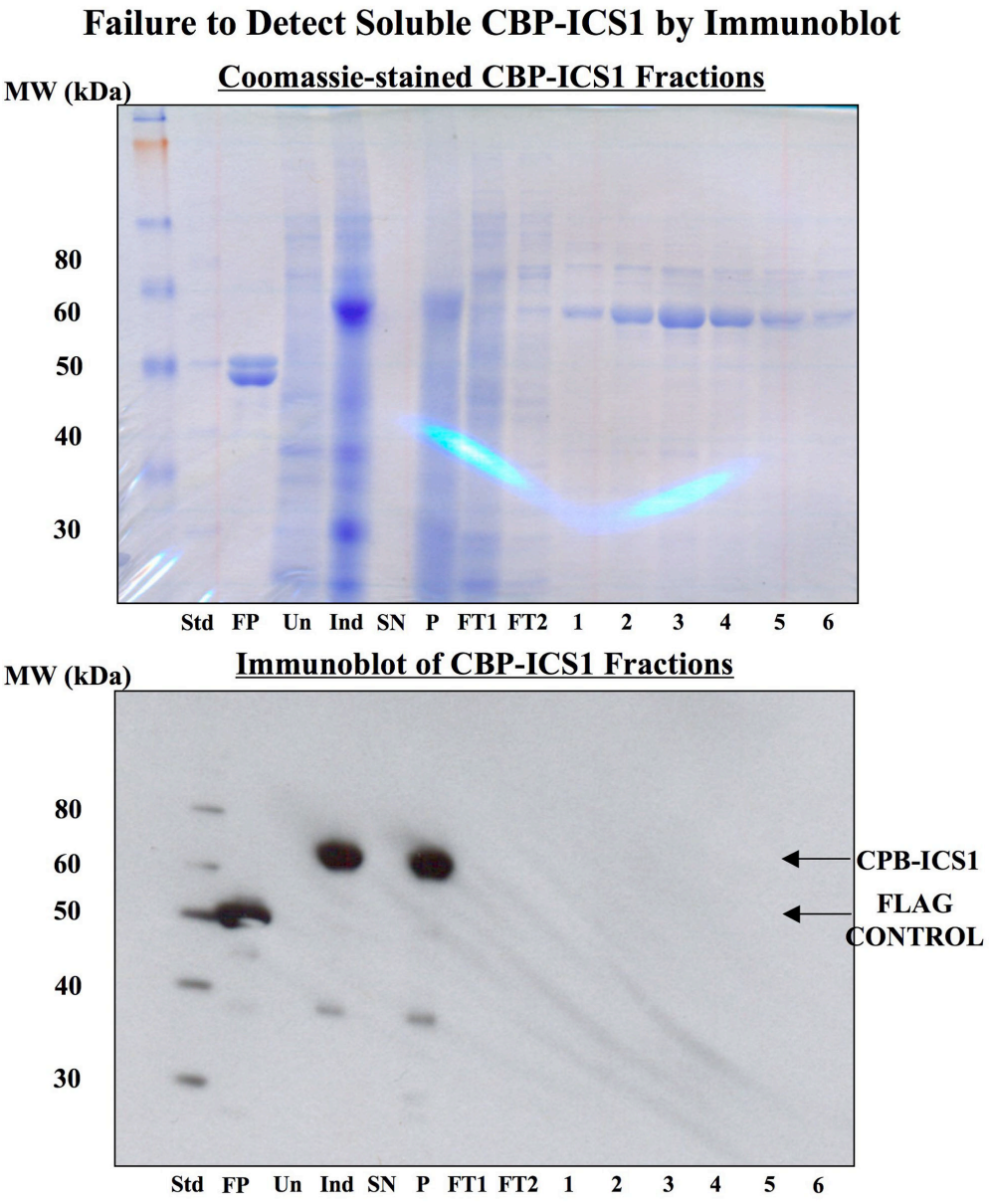

Figure A1.2. Immunoblot of CBP-AtICS1. Proteins were separated on a 10% SDS-PAGE gel and stained with Coomassie blue (above) or transferred to a membrane and incubated with anti-FLAG antibody (below). Abbreviations used are: Std, Invitrogen MagicMark Western protein standards, molecular masses in kDa are indicated on left; FP, Control FLAG Protein; Un, Uninduced *E. coli* total protein; Ind, IPTG-induced *E. coli* total protein; SN, Supernatant (crude extract) from lysed induced cells; P, Pellet from lysed induced cells; FT, Flow-through from column loading; Numbers are elution fractions; CPB, Calmodulin-binding peptide.

MBP-ICS1 Amylose Affinity Column Purification

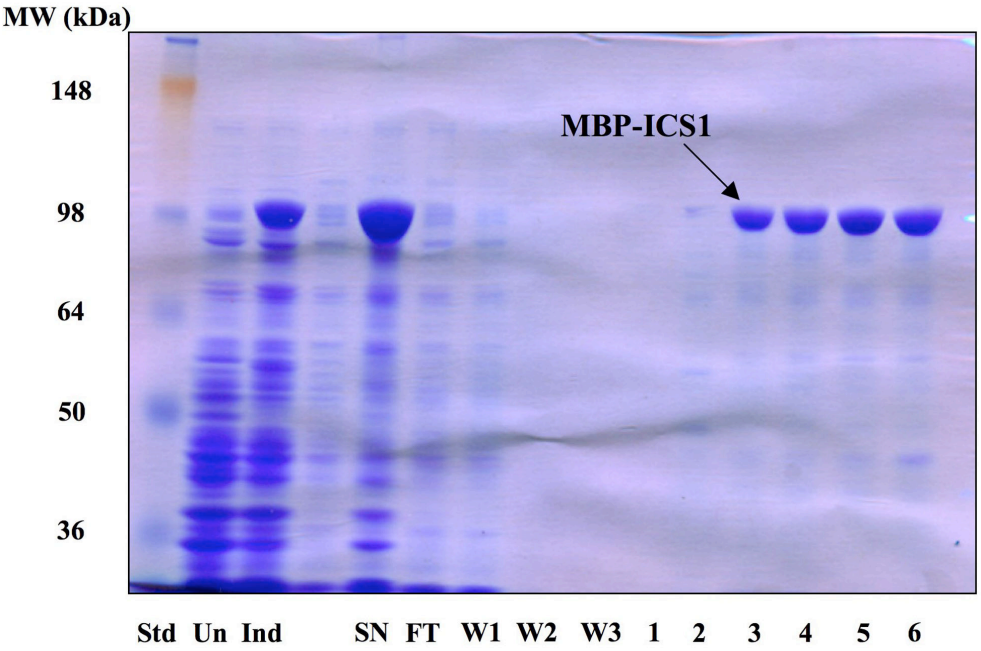

Fraction	P	SN	FT	W	1	2	3	Comb
Protein (mg/ml)	7.1	3.2	2.3	2.1	0.63	0.35	0.27	1.2
Specific Activity (nmol/min/mg)	1.08	3.50	0.06	1.82	11.9	9.9	9.9	46.0

Figure A1.3. SDS-PAGE on Amylose Affinity Column Fractions from the Purification of MBP-AtICS1. Proteins were separated on a 10% SDS-PAGE gel and stained with Coomassie blue. Abbreviations used are: Std, Invitrogen SeeBlue Plus2 pre-stained protein standards, molecular masses in kDa are indicated on left; Un, Uninduced *E. coli* total protein; Ind, IPTG-induced *E. coli* total protein; SN, Supernatant (crude extract) from lysed induced cells; P, Pellet from lysed induced cells; FT, Flow-through from column loading; W, Wash fractions; Numbers are elution fractions; MBP, Maltose-binding protein.

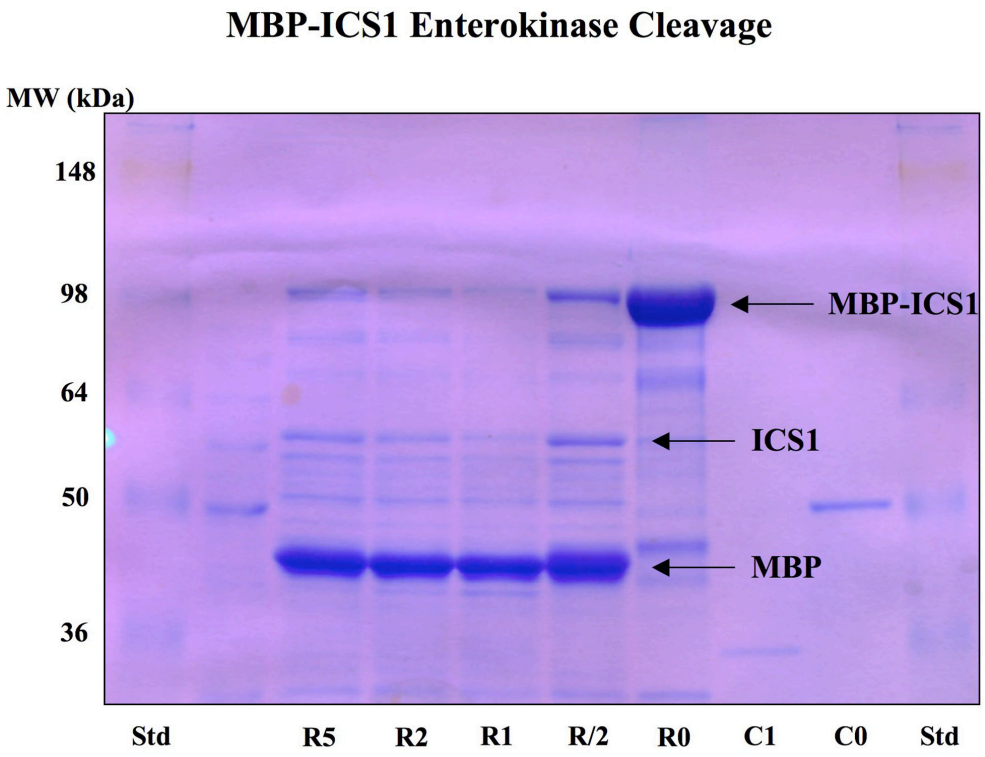

Figure A1.4. SDS-PAGE on Cleavage of MBP-AtICS1 by Enterokinase. Proteins were treated with varying levels of enterokinase, and then separated on a 10% SDS-PAGE gel and stained with Coomassie blue. Abbreviations used are: Std, Std, Invitrogen SeeBlue Plus2 pre-stained protein standards (3.6 μg protein loaded), molecular masses in kDa are indicated on left; C0, Control protein exposed to no enterokinase; C1, Control protein exposed to 1 unit of enterokinase; R0, MBP-ICS1 protein exposed to no enterokinase; R/2, MBP-ICS1 protein exposed to 0.5 units of enterokinase; R1, MBP-ICS1 protein exposed to 1 unit of enterokinase; R2, MBP-ICS1 protein exposed to 2 units of enterokinase; R5, MBP-ICS1 protein exposed to 5 units of enterokinase; MBP, Maltose-binding protein.

it was later demonstrated by immunoblot analysis to be a different protein than had been targeted. The immunoblot shows conclusively that the protein in question has no FLAG epitope, meaning either that the FLAG had been removed approximately at the enterokinase cleavage site by some type of proteolysis, or that the protein in question has no identity to the CBP-AtICS1 target. The complete lack of ICS activity of this protein suggests the latter possibility.

Though a successful procedure was ultimately developed for the production of AtICS1 using a His_6-tag (see Chapter 2), each individual 2 L preparation gave a yield of only 1 mg of AtICS1 typically. As far more than that was needed for biochemical study, an attempt was made to develop an MBP-AtICS1 fusion protein that could be purified in large amounts. In addition, the cloning was performed in a manner such that there was a FLAG epitope intermediate between the MBP domain and the AtICS1 target. Though the MBP tag may have impaired the function of the AtICS1 fused to it, a Factor Xa cleavage site between the MBP domain and the FLAG epitope allows for separation of MBP and ICS1. The existence of two cleavage sites also provides versatility – either the native AtICS1 or the FLAG-AtICS1 can be produced by cleavage with enterokinase or Factor Xa, respectively. This strategy remains sound, though this particular protein was inactive whether present as an MBP-AtICS1 fusion or in its native form. However, the solubility of this MBP fusion protein (17 mg of MBP-AtICS1 were isolated) does demonstrate the ability of the MBP tag to solubilize relatively insoluble target proteins like AtICS1.

APPENDIX II

DEVELOPMENT OF COUPLED CONTINUOUS SPECTROPHOTOMETRIC ASSAY FOR ICS ACTIVITY

INTRODUCTION

The characterization of an enzyme necessarily involves the use of a reliable assay for its activity. Though endpoint assays do provide useful information, a time course assay allows observation of the progress of the reaction. The progress curve of an enzyme reaction is a plot of product concentration as a function of time, and it has several phases, the most widely observed of these being the steady-state phase. This is a linear region of the progress curve, wherein each of the enzyme-bound intermediates in the course of the overall reaction is at a concentration that remains relatively constant. The steady-state phase is usually achieved fairly quickly after initiation of the reaction and, under ideal conditions, can last for hundreds of seconds. The slope of this steady-state region of the progress curve is taken as the value for initial velocity in Michaelis-Menton kinetics.

The use of the progress curve slope to determine the initial velocity of the enzyme reaction is only valid if it is linear within the time frame of the reaction. It is a general guideline that initial rate conditions no longer prevail when more than 10% of the substrate has been processed [366, 367]. This rule of thumb certainly applies to exergonic reactions ($\Delta G < 0$) with large equilibrium constants. However, when the equilibrium constant for the reaction is close to 1, the steady-state phase of the reaction is generally much shorter than in the above case, and a much more sensitive assay is required to detect even a short linear range of activity. Furthermore, product accumulation results in a significant rate of back-reaction, and even when this rate is low, it can greatly distort the value for the forward reaction rate determined thusly [366].

The preferred means of overcoming the obstacle of non-linearity is to add a secondary enzyme that reacts with the product of the enzyme of interest. Provided that this secondary enzyme is present in excess – or that it at least provides turnover in excess of that which allows buildup of intermediate – the rate of back-reaction of the primary enzyme is effectively eliminated. This assures that the rate measured – now of secondary enzyme product formation – accurately describes the kinetics of the primary enzyme. A particularly attractive feature of many of the coupled assays that have been developed is the incorporation of the chromophore NADH, which requires the use of the appropriate dehydrogenase as a secondary enzyme. NADH experiences a large change in absorbance at 340 nm ($\varepsilon_{340} = 6220\ M^{-1}\ cm^{-1}$) as it is oxidized to NAD^+. This process can be visualized spectrophotometrically in real time, giving the researcher the option of obtaining much better estimates for initial rates of reaction than would be provided by an endpoint assay. These so-called coupled continuous spectrophotometric assays are the method of choice for the determination of kinetic constants, as they give smooth reaction progress curves that are the product of a long series of time points, each of which is an individual endpoint assay.

Lactic dehydrogenase (LDH) has historically been among the most assayed enzymes, as it is present in serum after tissue damage. The increase in serum levels of one heart LDH isozyme (H_4) relative to another (H_3M), for example, is used as clinical evidence that a heart attack has occurred [368]. LDH catalyzes the reduction of pyruvate to lactate, with a concomitant oxidation of NADH to NAD^+. Though this reaction is reversible, and LDH is often used to assay the rate of the reverse reaction as well, the equilibrium in the forward direction is quite high ($3.62 \times 10^{11}\ M^{-1}$ at 25 °C and pH 7.0) [369], the maximal velocity in this direction more favorable [370, 371], and the NADH component more stable (than NAD^+). In addition, its K_M for NADH is very low (NADH K_M = 10.7 μM; see [372]), ensuring that LDH remains

saturated with NADH for most of the reaction, and that the velocity will not therefore fall significantly. The high velocity and long-lasting reaction time of LDH combine to make it an ideal coupling enzyme for the oxidation of NADH in continuous assays. After a steady-state velocity of pyruvate reduction is achieved at the end of the initial lag time, LDH is rarely rate limiting in any system even at low concentrations.

PchB, on the other hand, has not been used a great deal as a coupling enzyme. It is a 101-amino acid homodimer that functions as an IPL enzyme in the production of pyochelin by *Pseudomonas aeruginosa* [298]. It also has CM activity, though it proceeds with a catalytic efficiency (k_{cat}/K_M) that is over two orders of magnitude lower than that of the IPL activity. PchB has been used effectively in one instance as a secondary coupling enzyme for the assay of ICS activity in PchA [296]. In a discontinuous assay, 48 units of PchB and ~2 units of PchA were incubated at 37 °C with 500 μM chorismate, the reaction was quenched by addition of concentrated acid, extracted with ethyl acetate, and the salicylate product isolated was quantified by fluorescence using HPLC. Further analysis in this work of the coupled process showed that PchA activity, not PchB activity, was the limiting factor in the rate of overall salicylate production.

Apart from the PchA study [296], and one other on EntC [55], no coupled reactions have been used to assay ICS activity. One discontinuous assay used by many researchers studying ICS enzymes involves quantification of the isochorismate formed in the reaction by non-enzymatic conversion to salicylate at 100 °C, but the efficiency of this reaction is low (~25%) and the results are highly variable [373]. A more straightforward discontinuous assay requires simply developing conditions wherein chorismate and isochorismate can be separated by HPLC. Aliquots of the reaction can then be injected, the absorbance peak areas at any given wavelength determined by spectrophotometer, and the amounts of both molecules quantified by either reference of the peak areas to their corresponding calibration curves, or by use of known extinction coefficients for each molecule (chorismate $\varepsilon_{273} = 2630\ cm^{-1}\ M^{-1}$ [40], and isochorismate $\varepsilon_{280} = 8300\ cm^{-1}\ M^{-1}$ [299]). I developed one such assay that proved very useful for examining the effects of changing reaction conditions on the extent of the conversion of chorismate to isochorismate by ICS (see the HPLC ICS Activity Assay in Chapter 2), and many other similar assays have been used in the past by other researchers. Unfortunately, this assay, as well as all the others like it, is not appropriate for measuring ICS initial velocities, as the reaction progress curve is non-linear. A comprehensive study of purified EntC (Figure A2.1, see Chapter 1 and Figure 1.10 for background) reactivity revealed a non-linear time course (shown in Figure A2.2). In all cases, regardless of how many data points were used, the rate of back-reaction of the ICS enzyme was significant from the very beginning. Any kinetic data obtained from an assay such as this is suspect, and consideration of the shortcomings of this assay motivated the development of a coupled assay for ICS activity that would be reasonably accurate.

MATERIALS AND METHODS

Materials and General Protocols

All specialty reagents and chemicals were obtained from Sigma-Aldrich unless otherwise specified. HPLC-grade solvents (EMD Biosciences) were employed in the HPLC analyses. Barium chorismate (Sigma C-1259, 60-80% purity) was used in all assays. L-Lactic Dehydrogenase (Sigma L-1254, Type XI: from Rabbit Muscle) was used in all procedures

His-EntC Ni^{2+}-NTA Affinity Column Purification

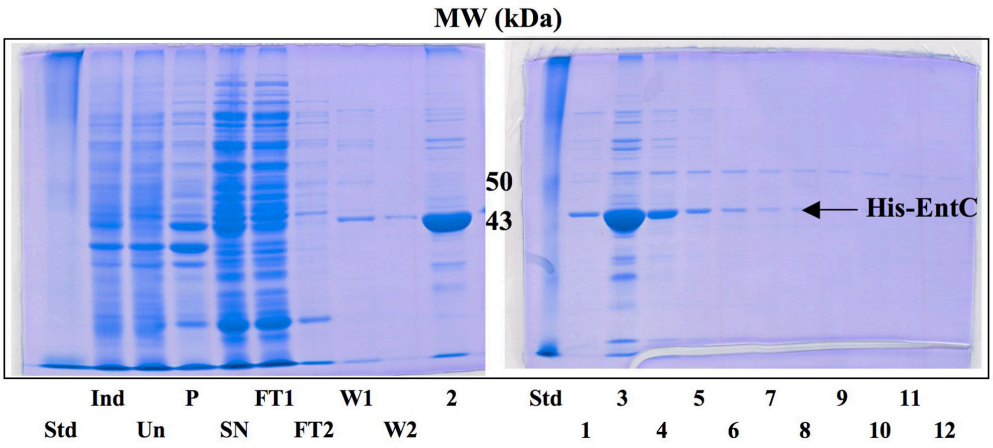

Fraction	1	2	3	4
Protein (mg/ml)	0.14	3.98	2.24	0.51
Specific Activity (μmol/min/mg)		2.3		

Figure A2.1. SDS-PAGE on Ni^{2+}-NTA Affinity Column Fractions from the Purification of His-EntC. Proteins were separated on a 10% SDS-PAGE gel and stained with Coomassie blue. Abbreviations used are: Std, Invitrogen BenchMark protein standards, molecular masses in kDa are indicated in the center between gels; Un, Uninduced *E. coli* total protein; Ind, IPTG-induced *E. coli* total protein; SN, Supernatant (crude extract) from lysed induced cells; P, Pellet from lysed induced cells; FT, Flow-through from column loading; W, Wash fractions; Numbers are elution fractions.

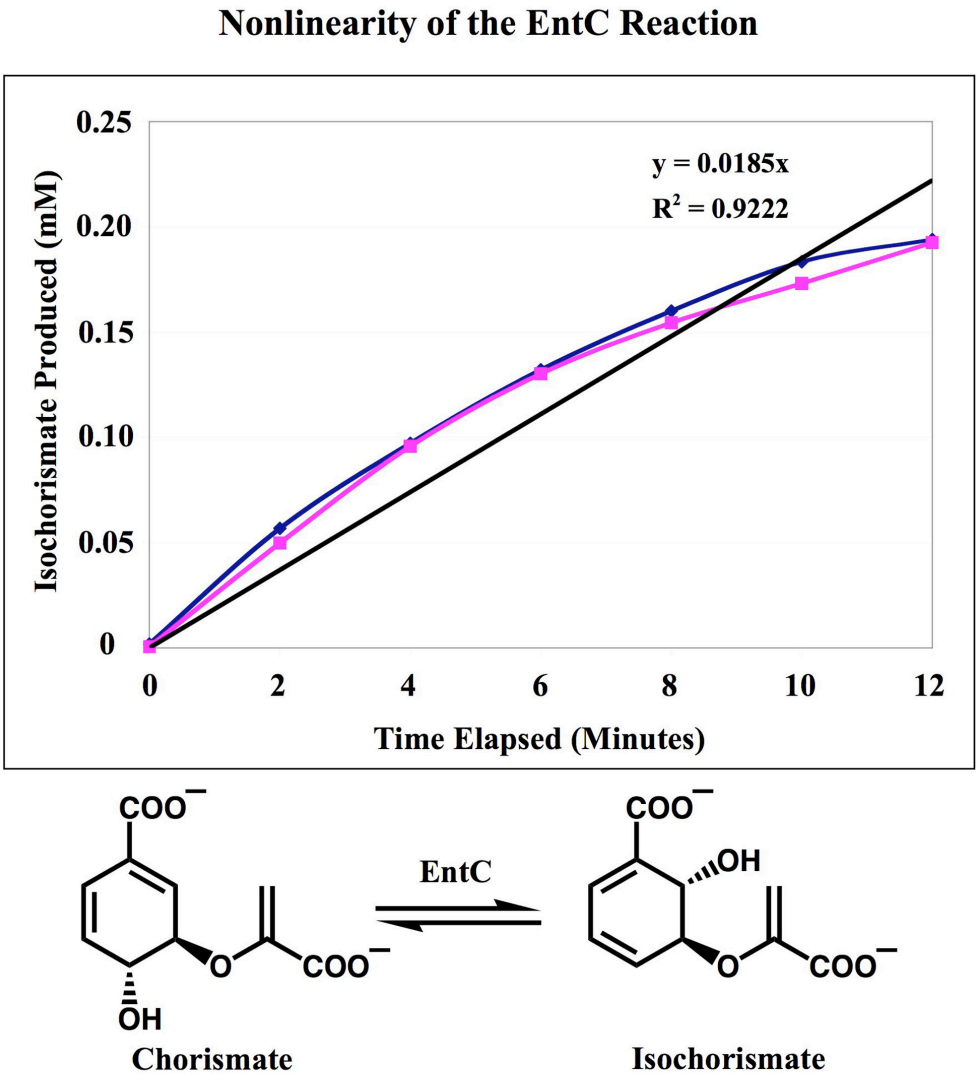

Figure A2.2. Early Reaction Progress Curve for EntC ICS Reaction. Aliquots of duplicate EntC reactions (purple and blue curves) were removed every two minutes, and isochorismate content was determined by HPLC. A line (in black, with the line equation and coefficient of determination shown) obtained by least squares fitting of the points in the purple curve is shown to emphasize the nonlinearity of the reaction progress curve. The reversible reaction catalyzed by EntC is shown below.

involving LDH. For selection and growth of transformed cells (described below), pET-28 derivatives were selected with 50 μg/ml kanamycin. Commonly utilized protein and molecular biological reagents and protocols were prepared/performed as in *Current Protocols in Molecular Biology* [295]. 96-well microtiter plates were used for all spectrophotometric assays, and absorbances were measured by a Spectramax Plus microplate spectrophotometer (Molecular Devices) that had been preheated to 30 °C. An extinction coefficient for NADH of 6220 M^{-1} cm^{-1} at 340 nm was used for conversion of these values to units of μM/min [55].

Expression and Purification of Recombinant Eco EntC

The construct pIC5-1 was derived from the *E. coli* EntC coding region of pJLT5053 [55], and subcloned by Isabel Chon into the pET-28a vector (Novagen) in register with an amino-terminal His_6-tag. Crude cell extracts prepared from a 500 ml culture of *E. coli* Rosetta2 (DE3) cells (Novagen) transformed with pIC5-1 were grown in LB media containing 50 μg/ml kanamycin and 30 μg/ml chloramphenicol. Cultures were grown at 37 °C to mid-log phase, 1 mM IPTG was added to induce His_6-EntC synthesis, cells were harvested after 4 hours (~3.99 g wet weight) and stored overnight at –20 °C. Cells were resuspended in 10 ml BugBuster Master Mix (Novagen) containing 100 μM leupeptin, 500 μM PMSF, 2 mM $MgCl_2$, and 5 μM Tris(hydroxypropyl)phosphine (THP). This suspension was gently agitated for 30 minutes at room temperature in order to allow for complete lysis, and then centrifuged at 12000 × *g* for 40 minutes. After isolating the supernatant from the pellet, it was mixed with 2.5 ml of pre-rinsed 50% Ni^{2+}-NTA His-Bind Resin (Novagen) and gently agitated for one hour on a rotary spinner at 4 °C. The mixture was then loaded into a column and flow-through was collected. After washing the column two times each with 13 ml of Ni^{2+}-NTA Wash Buffer (50 mM sodium phosphate buffer, pH 8.0, 300 mM sodium chloride, 20 mM imidazole), His_6-EntC was eluted with 13 ml of Ni^{2+}-NTA Elution Buffer (50 mM sodium phosphate buffer, pH 8.0, 300 mM sodium chloride, 250 mM imidazole). The protein was collected in 1.0 ml portions. Fractions were analyzed by SDS-PAGE, and those containing His_6-EntC were dialyzed overnight into 100 mM Tris, pH 7.7, containing 10% glycerol, 2 mM $MgCl_2$, and 1.0 mM DTT. The protein was aliquoted and stored at –80 °C.

Expression and Purification of Recombinant Pae PchB

The construct pSM147-1 was derived from the *P. aeruginosa* PchB coding region from pME3368 [90], and cloned into pBAD33 [374]. After being subcloned by Dr. Sharon Marr into the pET-28a vector (Novagen), the construct contained an amino-terminal His_6-tag and 135 nucleotides of the PchA coding region downstream of the PchB stop codon.

This procedure was adapted from Ni^{2+}-NTA His-Bind Resin Technical Bulletin (Novagen). *E. coli* Rosetta2 (DE3) cells (Novagen) were transformed with pSM147-1. Crude cell extracts were prepared from a 2 L culture in TB media containing 0.2% glucose, 50 μg/ml kanamycin and 30 μg/ml chloramphenicol. The culture was grown at 37 °C with shaking until an OD_{600} of 0.594 was reached, at which point IPTG was added to a final concentration of 1.0 mM to induce His_6-PchB synthesis. Cells were harvested after shaking for 4 hours at 37 °C (24.34 g wet weight) and stored overnight at –20 °C. After thawing on ice, cells were resuspended in 125 ml of ice-cold Ni^{2+}-NTA Binding Buffer (50 mM sodium phosphate buffer, pH 8.0, 300 mM sodium chloride, 10 mM imidazole) containing 2 mM PMSF, 5 μM leupeptin and 10 μg/ml DNase. All subsequent operations were carried out at 4 °C. The cells were lysed by two passages through a French press at 18000 psi at the orifice. The lysate was centrifuged at

12500 × *g* for 40 minutes, and the supernatant was separated. Supernatant (~135 ml) was mixed with 30 ml of pre-rinsed 50% Ni^{2+}-NTA His-Bind Resin (Novagen) and agitated for 21 hours on a rotary spinner. The mixture was then loaded into a column and flow-through was collected. After washing column two times each with 120 ml of Ni^{2+}-NTA Wash Buffer, His_6-PchB was eluted with 40 ml of Ni^{2+}-NTA Elution Buffer. Protein was collected in 1.0 ml portions. Fractions were analyzed by SDS-PAGE, and those containing His_6-PchB (40 ml) were pooled and concentrated using an Amicon Ultra-15 (10 kDa MWCO) ultrafiltration device (Millipore) to a final volume of 12 ml. This solution was dialyzed overnight into 100 mM Tris, pH 7.7, containing 10% glycerol and 1.0 mM DTT. The protein was aliquoted and stored at –80 °C.

Determination of Protein Concentration

Protein concentrations were determined by the method of Bradford, modified as described in *Current Protocols in Molecular Biology* [295].

Isochorismate Synthase Activity Assay

The HPLC isochorismate synthase activity assay was performed using purified EntC as described in Chapter 2. The reaction was performed in duplicate in total volumes of 1.0 ml using a working concentration of 3.27 μg/ml EntC, and 50 μl aliquots were removed at 0, 2, 4, 6, 8, 10, and 12 minutes and submitted to the HPLC protocol for isochorismate determination described in Chapter 2. The working concentrations of all other substrates and reagents were the same as described in Chapter 2. Isochorismate absorbance at 280 nm was converted to units of concentration by using a value for the extinction coefficient of 8.3 mM^{-1} cm^{-1} [299].

Coupled Discontinuous HPLC Assay for ICS Activity

The coupled discontinuous HPLC ICS activity assay described in Chapter 2 was modified in order to examine the dependence of SA production on time and on PchB concentration. EntC was substituted for AtICS1, and the following modifications were made. Assays were run with working concentrations of 3.27 μg/ml recombinant EntC, 500 μM chorismate, and either 32.0 μg/ml or 4.0 μg/ml recombinant PchB in a buffer of 100 mM potassium phosphate buffer, pH 7.0, 15 mM $MgCl_2$, 10% glycerol and 1 mM DTT. The reaction was always initiated by addition of chorismate, and each reaction was incubated for a variable amount of time at 30 °C. Each reaction was performed in duplicate in total volumes of 1.0 ml, and 50 μl aliquots were removed at 0, 5, 10, 15, and 20 minutes and submitted to the HPLC protocol for SA determination described in Chapter 2.

LDH Activity in Various Media

An endpoint spectrophotometric assay for lactic dehydrogenase activity was performed as described below. The extent of LDH reaction was measured by mixing variable amounts of sodium pyruvate with a defined concentration of NADH and LDH, and then observing how much NADH disappears as pyruvate is converted to lactate. Concentrations of LDH and NADH used were consistent with those from previous assays [55, 299]. All assay volumes were 200 μl per well, and contained working concentrations of 0.2 mM NADH and 0.833 μg/ml LDH. The buffer used was 100 mM Tris, pH 7.7, with or without 10% glycerol, 10 mM $MgCl_2$, and 1 mM DTT in addition. The reaction was initiated by addition of pyruvate to the reaction mixture, and the change in absorbance at 340 nm was measured after incubating for 5 minutes at 30 °C. Distilled water was used as a cuvette reference.

Coupled Continuous Spectrophotometric Assay for ICS Activity

A reaction buffer composed of 100 mM Tris, pH 7.7, 10% glycerol, 10 mM $MgCl_2$, and 1 mM DTT was used for all assays. A master mix of all common enzymes and coenzymes was prepared by mixing 20 µl per well of 10× solutions of each reaction component (save chorismate) with 100 µl per well of reaction buffer. 180 µl per well of this mixture was distributed in the 96-well plate, and the plate was preheated in the spectrophotometer at 30 °C for 5 minutes. The reaction was then initiated by addition of 20 µl per well of 10× chorismate solution, and the change in absorbance at 340 nm was measured in each well in increments of 60 seconds and monitored for 60 minutes total. Each 200 µl (per well) reaction assay volume contained final working concentrations of 0.2 mM NADH, 0.833 µg/ml LDH, 32.0 µg/ml His_6-PchB, and 2 mM chorismic acid in reaction buffer. Controls were performed that were missing one of each of the preceding components. The following working concentrations of His_6-EntC were employed: 6.0 µg/ml, 4.0 µg/ml, 2.67 µg/ml, 1.78 µg/ml, 1.19 µg/ml, 0.79 µg/ml, 0.52 µg/ml, and 0 µg/ml. Each of these reactions was performed in triplicate. The initial reaction rate in each well was assessed for a period of 1000 seconds, beginning approximately 1000 seconds after initiation of the reaction. That the reaction rate was linear in this range was confirmed manually for every reaction (there are up to 96 reactions per microtiter plate), and each rate was calculated using least squares fitting of the curve from the corresponding well. Velocity was linear with time (following an initial lag) for >15 min at all concentrations of His_6-EntC.

Coupled Continuous Spectrophotometric Assay of AtICS1 Activity Using Various PchB Concentrations

The coupled continuous spectrophotometric assay was performed using AtICS1 in place of His_6-EntC, using the conditions described in Chapter 2, but with the following modifications. Three different working concentrations of PchB were used (96.0 µg/ml, 32.0 µg/ml, and 9.6 µg/ml), and for each of these, 4 different working concentrations of AtICS1 were used (10.0 µg/ml, 4.0 µg/ml, 1.0 µg/ml, and 0 µg/ml). All reactions were performed in duplicate. The initial reaction rate in each well was assessed for a period of 500 seconds, beginning approximately 350 seconds after initiation of the reaction, and each rate was calculated using least squares fitting of the curve from the corresponding well.

Revision of the Chorismate Levels Present in the ICS Coupled Assay

To determine the effective chorismate concentrations of the coupled continuous spectrophotometric ICS assay, I assessed the non-productive conversion of chorismate to prephenate by PchB in parallel. As modified from [298], each 200 µl standard coupled reaction volume (including AtICS1) in the 96-well plate was treated with 100 µl 1M HCl to convert prephenate to phenylpyruvate after the reaction had progressed for 0, 5, 10, 15, or 20 minutes. Each individual reaction was transferred separately to an Eppendorf tube and heated at 37 °C for 10 minutes. After cooling, 700 µl 2.5 M NaOH was added to each tube and the contents were mixed thoroughly. A 200 µl aliquot of each tube was then added to a new 96-well plate, and an absorbance measurement was taken at 320 nm. Distilled water was used as a cuvette reference. Prephenate standard curves were run in parallel for quantification. Chorismate utilization via PchB was estimated as equal on a molar basis to prephenate. Each reaction was performed in triplicate.

RESULTS

The HPLC ICS activity assay does not give a linear reaction progress curve. His_6-EntC, an ICS enzyme from *E. coli*, was overexpressed and purified as described above (Figure A2.1). Further analysis of fraction 2 from this purification showed that EntC was present at a high concentration (3.98 mg/ml), and the protein was subsequently shown to have a very high specific activity (2.3 μmol/min/mg). This protein fraction was used for all the assays described hereafter that involve EntC. This protein was initially assayed by the HPLC ICS activity assay described in Chapter 2. As shown in Figure A2.2, the rate of isochorismate production by EntC is never found to be constant, even in the earliest phases of the reaction. A line obtained by least squares fitting of all the points is shown in black. It serves to emphasize the non-linearity of the reaction progress curve using this assay.

The EntC-PchB coupled reaction produces salicylate at a linear rate when a high concentration of PchB is used. His_6-PchB, an IPL enzyme from *P. aeruginosa*, was overexpressed and purified as described above (Figure A2.3). Further analysis of fraction 4 from this purification showed that PchB was present at a very high concentration (9.53 mg/ml). This protein fraction was used for all the assays described hereafter that involve PchB. The coupled discontinuous HPLC assay for ICS activity from Chapter 2 was employed using EntC in place of AtICS1. This reaction progress curve (Figure A2.4), unlike that of the uncoupled reaction, was now found to be linear when a working concentration of 32.0 μg/ml of PchB is used. When a working concentration of 4.0 μg/ml of PchB was used instead, there is considerably more variation in each time point, and the reaction progress curve in no longer linear. At 32.0 μg/ml of PchB, the variation at each time point is relatively low. Both reactions were performed in duplicate.

LDH activity is not affected by the medium used in the coupled HPLC assay. The reaction of NADH and pyruvate catalyzed by LDH was examined using two different media (Figure A2.5). An endpoint assay was employed to detect the amount of NADH converted to NAD^+. Various concentrations of pyruvate in the presence of excess NADH were wholly converted to lactate within 5 minutes, as evidenced by a loss of absorbance at 340 nm corresponding to the amount of NADH that had disappeared. One such reaction was performed in 100 mM Tris, pH 7.7, and the other using the same buffer, but also including 10% glycerol, 10 mM $MgCl_2$, and 1 mM DTT. The curves have nearly identical slopes and intercepts, indicating that the enzyme performs normally in the presence of these additives. This experiment was repeated, and identical results were obtained (not shown).

A coupled continuous spectrophotometric assay for ICS activity incorporating PchB and LDH shows reactivity for EntC that is proportional to its concentration. A coupled continuous assay for ICS activity was performed using EntC as the primary enzyme, PchB as a secondary enzyme, and LDH as a tertiary enzyme; a reaction schematic is shown in Figures A2.6 and A2.7. The reaction buffer (100 mM Tris, pH 7.7) for all reactions contained 10% glycerol and 1 mM DTT for enzyme stability, excess $MgCl_2$ (10 mM) for maximal ICS enzyme activity, excess NADH (0.2 mM) for maximal LDH activity, and excess His_6-PchB (32.0 μg/ml) and LDH (0.833 μg/ml) to ensure that the secondary and tertiary reactions do not limit the rate of the

His-PchB Ni^{2+}-NTA Affinity Column Purification

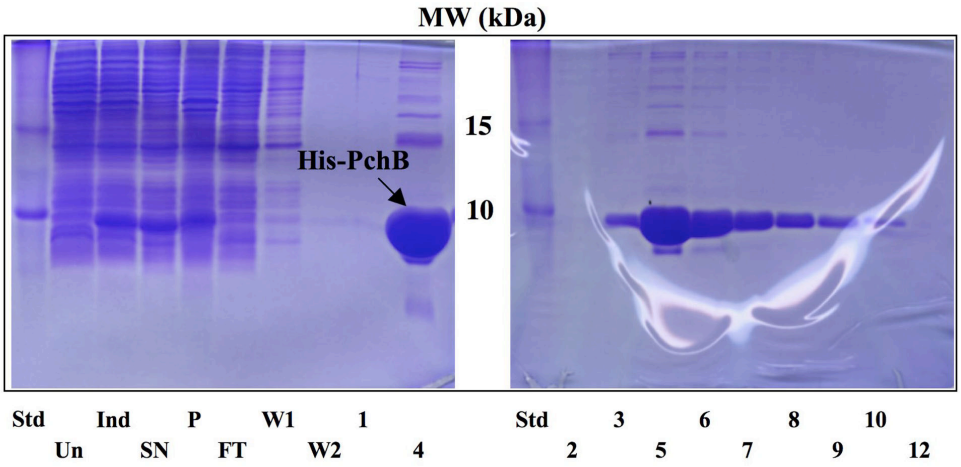

Fraction	2	3	4	5	6	7
Protein (mg/ml)	0	0.13	9.53	3.20	1.39	0.26

Figure A2.3. SDS-PAGE on Ni^{2+}-NTA Affinity Column Fractions from the Purification of His-PchB. Proteins were separated on a 10% SDS-PAGE gel and stained with Coomassie blue. Abbreviations used are: Std, Novagen Trail Mix protein standards, molecular masses in kDa are indicated in the center between gels; Un, Uninduced *E. coli* total protein; Ind, IPTG-induced *E. coli* total protein; SN, Supernatant (crude extract) from lysed induced cells; P, Pellet from lysed induced cells; FT, Flow-through from column loading; W, Wash fractions; Numbers are elution fractions.

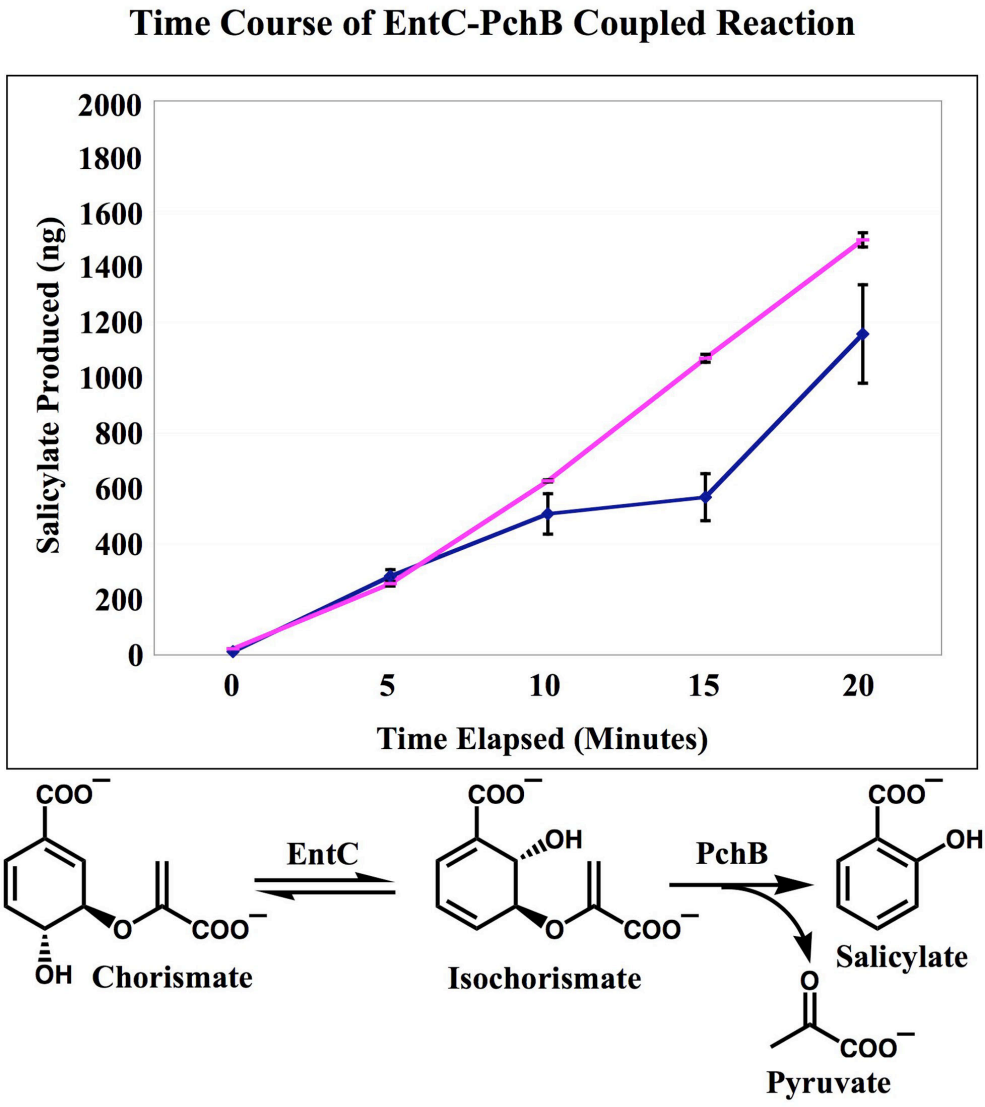

Figure A2.4. Early Reaction Progress Curve for EntC-PchB Coupled Reaction. Aliquots of coupled EntC-PchB reactions were removed every five minutes, and salicylate content was determined by HPLC. Two different reactions were performed, each in duplicate: one with 4.0 μg/ml PchB secondary enzyme (blue curve) and the other with 32.0 μg/ml PchB secondary enzyme (purple curve). The coupled reaction catalyzed by EntC and PchB is shown below.

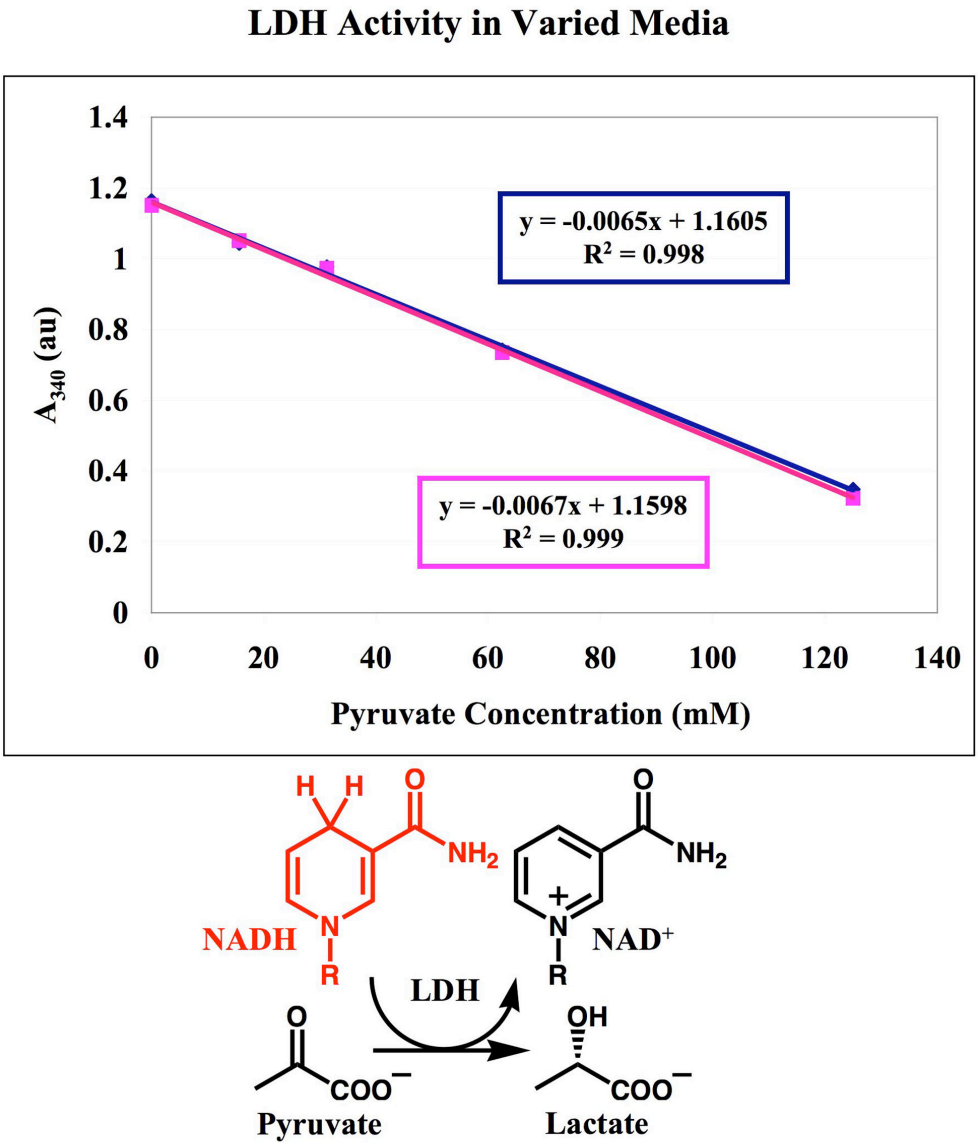

Figure A2.5. Effect of Additives on LDH Activity. Various working concentrations of substrate pyruvate were used in endpoint assays of LDH activity. After 5 minutes of reaction time, absorbance at 340 nm was measured to quantify NADH content. One series of reactions was performed in 100 mM Tris buffer, pH 7.7 (curve in blue), and the other in 100 mM Tris buffer, pH 7.7, 10% glycerol, 10 mM $MgCl_2$, and 1 mM DTT (curve in purple). Excess NADH was used for both sets of reactions. The line equation and coefficient of determination is shown for each curve. The reaction catalyzed by LDH is shown below - NADH is highlighted in red to indicate its UV activity (A_{340}). Abbreviations used are: LDH, Lactate dehydrogenase; Tris, Tris(hydroxymethyl)-aminomethane; DTT, Dithiothreitol.

overall reaction. Various amounts of His_6-EntC were used to determine an optimal working concentration of EntC for the coupled continuous assay. Every reaction was initiated by addition of enough chorismate solution to effect a final working concentration of 2 mM, an amount far in excess of that required for saturation of EntC (K_M = 14 μM for chorismate; see [55]). The assay was conducted in 96-well microtiter plates incubated at a constant temperature of 30 °C for 60 minutes, and the change in absorbance at 340 nm was measured at intervals of 60 seconds to quantify NADH disappearance. A value for the initial rate reaction was determined for each well of the plate by obtaining a least squares fit of the reaction progress curve (a typical example is shown in Figure A2.6), and converting this value to units of μM of NADH reacted per minute using the extinction coefficient of NADH (6220 M^{-1} cm^{-1}; see [55]). The linear nature of the graph indicates proportionality between reaction velocity and enzyme concentration, and suggests that substrate chorismate is saturating EntC. After analysis of the calculated initial velocities at various concentrations of EntC (shown in Figure A2.7), a working concentration of 3.0 μg/ml of His_6-EntC was selected as optimal for operation in the linear range of activity of this coupled continuous assay. As expected, wells missing the reaction components chorismate, LDH, His_6-PchB (all shown in Figure A2.7), or NADH (not shown) have no detectable reactivity. Importantly, the average initial velocity of several control reactions containing no ICS enzyme (which is generally low, but non-zero) must be subtracted from any initial velocity determined for an ICS enzyme in order to obtain an accurate value for initial velocity by this assay.

Intermediate Levels of PchB Give Maximal Activity in the Coupled Continuous Spectrophotometric Assay of AtICS1 Activity. To ensure that maximal velocities were being achieved in the coupled continuous ICS assay, PchB and AtICS1 levels were varied. As expected, ICS activity was roughly proportional to AtICS1 levels regardless of the PchB concentration used (Figure A2.8). However, this was not true for PchB. Though an intermediate concentration of PchB (32.0 μg/ml) gave greater velocities than a relatively low one (9.6 μg/ml) – indicating that PchB is not sufficiently in excess at the lower level – even higher levels of PchB (96.0 μg/ml) gave the lowest velocities of all. PchB has chorismate mutase activity in addition to its isochorismate pyruvate lyase activity [298], and very high PchB levels apparently lower the rate of the ICS reaction by limiting chorismate supply through prephenate production (Figure A2.8). All subsequent coupled continuous ICS assays employed PchB in intermediate concentrations (32.0 μg/ml) that maximize assay velocity.

Effective Chorismate Levels are Determined for K_M Experiments on ICS Enzymes. The previous experiment (see above and Figure A2.8) showed that a large excess of PchB diminishes ICS activity due to its secondary chorismate mutase activity – PchB is responsible for removing chorismate from solution, thus establishing less-than-saturating chorismate levels. The chorismate mutase activity of PchB is expected to be a significant problem as well during ICS enzyme K_M determination for chorismate, as the intermediate levels (32.0 μg/ml) of PchB required by the coupled continuous assay for ICS activity will establish lower effective levels of chorismate in solution. As a result of this, the coupled continuous assay for ICS activity will tend to overestimate the value of the K_M for chorismate (give a significantly higher K_M value than is accurate). To determine an accurate value for the K_M for chorismate of AtICS1, I obtained a value for the effective concentration of chorismate at every data point obtained in the K_M study and used it in place of each value for initial chorismate concentration. The amount of

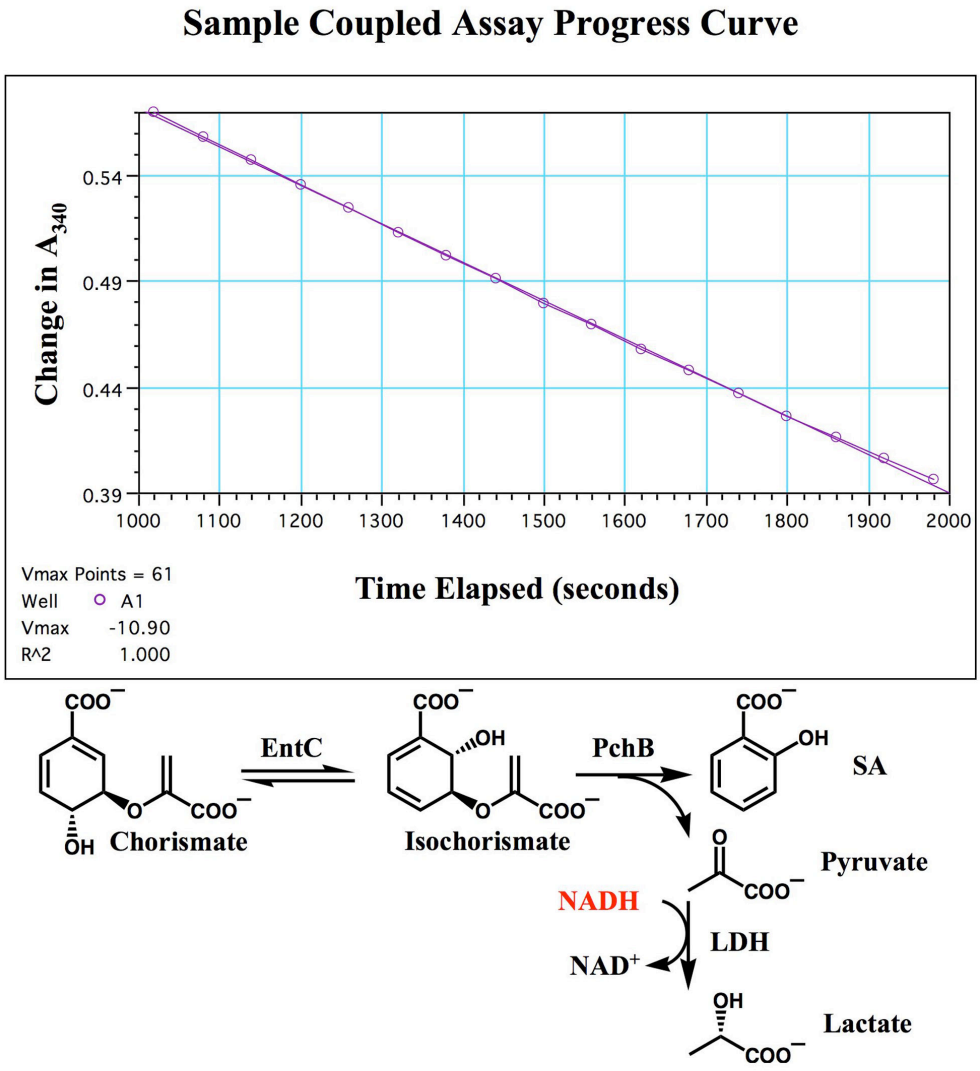

Figure A2.6. Sample of a Reaction Progress Curve From the Coupled Continuous ICS Assay. The change in absorbance (340 nm) over time of a sample coupled reaction is shown for a single well of the 96-well plate. A time period of reaction is manually selected, and a value for the rate of change of absorbance (absorbance units per second) is automatically calculated by least squares fitting. This value (called V_{max} above) must be converted to units of μM/min to properly describe the rate of formation of isochorismate by an ICS enzyme. A schematic of the overall coupled reaction is shown below, with NADH highlighted in red to indicate that its UV activity (A_{340}) is the feature of the reaction being observed. Abbreviations used are: LDH, Lactate dehydrogenase; ICS, Isochorismate synthase; SA, Salicylic acid.

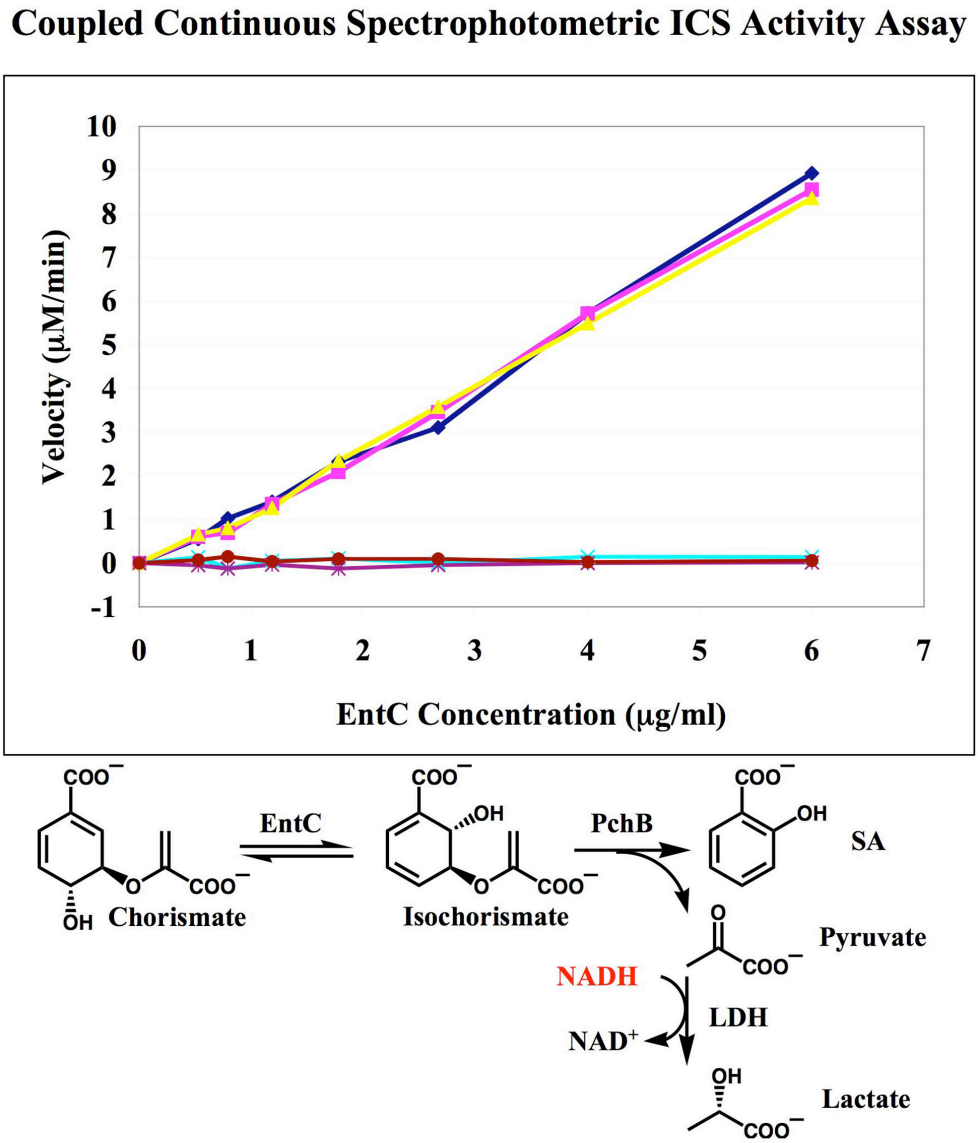

Figure A2.7. Initial Velocities of the Coupled Continuous ICS Assay Determined For Various Concentrations of EntC. Values for initial velocity of EntC were determined at different concentrations of the ICS enzyme. The reaction was performed in triplicate (blue diamonds, purple squares, and yellow triangles) with identical results. Control reactions with no PchB (red circles), LDH (light blue crosses), and chorismate (purple crosses) are shown to have no ICS activity at any EntC concentration. A schematic of the overall coupled reaction is shown below, with NADH highlighted in red to indicate that its UV activity (A_{340}) is the feature of the reaction being observed. Abbreviations used are: LDH, Lactate dehydrogenase; ICS, Isochorismate synthase; SA, Salicylic acid.

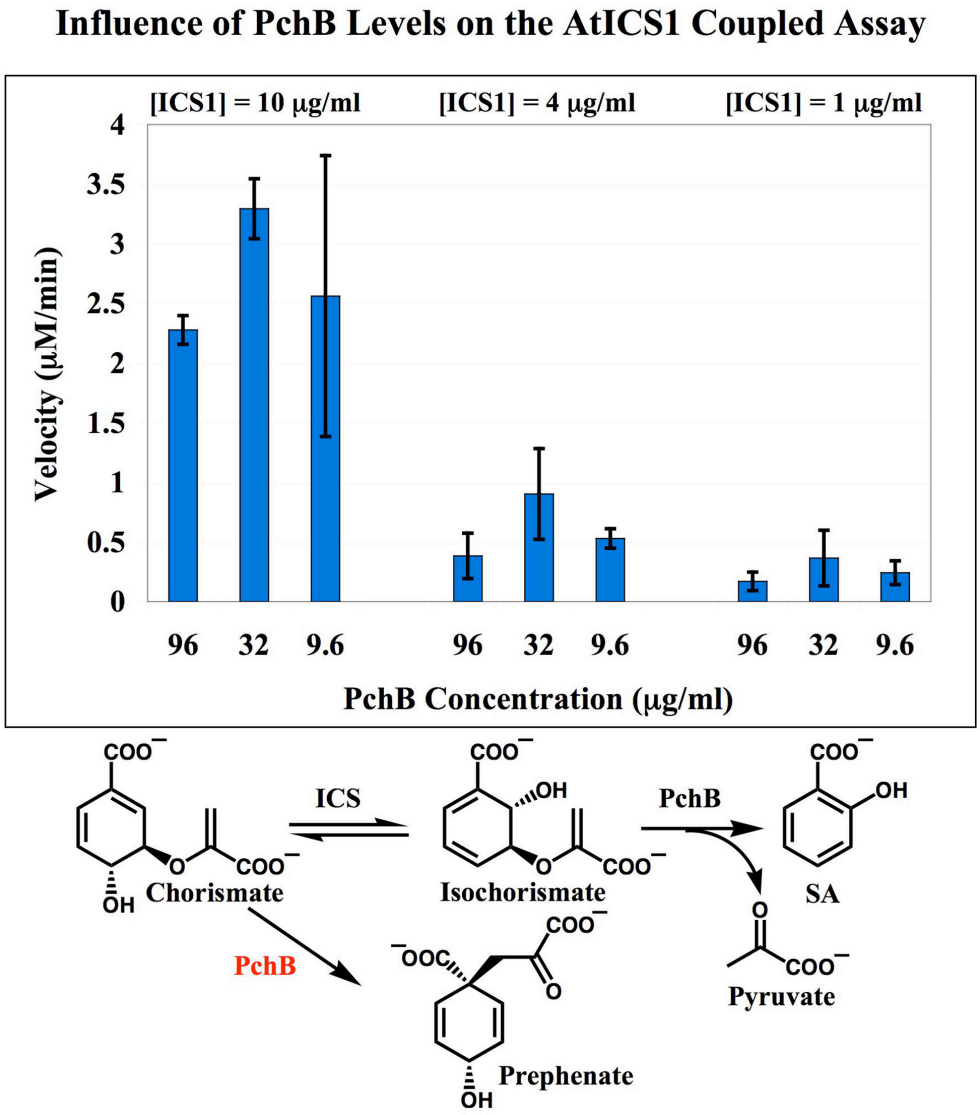

Figure A2.8. Influence of PchB Levels on the Velocity of the ICS Coupled Continuous Assay. Values for initial velocity of AtICS1 were determined for three different concentrations of enzyme (specified atop graph). For each unique AtICS1 concentration, the PchB level was varied (specified on x-axis of graph). All reactions were performed in duplicate. A schematic of the reactions catalyzed by PchB is shown below, with the chorismate mutase reactivity relevant at high PchB concentrations highlighted in red. Abbreviations used are: ICS, Isochorismate synthase; SA, Salicylic acid.

chorismate lost was assumed to be equivalent to the amount of prephenate formed by PchB, so prephenate content was determined at each initial chorismate concentration after a series of elapsed times (Figure A2.9). This was done by adding concentrated HCl to each well at the appropriate time point and then heating at 37 °C to convert all prephenate to phenylpyruvate (see schematic in Figure A2.9). Phenylpyruvate is a stable compound that is easily quantified by obtaining an absorbance reading at 320 nm and converting to units of concentration using the appropriate extinction coefficient (ε_{320} = 17,500 cm^{-1} M^{-1}; see [298]). Importantly, this assay showed that a significant amount of the chorismate (as much as 17%) has spontaneously rearranged to prephenate in a freshly prepared solution even before exposure to PchB (dark blue line in Figure A2.9), suggesting that prephenate is present already in the commercially available chorismate used for all the assays in this thesis. After 20 minutes of exposure to AtICS1 without PchB present, only slightly more prephenate has formed (dark blue line in Figure A2.9), indicating that uncatalyzed prephenate formation is a problem of only moderate significance in this assay. After 20 minutes of exposure to PchB without AtICS1 present, levels of prephenate formed are similar to those found when AtICS1 is present (brown line and light blue line, respectively, in Figure A2.9), suggesting that prephenate is formed by PchB at a similar rate regardless of whether ICS is present or not. The various curves in Figure A2.9 show increasingly higher levels of prephenate being formed as time has elapsed; however, the 10 minute, 15 minute, and 20 minute curves all show similar amounts of prephenate formed for each initial chorismate concentration. As the ICS enzyme is still actively catalyzing the production of isochorismate at these time points, this suggests that the active site of PchB is incompletely saturated with isochorismate before 10 minutes have elapsed. A typical measurement of ICS reactivity using the coupled assay involves analysis of the reaction progress curve beginning after 1000 seconds (16.7 minutes) have elapsed (see Figure A2.6). PchB is clearly saturated with isochorismate after 20 minutes have elapsed, and this time point was selected as a reasonable one to use to calculate effective chorismate concentrations (Figure A2.10). Each value for chorismate lost to prephenate production under the conditions of the assay after 20 minutes (see Figure A2.9) was subtracted from its corresponding value for initial chorismate concentration, and the results are shown in Figure A2.10. A similar analysis is performed for all determinations of the K_M for chorismate in this thesis, and values for effective chorismate concentration are used in place of those for initial chorismate concentration (y-axis values in place of x-axis values of the red curve in Figure A2.10) in each final calculation of kinetic constants.

DISCUSSION

The non-linearity of the ICS reaction progress curve is a phenomenon that has been ignored in the determinations of many of the kinetic constants of ICS enzymes. The central assumption of steady-state kinetics is that all reactive intermediates do not experience a change in concentration over the period of time analyzed, and this condition must be met for linearity to be achieved by a reaction progress curve. Removal of isochorismate from solution – by PchB-catalyzed conversion to SA – immediately after its formation ensures that only the rate of the forward reaction catalyzed by ICS is being measured. Addition of excess PchB (~2.78 μM) to a modest amount of EntC (~0.076 μM) effectively converted the nonlinear reaction progress curve for isochorismate production by EntC (Figure A2.2) to a highly linear curve for SA production

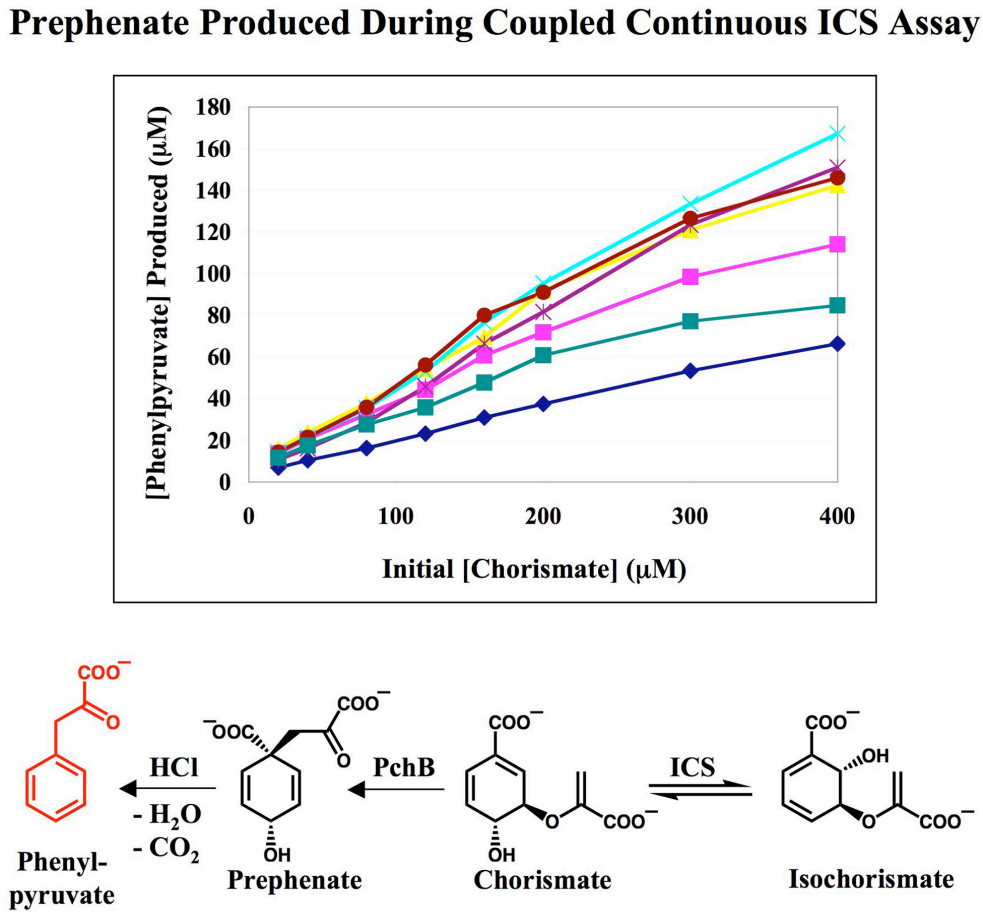

Figure A2.9. Determination of the Prephenate Produced in the Coupled Continuous ICS Assay. The graph shows the concentration of prephenate - measured as phenylpyruvate produced - for every value of initial chorismate concentration used in the determination of ICS kinetic constants. Each curve indicates the various levels of prephenate formed after a given time had elapsed: dark blue diamonds, 0 minutes; light purple squares, 5 minutes; yellow triangles, 10 minutes; dark purple crosses, 15 minutes; light blue crosses, 20 minutes; brown circles, 20 minutes with no ICS; dark green squares, 20 minutes with no PchB. Error bars were omitted for clarity. The reactions relevant to this experiment are shown in the schematic below, with only the chorismate mutase activity of PchB considered - phenylpyruvate is highlighted in red to indicate its UV activity (A_{320}). Abbreviation used is: ICS, Isochorismate synthase.

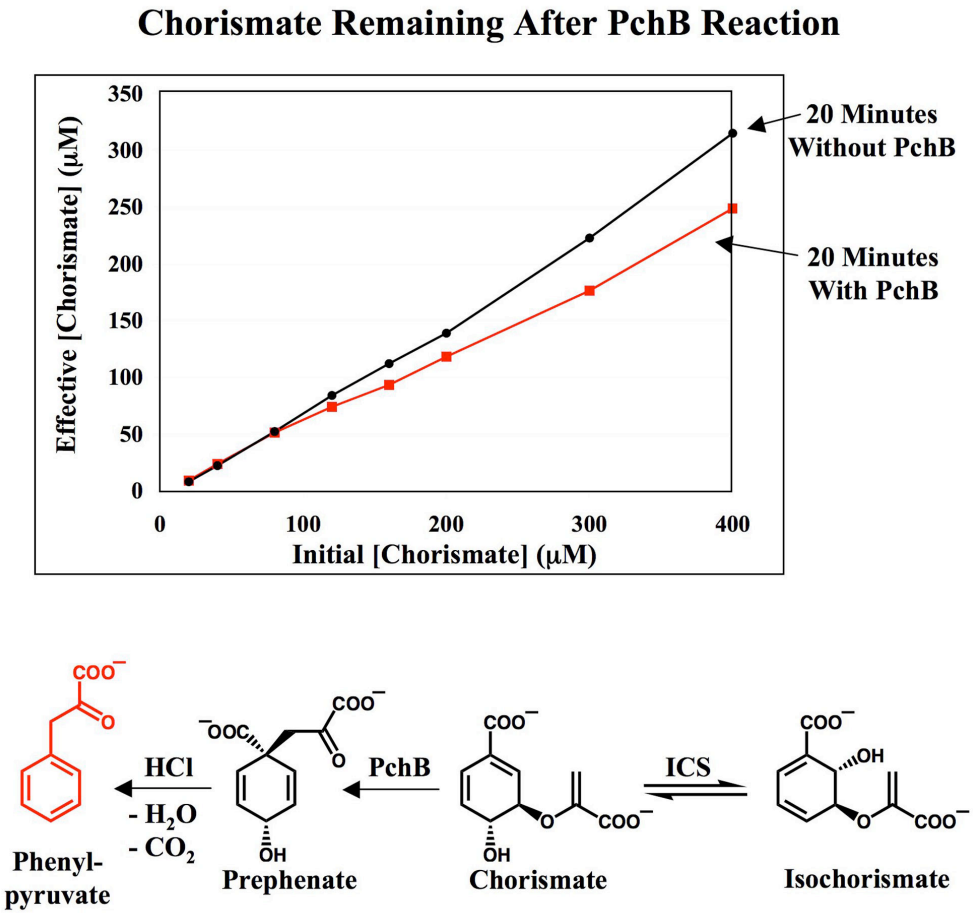

Figure A2.10. Revision of the Chorismate Levels Present in the Coupled Continuous ICS Assay. The graph shows the effective chorismate concentrations calculated for each initial chorismate concentration after 20 minutes of elapsed time, both with and without PchB present. Error bars were omitted for clarity. The reactions relevant to this experiment are shown in the schematic below, specifying only the chorismate mutase activity of PchB - phenylpyruvate is highlighted in red to indicate its UV activity (A_{320}). Abbreviation used is: ICS, Isochorismate synthase.

by EntC and PchB (Figure A2.4). The coupling of excess PchB with any ICS enzyme should be sufficient to allow for the performance of accurate steady-state kinetics.

However, the coupled reaction catalyzed by EntC and PchB suffers from the significant drawback that it is discontinuous, as aliquots must be removed periodically for analysis. It is time-consuming to individually acquire the data for each time point of the reaction progress curve, the manipulation of the sample for HPLC analysis necessarily introduces error to the data, and the large reaction volumes required to generate numerous data points necessitate the use of a wasteful amount of each reaction component. I sought a process that could be coupled to the EntC/PchB reaction that would enable continuous real-time acquisition of data. The enzyme LDH, which catalyzes the NADH-mediated reduction of pyruvate to lactate, was shown to operate normally under the conditions of the coupled EntC/PchB assay (Figure A2.5). The addition of LDH (~0.0060 μM) and excess NADH (0.2 mM) to the EntC/PchB reaction already developed allowed for the instantaneous acquisition of many time points for every microtiter plate well (Figure A2.6). Though each individual continuous coupled reaction was performed on a much smaller scale than each discontinuous coupled reaction, the ability of the former to acquire 100 or more data points per reaction, coupled with the presence of 96 wells per plate, make it possible for the continuous assay to, in a single hour, acquire up to 10,000 times more data than the discontinuous assay could.

The unfortunate chorismate mutase activity of the PchB secondary enzyme adds a complication to this assay. High concentrations of PchB lower the velocity of the coupled continuous ICS assay by removing substrate chorismate. Though using more modest concentrations of PchB gives maximal values for ICS activity at high saturating substrate concentrations (Figure A2.8), K_M determinations require the use of many low substrate concentrations. The K_M for chorismate of PchB is 150 μM [298], and at chorismate concentrations near to or above this, conversion of chorismate to prephenate by PchB significantly alters the effective chorismate concentration (Figure A2.10). Under the conditions of this assay, PchB has a k_{cat}/K_M for chorismate of 0.052 μM^{-1} min^{-1} [298] and is present at a concentration of ~2.78 μM, and AtICS1 has a k_{cat}/K_M for chorismate of 0.933 μM^{-1} min^{-1} and is present at a concentration of ~0.168 μM. These values suggest that at low substrate concentrations these enzymes will compete effectively with each other for substrate chorismate (the PchB value for $[E_t] \times k_{cat}/K_M$ is 0.145 min^{-1} and the AtICS1 value for $[E_t] \times k_{cat}/K_M$ is 0.157 min^{-1}, though this is technically only relevant when $[S] << K_M$). The non-enzymatic conversion of chorismate to prephenate alters the effective chorismate concentration to almost the same degree as the conversion due to PchB does (see Figure A2.10), and this appears to be due to the fact that the commercial preparation of chorismate used was as much as 17% prephenate (Figure A2.9). These factors both make the calculation of effective chorismate concentration by the method outlined above necessary for complete accuracy in the determination of ICS enzyme kinetic constants. The problem of chorismate depletion in this coupled continuous ICS assay can be overcome by using a secondary enzyme that generates pyruvate from isochorismate without binding to chorismate (like EntB, see Figure 1.10), and by laboratory preparation of chorismate – via biosynthesis from shikimate (see Figure 1.6) – that is much purer than that which is commercially available.

BIBLIOGRAPHY

1. Farnsworth, N.R. and R.W. Morris, *Higher plants--the sleeping giant of drug development*. Am J Pharm Sci Support Public Health, 1976. **148**(2): p. 46-52.
2. Schmidt, B.M., et al., *Revisiting the ancient concept of botanical therapeutics*. Nature Chemical Biology, 2007. **3**(7): p. 360-366.
3. Newman, D.J. and G.M. Cragg, *Natural products as sources of new drugs over the last 25 years*. Journal of Natural Products, 2007. **70**(3): p. 461-477.
4. Farnsworth, N.R., et al., *Medicinal Plants in Therapy*. Bulletin of the World Health Organization, 1985. **63**(6): p. 965-982.
5. Kinghorn, A.D., *Pharmacognosy in the 21st century*. Journal of Pharmacy and Pharmacology, 2001. **53**(2): p. 135-148.
6. Macías, F.A., *Allelopathy : chemistry and mode of action of allelochemicals*. 2004, Boca Raton, Fla.: CRC Press. 372 p.
7. Buchanan, B.B., W. Gruissem, and R.L. Jones, *Biochemistry & molecular biology of plants*. 2000, Rockville, Md.: American Society of Plant Physiologists. xxxix, 1367 p.
8. Lichtenthaler, H.K., *The 1-Deoxy-D-Xylulose-5-Phosphate Pathway of Isoprenoid Biosynthesis in Plants*. Annu Rev Plant Physiol Plant Mol Biol, 1999. **50**: p. 47-65.
9. Dewick, P.M., *Medicinal natural products : a biosynthetic approach*. 2nd ed. 2002, Chichester, West Sussex, England ; New York, NY, USA: John Wiley & Sons. xii, 507 p.
10. Taiz, L. and E. Zeiger, *Plant physiology*. 4th ed. 2006, Sunderland, Mass.: Sinauer Associates. xxvi, 764 p.
11. Karban, R. and I.T. Baldwin, *Induced responses to herbivory*. Interspecific interactions. 1997, Chicago: University of Chicago Press. ix, 319 p.
12. Arimura, G., et al., *Herbivory-induced volatiles elicit defence genes in lima bean leaves*. Nature, 2000. **406**(6795): p. 512-515.
13. Rosenthal, G.A. and M. Berenbaum, *Herbivores, their interactions with secondary plant metabolites*. 2nd ed. 1991, San Diego: Academic Press.
14. Seigler, D.S., *Plant secondary metabolism*. 1998, Boston: Kluwer Academic. ix, 759 p.
15. Glawischnig, E., et al., *Camalexin is synthesized from indole-3-acetaidoxime, a key branching point between primary and secondary metabolism in Arabidopsis*. Proceedings of the National Academy of Sciences of the United States of America, 2004. **101**(21): p. 8245-8250.
16. Glawischnig, E., *The role of cytochrome P450 enzymes in the biosynthesis of camalexin*. Biochem Soc Trans, 2006. **34**(Pt 6): p. 1206-8.
17. Poulton, J.E., *Cyanogenesis in Plants*. Plant Physiology, 1990. **94**(2): p. 401-405.
18. Kombrink, E. and I. Somssich, *Defense Responses of Plants to Pathogens*. Advances in Botanical Research, 1995. **21**: p. 1-34.
19. Bones, A.M. and J.T. Rossiter, *The myrosinase-glucosinolate system, its organisation and biochemistry*. Physiologia Plantarum, 1996. **97**(1): p. 194-208.
20. Austin, M.B. and A.J.P. Noel, *The chalcone synthase superfamily of type III polyketide synthases*. Natural Product Reports, 2003. **20**(1): p. 79-110.
21. Arnason, J.T., et al., *Psilotin, an Insect Feeding Deterrent and Growth Reducer from Psilotum-Nudum*. Biochemical Systematics and Ecology, 1986. **14**(3): p. 287-289.

22. Haberlein, H., G. Boonen, and M.A. Beck, *Piper methysticum: Enantiomeric separation of kavapyrones by high performance liquid chromatography*. Planta Medica, 1997. **63**(1): p. 63-65.
23. Beckert, C., et al., *Styrylpyrone biosynthesis in Equisetum arvense*. Phytochemistry, 1997. **44**(2): p. 275-283.
24. Bermejo, A., et al., *Styryl-pyrones from Goniothalamus arvensis*. Phytochemistry, 1998. **47**(7): p. 1375-1380.
25. Peris, E., et al., *3-acetylaltholactone and related styryl-lactones, mitochondrial respiratory chain inhibitors*. Phytochemistry, 2000. **54**(3): p. 311-315.
26. Jang, M.S., et al., *Cancer chemopreventive activity of resveratrol, a natural product derived from grapes*. Science, 1997. **275**(5297): p. 218-220.
27. Baur, J.A. and D.A. Sinclair, *Therapeutic potential of resveratrol: the in vivo evidence*. Nature Reviews Drug Discovery, 2006. **5**(6): p. 493-506.
28. Shibuya, M., et al., *Incorporation of three deuterium atoms excludes intermediacy of stilbenecarboxylic acid in stilbene synthase reaction*. Tetrahedron Letters, 2002. **43**(29): p. 5071-5074.
29. Hain, R., et al., *Disease Resistance Results from Foreign Phytoalexin Expression in a Novel Plant*. Nature, 1993. **361**(6408): p. 153-156.
30. Harris, T.M. and C.M. Harris, *Biomimetic Syntheses of Aromatic Polyketide Metabolites*. Pure and Applied Chemistry, 1986. **58**(2): p. 283-294.
31. Austin, M.B., et al., *An aldol switch discovered in stilbene synthases mediates cyclization specificity of type III polyketide synthases*. Chemistry & Biology, 2004. **11**(9): p. 1179-1194.
32. Li, J.Y., et al., *Arabidopsis Flavonoid Mutants Are Hypersensitive to Uv-B Irradiation*. Plant Cell, 1993. **5**(2): p. 171-179.
33. Lunau, K., *A new interpretation of flower guide colouration: absorption of ultraviolet light enhances colour saturation*. Plant Systematics and Evolution, 1992. **183**(1-2): p. 51-65.
34. Davis, S.R., et al., *Phytoestrogens in health and disease*. Recent Prog Horm Res, 1999. **54**: p. 185-210; discussion 210-1.
35. Winkel-Shirley, B., *Biosynthesis of flavonoids and effects of stress*. Current Opinion in Plant Biology, 2002. **5**(3): p. 218-223.
36. Herrmann, K.M. and L.M. Weaver, *The Shikimate Pathway*. Annu Rev Plant Physiol Plant Mol Biol, 1999. **50**: p. 473-503.
37. Herrmann, K.M., *The Shikimate Pathway - Early Steps in the Biosynthesis of Aromatic-Compounds*. Plant Cell, 1995. **7**(7): p. 907-919.
38. Dosselaere, F. and J. Vanderleyden, *A metabolic node in action: chorismate-utilizing enzymes in microorganisms*. Crit Rev Microbiol, 2001. **27**(2): p. 75-131.
39. Reuters, *Glyphosate Occupies More Than 30% of the Herbicide Sales Volume All Around the World*., in *Reuters*. 2008, M2 Presswire: Dublin.
40. Walsh, C.T., et al., *Molecular Studies on Enzymes in Chorismate Metabolism and the Enterobactin Biosynthetic-Pathway*. Chemical Reviews, 1990. **90**(7): p. 1105-1129.
41. Loscher, R. and L. Heide, *Biosynthesis of p-Hydroxybenzoate from p-Coumarate and p-Coumaroyl-Coenzyme A in Cell-Free Extracts of Lithospermum erythrorhizon Cell Cultures*. Plant Physiology, 1994. **106**(1): p. 271-279.

42. Khanjin, N.A., J.P. Snyder, and F.M. Menger, *Mechanism of chorismate mutase: Contribution of conformational restriction to catalysis in the Claisen rearrangement*. Journal of the American Chemical Society, 1999. **121**(50): p. 11831-11846.
43. Holden, M.J., et al., *Chorismate lyase: kinetics and engineering for stability*. Biochimica Et Biophysica Acta-Protein Structure and Molecular Enzymology, 2002. **1594**(1): p. 160-167.
44. Wright, S.K., et al., *Isotope effects on the enzymatic and nonenzymatic reactions of chorismate*. Journal of the American Chemical Society, 2005. **127**(37): p. 12957-12964.
45. Kolappan, S., et al., *Lysine 190 is the catalytic base in MenF, the menaquinone-specific isochorismate synthase from Escherichia coli: implications for an enzyme family*. Biochemistry, 2007. **46**(4): p. 946-53.
46. Goncharoff, P. and B.P. Nichols, *Nucleotide sequence of Escherichia coli pabB indicates a common evolutionary origin of p-aminobenzoate synthetase and anthranilate synthetase*. J Bacteriol, 1984. **159**(1): p. 57-62.
47. Goncharoff, P. and B.P. Nichols, *Evolution of aminobenzoate synthases: nucleotide sequences of Salmonella typhimurium and Klebsiella aerogenes pabB*. Mol Biol Evol, 1988. **5**(5): p. 531-48.
48. Ozenberger, B.A., T.J. Brickman, and M.A. Mcintosh, *Nucleotide-Sequence of Escherichia-Coli Isochorismate Synthetase Gene Entc and Evolutionary Relationship of Isochorismate Synthetase and Other Chorismate-Utilizing Enzymes*. Journal of Bacteriology, 1989. **171**(2): p. 775-783.
49. Knochel, T., et al., *The crystal structure of anthranilate synthase from Sulfolobus solfataricus: functional implications*. Proc Natl Acad Sci U S A, 1999. **96**(17): p. 9479-84.
50. Morollo, A.A. and M.J. Eck, *Structure of the cooperative allosteric anthranilate synthase from Salmonella typhimurium*. Nat Struct Biol, 2001. **8**(3): p. 243-7.
51. Spraggon, G., et al., *The structures of anthranilate synthase of Serratia marcescens crystallized in the presence of (i) its substrates, chorismate and glutamine, and a product, glutamate, and (ii) its end-product inhibitor, L-tryptophan*. Proc Natl Acad Sci U S A, 2001. **98**(11): p. 6021-6.
52. Parsons, J.F., et al., *Structure of Escherichia coli aminodeoxychorismate synthase: architectural conservation and diversity in chorismate-utilizing enzymes*. Biochemistry, 2002. **41**(7): p. 2198-208.
53. Parsons, J.F., K.M. Shi, and J.E. Ladner, *Structure of isochorismate synthase in complex with magnesium*. Acta Crystallogr D Biol Crystallogr, 2008. **64**(Pt 5): p. 607-10.
54. He, Z., et al., *Conservation of mechanism in three chorismate-utilizing enzymes*. Journal of the American Chemical Society, 2004. **126**(8): p. 2378-2385.
55. Liu, J., et al., *Overexpression, purification, and characterization of isochorismate synthase (EntC), the first enzyme involved in the biosynthesis of enterobactin from chorismate*. Biochemistry, 1990. **29**(6): p. 1417-25.
56. Basset, G.J.C., et al., *Foliate synthesis in plants: The p-aminobenzoate branch is initiated by a bifunctional PabA-PabB protein that is targeted to plastids*. Proceedings of the National Academy of Sciences of the United States of America, 2004. **101**(6): p. 1496-1501.

57. Huang, X.Y., H.M. Holden, and F.M. Raushel, *Channeling of substrates and intermediates in enzyme-catalyzed reactions*. Annual Review of Biochemistry, 2001. **70**: p. 149-180.
58. Kerbarh, O., et al., *Crystal structures of Yersinia enterocolitica salicylate synthase and its complex with the reaction products salicylate and pyruvate*. J Mol Biol, 2006. **357**(2): p. 524-34.
59. Kozlowski, M.C., et al., *Chorismate-Utilizing Enzymes Isochorismate Synthase, Anthranilate Synthase, and P-Aminobenzoate Synthase - Mechanistic Insight through Inhibitor Design*. Journal of the American Chemical Society, 1995. **117**(8): p. 2128-2140.
60. Summerfield, A.E., R. Bauerle, and C.M. Grisham, *Magnetic resonance and kinetic studies of the partial complex and Component I subunit forms of Salmonella typhimurium anthranilate synthase*. J Biol Chem, 1988. **263**(35): p. 18793-801.
61. Zwahlen, J., et al., *Structure and mechanism of MbtI, the salicylate synthase from Mycobacterium tuberculosis*. Biochemistry, 2007. **46**(4): p. 954-64.
62. Chook, Y.M., H. Ke, and W.N. Lipscomb, *Crystal structures of the monofunctional chorismate mutase from Bacillus subtilis and its complex with a transition state analog*. Proc Natl Acad Sci U S A, 1993. **90**(18): p. 8600-3.
63. Gallagher, D.T., et al., *The crystal structure of chorismate lyase shows a new fold and a tightly retained product*. Proteins, 2001. **44**(3): p. 304-11.
64. Schadt, H.S., et al., *2-Amino-2-deoxyisochorismate is a key intermediate in Bacillus subtilis p-aminobenzoic acid biosynthesis*. J Am Chem Soc, 2009. **131**(10): p. 3481-3.
65. Bulloch, E.M., et al., *Identification of 4-amino-4-deoxychorismate synthase as the molecular target for the antimicrobial action of (6s)-6-fluoroshikimate*. J Am Chem Soc, 2004. **126**(32): p. 9912-3.
66. Eberhard, J., et al., *Cytosolic and plastidic chorismate mutase isozymes from Arabidopsis thaliana: Molecular characterization and enzymatic properties*. Plant Journal, 1996. **10**(5): p. 815-821.
67. Mobley, E.M., B.N. Kunkel, and B. Keith, *Identification, characterization and comparative analysis of a novel chorismate mutase gene in Arabidopsis thaliana*. Gene, 1999. **240**(1): p. 115-123.
68. Niyogi, K.K. and G.R. Fink, *2 Anthranilate Synthase Genes in Arabidopsis - Defense-Related Regulation of the Tryptophan Pathway*. Plant Cell, 1992. **4**(6): p. 721-733.
69. Singh, B., *Plant amino acids : biochemistry and biotechnology*. Books in soils, plants, and the environment. 1999, New York: Marcel Dekker. ix, 621 p.
70. Niyogi, K.K., et al., *Suppressors of Trp1 Fluorescence Identify a New Arabidopsis Gene, Trp4, Encoding the Anthranilate Synthase Beta-Subunit*. Plant Cell, 1993. **5**(9): p. 1011-1027.
71. Zhao, J.M. and R.L. Last, *Coordinate regulation of the tryptophan biosynthetic pathway and indolic phytoalexin accumulation in Arabidopsis*. Plant Cell, 1996. **8**(12): p. 2235-2244.
72. Bohlmann, J., et al., *Purification and Cdna Cloning of Anthranilate Synthase from Ruta-Graveolens - Modes of Expression and Properties of Native and Recombinant Enzymes*. Plant Journal, 1995. **7**(3): p. 491-501.
73. Radwanski, E.R. and R.L. Last, *Tryptophan Biosynthesis and Metabolism - Biochemical and Molecular-Genetics*. Plant Cell, 1995. **7**(7): p. 921-934.

74. Facchini, P.J., D.A. Bird, and B. St-Pierre, *Can Arabidopsis make complex alkaloids?* Trends in Plant Science, 2004. **9**(3): p. 116-22.
75. Bernasconi, P., et al., *Functional expression of Arabidopsis thaliana anthranilate synthase subunit I in Escherichia coli*. Plant Physiology, 1994. **106**(1): p. 353-8.
76. Li, J. and R.L. Last, *The Arabidopsis thaliana trp5 mutant has a feedback-resistant anthranilate synthase and elevated soluble tryptophan*. Plant Physiology, 1996. **110**(1): p. 51-9.
77. Bohlmann, J., et al., *Anthranilate synthase from Ruta graveolens - Duplicated AS alpha genes encode tryptophan-sensitive and tryptophan-insensitive isoenzymes specific to amino acid and alkaloid biosynthesis*. Plant Physiology, 1996. **111**(2): p. 507-514.
78. Hughes, E.H., et al., *Expression of a feedback-resistant anthranilate synthase in Catharanthus roseus hairy roots provides evidence for tight regulation of terpenoid indole alkaloid levels*. Biotechnology and Bioengineering, 2004. **86**(6): p. 718-727.
79. Basset, G.J.C., et al., *Folate synthesis in plants: the last step of the p-aminobenzoate branch is catalyzed by a plastidial aminodeoxychorismate lyase*. Plant Journal, 2004. **40**(4): p. 453-461.
80. Sahr, T., et al., *Folate synthesis in plants: purification, kinetic properties, and inhibition of aminodeoxychorismate synthase*. Biochem J, 2006. **396**(1): p. 157-62.
81. Wildermuth, M.C., et al., *Isochorismate synthase is required to synthesize salicylic acid for plant defence*. Nature, 2001. **414**(6863): p. 562-5.
82. Strawn, M.A., et al., *Arabidopsis isochorismate synthase functional in pathogen-induced salicylate biosynthesis exhibits properties consistent with a role in diverse stress responses*. Journal of Biological Chemistry, 2007. **282**(8): p. 5919-5933.
83. Garcion, C., et al., *Characterization and biological function of the ISOCHORISMATE SYNTHASE2 gene of Arabidopsis*. Plant Physiology, 2008. **147**(3): p. 1279-1287.
84. Crosa, J.H., *Signal transduction and transcriptional and posttranscriptional control of iron-regulated genes in bacteria*. Microbiol Mol Biol Rev, 1997. **61**(3): p. 319-36.
85. Fischbach, M.A., et al., *How pathogenic bacteria evade mammalian sabotage in the battle for iron*. Nat Chem Biol, 2006. **2**(3): p. 132-8.
86. Meganathan, R., *Biosynthesis of menaquinone (vitamin K2) and ubiquinone (coenzyme Q): a perspective on enzymatic mechanisms*. Vitam Horm, 2001. **61**: p. 173-218.
87. Buss, K., et al., *Clustering of isochorismate synthase genes menF and entC and channeling of isochorismate in Escherichia coli*. Biochim Biophys Acta, 2001. **1522**(3): p. 151-7.
88. Dahm, C., et al., *The role of isochorismate hydroxymutase genes entC and menF in enterobactin and menaquinone biosynthesis in Escherichia coli*. Biochim Biophys Acta, 1998. **1425**(2): p. 377-86.
89. Daruwala, R., et al., *Menaquinone (vitamin K2) biosynthesis: overexpression, purification, and characterization of a new isochorismate synthase from Escherichia coli*. J Bacteriol, 1997. **179**(10): p. 3133-8.
90. Serino, L., et al., *Structural Genes for Salicylate Biosynthesis from Chorismate in Pseudomonas-Aeruginosa*. Molecular & General Genetics, 1995. **249**(2): p. 217-228.
91. Pelludat, C., D. Brem, and J. Heesemann, *Irp9, encoded by the high-pathogenicity island of Yersinia enterocolitica, is able to convert chorismate into salicylate, the precursor of the siderophore yersiniabactin*. J Bacteriol, 2003. **185**(18): p. 5648-53.

92. Liu, J., K. Duncan, and C.T. Walsh, *Nucleotide sequence of a cluster of Escherichia coli enterobactin biosynthesis genes: identification of entA and purification of its product 2,3-dihydro-2,3-dihydroxybenzoate dehydrogenase*. J Bacteriol, 1989. **171**(2): p. 791-8.
93. Raymond, K.N., E.A. Dertz, and S.S. Kim, *Enterobactin: An archetype for microbial iron transport*. Proceedings of the National Academy of Sciences of the United States of America, 2003. **100**(7): p. 3584-3588.
94. Kerbarh, O., et al., *Salicylate biosynthesis: overexpression, purification, and characterization of Irp9, a bifunctional salicylate synthase from Yersinia enterocolitica*. J Bacteriol, 2005. **187**(15): p. 5061-6.
95. Gross, J., et al., *A plant locus essential for phylloquinone (vitamin K1) biosynthesis originated from a fusion of four eubacterial genes*. J Biol Chem, 2006. **281**(25): p. 17189-96.
96. Rowland, B.M. and H.W. Taber, *Duplicate isochorismate synthase genes of Bacillus subtilis: Regulation and involvement in the biosyntheses of menaquinone and 2,3-dihydroxybenzoate*. Journal of Bacteriology, 1996. **178**(3): p. 854-861.
97. Berkner, K.L., *The vitamin K-dependent carboxylase*. Annual Review of Nutrition, 2005. **25**: p. 127-149.
98. Suttie, J.W., *The Importance of Menaquinones in Human-Nutrition*. Annual Review of Nutrition, 1995. **15**: p. 399-417.
99. Vermeer, C., et al., *Beyond deficiency: Potential benefits of increased intakes of vitamin K for bone and vascular health*. European Journal of Nutrition, 2004. **43**(6): p. 325-335.
100. Booth, S.L., *Roles for Vitamin K Beyond Coagulation*. Annual Review of Nutrition, 2009. **29**: p. 89-110.
101. Hiratsuka, T., et al., *An alternative menaquinone biosynthetic pathway operating in microorganisms*. Science, 2008. **321**(5896): p. 1670-1673.
102. Palaniappan, C., et al., *Menaquinone (Vitamin-K2) Biosynthesis - Evidence That the Escherichia-Coli Mend Gene Encodes Both 2-Succinyl-6-Hydroxy-2,4-Cyclohexadiene-1-Carboxylic Acid Synthase and Alpha-Ketoglutarate Decarboxylase Activities*. Journal of Bacteriology, 1992. **174**(24): p. 8111-8118.
103. Bhasin, M., J.L. Billinsky, and D.R.J. Palmer, *Steady-state kinetics and molecular evolution of Escherichia coli MenD [(1R,6R)-2-succinyl-6-hydroxy-2,4-cyclohexadiene-1-carboxylate synthase], an anomalous thiamin diphosphate-dependent decarboxylase-carboligase*. Biochemistry, 2003. **42**(46): p. 13496-13504.
104. Jiang, M., et al., *Menaquinone biosynthesis in Escherichia coli: Identification of 2-succinyl-5-enolpyruvyl-6-hydroxy-3-cyclohexene-l-carboxylate as a novel intermediate and re-evaluation of MenD activity*. Biochemistry, 2007. **46**(38): p. 10979-10989.
105. Jiang, M., et al., *Determination of the stereochemistry of 2-succinyl-5-enolpyruvyl-6-hydroxy-3-cyclohexene-1-carboxylate, a key intermediate in menaquinone biosynthesis*. Organic Letters, 2007. **9**(23): p. 4765-4767.
106. Jiang, M., et al., *Identification and characterization of (1R,6R)-2-succinyl-6-hydroxy-2,4-cyclohexadiene-1-carboxylate synthase in the menaquinone biosynthesis of Escherichia coli*. Biochemistry, 2008. **47**(11): p. 3426-3434.
107. Kwon, O., D.K. Bhattacharyya, and R. Meganathan, *Menaquinone (vitamin K2) biosynthesis: overexpression, purification, and properties of o-succinylbenzoyl-coenzyme A synthetase from Escherichia coli*. J Bacteriol, 1996. **178**(23): p. 6778-81.

108. Sharma, V., et al., *Menaquinone (Vitamin-K2) Biosynthesis - Nucleotide-Sequence and Expression of the Menb Gene from Escherichia-Coli*. Journal of Bacteriology, 1992. **174**(15): p. 5057-5062.
109. Truglio, J.J., et al., *Crystal structure of Mycobacterium tuberculosis MenB, a key enzyme in vitamin K-2 biosynthesis*. Journal of Biological Chemistry, 2003. **278**(43): p. 42352-42360.
110. Widhalm, J.R., et al., *A dedicated thioesterase of the Hotdog-fold family is required for the biosynthesis of the naphthoquinone ring of vitamin K1*. Proc Natl Acad Sci U S A, 2009. **106**(14): p. 5599-603.
111. Suvarna, K., et al., *Menaquinone (vitamin K-2) biosynthesis: Localization and characterization of the menA gene from Escherichia coli*. Journal of Bacteriology, 1998. **180**(10): p. 2782-2787.
112. Lee, P.T., et al., *A C-methyltransferase involved in both ubiquinone and menaquinone biosynthesis: isolation and identification of the Escherichia coli ubiE gene*. J Bacteriol, 1997. **179**(5): p. 1748-54.
113. Monzingo, A.F., et al., *The X-ray structure of Escherichia coli RraA (MenG), A protein inhibitor of RNA processing*. J Mol Biol, 2003. **332**(5): p. 1015-24.
114. Saxena, S.P., E.D. Israels, and L.G. Israels, *Novel vitamin K-dependent pathways regulating cell survival*. Apoptosis, 2001. **6**(1-2): p. 57-68.
115. Lochner, K., O. Doring, and M. Bottger, *Phylloquinone, what can we learn from plants?* Biofactors, 2003. **18**(1-4): p. 73-8.
116. Bridge, A., R. Barr, and D.J. Morre, *The plasma membrane NADH oxidase of soybean has vitamin K-1 hydroquinone oxidase activity*. Biochimica Et Biophysica Acta-Biomembranes, 2000. **1463**(2): p. 448-458.
117. Schultz, G., B.H. Ellerbrock, and J. Soll, *Site of Prenylation Reaction in Synthesis of Phylloquinone (Vitamin-K1) by Spinach-Chloroplasts*. European Journal of Biochemistry, 1981. **117**(2): p. 329-332.
118. Gaudilliere, J.P., et al., *Prenylation and Methylation Reactions in Phylloquinone (Vitamin-K1) Synthesis in Capsicum-Annuum Plastids*. Plant Cell Reports, 1984. **3**(6): p. 240-242.
119. Simantiras, M. and E. Leistner, *Formation of Orthosuccinylbenzoic Acid from Iso-Chorismic Acid in Protein Extracts from Anthraquinone-Producing Plant-Cell Suspension-Cultures*. Phytochemistry, 1989. **28**(5): p. 1381-1382.
120. Seeger, J.W. and R. Bentley, *Phylloquinone (Vitamin-K1) Biosynthesis in Euglena-Gracilis Strain-Z*. Phytochemistry, 1991. **30**(11): p. 3585-3589.
121. Johnson, T.W., et al., *Recruitment of a foreign quinone into the A(1) site of photosystem I. I. Genetic and physiological characterization of phylloquinone biosynthetic pathway mutants in Synechocystis sp. pcc 6803*. J Biol Chem, 2000. **275**(12): p. 8523-30.
122. Wade Johnson, T., et al., *The menD and menE homologs code for 2-succinyl-6-hydroxyl-2,4-cyclohexadiene-1-carboxylate synthase and O-succinylbenzoic acid-CoA synthase in the phylloquinone biosynthetic pathway of Synechocystis sp. PCC 6803*. Biochim Biophys Acta, 2003. **1557**(1-3): p. 67-76.
123. Sakuragi, Y., et al., *Insertional inactivation of the menG gene, encoding 2-phytyl-1,4-naphthoquinone methyltransferase of Synechocystis sp. PCC 6803, results in the incorporation of 2-phytyl-1,4-naphthoquinone into the A(1) site and alteration of the*

equilibrium constant between A(1) and F(X) in photosystem I. Biochemistry, 2002. **41**(1): p. 394-405.
124. Lefebvre-Legendre, L., et al., *Loss of phylloquinone in Chlamydomonas affects plastoquinone pool size and photosystem II synthesis*. J Biol Chem, 2007. **282**(18): p. 13250-63.
125. Lange, B.M. and M. Ghassemian, *Genome organization in Arabidopsis thaliana: a survey for genes involved in isoprenoid and chlorophyll metabolism*. Plant Mol Biol, 2003. **51**(6): p. 925-48.
126. Kim, H.U., et al., *The AAE14 gene encodes the Arabidopsis o-succinylbenzoyl-CoA ligase that is essential for phylloquinone synthesis and photosystem-I function*. Plant Journal, 2008. **54**(2): p. 272-83.
127. Shimada, H., et al., *Inactivation and deficiency of core proteins of photosystems I and II caused by genetical phylloquinone and plastoquinone deficiency but retained lamellar structure in a T-DNA mutant of Arabidopsis*. Plant Journal, 2005. **41**(4): p. 627-37.
128. Lohmann, A., et al., *Deficiency in phylloquinone (vitamin K1) methylation affects prenyl quinone distribution, photosystem I abundance, and anthocyanin accumulation in the Arabidopsis AtmenG mutant*. J Biol Chem, 2006. **281**(52): p. 40461-72.
129. Dandekar, T., et al., *Conservation of gene order: a fingerprint of proteins that physically interact*. Trends Biochem Sci, 1998. **23**(9): p. 324-8.
130. Overbeek, R., et al., *The use of gene clusters to infer functional coupling*. Proceedings of the National Academy of Sciences of the United States of America, 1999. **96**(6): p. 2896-2901.
131. Winkel, B.S.J., *Metabolic channeling in plants*. Annual Review of Plant Biology, 2004. **55**: p. 85-107.
132. Muller, W.U. and E. Leistner, *Metabolic Relation between Naphthalene Derivatives in Juglans*. Phytochemistry, 1978. **17**(10): p. 1735-1738.
133. Han, Y.S., et al., *Biosynthesis of anthraquinones in cell cultures of Cinchona 'Robusta' proceeds via the methylerythritol 4-phosphate pathway*. Phytochemistry, 2002. **59**(1): p. 45-55.
134. Polya, G.M., *Biochemical targets of plant bioactive compounds a pharmacological reference guide to sites of action and biological effects*. 2003, Taylor & Francis: London ; New York.
135. D'Auria, J.C. and J. Gershenzon, *The secondary metabolism of Arabidopsis thaliana: growing like a weed*. Curr Opin Plant Biol, 2005. **8**(3): p. 308-16.
136. Fieser, L.F., *The Discovery of Synthetic Alizarin*. Journal of Chemical Education, 1930. **7**(11): p. 2609-2633.
137. Brodersen, P., et al., *The role of salicylic acid in the induction of cell death in Arabidopsis acd11*. Plant Physiology, 2005. **138**(2): p. 1037-1045.
138. Muljono, R.A.B., J.C. Scheffer, and R. Verpoorte, *Isochorismate is an intermediate in 2,3-dihydroxybenzoic acid biosynthesis in Catharanthus roseus cell cultures*. Plant Physiology and Biochemistry, 2002. **40**(3): p. 231-234.
139. van Tegelen, L.J.P., et al., *Purification and cDNA cloning of isochorismate synthase from elicited cell cultures of Catharanthus roseus*. Plant Physiology, 1999. **119**(2): p. 705-712.
140. Dempsey, D.A., J. Shah, and D.F. Klessig, *Salicylic acid and disease resistance in plants*. Critical Reviews in Plant Sciences, 1999. **18**(4): p. 547-575.

141. Lee, H.I., J. Leon, and I. Raskin, *Biosynthesis and metabolism of salicylic acid*. Proc Natl Acad Sci U S A, 1995. **92**(10): p. 4076-9.
142. Yalpani, N., et al., *Pathway of Salicylic-Acid Biosynthesis in Healthy and Virus-Inoculated Tobacco*. Plant Physiology, 1993. **103**(2): p. 315-321.
143. Leon, J., et al., *Benzoic acid 2-hydroxylase, a soluble oxygenase from tobacco, catalyzes salicylic acid biosynthesis*. Proc Natl Acad Sci U S A, 1995. **92**(22): p. 10413-7.
144. Hooykaas, P.J.J., M.A. Hall, and K.R. Libbenga, *Biochemistry and molecular biology of plant hormones*. 1st ed. New comprehensive biochemistry v. 33. 1999, Amsterdam ; New York: Elsevier. xxii, 541 p.
145. Wildermuth, M.C., *Variations on a theme: synthesis and modification of plant benzoic acids*. Curr Opin Plant Biol, 2006. **9**(3): p. 288-96.
146. Coquoz, J.L., A. Buchala, and J.P. Metraux, *The biosynthesis of salicylic acid in potato plants*. Plant Physiology, 1998. **117**(3): p. 1095-1101.
147. Mauch-Mani, B. and A.J. Slusarenko, *Production of Salicylic Acid Precursors Is a Major Function of Phenylalanine Ammonia-Lyase in the Resistance of Arabidopsis to Peronospora parasitica*. Plant Cell, 1996. **8**(2): p. 203-212.
148. Nawrath, C. and J.P. Metraux, *Salicylic acid induction-deficient mutants of Arabidopsis express PR-2 and PR-5 and accumulate high levels of camalexin after pathogen inoculation*. Plant Cell, 1999. **11**(8): p. 1393-1404.
149. Dewdney, J., et al., *Three unique mutants of Arabidopsis identify eds loci required for limiting growth of a biotrophic fungal pathogen*. Plant Journal, 2000. **24**(2): p. 205-218.
150. Dean, J.V., L.A. Mohammed, and T. Fitzpatrick, *The formation, vacuolar localization, and tonoplast transport of salicylic acid glucose conjugates in tobacco cell suspension cultures*. Planta, 2005. **221**(2): p. 287-296.
151. Oerke, E.C., *Crop production and crop protection : estimated losses in major food and cash crops*. 1994, Amsterdam ; New York: Elsevier. xxii, 808 p.
152. van Loon, L.C., M. Rep, and C.M.J. Pieterse, *Significance of inducible defense-related proteins in infected plants*. Annual Review of Phytopathology, 2006. **44**: p. 135-162.
153. Glazebrook, J., *Contrasting mechanisms of defense against biotrophic and necrotrophic pathogens*. Annual Review of Phytopathology, 2005. **43**: p. 205-227.
154. Robert-Seilaniantz, A., et al., *Pathological hormone imbalances*. Curr Opin Plant Biol, 2007. **10**(4): p. 372-9.
155. Wiermer, M., B.J. Feys, and J.E. Parker, *Plant immunity: the EDS1 regulatory node*. Current Opinion in Plant Biology, 2005. **8**(4): p. 383-389.
156. Zhao, J., L.C. Davis, and R. Verpoorte, *Elicitor signal transduction leading to production of plant secondary metabolites*. Biotechnol Adv, 2005. **23**(4): p. 283-333.
157. Ebel, J. and A. Mithofer, *Early events in the elicitation of plant defence*. Planta, 1998. **206**(3): p. 335-348.
158. Chisholm, S.T., et al., *Host-microbe interactions: shaping the evolution of the plant immune response*. Cell, 2006. **124**(4): p. 803-14.
159. Nurnberger, T., et al., *Innate immunity in plants and animals: striking similarities and obvious differences*. Immunological Reviews, 2004. **198**(1): p. 249-266.
160. Jones, J.D. and J.L. Dangl, *The plant immune system*. Nature, 2006. **444**(7117): p. 323-9.
161. Asai, T., et al., *MAP kinase signalling cascade in Arabidopsis innate immunity*. Nature, 2002. **415**(6875): p. 977-983.

162. Eulgem, T., et al., *The WRKY superfamily of plant transcription factors*. Trends in Plant Science, 2000. **5**(5): p. 199-206.
163. Eulgem, T. and I.E. Somssich, *Networks of WRKY transcription factors in defense signaling*. Curr Opin Plant Biol, 2007. **10**(4): p. 366-71.
164. Zipfel, C., et al., *Bacterial disease resistance in Arabidopsis through flagellin perception*. Nature, 2004. **428**(6984): p. 764-767.
165. Bowles, D.J., *Defense-Related Proteins in Higher-Plants*. Annual Review of Biochemistry, 1990. **59**: p. 873-907.
166. Blume, B., et al., *Receptor-mediated increase in cytoplasmic free calcium required for activation of pathogen defense in parsley*. Plant Cell, 2000. **12**(8): p. 1425-1440.
167. Levine, A., et al., *Calcium-mediated apoptosis in a plant hypersensitive disease resistance response*. Current Biology, 1996. **6**(4): p. 427-37.
168. Apel, K. and H. Hirt, *Reactive oxygen species: Metabolism, oxidative stress, and signal transduction*. Annual Review of Plant Biology, 2004. **55**: p. 373-399.
169. Shirasu, K., et al., *Salicylic acid potentiates an agonist-dependent gain control that amplifies pathogen signals in the activation of defense mechanisms*. Plant Cell, 1997. **9**(2): p. 261-270.
170. Bradley, D.J., P. Kjellbom, and C.J. Lamb, *Elicitor- and wound-induced oxidative cross-linking of a proline-rich plant cell wall protein: a novel, rapid defense response*. Cell, 1992. **70**(1): p. 21-30.
171. Buchanan, B.B. and Y. Balmer, *Redox regulation: a broadening horizon*. Annu Rev Plant Biol, 2005. **56**: p. 187-220.
172. Hess, D.T., et al., *Protein S-nitrosylation: Purview and parameters*. Nature Reviews Molecular Cell Biology, 2005. **6**(2): p. 150-166.
173. Delledonne, M., *NO news is good news for plants*. Current Opinion in Plant Biology, 2005. **8**(4): p. 390-396.
174. Delledonne, M., et al., *Nitric oxide functions as a signal in plant disease resistance*. Nature, 1998. **394**(6693): p. 585-588.
175. Mur, L.A., T.L. Carver, and E. Prats, *NO way to live; the various roles of nitric oxide in plant-pathogen interactions*. J Exp Bot, 2006. **57**(3): p. 489-505.
176. Zeidler, D., et al., *Innate immunity in Arabidopsis thaliana: Lipopolysaccharides activate nitric oxide synthase (NOS) and induce defense genes*. Proceedings of the National Academy of Sciences of the United States of America, 2004. **101**(44): p. 15811-15816.
177. Moreau, M., et al., *AtNOS/AtNOA1 is a functional Arabidopsis thaliana cGTPase and not a nitric-oxide synthase*. J Biol Chem, 2008. **283**(47): p. 32957-67.
178. Feechan, A., et al., *A central role for S-nitrosothiols in plant disease resistance*. Proc Natl Acad Sci U S A, 2005. **102**(22): p. 8054-9.
179. Lindermayr, C., G. Saalbach, and J. Durner, *Proteomic identification of S-nitrosylated proteins in Arabidopsis*. Plant Physiology, 2005. **137**(3): p. 921-30.
180. Courtois, C., et al., *Nitric oxide signalling in plants: interplays with Ca2+ and protein kinases*. J Exp Bot, 2008. **59**(2): p. 155-63.
181. Jabs, T., et al., *Elicitor-stimulated ion fluxes and O2- from the oxidative burst are essential components in triggering defense gene activation and phytoalexin synthesis in parsley*. Proc Natl Acad Sci U S A, 1997. **94**(9): p. 4800-5.

182. Szatmari, A., et al., *Characterisation of basal resistance (BR) by expression patterns of newly isolated representative genes in tobacco*. Plant Cell Reports, 2006. **25**(7): p. 728-740.
183. Hayat, S. and A. Ahmad, *Salicylic acid : a plant hormone*. 2007, Dordrecht: Springer. xv, 401 p.
184. Schmelz, E.A., et al., *Simultaneous analysis of phytohormones, phytotoxins, and volatile organic compounds in plants*. Proceedings of the National Academy of Sciences of the United States of America, 2003. **100**(18): p. 10552-10557.
185. Schmelz, E.A., et al., *Phytohormone-based activity mapping of insect herbivore-produced elicitors*. Proceedings of the National Academy of Sciences of the United States of America, 2009. **106**(2): p. 653-657.
186. De Vos, M., et al., *Signal signature and transcriptome changes of Arabidopsis during pathogen and insect attack*. Molecular Plant-Microbe Interactions, 2005. **18**(9): p. 923-937.
187. Thomma, B.P.H.J., et al., *The complexity of disease signaling in Arabidopsis*. Current Opinion in Immunology, 2001. **13**(1): p. 63-68.
188. McConn, M., et al., *Jasmonate is essential for insect defense in Arabidopsis*. Proc Natl Acad Sci U S A, 1997. **94**(10): p. 5473-7.
189. Kutchan, T.M., *Alkaloid Biosynthesis[mdash]The Basis for Metabolic Engineering of Medicinal Plants*. Plant Cell, 1995. **7**(7): p. 1059-1070.
190. Facchini, P.J., *Alkaloid biosynthesis in plants: Biochemistry, cell biology, molecular regulation, and metabolic engineering applications*. Annual Review of Plant Physiology and Plant Molecular Biology, 2001. **52**: p. 29-66.
191. Farmer, E.E., E. Almeras, and V. Krishnamurthy, *Jasmonates and related oxylipins in plant responses to pathogenesis and herbivory*. Current Opinion in Plant Biology, 2003. **6**(4): p. 372-378.
192. Ziegler, J. and P.J. Facchini, *Alkaloid biosynthesis: Metabolism and trafficking*. Annual Review of Plant Biology, 2008. **59**: p. 735-769.
193. Kirby, J. and J.D. Keasling, *Biosynthesis of Plant Isoprenoids: Perspectives for Microbial Engineering*. Annual Review of Plant Biology, 2009. **60**: p. 335-355.
194. Hammerschmidt, R., *PHYTOALEXINS: What Have We Learned After 60 Years?* Annu Rev Phytopathol, 1999. **37**: p. 285-306.
195. Rogers, E.E., J. Glazebrook, and F.N. Ausubel, *Mode of action of the Arabidopsis thaliana phytoalexin camalexin and its role in Arabidopsis-pathogen interactions*. Molecular Plant-Microbe Interactions, 1996. **9**(8): p. 748-757.
196. Ferrari, S., et al., *Arabidopsis local resistance to Botrytis cinerea involves salicylic acid and camalexin and requires EDS4 and PAD2, but not SID2, EDS5 or PAD4*. Plant Journal, 2003. **35**(2): p. 193-205.
197. Shapiro, A.D. and A.T. Gutsche, *Capillary electrophoresis-based profiling and quantitation of total salicylic acid and related phenolics for analysis of early signaling in Arabidopsis disease resistance*. Analytical Biochemistry, 2003. **320**(2): p. 223-233.
198. Tsuda, K., et al., *Interplay between MAMP-triggered and SA-mediated defense responses*. Plant Journal, 2008. **53**(5): p. 763-775.
199. Feys, B.J., et al., *Direct interaction between the Arabidopsis disease resistance signaling proteins, EDS1 and PAD4*. Embo Journal, 2001. **20**(19): p. 5400-11.
200. Dong, X., *NPR1, all things considered*. Curr Opin Plant Biol, 2004. **7**(5): p. 547-52.

201. Horvath, D.M. and N.H. Chua, *Identification of an immediate-early salicylic acid-inducible tobacco gene and characterization of induction by other compounds*. Plant Molecular Biology, 1996. **31**(5): p. 1061-1072.
202. Uquillas, C., et al., *NPR1-independent activation of immediate early salicylic acid-responsive genes in Arabidopsis*. Molecular Plant-Microbe Interactions, 2004. **17**(1): p. 34-42.
203. DebRoy, S., et al., *A family of conserved bacterial effectors inhibits salicylic acid-mediated basal immunity and promotes disease necrosis in plants*. Proc Natl Acad Sci U S A, 2004. **101**(26): p. 9927-32.
204. Fobert, P.R. and C. Despres, *Redox control of systemic acquired resistance*. Curr Opin Plant Biol, 2005. **8**(4): p. 378-82.
205. Cao, H., X. Li, and X. Dong, *Generation of broad-spectrum disease resistance by overexpression of an essential regulatory gene in systemic acquired resistance*. Proc Natl Acad Sci U S A, 1998. **95**(11): p. 6531-6.
206. Mou, Z., W. Fan, and X. Dong, *Inducers of plant systemic acquired resistance regulate NPR1 function through redox changes*. Cell, 2003. **113**(7): p. 935-44.
207. Despres, C., et al., *The Arabidopsis NPR1 disease resistance protein is a novel cofactor that confers redox regulation of DNA binding activity to the basic domain/leucine zipper transcription factor TGA1*. Plant Cell, 2003. **15**(9): p. 2181-2191.
208. Ndamukong, I., et al., *SA-inducible Arabidopsis glutaredoxin interacts with TGA factors and suppresses JA-responsive PDF1.2 transcription*. Plant Journal, 2007. **50**(1): p. 128-39.
209. Shah, J., *The salicylic acid loop in plant defense*. Curr Opin Plant Biol, 2003. **6**(4): p. 365-71.
210. Chang, J.H., et al., *A high-throughput, near-saturating screen for type III effector genes from Pseudomonas syringae*. Proc Natl Acad Sci U S A, 2005. **102**(7): p. 2549-54.
211. Dangl, J.L. and J.D. Jones, *Plant pathogens and integrated defence responses to infection*. Nature, 2001. **411**(6839): p. 826-33.
212. Lam, E., N. Kato, and M. Lawton, *Programmed cell death, mitochondria and the plant hypersensitive response*. Nature, 2001. **411**(6839): p. 848-53.
213. Grant, M., et al., *The RPM1 plant disease resistance gene facilitates a rapid and sustained increase in cytosolic calcium that is necessary for the oxidative burst and hypersensitive cell death*. Plant Journal, 2000. **23**(4): p. 441-50.
214. Lecourieux, D., et al., *Analysis and effects of cytosolic free calcium increases in response to elicitors in Nicotiana plumbaginifolia cells*. Plant Cell, 2002. **14**(10): p. 2627-41.
215. Desikan, R., et al., *Harpin and hydrogen peroxide both initiate programmed cell death but have differential effects on defence gene expression in Arabidopsis suspension cultures*. Biochem J, 1998. **330 (Pt 1)**: p. 115-20.
216. Solomon, M., et al., *The involvement of cysteine proteases and protease inhibitor genes in the regulation of programmed cell death in plants*. Plant Cell, 1999. **11**(3): p. 431-443.
217. Laloi, C., et al., *The Arabidopsis cytosolic thioredoxin h5 gene induction by oxidative stress and its W-box-mediated response to pathogen elicitor*. Plant Physiology, 2004. **134**(3): p. 1006-1016.
218. Diaz, M., et al., *The gene encoding glutathione-dependent formaldehyde dehydrogenase/GSNO reductase is responsive to wounding, jasmonic acid and salicylic acid*. Febs Letters, 2003. **543**(1-3): p. 136-139.

219. Clarke, A., et al., *NO way back: nitric oxide and programmed cell death in Arabidopsis thaliana suspension cultures*. Plant Journal, 2000. **24**(5): p. 667-77.
220. Gechev, T.S., I.Z. Gadjev, and J. Hille, *An extensive microarray analysis of AAL-toxin-induced cell death in Arabidopsis thaliana brings new insights into the complexity of programmed cell death in plants*. Cellular and Molecular Life Sciences, 2004. **61**(10): p. 1185-1197.
221. Krzymowska, M., et al., *Infection of tobacco with different Pseudomonas syringae pathovars leads to distinct morphotypes of programmed cell death*. Plant Journal, 2007. **50**(2): p. 253-264.
222. Tada, Y., et al., *Nitric oxide and reactive oxygen species do not elicit hypersensitive cell death but induce apoptosis in the adjacent cells during the defense response of oat*. Molecular Plant-Microbe Interactions, 2004. **17**(3): p. 245-253.
223. Torres, M.A., J.D.G. Jones, and J.L. Dangl, *Pathogen-induced, NADPH oxidase-derived reactive oxygen intermediates suppress spread of cell death in Arabidopsis thaliana*. Nature Genetics, 2005. **37**(10): p. 1130-1134.
224. Dorey, S., et al., *Hydrogen peroxide from the oxidative burst is neither necessary nor sufficient for hypersensitive cell death induction, phenylalanine ammonia lyase stimulation, salicylic acid accumulation, or scopoletin consumption in cultured tobacco cells treated with elicitin*. Plant Physiology, 1999. **121**(1): p. 163-171.
225. Zheng, Z.Y., et al., *Functional analysis of Arabidopsis WRKY25 transcription factor in plant defense against Pseudomonas syringae*. Bmc Plant Biology, 2007. **7**: p. -.
226. DeFraia, C.T., E.A. Schmelz, and Z.L. Mou, *A rapid biosensor-based method for quantification of free and glucose-conjugated salicylic acid*. Plant Methods, 2008. **4**: p. -.
227. Glazebrook, J., et al., *Topology of the network integrating salicylate and jasmonate signal transduction derived from global expression phenotyping*. Plant Journal, 2003. **34**(2): p. 217-28.
228. Enyedi, A.J., et al., *Localization, Conjugation, and Function of Salicylic-Acid in Tobacco during the Hypersensitive Reaction to Tobacco Mosaic-Virus*. Proceedings of the National Academy of Sciences of the United States of America, 1992. **89**(6): p. 2480-2484.
229. Kawano, T. and S. Muto, *Mechanism of peroxidase actions for salicylic acid-induced generation of active oxygen species and an increase in cytosolic calcium in tobacco cell suspension culture*. J Exp Bot, 2000. **51**(345): p. 685-93.
230. Van Camp, W., M. Van Montagu, and D. Inze, *H2O2 and NO: redox signals in disease resistance*. Trends in Plant Science, 1998. **3**(9): p. 330-334.
231. Kliebenstein, D.J., et al., *LSD1 regulates salicylic acid induction of copper zinc superoxide dismutase in Arabidopsis thaliana*. Molecular Plant-Microbe Interactions, 1999. **12**(11): p. 1022-1026.
232. Durner, J. and D.F. Klessig, *Inhibition of ascorbate peroxidase by salicylic acid and 2,6-dichloroisonicotinic acid, two inducers of plant defense responses*. Proc Natl Acad Sci U S A, 1995. **92**(24): p. 11312-6.
233. Durner, J. and D.F. Klessig, *Salicylic acid is a modulator of tobacco and mammalian catalases*. J Biol Chem, 1996. **271**(45): p. 28492-501.
234. Klessig, D.F., et al., *Nitric oxide and salicylic acid signaling in plant defense*. Proc Natl Acad Sci U S A, 2000. **97**(16): p. 8849-55.

235. Delledonne, M., et al., *Signal interactions between nitric oxide and reactive oxygen intermediates in the plant hypersensitive disease resistance response*. Proceedings of the National Academy of Sciences of the United States of America, 2001. **98**(23): p. 13454-13459.
236. Mittler, R., et al., *Transgenic tobacco plants with reduced capability to detoxify reactive oxygen intermediates are hyperresponsive to pathogen infection*. Proc Natl Acad Sci U S A, 1999. **96**(24): p. 14165-70.
237. Zottini, M., et al., *Salicylic acid activates nitric oxide synthesis in Arabidopsis*. Journal of Experimental Botany, 2007. **58**(6): p. 1397-1405.
238. Clark, D., et al., *Nitric oxide inhibition of tobacco catalase and ascorbate peroxidase*. Mol Plant Microbe Interact, 2000. **13**(12): p. 1380-4.
239. Durner, J., D. Wendehenne, and D.F. Klessig, *Defense gene induction in tobacco by nitric oxide, cyclic GMP, and cyclic ADP-ribose*. Proc Natl Acad Sci U S A, 1998. **95**(17): p. 10328-33.
240. Shirano, Y., et al., *A gain-of-function mutation in an Arabidopsis Toll Interleukin-1 Receptor-Nucleotide Binding Site-Leucine-Rich Repeat type R gene triggers defense responses and results in enhanced disease resistance*. Plant Cell, 2002. **14**(12): p. 3149-3162.
241. Delaney, T.P., et al., *A Central Role of Salicylic-Acid in Plant-Disease Resistance*. Science, 1994. **266**(5188): p. 1247-1250.
242. Ross, A.F., *Systemic acquired resistance induced by localized virus infections in plants*. Virology, 1961. **14**: p. 340-58.
243. Durrant, W.E. and X. Dong, *Systemic acquired resistance*. Annu Rev Phytopathol, 2004. **42**: p. 185-209.
244. Gozzo, F., *Systemic acquired resistance in crop protection: from nature to a chemical approach*. J Agric Food Chem, 2003. **51**(16): p. 4487-503.
245. Maleck, K., et al., *The transcriptome of Arabidopsis thaliana during systemic acquired resistance*. Nat Genet, 2000. **26**(4): p. 403-10.
246. Gaffney, T., et al., *Requirement of Salicylic-Acid for the Induction of Systemic Acquired-Resistance*. Science, 1993. **261**(5122): p. 754-756.
247. Malamy, J. and D.F. Klessig, *Salicylic-Acid and Plant-Disease Resistance*. Plant Journal, 1992. **2**(5): p. 643-654.
248. Alvarez, M.E., et al., *Reactive oxygen intermediates mediate a systemic signal network in the establishment of plant immunity*. Cell, 1998. **92**(6): p. 773-84.
249. Felton, G.W., et al., *Inverse relationship between systemic resistance of plants to microorganisms and to insect herbivory*. Current Biology, 1999. **9**(6): p. 317-20.
250. White, R.F., *Acetylsalicylic acid (aspirin) induces resistance to tobacco mosaic virus in tobacco*. Virology, 1979. **99**(2): p. 410-2.
251. Malamy, J., et al., *Salicylic Acid: A Likely Endogenous Signal in the Resistance Response of Tobacco to Viral Infection*. Science, 1990. **250**(4983): p. 1002-1004.
252. Metraux, J.P., et al., *Increase in Salicylic Acid at the Onset of Systemic Acquired Resistance in Cucumber*. Science, 1990. **250**(4983): p. 1004-1006.
253. Shulaev, V., J. Leon, and I. Raskin, *Is Salicylic-Acid a Translocated Signal of Systemic Acquired-Resistance in Tobacco*. Plant Cell, 1995. **7**(10): p. 1691-1701.

254. Willits, M.G. and J.A. Ryals, *Determining the relationship between salicylic acid levels and systemic acquired resistance induction in tobacco*. Molecular Plant-Microbe Interactions, 1998. **11**(8): p. 795-800.
255. Vernooij, B., et al., *Salicylic-Acid Is Not the Translocated Signal Responsible for Inducing Systemic Acquired-Resistance but Is Required in Signal Transduction*. Plant Cell, 1994. **6**(7): p. 959-965.
256. Chen, F., et al., *An Arabidopsis thaliana gene for methylsalicylate biosynthesis, identified by a biochemical genomics approach, has a role in defense*. Plant Journal, 2003. **36**(5): p. 577-588.
257. Kumar, D. and D.F. Klessig, *High-affinity salicylic acid-binding protein 2 is required for plant innate immunity and has salicylic acid-stimulated lipase activity*. Proceedings of the National Academy of Sciences of the United States of America, 2003. **100**(26): p. 16101-16106.
258. Forouhar, F., et al., *Structural and biochemical studies identify tobacco SABP2 as a methyl salicylate esterase and implicate it in plant innate immunity*. Proceedings of the National Academy of Sciences of the United States of America, 2005. **102**(5): p. 1773-1778.
259. Park, S.W., et al., *Methyl salicylate is a critical mobile signal for plant systemic acquired resistance*. Science, 2007. **318**(5847): p. 113-116.
260. Park, S.W., et al., *Use of a Synthetic Salicylic Acid Analog to Investigate the Roles of Methyl Salicylate and Its Esterases in Plant Disease Resistance*. Journal of Biological Chemistry, 2009. **284**(11): p. 7307-7317.
261. Maldonado, A.M., et al., *A putative lipid transfer protein involved in systemic resistance signalling in Arabidopsis*. Nature, 2002. **419**(6905): p. 399-403.
262. Truman, W., et al., *Arabidopsis systemic immunity uses conserved defense signaling pathways and is mediated by jasmonates*. Proceedings of the National Academy of Sciences of the United States of America, 2007. **104**(3): p. 1075-1080.
263. Huffaker, A., G. Pearce, and C.A. Ryan, *An endogenous peptide signal in Arabidopsis activates components of the innate immune response*. Proceedings of the National Academy of Sciences of the United States of America, 2006. **103**(26): p. 10098-10103.
264. Jung, H.W., et al., *Priming in Systemic Plant Immunity*. Science, 2009. **324**(5923): p. 89-91.
265. Vlot, A.C., D.F. Klessig, and S.W. Park, *Systemic acquired resistance: the elusive signal(s)*. Curr Opin Plant Biol, 2008. **11**(4): p. 436-42.
266. Nawrath, C., et al., *EDS5, an essential component of salicylic acid-dependent signaling for disease resistance in Arabidopsis, is a member of the MATE transporter family*. Plant Cell, 2002. **14**(1): p. 275-286.
267. Sharma, Y.K., et al., *Ozone-induced responses in Arabidopsis thaliana: The role of salicylic acid in the accumulation of defense-related transcripts and induced resistance*. Proceedings of the National Academy of Sciences of the United States of America, 1996. **93**(10): p. 5099-5104.
268. Scott, I.M., et al., *Salicylate accumulation inhibits growth at chilling temperature in Arabidopsis*. Plant Physiology, 2004. **135**(2): p. 1040-1049.
269. Clarke, S.M., et al., *Salicylic acid dependent signaling promotes basal thermotolerance but is not essential for acquired thermotolerance in Arabidopsis thaliana*. Plant Journal, 2004. **38**(3): p. 432-447.

270. Larkindale, J., et al., *Heat stress phenotypes of arabidopsis mutants implicate multiple signaling pathways in the acquisition of thermotolerance*. Plant Physiology, 2005. **138**(2): p. 882-897.
271. Borsani, O., V. Valpuesta, and M.A. Botella, *Evidence for a role of salicylic acid in the oxidative damage generated by NaCl and osmotic stress in Arabidopsis seedlings*. Plant Physiology, 2001. **126**(3): p. 1024-1030.
272. Martinez, C., et al., *Salicylic acid regulates flowering time and links defence responses and reproductive development*. Plant Journal, 2004. **37**(2): p. 209-217.
273. Morris, K., et al., *Salicylic acid has a role in regulating gene expression during leaf senescence*. Plant Journal, 2000. **23**(5): p. 677-685.
274. Warner, T.D. and J.A. Mitchell, *Cyclooxygenase-3 (COX-3): Filling in the gaps toward a COX continuum?* Proceedings of the National Academy of Sciences of the United States of America, 2002. **99**(21): p. 13371-13373.
275. Weissmann, G., *Aspirin*. Sci Am, 1991. **264**(1): p. 84-90.
276. Rainsford, K.D., *Aspirin and related drugs*. 2004, London ; New York: Taylor & Francis. xxi, 770 p.
277. Masferrer, J.L. and P. Needleman, *Anti-inflammatories for cardiovascular disease*. Proc Natl Acad Sci U S A, 2000. **97**(23): p. 12400-1.
278. Vane, J.R., *Inhibition of prostaglandin synthesis as a mechanism of action for aspirin-like drugs*. Nat New Biol, 1971. **231**(25): p. 232-5.
279. Ferreira, S.H., S. Moncada, and J.R. Vane, *Indomethacin and aspirin abolish prostaglandin release from the spleen*. Nat New Biol, 1971. **231**(25): p. 237-9.
280. Roth, G.J. and P.W. Majerus, *The mechanism of the effect of aspirin on human platelets. I. Acetylation of a particulate fraction protein*. J Clin Invest, 1975. **56**(3): p. 624-32.
281. Kujubu, D.A., et al., *TIS10, a phorbol ester tumor promoter-inducible mRNA from Swiss 3T3 cells, encodes a novel prostaglandin synthase/cyclooxygenase homologue*. J Biol Chem, 1991. **266**(20): p. 12866-72.
282. Xie, W.L., et al., *Expression of a mitogen-responsive gene encoding prostaglandin synthase is regulated by mRNA splicing*. Proc Natl Acad Sci U S A, 1991. **88**(7): p. 2692-6.
283. Kopp, E. and S. Ghosh, *Inhibition of NF-kappa B by sodium salicylate and aspirin*. Science, 1994. **265**(5174): p. 956-9.
284. Yin, M.J., Y. Yamamoto, and R.B. Gaynor, *The anti-inflammatory agents aspirin and salicylate inhibit the activity of I kappa B kinase-beta*. Nature, 1998. **396**(6706): p. 77-80.
285. DiDonato, J.A., et al., *A cytokine-responsive IkappaB kinase that activates the transcription factor NF-kappaB*. Nature, 1997. **388**(6642): p. 548-54.
286. Baker, B., et al., *Signaling in plant-microbe interactions*. Science, 1997. **276**(5313): p. 726-33.
287. Ryals, J., et al., *The Arabidopsis NIM1 protein shows homology to the mammalian transcription factor inhibitor I kappa B*. Plant Cell, 1997. **9**(3): p. 425-439.
288. Spoel, S.H., et al., *NPR1 modulates cross-talk between salicylate- and jasmonate-dependent defense pathways through a novel function in the cytosol*. Plant Cell, 2003. **15**(3): p. 760-770.
289. Leduc, C., P. Ruhnau, and E. Leistner, *Isochorismate Hydroxymutase from Rubiaceae Cell-Suspension Cultures*. Plant Cell Reports, 1991. **10**(6-7): p. 334-337.

290. Leduc, C., et al., *Isochorismate hydroxymutase from a cell-suspension culture of Galium mollugo L.* Planta, 1997. **202**(2): p. 206-210.
291. van Tegelen, L.J.P., et al., *Isochorismate synthase isoforms from elicited cell cultures of Rubia tinctorum*. Phytochemistry, 1999. **51**(2): p. 263-269.
292. Stalman, M., et al., *Regulation of anthraquinone biosynthesis in cell cultures of Morinda citrifolia*. Journal of Plant Physiology, 2003. **160**(6): p. 607-614.
293. Uppalapati, S.R., et al., *The phytotoxin coronatine contributes to pathogen fitness and is required for suppression of salicylic acid accumulation in tomato inoculated with Pseudomonas syringae pv. tomato DC3000*. Mol Plant Microbe Interact, 2007. **20**(8): p. 955-65.
294. Catinot, J., et al., *Salicylic acid production in response to biotic and abiotic stress depends on isochorismate in Nicotiana benthamiana*. FEBS Lett, 2008. **582**(4): p. 473-8.
295. Ausubel, F.M., et al., *Current protocols in molecular biology*. 2005, Brooklyn, N. Y.; Media, Pa.: Greene Publishing Associates; J. Wiley, order fulfillment. 5 v. (loose-leaf).
296. Gaille, C., C. Reimmann, and D. Haas, *Isochorismate synthase (PchA), the first and rate-limiting enzyme in salicylate biosynthesis of Pseudomonas aeruginosa*. J Biol Chem, 2003. **278**(19): p. 16893-8.
297. Rudolph, F.B. and H.J. Fromm, *Plotting methods for analyzing enzyme rate data*. Methods Enzymol, 1979. **63**: p. 138-59.
298. Gaille, C., P. Kast, and D. Haas, *Salicylate biosynthesis in Pseudomonas aeruginosa. Purification and characterization of PchB, a novel bifunctional enzyme displaying isochorismate pyruvate-lyase and chorismate mutase activities*. J Biol Chem, 2002. **277**(24): p. 21768-75.
299. Rusnak, F., et al., *Subcloning of the enterobactin biosynthetic gene entB: expression, purification, characterization, and substrate specificity of isochorismatase*. Biochemistry, 1990. **29**(6): p. 1425-35.
300. Morollo, A.A. and R. Bauerle, *Characterization of composite aminodeoxyisochorismate synthase and aminodeoxyisochorismate lyase activities of anthranilate synthase*. Proc Natl Acad Sci U S A, 1993. **90**(21): p. 9983-7.
301. Zimmermann, P., et al., *GENEVESTIGATOR. Arabidopsis microarray database and analysis toolbox*. Plant Physiology, 2004. **136**(1): p. 2621-32.
302. Craigon, D.J., et al., *NASCArrays: a repository for microarray data generated by NASC's transcriptomics service*. Nucleic Acids Res, 2004. **32**(Database issue): p. D575-7.
303. Poulsen, C., R. Vanderheijden, and R. Verpoorte, *Assay of Isochorismate Synthase from Plant-Cell Cultures by High-Performance Liquid-Chromatography*. Phytochemistry, 1991. **30**(9): p. 2873-2876.
304. Young, I.G., Batterha.Tj, and F. Gibson, *Isolation Identification and Properties of Isochorismic Acid . An Intermediate in Biosynthesis of 2,3-Dihydroxybenzoic Acid*. Biochimica Et Biophysica Acta, 1969. **177**(3): p. 389-&.
305. DeClue, M.S., et al., *Experimental and computational investigation of the uncatalyzed rearrangement and elimination reactions of isochorismate*. Journal of the American Chemical Society, 2006. **128**(6): p. 2043-2051.
306. Cornish-Bowden, A., *Fundamentals of enzyme kinetics*. 1979, London ; Boston: Butterworths. xiii, 230 p.
307. Genoud, T., et al., *Phytochrome signalling modulates the SA-perceptive pathway in Arabidopsis*. Plant Journal, 2002. **31**(1): p. 87-95.

308. Fall, R. and M.C. Wildermuth, *Isoprene synthase: From biochemical mechanism to emission algorithm*. Journal of Geophysical Research-Atmospheres, 1998. **103**(D19): p. 25599-25609.
309. Entus, R., M. Poling, and K.M. Herrmann, *Redox regulation of arabidopsis 3-deoxy-D-arabino-heptulosonate 7-phosphate synthase*. Plant Physiology, 2002. **129**(4): p. 1866-1871.
310. Pigliucci, M. *Ecology and Evolutionary Biology of Arabidopsis*. The Arabidopsis Book 2002; Available from: http://www.aspb.org/publications/arabidopsis.
311. Wolfenden, R., et al., *The temperature dependence of enzyme rate enhancements*. Journal of the American Chemical Society, 1999. **121**(32): p. 7419-7420.
312. Verberne, M.C., et al., *Overproduction of salicylic acid in plants by bacterial transgenes enhances pathogen resistance*. Nat Biotechnol, 2000. **18**(7): p. 779-83.
313. Mauch, F., et al., *Manipulation of salicylate content in Arabidopsis thaliana by the expression of an engineered bacterial salicylate synthase*. Plant Journal, 2001. **25**(1): p. 67-77.
314. Chandran, D., et al., *Temporal global expression data reveal known and novel salicylate-impacted processes and regulators mediating powdery mildew growth and reproduction on Arabidopsis*. Plant Physiology, 2009. **149**(3): p. 1435-51.
315. Tewari, Y.B., et al., *A thermodynamic study of the conversion of chorismate to isochorismate*. Journal of Chemical Thermodynamics, 2000. **32**(8): p. 1057-1070.
316. Andrews, P.R., G.D. Smith, and I.G. Young, *Transition-State Stabilization and Enzymic Catalysis - Kinetic and Molecular-Orbital Studies of Rearrangement of Chorismate to Prephenate*. Biochemistry, 1973. **12**(18): p. 3492-3498.
317. Harrison, A.J., et al., *The structure of MbtI from Mycobacterium tuberculosis, the first enzyme in the biosynthesis of the siderophore mycobactin, reveals it to be a salicylate synthase*. Journal of Bacteriology, 2006. **188**(17): p. 6081-6091.
318. Sakurai, T., et al., *RARGE: a large-scale database of RIKEN Arabidopsis resources ranging from transcriptome to phenome*. Nucleic Acids Research, 2005. **33**: p. D647-D650.
319. Yamada, K., et al., *Empirical analysis of transcriptional activity in the Arabidopsis genome*. Science, 2003. **302**(5646): p. 842-6.
320. Calhoun, D.H., et al., *The emerging periplasm-localized subclass of AroQ chorismate mutases, exemplified by those from Salmonella typhimurium and Pseudomonas aeruginosa*. Genome Biol, 2001. **2**(8): p. RESEARCH0030.
321. Quadri, L.E.N., et al., *Identification of a Mycobacterium tuberculosis gene cluster encoding the biosynthetic enzymes for assembly of the virulence-conferring siderophore mycobactin*. Chemistry & Biology, 1998. **5**(11): p. 631-645.
322. Tso, J.Y. and H. Zalkin, *Chemical Modifications of Serratia-Marcescens Anthranilate Synthase Component-I*. Journal of Biological Chemistry, 1981. **256**(19): p. 9901-9908.
323. Payne, R.J., et al., *Inhibition studies on salicylate synthase*. Organic & Biomolecular Chemistry, 2005. **3**(10): p. 1825-1827.
324. Copley, S.D. and J.R. Knowles, *The Uncatalyzed Claisen Rearrangement of Chorismate to Prephenate Prefers a Transition-State of Chairlike Geometry*. Journal of the American Chemical Society, 1985. **107**(18): p. 5306-5308.

325. Sogo, S.G., et al., *Stereochemistry of the Rearrangement of Chorismate to Prephenate - Chorismate Mutase Involves a Chair Transition-State*. Journal of the American Chemical Society, 1984. **106**(9): p. 2701-2703.
326. Asano, Y., et al., *Steric Course of the Reactions Catalyzed by 5-Enolpyruvylshikimate-3-Phosphate Synthase, Chorismate Mutase, and Anthranilate Synthase*. Journal of the American Chemical Society, 1985. **107**(14): p. 4314-4320.
327. Zamir, L.O., et al., *Evidence for Enzymatic Formation of Isoprephenate from Isochorismate*. Bioorganic & Medicinal Chemistry Letters, 1993. **3**(7): p. 1441-1446.
328. Copley, S.D. and J.R. Knowles, *The Conformational Equilibrium of Chorismate in Solution - Implications for the Mechanism of the Nonenzymatic and the Enzyme-Catalyzed Rearrangement of Chorismate to Prephenate*. Journal of the American Chemical Society, 1987. **109**(16): p. 5008-5013.
329. DeClue, M.S., et al., *Isochorismate pyruvate lyase: A pericyclic reaction mechanism?* Journal of the American Chemical Society, 2005. **127**(43): p. 15002-15003.
330. Kunzler, D.E., et al., *Mechanistic insights into the isochorismate pyruvate lyase activity of the catalytically promiscuous PchB from combinatorial mutagenesis and selection*. J Biol Chem, 2005. **280**(38): p. 32827-34.
331. Smith, N., et al., *Structural analysis of ligand binding and catalysis in chorismate lyase*. Archives of Biochemistry and Biophysics, 2006. **445**(1): p. 72-80.
332. Luo, Q., J. Olucha, and A.L. Lamb, *Structure-function analyses of isochorismate-pyruvate lyase from Pseudomonas aeruginosa suggest differing catalytic mechanisms for the two pericyclic reactions of this bifunctional enzyme*. Biochemistry, 2009. **48**(23): p. 5239-45.
333. Zaitseva, J., et al., *Two crystal structures of the isochorismate pyruvate lyase from Pseudomonas aeruginosa*. Journal of Biological Chemistry, 2006. **281**(44): p. 33441-33449.
334. Bartlett, P.A. and C.R. Johnson, *An Inhibitor of Chorismate Mutase Resembling the Transition-State Conformation*. Journal of the American Chemical Society, 1985. **107**(25): p. 7792-7793.
335. Bartlett, P.A., et al., *Chorismate Mutase Inhibitors - Synthesis and Evaluation of Some Potential Transition-State Analogs*. Journal of Organic Chemistry, 1988. **53**(14): p. 3195-3210.
336. Payne, R.J., et al., *Design and synthesis of aromatic inhibitors of anthranilate synthase*. Organic & Biomolecular Chemistry, 2005. **3**(20): p. 3629-3635.
337. Payne, R.J., et al., *Synthesis and evaluation of 2,5-dihydrochorismate analogues as inhibitors of the chorismate-utilising enzymes*. Organic & Biomolecular Chemistry, 2009. **7**(11): p. 2421-2429.
338. Payne, R.J., et al., *Design and synthesis of aromatic inhibitors of anthranilate synthase*. Organic & Biomolecular Chemistry, 2005. **3**(12): p. 2271-2281.
339. Gilchrist, D.G. and J.A. Connelly, *Chorismate Mutase from Mung Bean and Sorghum*. Methods in Enzymology, 1987. **142**: p. 450-463.
340. Thompson, J.D., D.G. Higgins, and T.J. Gibson, *CLUSTAL W: improving the sensitivity of progressive multiple sequence alignment through sequence weighting, position-specific gap penalties and weight matrix choice*. Nucleic Acids Res, 1994. **22**(22): p. 4673-80.

341. Emanuelsson, O., H. Nielsen, and G. von Heijne, *ChloroP, a neural network-based method for predicting chloroplast transit peptides and their cleavage sites*. Protein Sci, 1999. **8**(5): p. 978-84.
342. Fiser, A. and A. Sali, *Modeller: generation and refinement of homology-based protein structure models*. Methods Enzymol, 2003. **374**: p. 461-91.
343. Emsley, P. and K. Cowtan, *Coot: model-building tools for molecular graphics*. Acta Crystallogr D Biol Crystallogr, 2004. **60**(Pt 12 Pt 1): p. 2126-32.
344. Kuroki, G.W. and E.E. Conn, *Purification and characterization of an inducible aromatic amino acid-sensitive form of chorismate mutase from Solanum tuberosum L. tubers*. Archives of Biochemistry and Biophysics, 1988. **260**(2): p. 616-21.
345. Kuroki, G.W. and E.E. Conn, *Differential Activities of Chorismate Mutase Isozymes in Tubers and Leaves of Solanum tuberosum L.* Plant Physiology, 1989. **89**(2): p. 472-476.
346. Hertel, S.C., M. Hieke, and D. Groger, *Purification and Characterization of Chorismate Mutase Isoenzymes from Ruta-Graveolens L.* Acta Biotechnologica, 1991. **11**(1): p. 39-48.
347. Eberhard, J., et al., *Isolation of a cDNA from tomato coding for an unregulated, cytosolic chorismate mutase*. Plant Mol Biol, 1996. **31**(4): p. 917-22.
348. Zamir, L.O., R. Tiberio, and R.A. Jensen, *Differential Acid-Catalyzed Aromatization of Prephenate, Arogenate, and Spiro-Arogenate*. Tetrahedron Letters, 1983. **24**(28): p. 2815-2818.
349. Kerbarh, O., et al., *Nucleophile selectivity of chorismate-utilizing enzymes*. Chembiochem, 2007. **8**(6): p. 622-4.
350. Kanno, T., et al., *Structure-based in vitro engineering of the anthranilate synthase, a metabolic key enzyme in the plant tryptophan pathway*. Plant Physiology, 2005. **138**(4): p. 2260-8.
351. Vance, R.L., et al., *Transition Structures for the Claisen Rearrangement*. Journal of the American Chemical Society, 1988. **110**(7): p. 2314-2315.
352. Poulsen, C., R.J. Bongaerts, and R. Verpoorte, *Purification and characterization of anthranilate synthase from Catharanthus roseus*. Eur J Biochem, 1993. **212**(2): p. 431-40.
353. Orsomando, G., et al., *Evidence for folate-salvage reactions in plants*. Plant Journal, 2006. **46**(3): p. 426-435.
354. Mavrodi, D.V., W. Blankenfeldt, and L.S. Thomashow, *Phenazine compounds in fluorescent Pseudomonas spp. biosynthesis and regulation*. Annu Rev Phytopathol, 2006. **44**: p. 417-45.
355. McDonald, M., et al., *Phenazine biosynthesis in Pseudomonas fluorescens: branchpoint from the primary shikimate biosynthetic pathway and role of phenazine-1,6-dicarboxylic acid*. J Am Chem Soc, 2001. **123**(38): p. 9459-60.
356. Van Lanen, S.G., S.J. Lin, and B. Shen, *Biosynthesis of the enediyne antitumor antibiotic C-1027 involves a new branching point in chorismate metabolism*. Proceedings of the National Academy of Sciences of the United States of America, 2008. **105**(2): p. 494-499.
357. Gu, Z.L., et al., *Role of duplicate genes in genetic robustness against null mutations*. Nature, 2003. **421**(6918): p. 63-66.
358. Chen, B.S., et al., *A new measure of the robustness of biochemical networks*. Bioinformatics, 2005. **21**(11): p. 2698-2705.

359. Makridakis, N., A. Akalu, and J.K. Reichardt, *Identification and characterization of somatic steroid 5alpha-reductase (SRD5A2) mutations in human prostate cancer tissue*. Oncogene, 2004. **23**(44): p. 7399-405.
360. Woycechowsky, K.J. and D. Hilvert, *Deciphering enzymes - Genetic selection as a probe of structure and mechanism*. European Journal of Biochemistry, 2004. **271**(9): p. 1630-1637.
361. Scopes, R.K., *Protein purification : priciples and practice*. 3rd ed. Springer advanced texts in chemistry. 1994, New York: Springer-Verlag. xix, 380 p.
362. Sharma, R.K., W.A. Taylor, and J.H. Wang, *Use of calmodulin affinity chromatography for purification of specific calmodulin-dependent enzymes*. Methods Enzymol, 1983. **102**: p. 210-9.
363. Kellermann, O.K. and T. Ferenci, *Maltose-binding protein from Escherichia coli*. Methods Enzymol, 1982. **90 Pt E**: p. 459-63.
364. Kapust, R.B. and D.S. Waugh, *Escherichia coli maltose-binding protein is uncommonly effective at promoting the solubility of polypeptides to which it is fused*. Protein Science, 1999. **8**(8): p. 1668-1674.
365. Hammarstrom, M., et al., *Rapid screening for improved solubility of small human proteins produced as fusion proteins in Escherichia coli*. Protein Science, 2002. **11**(2): p. 313-321.
366. Coligan, J.E., *Current protocols in protein science*. 1996, John Wiley and Sons: New York. p. <1- > (loose-leaf).
367. Eisenthal, R. and M.J. Danson, *Enzyme assays : a practical approach*. 2nd ed. The practical approach series 257. 2002, Oxford, OX ; New York: Oxford University Press. xix, 282 p.
368. Berg, J.M., J.L. Tymoczko, and L. Stryer, *Biochemistry*. 6th ed. 2007, New York: W.H. Freeman. 1 v. (various pagings).
369. Hakala, M.T., A.J. Glaid, and G.W. Schwert, *Lactic dehydrogenase. II. Variation of kinetic and equilibrium constants with temperature*. J Biol Chem, 1956. **221**(1): p. 191-209.
370. Howell, B.F., S. McCune, and R. Schaffer, *Lactate-to-pyruvate or pyruvate-to-lactate assay for lactate dehydrogenase: a re-examination*. Clin Chem, 1979. **25**(2): p. 269-72.
371. Bergmeyer, H.U., J. Bergmeyer, and M. Grassl, *Methods of enzymatic analysis*. 3rd ed. 1983, Weinheim ; Deerfield Beach, Fla.: Verlag Chemie. v. <1-9, 14 >.
372. Zewe, V. and H.J. Fromm, *Kinetic studies of rabbit muscle lactate dehydrogenase*. J Biol Chem, 1962. **237**: p. 1668-75.
373. Young, I.G. and F. Gibson, *Regulation of Enzymes Involved in Biosynthesis of 2,3-Dihydroxybenzoic Acid in Aerobacter Aerogenes and Escherichia Coli*. Biochimica Et Biophysica Acta, 1969. **177**(3): p. 401-&.
374. Guzman, L.M., et al., *Tight regulation, modulation, and high-level expression by vectors containing the arabinose PBAD promoter*. J Bacteriol, 1995. **177**(14): p. 4121-30.